Herausgeber: Prof. Dr.-Ing. Viktor Mechtcherine
Institut für Baustoffe
Fakultät Bauingenieurwesen
Technische Universität Dresden
01062 Dresden

Telefon: (0351) 463 36311
Telefax: (0351) 463 37268
E-Mail: i.baustoffe@tu-dresden.de

Druck: addprint AG, Am Spitzberg 8a, 01728 Bannewitz

ISBN 978-3-86780-381-6

Mechanisms of the interaction between continuous and short fibres in textile-reinforced concrete (TRC)

Mechanismen der Wechselwirkungen zwischen Endlos- und Kurzfasern in textilbewehrtem Beton

An der Fakultät Bauingenieurwesen der Technischen Universität Dresden

zur Erlangung der Würde eines Doktor-Ingenieurs (Dr.-Ing.)

eingereichte

DISSERTATION

vorgelegt von
Rabea Barhum, M. Sc.
aus Latakia – Syrien

eingereicht am 26. Juli 2013

Tag der mündlichen Prüfung: 21. November 2013

Gutachter:
Prof. Dr.-Ing. Viktor Mechtcherine,
Prof. Dr.-Ing. Marco di Prisco

Abstract

This thesis reports on experimental investigations of the mechanisms inherent in the joint action of short and continuous fibres in high-performance, cement-based composites. Experiments on different levels of observation (macro- meso- and micro-levels) were performed to provide detailed insights into the various effects of adding different types of short fibres (dispersed AR glass, integral AR glass and dispersed carbon fibres) on the strength, deformation, and failure behaviour of textile-reinforced concrete (TRC) subjected to tensile loading. Moreover, visual inspections of the specimens' surfaces and microscopic investigation of the fracture surfaces and the interface zone between fibre and matrix were performed and evaluated. Subsequently, the mathematical descriptions for TRC with short fibres under deformation controlled tensile loading conditions were derived based on a multi-scale rheological-statistical modelling approach.

Based on a literature review, the state of the art is presented and discussed to identify key questions that are yet to be answered satisfactorily. This provides the starting point for the investigations presented in this thesis.

The experimental program on the macro-level included uniaxial tension tests performed on thin, narrow plates reinforced by: a) only textile reinforcement, b) only short fibres, and c) hybrid reinforcement (both textile reinforcement with the addition of short fibres). Special attention was directed toward the course of the stress-strain relationship, crack pattern development, and fibre failure behaviour. The stress-strain curves resulting from uniaxial tension testing demonstrated clearly the positive influence of all types of short fibre on the mechanical performance of TRC. While the first-crack stress in TRC specimens increased significantly due to the addition of short fibres, an expansion of the strain region, where multiple cracks form, was observed for the stress-strain curves for TRC with added short fibres. The visual inspection of the specimens' surfaces showed a higher number of cracks and finer crack patterns for given strain levels in the cases when short fibres were added to TRC. Moreover, depending on fibre type, the positive effects of the addition of short fibres on both tensile strength and work-to-fracture of the composite were found to vary significantly.

The findings at the micro- and meso-levels of observation provided to a great extent a core of understanding of some particular mechanical behavioural properties of TRC with short fibres at the macro-level of observation. Thus, in addition to the experimental testing performed on composite materials with different parameter combinations, investigations of the action of individual material components, i.e., multifilament-yarns and single short fibres, embedded into cement-based matrices were carried out. It was found that short fibres indeed improve the bond between multifilament-yarns and the surrounding matrix. By their random positioning on the yarn's surface, short fibres built new adhesive cross-links which provided extra connecting points to the surrounding matrix. Furthermore, the water-to-binder ratio of the matrix influenced bond quality between fibre and matrix, i.e., various degrees of matrix-fibre bond were observed. As a result, the mechanical behaviour of the composite varied with w/b: While the good bond of the fibre embedded in a matrix with a low water-to-binder ratio leads to increase in stiffness and strength of the composite, fibres with weak bonding can be considered as defects with respect to stiffness as they lead to a decrease in the value.

The thesis further derives the mathematical relationships for TRC with the addition of short fibres under deformation-controlled tensile loading. A physically based rheological model consisting of simple rheological elements was developed based on the experimental results on the micro-scale, using single-fibre pullout tests. Special attention was paid to the gradual de-bonding

process and the resulting force-displacement branch. The model adequately reproduced both relevant fibre failure scenarios: fibre fracture and fibre pullout.

By means of statistical procedures the combination of these models led to description of the stress-crack opening behaviour of an individual crack bridged by the given number of short fibres.

The stress-strain relation for TRC with short fibres subjected to tensile loading was then derived. The concept followed at the macro-level of observation was modelling separately the three main regions of the characteristic stress-strain curve. The regions of crack-free material and crack-widening were considered linear and described based on the corresponding characteristic values of each region. The behaviour of the multiple cracking region was derived by considering an increasing number of cracks in serial interconnection and the contribution of the uncracked matrix in between. The stress transfer, i.e., bridging stress, across the crack was determined based on the contribution of both short fibres and multifilament-yarns. Behaviour of individual cracks was adjusted by varying the number of bridging fibres in different cracks and by varying the yarn bridging stress according to range observed in the pullout experiments.

Kurzfassung

In der vorliegenden Arbeit wird über Untersuchungen zu den Mechanismen der Wechselwirkungen zwischen Kurz- und Endlosfasern in zement-basierenten Hochleistungskompositen berichtet.

Hierzu wurden experimentelle Untersuchungen auf verschiedenen Betrachtungsebenen (Makro-, Meso- und Mikroebene) durchgeführt mit dem Ziel, detaillierte Erkenntnisse zu den Auswirkungen der Zugabe von verschiedenen Arten von Kurzfasern (disperse und integrale AR-Glasfasern, Kohlenstofffasern) hinsichtlich des Festigkeits-, Verformungs- und Bruchverhaltens von Textilbeton (engl.: textile-reinforced concrete = TRC) unter Zugbeanspruchung zu gewinnen. Die Bruchflächen sowie die Gestalt der Interphase zwischen der Bewehrung aus Textilien oder Kurzfasern und der umhüllenden zemengebundenen Matrix wurden mit optischen und elektronenmikroskopischen Verfahren hinsichtlich der Wechselwirkungsphänomene ausgewertet. Die Ergebnisse der experimentellen Arbeiten bildeten den Ausgangspunkt für die mathematischen Beschreibungen für TRC mit Kurzfasern unter verformungsgesteuerter Zugbelastung. Die Formulierungen erfolgten auf Grundlage multiskalarer rheologisch-statistischer Modellansätze.

In einer Literatursichtung wurde zunächst der Kenntnisstand zu den Materialien und zum Verhalten von TRC und Faserbeton unter Zugbeanspruchung dargestellt und diskutiert. Die noch zu erforschenden Fragen wurden präzisiert und die Grundlagen für deren Untersuchung geschaffen.

Bei den Experimenten auf der Makroebene wurden drei Bewehrungsvarianten betrachtet: a) textile Bewehrung, b) Kurzfaserbewehrung, und c) hybride Bewehrung (Textil und Kurzfasern). An Dehnkörpern wurde die Spannungs-Dehnungsbeziehung unter einachsiger Zugbelastung studiert und dabei das Rissbild und die Phänomene des Faserversagens detailliert beobachtet. Anhand der Spannungs-Dehnungsbeziehungen konnte gezeigt werden, dass die Zugabe von Kurzfasern bei allen untersuchten Kurzfaserarten zu einer erheblichen Verbesserung der Leistungsfähigkeit von Textilbeton führt. Dies zeigte sich unter anderem in einer ausgeprägten Anhebung der Erstrissspannung sowie der Entwicklung von zahlreicheren und damit feineren Rissen, die zu einer Verbesserung der Duktilität führten. Ebenso wurden Steigerungen der Zugfestigkeit und der Energiedissipation festgestellt. In welchem Maß diese Änderungen stattfinden, hängt von der Art der Kurzfasern ab.

Die Experimente auf der Mikro- und Mesoebene wurden so konzipiert, dass sie die Erkundung der Mechanismen, die den auf der Makroebene beobachteten Phänomenen zugrunde liegen, unterstützten. Auf der Mesoebene wurden Mulitifilamentgarnauszugversuche (mit und ohne Kurzfasern in der Matrix) und auf der Mikroebene Einzelfaserauszugsversuche für alle betrachteten Kurzfasertypen durchgeführt.

Es wurde festgestellt, dass die Kurzfasern den Verbund zwischen Matrix und Multifilamentgarn verbessern. Kurzfasern können bei zufälliger Positionierung an der Garnoberfläche zusätzliche Haftbrücken bzw. Verbindungsstellen zu umgebender Matrix bilden. Für die Verbundqualität zwischen Faser und Matrix ist der Wasser-Bindemittel-Wert (W/B-Wert) von entscheidender Bedeutung. Bei einer Matrix mit niedrigem W/B-Wert führt die gute Qualität des Verbunds der eingebetteten Fasern zu einer Erhöhung der Steifigkeit sowie der Festigkeit des Komposites. Bei hohem W/B-Wert haben die Fasern einen schlechten Verbund zur Matrix und müssen überwiegend als Fehl- bzw. Schwachstellen betrachtet werden. Festigkeit und Steifigkeit des Komposits nehmen daher ab.

Die Ableitung mathematischer Beziehungen für Textilbeton mit Zugabe von Kurzfasern unter verformungsgesteuerter Zugbelastung erfolgte aufbauend auf den Ergebnissen der experimentellen Untersuchungen auf der Mikroebene. Die Einzelfaserauszugsversuche wurden mit Hilfe eines physikalisch basierten Modelles nachgebildet, das aus einfachen rheologischen Elementen besteht. Phänomene wie die graduelle Ablösung der Faser, Faserbruch und Faserauszug wurden durch eine entsprechende Kombination und Parametrierung der rheologischen Elemente abgebildet. Im Ergebnis wurden zutreffende Kraft-Rissöffnungsbeziehungen modelliert.

Auf der Mesoebene wurde ein einzelner Riss modelliert, der sowohl durch Multifilamentgarne als auch Kurzfasern überbrückt werden kann. Der rissüberbrückenden Wirkung der zahlreichen Kurzfasern wurde mit Hilfe statistischer Methoden rechnung getragen, die unterschiedliche Faser-Risswinkel und Einbindelängen berücksichtigen. Die resultierende Spannungs-Rissöffnungskurve umfasst die rissüberbrückende Wirkung von Multifilamentgarnen und Kurzfasern.

Auf der Makroebene kann die charakteristische Spannungs-Dehnungsbeziehung von TRC unter Zugbelastung in 3 Bereiche (Zustände I, IIa, IIb) unterteilt werden. Die Kurvenverläufe im Zustand I (ungerissenen) sowie Zustand IIb (abgeschlossenes Rissbild) wurden als linear betrachtet und basierend auf den entsprechenden charakteristischen Werten des jeweiligen Zustands beschrieben. Das Verhalten im Zustand IIa (multiple Rissbildung) wurde durch die Reihenschaltung einer zunehmenden Anzahl von Rissen sowie den Beitrags der ungerissenen Matrix zwischen den Rissen modelliert.

Vorwort des Herausgebers

Bisherige Untersuchungen mechanischer Eigenschaften von textilbewehrtem Beton haben ergeben, dass die Zugabe von Kurzfasern das Verformungs- und Festigkeitsverhalten dieses Verbundwerkstoffs positiv beeinflussen kann. Die Mechanismen der Wechselwirkungen zwischen "Endlos"- und Kurzfasern in Textilbeton wurden jedoch nicht untersucht. Aufgrund des fehlenden Verständnisses dieser Wirkungsmechanismen war bislang eine gezielte Optimierung des komplexen Verbundwerkstoffs Textilbeton mit Kurzfasern nicht möglich.

Die vorliegende Dissertation hatte zum Ziel, das mechanische Verhalten von Textilbeton mit zusätzlicher Kurzfaserbewehrung unter quasistatischer monotoner Beanspruchung systematisch zu untersuchen. Eine besondere Stärke der Arbeit von Herrn Barhum ist der gut durchdachte und ausgezeichnet umgesetzte mehrskalige experimentelle Forschungsansatz begleitet von gefügemorphologischen Untersuchungen. Dadurch konnte das makroskopische Materialverhalten auf der Grundlage der meso- und mikromechanischen Vorgänge schlüssig erläutert werden. Durch die anschließende Entwicklung eines rheologisch-statistischen mehrskaligen Modells wird das Verständnis des Werkstoffverhaltens noch weiter vertieft. Hiermit schuf Herr Barhum eine überaus wertvolle Grundlage für eine gezielte Gestaltung der zementbasierten Verbundwerkstoffe mit hybrider Bewehrung bestehend aus "endlosen" und kurzen Fasern. Durch die gewonnenen Erkenntnisse zum spezifischen mechanischen Verhalten von Textil mit Kurzfasern leistet die Dissertation außerdem einen bedeutenden Beitrag zur Vorbereitung der Überführung dieses neuen Verbundwerkstoffes in die Baupraxis.

Die Arbeit von Herrn Barhum beruht auf den Ergebnissen eines anspruchsvollen, vom Autor mitbearbeiteten Forschungsvorhabens im Rahmen des Sonderforschungsbereiches 528 "Textile Bewehrungen zur bau-technischen Verstärkung und Instandsetzung" der Deutschen Forschungsgemeinschaft (DFG). Die intensive Zusammenarbeit mit den anderen Fachgebieten innerhalb des SFB war für die vorliegende Dissertation überaus vorteilhaft. Das gleiche gilt für den Forschungsaufenthalt von Herrn Barhum an der Bundesuniversität von Rio de Janeiro (UFRJ), Brasilien (Prof. Romildo Toledo Filho) im Rahmen des gemeinsamen Projektes der COPPE/UFRJ und der TU Dresden "Development and characterization of textile reinforced concrete with natural and man-made fibre". Schließlich hat die Vorbereitung von Publikationen in referierten internationalen Zeitschriften sowie seine Beiträge auf nationalen und internationalen Tagungen die Qualität seiner Arbeit zusätzlich gefördert.

Ich kenne Herrn Barhum noch aus seiner Zeit als Student des internationalen Masterstudienganges "Rehabilitation Engineering" an der TU Dresden. Seine wissenschaftliche Tätigkeit begann er mit seiner Masterarbeit zum Thema "Textile reinforced concrete – Transport mechanisms of gases and water". Ich freue mich, dass er sich durch seine Promotionsarbeit als Ingenieur und Wissenschaftler sehr gut weiterentwickelt und so auch die nächste Herausforderung mit Erfolg gemeistert hat. Außerdem freut mich, dass er seine Kenntnisse aus dem Masterstudium, der Promotionszeit und der Mitarbeit am Institut im Rahmen seiner heutigen Tätigkeit in einem renommierten Münchener Ingenieurbüro einsetzen kann. Für seine berufliche Karriere wünsche ich ihm viel Erfolg und privat alles Gute!

Viktor Mechtcherine

Acknowledgement

First of all I would like to express my gratitude to Prof. Viktor Mechtcherine and to the German Academic Exchange Service (DAAD) for the financial support provided through its graduate scholarship program. I am especially grateful to Prof. Mechtcherine for the continuous encouragement and the constructive feedbacks in combination with his warm treatment and support personally and professionally.

Sincere thanks are given to Prof. Marco di Prisco for his interest in my work his invaluable suggestions and discussions.

Further to that, I would like to thank my colleagues at the Institute of Construction Materials at Technische Universität Dresden:

- My deepest thankfulness is to Dr.-Ing. Marko Butler not only for his ongoing interest in my work, willingness to engage in discussions and expert assistance, but also for his very kind treatment, friendship and the handicraft works,
- Renate Franke, Isabell Schur, Christian Stahn and all trainees for their assistance in the variour laboratory work,
- Kai-Uwe Mehlisch and Tilo Günzel for the precise laboratory testing and manufacturing of the necessary moulds,
- Martina Götze, Mirella Kratz, Annegret Lindner, Dr. rer. nat. Christof Schröfl and Annett Willomitzer for the precise organization of laboratory work and the lovely personal support; I am deeply indebted to them,
- Simone Hempel for her excellent microscopy work and discussions of morphologic phenomena,
- Claudia Bellmann, Arnd-Eike Brüdern, Lukasz Dudziak, Michaela Gorges, Steffen Müller and Eric Mündecke for the tireless assistance, kind support and of course "kickern",
- Dr.-Ing. Frank Altmann, Dr.-Ing. Petr Jun and Dr.-Ing. Matthias Lieboldt for their support and exchange of experiences.

My sincere appreciation is further extended to the directors of Zilch + Müller Ingenieure for their support and understanding, especially in the period before the doctoral defense.

Finally, and most importantly, I would like to express my gratefulness to my Family for their support throughout my whole life, to my wife Lara for her continuous support and understanding and to my wonderful daughter Laura for the necessary distraction.

München, February 2014

Rabea Barhum

Contents

1 Introduction **1**
- 1.1 Problem to be solved . . . 1
- 1.2 Objectives and investigation concept . . . 2
- 1.3 Thesis structure . . . 4

2 Literature review **5**
- 2.1 Introduction . . . 5
- 2.2 Textile-reinforced concrete . . . 5
  - 2.2.1 Introduction . . . 5
  - 2.2.2 Fine-grained cement-based concrete . . . 5
    - 2.2.2.1 Structure of concrete . . . 5
    - 2.2.2.2 Matrix composition . . . 6
    - 2.2.2.3 Fresh concrete properties . . . 7
  - 2.2.3 Textile reinforcement . . . 7
  - 2.2.4 Production technologies . . . 8
  - 2.2.5 Characteristic behaviour . . . 8
  - 2.2.6 Failure mechanisms and yarn-matrix bond . . . 10
    - 2.2.6.1 Failure mechanisms . . . 10
    - 2.2.6.2 Bond mechanisms and pullout models . . . 12
- 2.3 Concrete with short fibres . . . 16
  - 2.3.1 Effect of short fibres on fresh concrete properties . . . 16
  - 2.3.2 Advantages of short fibres in hardened concrete . . . 16
  - 2.3.3 Orientation and distribution of fibres . . . 18
  - 2.3.4 Mechanisms of formation and propagation of cracks in fibre-reinforced concrete . . . 20
    - 2.3.4.1 Action of fibres in pre-cracking stage . . . 21
    - 2.3.4.2 Action of fibres in post-cracking stage . . . 22
    - Aggregate bridging . . . 23
    - Fibre bridging . . . 24
- 2.4 Rheological modelling . . . 29
- 2.5 Summary – Conclusions to the own work . . . 32

3 Experimental program **33**
- 3.1 Materials . . . 33
  - 3.1.1 Fine-grained cement-based matrix . . . 33
  - 3.1.2 Continuous fibres – Textile reinforcement . . . 34
  - 3.1.3 Short fibres . . . 34
- 3.2 Production of specimens . . . 35
  - 3.2.1 Mixing procedure . . . 36
  - 3.2.2 Specimen fabrication . . . 37
  - 3.2.3 Curing condition . . . 38
- 3.3 Experimental methods and parameters combination . . . 40
  - 3.3.1 Uniaxial tensile tests – Macro-level . . . 40

3.3.2 Multifilament-yarn pullout tests – Meso-level . . . 42
3.3.3 Single-fibre pullout tests – Micro-level . . . 43

4 Experimental results and discussion 47
4.1 Behaviour of the TRC with short fibres under uniaxial tension . . . 47
4.1.1 General effects of the addition of short fibres on TRC behaviour under tension . . . 47
4.1.2 Influence of short fibre on the behaviour of crack-free TRC – First-crack stress . . . 50
4.1.3 Influence of short fibres on crack formation and crack pattern . . . 52
4.1.4 Influence on short fibres on tensile strength and energy dissipation . . . 55
4.1.5 Discussion of the test results obtained from TRC specimens with and without short fibres . . . 56
4.2 Contribution of the components of TRC to its behaviour under uniaxial tensile loading . . . 61
4.2.1 Uniaxial tensile tests – Effect of w/b on macro-level . . . 61
4.2.1.1 Finely grained concrete – Plain matrix . . . 61
4.2.1.2 Specimens with textile reinforcement . . . 61
4.2.1.3 Specimens reinforced by short fibres only . . . 62
4.2.2 Multifilament-yarn pullout tests – Effect of w/b on meso-level . . . 67
4.2.3 Single-fibre pullout tests – Effect of w/b on micro-level . . . 67
4.3 Effect of short fibre on yarn-matrix bond . . . 71
4.3.1 Multifilament-yarn pullout tests – Effect of short fibres on meso-level . . . 71
4.4 Effect of short fibres' type and orientation . . . 77
4.4.1 Uniaxial tensile tests – Effect of fibre type on macro-level . . . 77
4.4.2 Single-fibre pullout tests – Effect of fibre type and orientation on micro-level 80
4.4.2.1 Single-fibre pullout parallel to the fibre axis . . . 81
4.4.2.2 Pullout of inclined fibres . . . 82
4.5 Summary . . . 86

5 Rheological-statistical model 89
5.1 Introduction . . . 89
5.2 Modelling at micro-level of observation – Single fibre . . . 89
5.2.1 Fibre fracture . . . 92
5.2.2 Fibre pullout . . . 98
5.3 Statistical study of fibre distribution and orientation at fracture surface – Meso-level 100
5.3.1 Introduction . . . 100
5.3.2 Fibre embedded length . . . 100
5.3.3 Orientation and number of fibres . . . 104
5.4 Multi-scale modelling approach . . . 108
5.4.1 Introduction . . . 108
5.4.2 Mathematical description of single-fibre pullout response – Micro-level . . . 108
5.4.3 Mathematical description of single crack behaviour – Meso-level . . . 111
5.4.4 Mathematical description of the TRC behaviour at macro-level . . . 115

6 Conclusions and outlook 119
6.1 Conclusions . . . 119
6.1.1 Introduction . . . 119
6.1.2 Experimental multi-level investigation . . . 119

6.1.3 Modelling 120
6.2 Outlook 121

Bibliography **123**

A Appendix – Slump flow tests **133**

B Appendix – Results of uniaxial tensile tests (4 layers of textile with and without short fibres) **135**

C Appendix – Effect of short fibres on crack pattern **137**

D Appendix – List of Symbols **139**

1 Introduction

1.1 Problem to be solved

Steel-reinforced concrete is the most frequently used and important material in civil engineering. This composite material is comprised of concrete characterized by high compressive strength values and steel reinforcement with high tensile strength. Steel-reinforced concrete is very appropriate for load-bearing structures subjected to a wide range of loading conditions.

Textile-reinforced concrete (TRC) is a relatively newly developed composite material consisting of multiaxial fabrics used in combination with finely grained concrete. The use of textiles, mainly made of alkali resistant (AR) glass and carbon, leads to a considerable reduction in element thickness. This novel material allows the design of curved and complex element shapes with high-quality of concrete surfaces and very thinly structured concrete elements, as low as 10 mm, with high strength under compression as well as under tension. An overview of the first applications is given in Brameshuber [1]. Textile-reinforced concrete offers today a wide spectrum of applications in both new structures, (in the manufacture of thinly walled façade elements, load-bearing integrated formwork, tunnel linings etc.) and in the strengthening and repair of existing reinforced concrete structural elements, some examples may be found in Brameshuber [1], Butler et al. [2] and Mechtcherine [3].

Previous investigations have shown that the high values of tensile strength in textile-reinforced concrete is typically reached at relatively large deformations and accompanied by the formation of a considerable number of cracks; see Jesse [4]. Such large deformations prior to material failure are crucial in respect of structural safety as well as energy dissipation, particularly in the case of impact loading; see, for example, Silva et al. [5]. However, since high strength levels can only be reached at high deformations, in the service state, where only small deformations are acceptable, the design load-bearing capacity of TRC must be much lower than its tensile strength. Moreover, Mechtcherine and Lieboldt in [6] and [7] and Lieboldt in [8] investigated the effects of multiple cracking on the permeation of fluids and gases through TRC. The resistance of TRC to the transport of fluids and gases into and through the repair material influences to a great extent the durability of restored structures with such TRC layers. They observed, based on the *in situ* permeation tests on cracked TRC subjected to uniaxial tensile loading, a pronounced increase in the transport rates of fluids and gases perpendicular to the composite surface through the TRC with increasing strain, in correspondence with greater crack widths. One of the challenges was to restrict the degree of permeability by decreasing the average crack widths.

In order to increase the load-carrying capacity of TRC, a higher degree of multifilament-yarn fineness and/or more textile reinforcement layers could be used, as shown in Figure 1.1 and Figure 1.2, respectively. However, this leads to an over-proportional increase in tensile strength, but to an under-proportional increase in load-bearing capacity with small deformations. Therefore, this costly measure seems inappropriate to a workable solution of the problem.

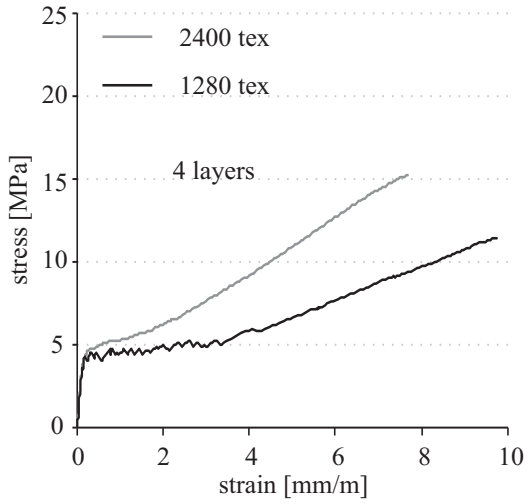

Figure 1.1: Influence of the fineness of multifilament-yarn on the behaviour of textile-reinforced concrete specimens in tensile test; Lieboldt [8]

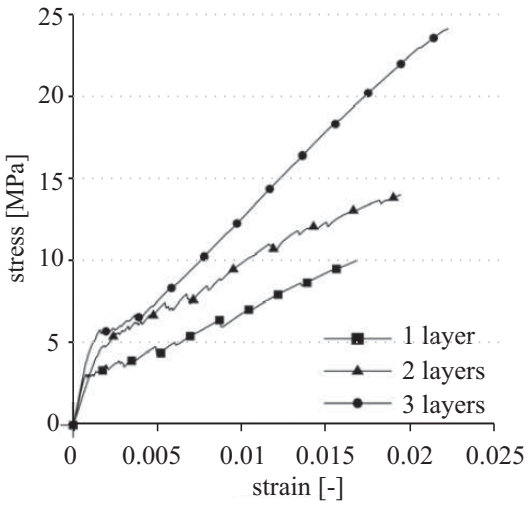

Figure 1.2: Influence of the reinforcement ratio on the behaviour of textile-reinforced concrete specimens in tensile test; Colombo et al. [9]

In recent years researchers have performed several test series to investigate the influence of short fibres on various properties of textile-reinforced concrete. A pronounced improvement of the behaviour of TRC under tensile loading was achieved successfully due to the addition of different types of short fibres: For example, the tests undertaken by Butler et al. [10], Hinzen and Brameshuber [11] and Korb [12]. Furthermore, the addition of short fibres to TRC led to a larger number of cracks in the TRC specimens at given strain levels, but these cracks were considerably finer and of lower permeability for gases and liquids in passing through the TRC, as shown by Lieboldt in [8]. However, the mechanisms inherent in the joint action of short fibre and continuous fibres, i.e., textile reinforcement, and how such complex materials with hybrid reinforcement work have not been fully investigated and understood; indeed this is not straightforward.

The thesis presented here reports of systematic investigations on the influence on the fracture behaviour of textile-reinforced concrete under tensile loading when various types of short fibres are added. The program of investigation has been initiated in order to gain more and better insight into the specific material behaviour of the finely grained concrete with such hybrid reinforcement.

1.2 Objectives and investigation concept

The goal of the thesis at hand is an in-depth analysis of the interaction between textile reinforcement and short fibres embedded in cement-based matrices and an understanding of the mechanisms of their mutual influences. A multiscale investigation program is necessary to provide details regarding the contribution of individual components of such complex material with hybrid reinforcement. The findings at the micro- and meso-levels of observation provide to a great extent a core of understanding of some particular mechanical behavioural properties of TRC

with short fibres at the macro-level of observation. Thus, in addition to the experimental testing performed on composite materials with different parameter combinations, investigations of the action of individual material components, i.e., multifilament-yarns and single short fibres, embedded into cement-based matrices are carried out, cf. Figure 1.3. Such an approach is followed in order to provide detailed information on the different failure mechanisms dominating the material behaviour at different levels of observation. The experimental program on the macro-level includes uniaxial tension tests performed on thin, narrow plates reinforced by: a) only textile reinforcement, b) only short fibres, and c) hybrid reinforcement (both textile reinforcement with the addition of short fibres). Special attention is directed toward the course of the stress-strain relationship, crack pattern development, and fibre failure behaviour. Moreover, visual inspections of the specimens' surfaces and microscopic investigation of the fracture surfaces and the interface zone between fibre and matrix are performed and evaluated.

To provide detailed insights into the various failure mechanisms observed in the tests and to clarify the fracture process, the experimental program is extended to the meso- and micro-levels of observation. Therefore, investigation of bond behaviour between multifilament-yarn or short fibres and the surrounding fine-grained matrix is studied by performing multifilament-yarn and single-fibre pullout tests, respectively.

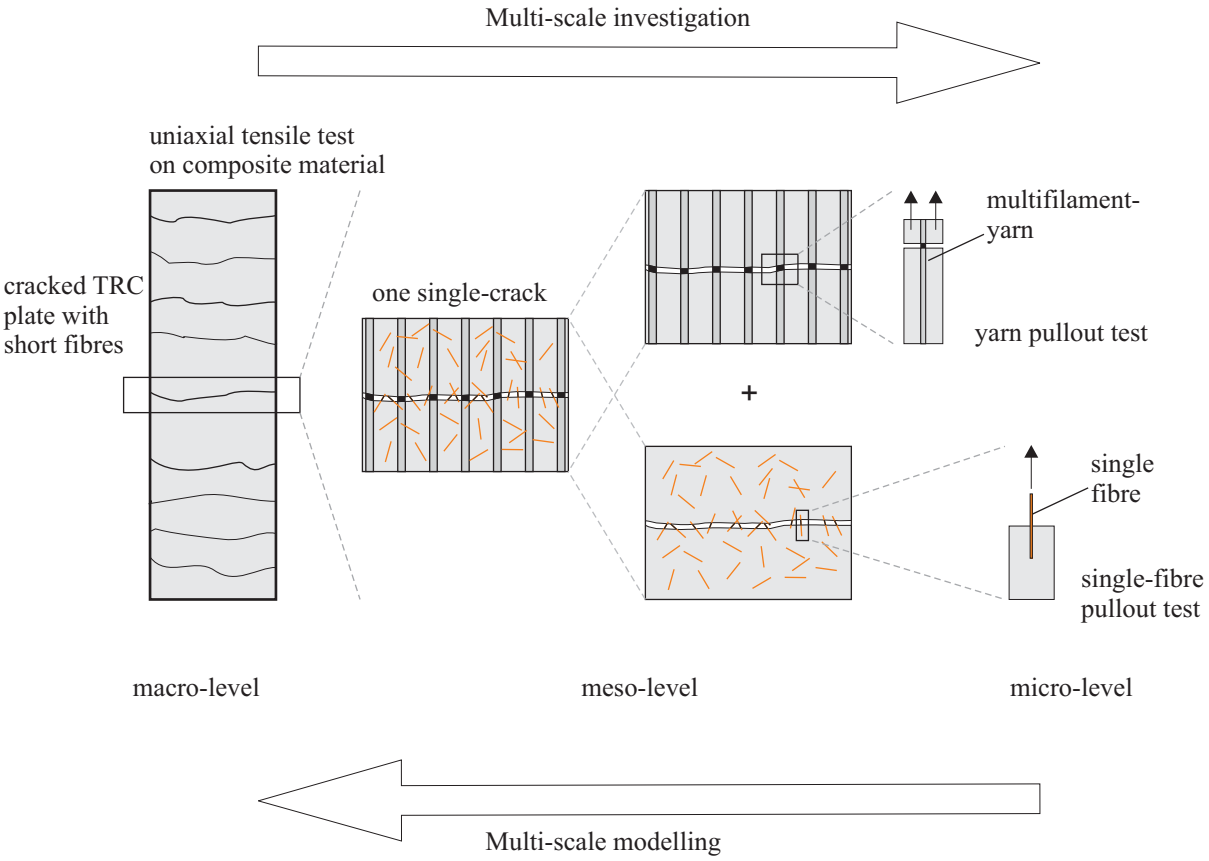

Figure 1.3: Schematic view of the tests used in order to consider the contribution of individual components of the composite to the overall mechanical behaviour of TRC with short fibres

Based on the experimental results and the phenomena observed on the micro-scale, i.e., single-fibre pullout tests, a physically based, rheological model consisting of simple rheological elements was developed. By means of statistical procedures the combination of these models enabled a sound description of the material behaviour on the meso-scale, i.e., the opening of one single-

crack. On the basis of this model and the results of mechanical fracture and phenomenological investigations, a material behaviour on the macro-scale has been described.

1.3 Thesis structure

The thesis at hand consists of six chapters:

Chapter 1 presents briefly the purpose of the research, the investigation concept and an overview of the thesis structure.

Chapter 2 gives a survey of the literature regarding the materials used in this investigation, textile-reinforced concrete (TRC) and fibre-reinforced concrete, relevant to this thesis. A general introduction of the components of TRC, the behaviour of TRC under tensile loading and some details regarding bond and failure mechanisms in TRC are introduced firstly. Subsequently, details with respect to the orientation and distribution of short fibres as well as the mechanics of crack formation and crack development in cementitious material are given. Finally, information concerning rheological models used to describe fracture in concrete are presented.

In **Chapter 3** the composition and properties of the material used in the experiments are described: finely grained concrete, textile reinforcement and different types of short fibres. Moreover, this chapter details the testing methods applied. The different arrangements and test setups of experiments at the macro-, meso-, and micro-level of observation are explained.

Chapter 4 presents the results obtained from the aforementioned materials and methods. First, the findings of experiments at the macro-level of observation by means of uniaxial tensile tests performed on composite materials are described in detail, discussed, and compared to each other. Based on this discussion, the need for further investigation at the meso- and micro-levels of observation is presented. Following that, the results obtained from multifilament-yarn and single-fibre pullout tests are presented and discussed.

In **Chapter 5**, the rheological-statistical model of fibre fracture, fibre pullout, and the steps followed in accomplishing this is derived. Furthermore, a statistical study of fibre distribution and fibre orientation on fracture surfaces is described. Next, the mathematical formula for description of tensile behaviour of TRC with the addition of short fibres are derived based on a multi-scale modelling approach. For this, the rheological model developed is used to describe the material behaviour in the micro-scale. Single-fibre pullout tests serve here as reference. Subsequently, the material behaviour at the meso- and macro-levels of observation is modelled under use of appropriate statistical functions and compared with the experimental results.

Chapter 6 summarizes the main findings with an eye to understanding the mechanisms of interaction between continuous fibres and short fibre in cement based composites. Some suggestions for possible upcoming investigation are provided as well.

2 Literature review

2.1 Introduction

This chapter is a survey of the recent knowledge on textile-reinforced concrete (TRC) and fibre-reinforced concrete (FRC) relevant to the scope of this investigation. First, general information regarding TRC components, its characteristic behaviour under tensile loading, a brief overview of the roving-matrix bond, and failure modes are presented. Subsequently, information concerning the mechanical properties of FRC with a special focus on the influence of fibre orientation and distribution is discussed. Finally, some rheological models used to describe fracture in concrete are presented.

2.2 Textile-reinforced concrete

2.2.1 Introduction

Textile-reinforced concrete is a composite construction material consisting of a finely grained, cement-based concrete matrix and high-performance, continuous multifilament-yarns made of alkali-resistant (AR) glass, carbon or polymer fibres.

2.2.2 Fine-grained cement-based concrete

2.2.2.1 Structure of concrete

Concrete in its simplest form is a mixture of cement, water and aggregates. However, improvement of fresh and hardened concrete properties can be achieved by using additives such as fly ash and silica fume or chemical admixtures, as an example plasticizers. In order to investigate the fracture process, crack formation and fracture mechanisms in composite materials such as concrete, it is essential to distinguish among the different levels of observation. On the macro-level of observation concrete seems a homogeneous material (Figure 2.1c). Accordingly, specific fracture behaviour observed on this scale can only be explained by considering the characteristic material structure and processes on the more detailed meso- and micro-levels. On the meso-level concrete is assumed to be a three-phase system, cement paste and aggregates as well as an interface zone (Figure 2.1b). However, each single component has an extremely complex structure and a high degree of heterogeneity on the micro-level of observation (Figure 2.1a). These three levels of material observation have been defined in detail by many researchers; see for example Wittmann [13]. It is important to note that concrete always contains air voids. They can be considered as an additional phase with zero-strength and zero-weight; see Snyder and Clifton [14].

Dealing with the properties of concrete components at the micro-level is meaningful only with a sufficient understanding of the hydration process. The hydration process of cement starts directly after the addition of water by the formation of calcium hydroxide ($Ca(OH)_2$), with a gel film building up on the cement grains' surfaces. As a result of the hydration of calcium silicates, solid crystallites (calcium silicate hydrate – C-S-H phases) are formed. This leads to a gradual

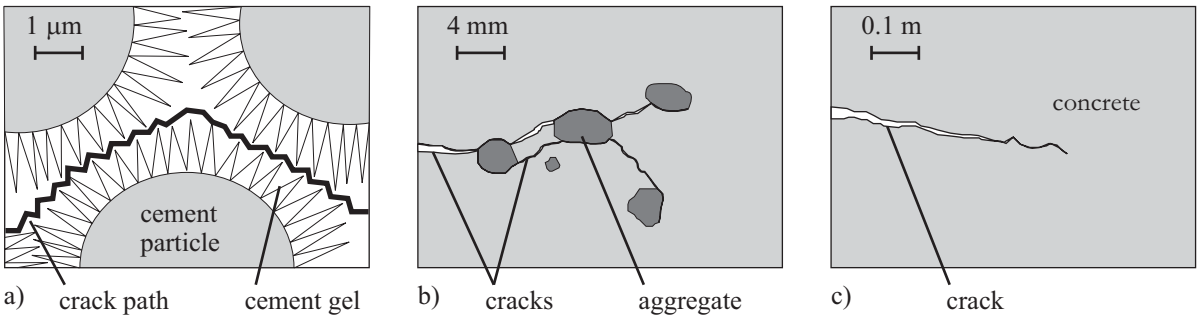

Figure 2.1: View of concrete on a) micro-, b) meso-, c) macro-level, adapted from Mechtcherine [15]

hardening of the cement paste. In the progress of hydration, existing crystallites grow further and new crystallites develop. To a great extent C-S-H phases are responsible for the development of the concrete's strength. Hydration is greatly influenced by a number of parameters: water-to-cement ratio, type of cement, clinker components, pozzolanic additives such as fly ash and micro-silica, admixtures such as superplasticizer, accelerator, retarder, and, of course, temperature. More detailed descriptions of hydration processes and structure of cement paste can be found in Stark and Wicht [16] and Plank et al. [17]. Basically, the main aspect influencing the concrete micro- and meso-structure is the matrix composition.

2.2.2.2 Matrix composition

The binder system used as a matrix for TRC has to be designed to meet special requirements regarding production processes, mechanical performance of the composite, and durability of textile reinforcements. The maximum aggregate diameter is limited by both the distance between reinforcement textile layers to each other or to the outer surface of the element and the mesh size of the textile reinforcement. In order to achieve good workability and penetration between matrix and textile layers, the maximum aggregate size should not exceed 1/5 of the mesh size. In most cases a maximum grain size under 2 mm is used, see Brameshuber [1], Brockmann [18] and Butler [19]. The special features of textile reinforcement impose their particular characteristics on the concrete used. One essential requirement of the matrix composition for the use in TRC is to ensure all-round envelopment and the partial, effectual penetration into the multifilament-yarn, which ensures adequate bonding between reinforcement and surrounding matrix and, thus, good mechanical behaviour of the composite. A sufficiently fluid consistency of the matrix is also required. With all this in mind, high binder contents, pozzolanic additives, and plasticizers are utilized. It was found that matrices with a high content of ground, granulated blast furnace slag in the cement (CEM III), and added pozzolans, fly ash, and micro-silica yielded favourable mechanical behaviour properties, i.e., for bonding between the filaments and the cementitious matrix as well as for the durability of the glass fibre reinforcement; see, for example, Majumdar and Laws [20], Butler et al. [21] and Mechtcherine [22]. Langlois et al. [23] obtained good results by using a matrix based on CEM III (approximately 25 % cement cilker and approximately 75 % blast furnace slag) in respect of bond behaviour and durability of continuous glass yarns. Alkali-resistant (AR) glass shows only limited stability in a high-alkaline environment. Pronounced improvement in durability can be achieved by reducing the ordinary portland cement clinker content and using pozzolanic additives like fly ash and silica fume. More details regarding the investigations in this field can be found in Butler [19], Schorn et al. [24, 25] and Orlowsky [26] for TRC and Majumdar and Laws [20] for fibre reinforced concrete.

Moreover, the influence of water-to-binder ratio on the bond properties is of crucial importance and has been investigated by many researchers. For example, Katz et al. [27] investigated the interface properties of carbon fibre in cement matrices and found that reducing the w/b from 0.5 to 0.35 led to a greater bonding value by factor of 2. Furthermore, previous research showed that with lower w/b the porosity around the fibre decreased, thus yielding better fibre-matrix bonds; for example, see Rieger [28] and [29]. Rieger performed his investigation by means of single-fibre pullout tests of steel fine-wire with a diameter of 50 μm.

2.2.2.3 Fresh concrete properties

The consistency of fresh concrete is determined by flow testing according to the German Standard for Mortars [DIN 18555-2]. Slump flow tests with a small cone are used to evaluate the workability of the mixture. More details concerning the testing procedures and typical results are described in Brockmann [18] and Brameshuber and Brockmann [30]. In such "binder-rich" concretes, as mentioned in Section 2.2.2.2, a suitable consistency with regard to the various production processes of TRC elements is achievable. In [1] some fresh concrete properties as air content, density, flow and flow time of different binder systems are presented.

2.2.3 Textile reinforcement

A furnace containing nozzles through which the fibre is to be formed is used to produce fibres by drawing the melted glass; see Figure 2.2. This manufacturing process is called nozzle drawing.

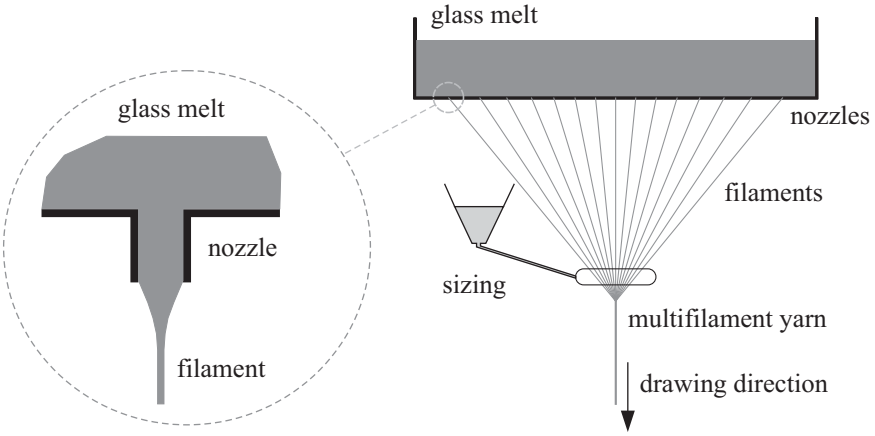

Figure 2.2: Schematic representation of the pulling of glass filaments from a melt using the nozzle drawing process [19]

The diameter of the glass filament is determined by the speed at which the filament is drawn from the glass melt. Typically, the diameter of a glass filament is 5 to 30 μm. The rate of drawing is between 25 and 150 m/s [31]. Immediately after drawing, the filaments are rapidly cooled and the surface is coated with sizing, cf. Figure 2.3 (left). Finally, individual filaments are grouped together into a multifilament-yarn, which is defined as a bundle of several hundreds, up to thousands, of single filaments, cf. Figure 2.3 (middle). The fineness of the multifilament-yarn is indicated in tex (mass in g of 1 km yarn; tex = g/km). The multifilament-yarn is then impregnated in order to improve the properties of the yarn by the pronounced enhancement of the adhesive capacity among the filaments and thus improve load-bearing performance.

Continuous, multifilament-yarns are manufactured together, taking into account many criteria regarding their use in the textile reinforcement of concrete Figure 2.3. The most often used types of fabrics are bi- or multi-axial warp knits due to the outstanding flexibility of their various properties and their suitability for many applications. More details concerning the fabrication of textile reinforcements are summarized in Gries et al. [32].

Figure 2.3: Textile reinforcement fabrication: AR-glass filament with sizing (left), multifilament-yarn (middle) and an example of bi-axial AR-glass textile fabric (right)

2.2.4 Production technologies

The main feature of each production process of TRC is the respective manner of bringing together the fine-grained matrix and the textile reinforcement layers. One of the simplest and most commonly used methods is a lamination technique both for new elements and the strengthening/repair of elements already in use. This method is also used to produce the TRC specimens for the investigation presented in this dissertation.

In preparing and in assisting with demoulding of the element after hardening, a release agent, i.e., release film, is applied to the mould surface. The laminating process begins then with the even spreading of a thin concrete layer on the bottom of the mould. The first sheet of textile reinforcement is laid on this fresh concrete layer and then, gently, partially pressed in and smoothed. The complete embedding of the first textile layer takes place during the application of the second concrete layer. The thicknesses of the concrete layers depend on the desired number of textile layers. These production steps are repeated until all reinforcing layers are placed and incorporated into the finely grained concrete.

Details concerning other production techniques such as extrusion technologies, quasi-continuous production and technology of prestressed TRC, depending on mixture design, size of structure, and planned application are presented in Mott et al. [33].

2.2.5 Characteristic behaviour

Similar to every composite material, the bonding properties among the material's components are of crucial importance to the mechanical performance of TRC. The stress-strain behaviour of textile-reinforced concrete under tensile loading is described in this section. The behaviour of TRC under tensile loading, as shown in Figure 2.4 and can be subdivided into three states: I, crack-free; IIa, crack formation; and IIb, stabilized crack pattern. Because of the brittle failure of the reinforcement under tension, no softening branch is to be observed.

In the following an overview of the special features of TRC behaviour under tensile loading is given based on the findings of Jesse [4].

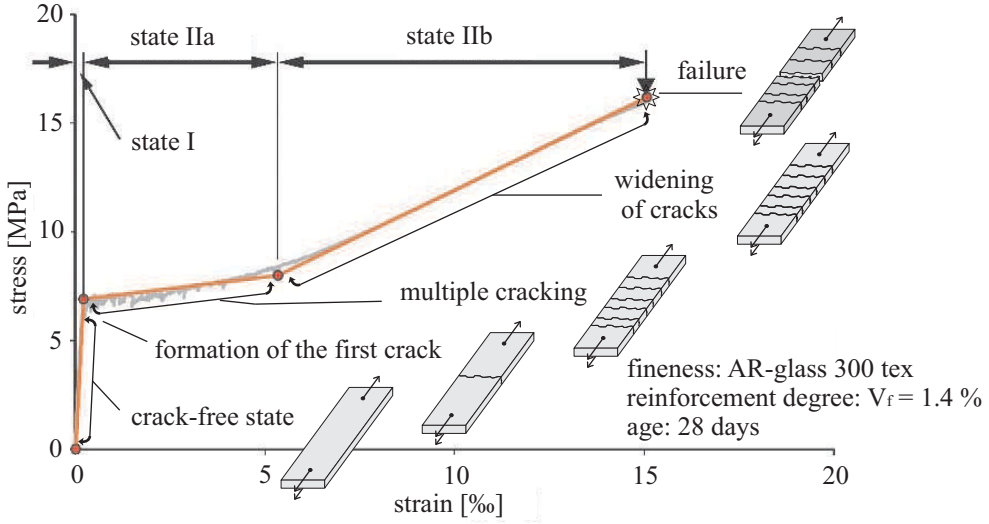

Figure 2.4: Stress-strain response of textile-reinforced concrete under tensile loading; result of a TRC specimen from Jesse [4]

The first state (I) is the **crack-free state**; the stiffness of both matrix and fibres determines the slope of this part of the curve. While Young's modulus of the fine concrete dominates to a great extent Young's modulus of the composite, a noticeable increase is recorded depending on fibre stiffness and fibre volume fraction. However, a significant reduction in composite stiffness from yarns not aligned to the direction of loading, i.e., transverse thread, should be considered. Richter [34] provided a suitable approach in analysing this effect and showed that modulus reduction depends on fibre volume fraction and fibre alignment.

TRC shows nearly linear-elastic behaviour up to the point at which the increase in stress leads to the formation of the first macro-crack and the entire load transferred across the crack is carried by the reinforcement. First-crack stress depends mainly on the tensile strength of the matrix and the degree of reinforcement. An increase in the degree of reinforcement leads to an increase in first-crack stress; however, this increase is moderate because of the limited micro-crack bridging ability of relatively thick multifilament-yarns. First-crack stress is usually defined as the first "jump" in the measured curve associated with the formation of the first macro-crack.

The second state (IIa) is the **state of crack formation**, leading to pronounced quasi-ductile behaviour in the composite. Due to the bonding between the filaments and the surrounding concrete, forces are transmitted to both sides of the first macro-crack and the tensile strength of the next weak cross-section is reached, i.e., the second macro-crack is formed. In this state more and more relatively fine cracks form gradually due to the increase in the tensile stress applied. The length and smoothness of this portion of the curve depend on the quality of the bond between textile and matrix; see Hartig et al. [35]. They depend as well on the volume proportion of fibres in the composite activated for load transfer. Indeed the appearance of this part of the stress-strain curves can be related to the number of cracks and the crack widths. It is worth noting here that transverse multifilament-yarns can almost be considered as defects at the corresponding cross-section and, through, they influence the crack pattern strongly.

The final state is the **crack widening state** (IIb). Here either no new cracks or only a few appear, but the existing cracks become wider until the tensile strength, actually the so-called apparent strength, of the multifilament yarns of the textile reinforcement is reached and the composite

fails. Here the slope of the corresponding section of the stress-strain curve depends primarily on the stiffness of the fibre material, the bond quality between matrix and multifilament-yarns, and on the volume fraction of activated fibres in the textile. More details concerning the factors determining the material's stiffness in this region are discussed by Weiland [36]. A combination of these factors is relevant to the experimental results. Actually, the stiffness of the composite in this state is lower than Young's modulus for the textile reinforcement. This can be traced back to the reduction in fibre volume content resulted from the damage in reinforcement in the previous two states already before the beginning of the this state. Ohno and Hannant [37] developed a mechanical model which took into account the reduction in the fibre volume fraction in order to describe behaviour after multiple cracking and applied it to continuous, polypropylene-fibrillated fibres.

The failure of the composite is seen to be brittle. The material fails in that the multifilament-yarns break at one of the cracks. It should be mentioned that the composite tensile strength is less than the tensile strength of the multifilament-yarns of the textile reinforcement, tested separately. This has been shown by many researchers; see for example Jesse and Curbach [38]. The reason for this is based on the failure of outer filaments from multifilament-yarns and the resulting smaller size of the stressed cross-section.

The sequence of the three states as described above can be observed by monitoring the crack formation on the specimen's surface, even with the naked eye, during testing under tensile load.

As indicated in this sub-chapter, fundamental information on the force transmission between the concrete matrix and the multifilament-yarns is necessary in order to understand and improve the specific load-carrying behaviour of TRC. The details of the bond and failure mechanisms are presented in the next sub-chapter.

2.2.6 Failure mechanisms and yarn-matrix bond

2.2.6.1 Failure mechanisms

The failure of textile-reinforced concrete is actually a combination of the different failure phenomena of the individual components of the composite; see Figures 2.5 and 2.6. The most important failure mechanisms, according to Zastrau et al. [39], are:

- development of micro-cracks in the concrete matrix between the reinforcement layers
- development of micro-cracks in the vicinity of the yarn
- de-bonding and slip of fibre from the surrounding matrix
- slippage between filaments in a yarn
- fibre fracture
- delamination of textile reinforcement layer from matrix.

A sufficient degree of reinforcement leads to the formation of multiple macro-cracks, a result of the development and merging of micro-cracks. After the formation of the last macro-crack and the development of the final crack pattern, the residual stiffness depends on the stiffness of the fibre and is influenced to a great extent by the bond properties between multifilament-yarn and matrix. Actually, the bond behaviour among the components, which is based on the stress transfer due to adhesion and friction, is one of the most essential criteria in determining

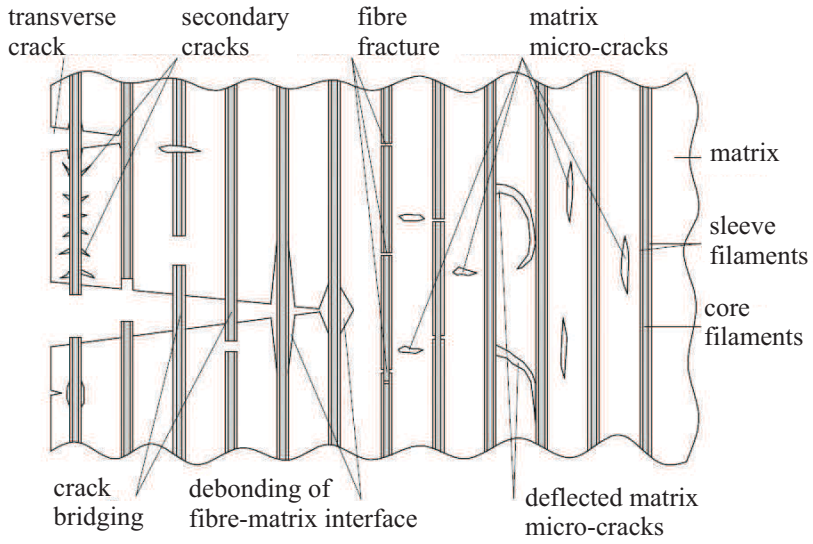

Figure 2.5: Compilation of different failure mechanisms in textile-reinforced concrete; according to Zastrau et al. [39]

composite behaviour. Many factors influence the failure of the bond between reinforcement and matrix: surface structure of the reinforcement, e. g., Lorenz et al. [40]; type of applied load, e. g., Silva et al. [5] and Möller et al. [41] for dynamic loading and Kang [42] for cyclic loading; environmental conditions in Orlowsky and Raupach [43]; geometry of specimen in Chudoba [44]; and test setup in Hartig et al. [45]. This wide range of factors complicates the comparison of the interface investigations performed by the researchers.

In this work the influence of water-to-binder ratio as well as the effect of the addition of different types short fibres on the bond and failure mechanism of textile-reinforced concrete subjected to tensile loading is investigated in depth. Special attention has been paid to clarify the fracture criteria, and deep microscopic investigations were performed in order to understand the bases of the various fracture mechanisms observed in the tests carried out in the framework of this dissertation.

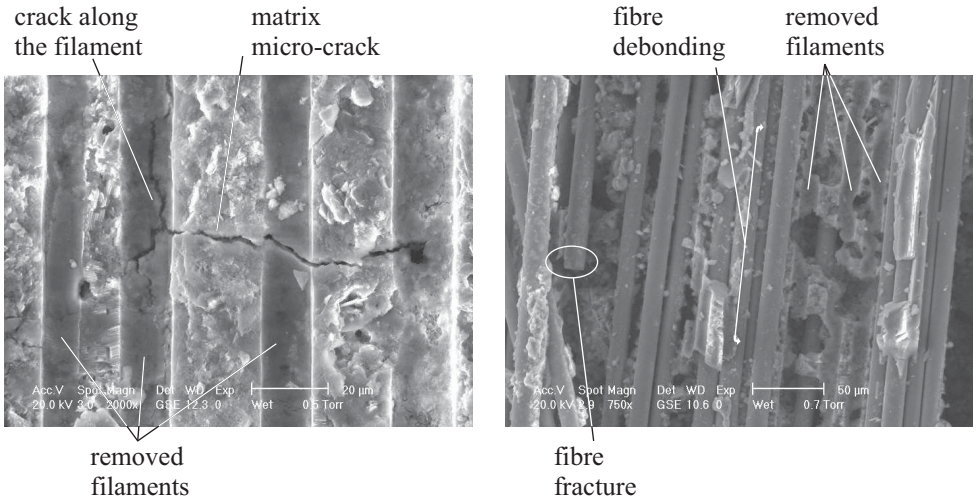

Figure 2.6: ESEM images of different failure mechanisms in textile-reinforced concrete

2.2.6.2 Bond mechanisms and pullout models

The bonding behaviour of textile reinforcement with the surrounding cement-based matrix is complex, since the intensity of bonding may vary considerably over the cross-sections of the multifilament-yarns. Filaments in the yarn can be subdivided into (a) sleeve filaments, i.e., outer filaments connected directly to concrete, which leads to better bond performance than that of the (b) core filaments, i.e., inner filaments, which have no direct connection to the matrix and only the friction between the filaments ensures the transmission of force. However, the bond between outer and inner filaments as well as the quality of yarn cross-section can be improved by impregnation, as presented in Figure 2.7. The degree of impregnation is set as a mass proportion of the yarn material in such a manner as to ensure a uniform distribution over the entire cross-section of the multifilament-yarn. The textile reinforcement used in this investigation is made of polymer-impregnated AR glass; see Section 3.1.2. Details concerning the different surface modifications and interface properties are discussed by Scheffler et al. [46, 47].

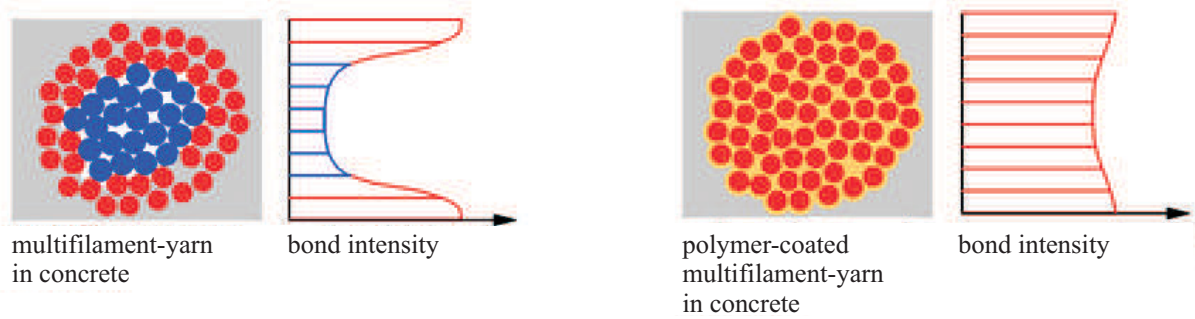

Figure 2.7: Schematic representation of improvement in bond quality of multifilament-yarn by impregnation, adapted from Lepenies [48]

As a result of this special feature, the idealisation of cross-sections of the multifilament-yarn due to the differentiated bond behaviour was necessary. Different models for idealising the yarn were discussed by Zastrau et al. [49] and Lepenies [48]. For the multifilament-yarns and short integral glass fibres used in this investigation, the cross-section is considered to consist of two groups of filaments: inner filaments (without) and outer filaments with direct contact to the matrix. This feature is used to explain the behaviour of multifilament-yarns in pullout tests and single-fibre pullout tests performed on short integral glass fibres in the framework of this dissertation; see Section 4.4.2.

Various models have been developed in order to simulate the bond behaviour of multifilament-yarns in cementitious matrices based on multifilament-yarn pullout tests and microscopic investigations.

Microscopic investigations of embedded, multifilament-yarns showed that the distribution of the hydration products responsible for the bond between filament and filament and/or filament and matrix is non-uniform; see Figure 2.8. Based on this observation Schorn [50] proposed the "adhesive cross linkage model". Using this model he showed that all filaments, depending on their location in the cross-section, are bonded to each other by a pattern of adhesive cross-links. The piece of filament between two cross-links and the bridge over a crack can be deformed along the available deformation length L_0. In Figure 2.8 different types of bonding between filament and matrix and, therefore, different available deformation lengths are presented according to Butler et al. [51]. Due to the shear stiffness of the cross-links, a so-called effective length L_w is defined.

The effective length can be greater than or equal to the deformation length *L0* depending on the stiffness of the cross-links. On the other hand, since the distances between the filaments are tiny, the penetration of the hydrated cement particles into the core of the multifilament-yarn will be limited. It can be assumed, therefore, that the number of cross-links decreases towards the inner part of the yarn. After concrete cracking the stress is redistributed among the crack-bridging filaments: the filaments with the smallest effective length will receive the greatest stress. Subsequently, because of the opening of the crack the strain capacity of these filaments is reached and they fail, the stress being redistributed again among the remaining filaments still intact. Further increases in crack width lead to successive failures in the filaments.

It should be mentioned here that this model is developed for non-impregnated multifilament-yarns where the hydration products can penetrate into the yarn's cross-section. For impregnated multifilament-yarns the hydration products are located only on the yarn's surface. However, the non-uniform distribution of these cross-links on the yarn and fibre surface holds true and can be used to describe the bond to the surrounding matrix.

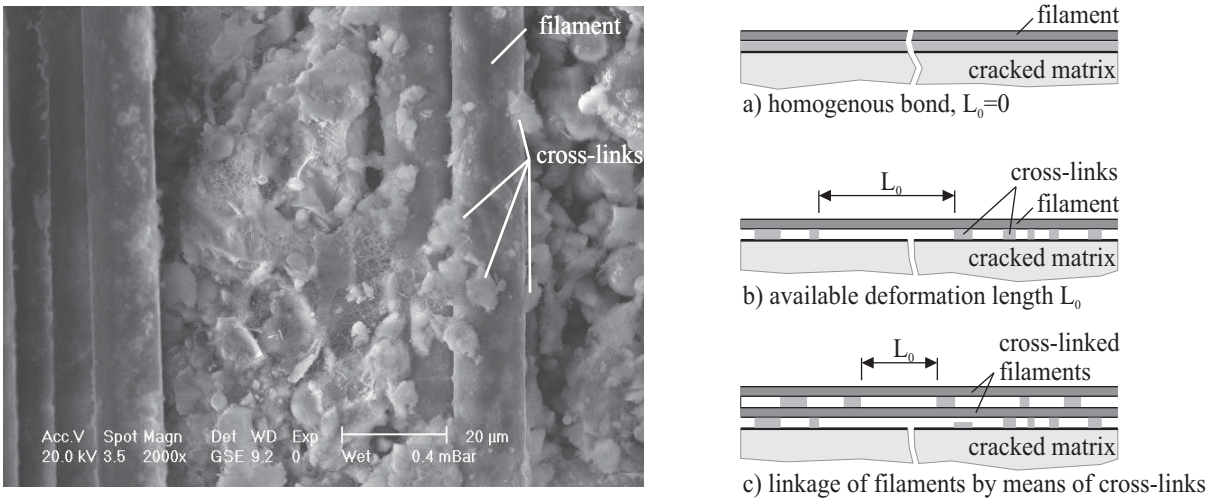

Figure 2.8: ESEM image of AR glass filaments in cementitious matrix (left) and different types of bonding due to different positions of cross-links based on "adhesive cross linkage model" (right) [51]

In order to model the adhesive cross-links Lepenies et al. [52] idealised the random distribution of the cross-links by "... lumping them together into a continuous plug, leaving a free length without any bond..." as shown in Figure 2.9. Lepenies introduced this idea in combination with the gradual failure of filaments according to their effective length into his Micro-Meso-Macro model and developed it further so that he could, based on yarn pullout-testing, identify the bond parameters and predict the behaviour of TRC.

Banholzer [53, 54] presented alternative assumptions in order to describe the pullout behaviour of yarn embedded in a fine-grained matrix by means of one-sided pullout tests. He idealised the multifilament-yarn as a layered system made of m layers, each with a given number of filaments as shown in Figure 2.10 (left). The active filaments-versus-displacement relationship was matched by using a step function corresponding to the number of layers. The number of steps used corresponded to the number of layers assumed in the idealisation. The width of each step referred to the displacement range in which the filaments of each layer fail; see Figure 2.10 (middle). Using the cross-links model proposed by Schorn [50], and by assuming that the

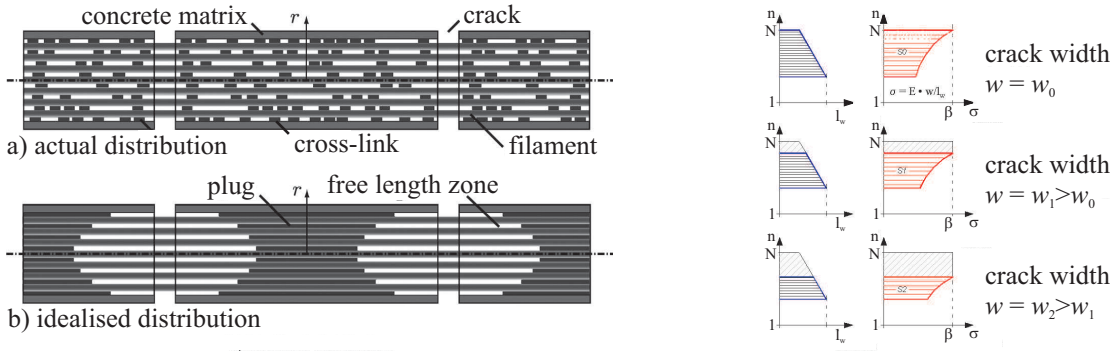

Figure 2.9: Plug model according to [52] (left) and effective length of filaments of a yarn and the corresponding stress distribution with increasing crack width (right) [50]

corresponding displacement consists of both slip of the filament (ω) and elongation over the filament's free length (Δ) (see Equation 2.1) Banholzer [54] confirmed the validation of his model by comparison of the experimental results obtained from one-side yarn pullout tests with the simulated responses of two different yarns' idealisation: 5 layers and 100 layers, as shown in Figure 2.10 (right).

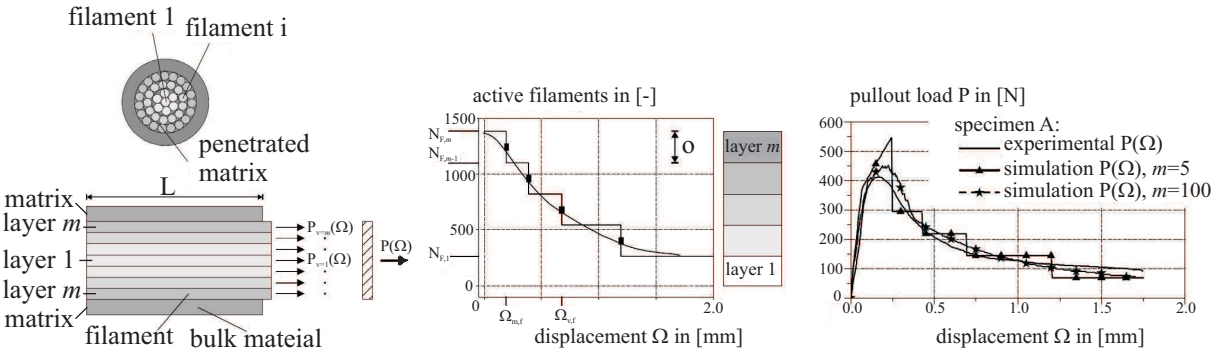

Figure 2.10: Idealisation of a yarn (left), adaption of active filaments-displacement relation (middle) and pullout responses of multifilament-yarn; experimental results and simulation (right) [54]

$$P(\Omega) = \sum_{v=1}^{m} p_v(\Omega = \omega + \Delta) \equiv \sum_{v=1}^{m} P_v(\omega) \cdot o, \qquad \Delta = \frac{P_v(\omega)}{E_F A_F} \frac{(\Omega_{v,f} - \omega_{v,f}) \cdot E_F}{f_v, t} \tag{2.1}$$

Where: $p_v(\Omega)$: the pullout response of layer v, $P_v(\omega)$: the pullout response of single filament, o: number of filaments per layer, m: number of layers, E_F: Young's modulus of the filament and A_F: the cross-sectional area of the filament.

Soranakom and Mobasher [55] proposed another approach based on the nonlinear finite difference method. They demonstrated and evaluated three main constituents of fabric pullout response by a nonlinear interface bond model of the pre- and post-peak response as a function of slip (Figure 2.11a), a typical stress-strain model of a longitudinal warp yarns beginning with a slack (Figure 2.11b) and, finally, mechanical anchorage at the junction points provided by transverse yarn simulated by nonlinear springs (Figure 2.11c). Analysis of the load transfer mechanisms between yarn and matrix with and without nonlinear springs by using "nodal

equilibrium equations" was performed. Parametric studies showed that the pullout strength increases due to the increase in the interface's bond strength. Moreover, a pronounced increase in pullout resistance was recorded due to the mechanical anchorage by the bonded transverse yarns. However, the presence of slack in longitudinal yarn led to a weaker pullout. The simulation also showed that the first phase of pullout resistance was contributed by the bond and by transverse "springs". A drop in stress because of junction failure, similar to experimental measurements, was presented. The second phase, occurring after the sequential failure of the springs, was due exclusively to the bond, as shown in Figure 2.11. However, this approach deals with the bonding properties and de-bonding processes only on one side of the crack and can be considered as a one-side pullout test.

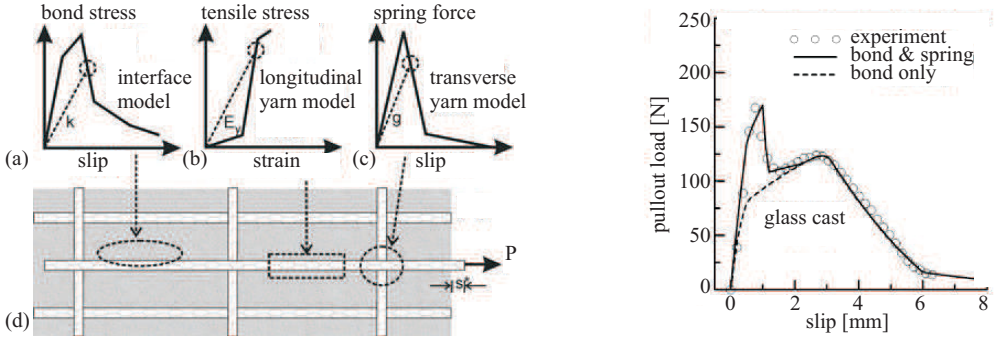

Figure 2.11: Yarn pullout mechanisms: a) interface bond, b) longitudinal yarn, c) spring simulation and d) textile pullout specimen (left), and pullout response of AR glass yarn using shear interface bond model and bond and junction model (right) [55]

It should be mentioned here that the one-side yarn pullout tests give an insufficient description of the behaviour under investigation. This is due to the inaccuracy arising out of the assumption that the pullout displacement is equivalent to a half of the crack width. In reality the de-bonding and pullout of the multifilament-yarn may occur partially and, in most cases, from both sides of the crack.

Lorenz and Ortlepp [56] developed further the setup of pullout test designed by Krueger et al. [57]. In this test setup the multifilament-yarn is anchored in the fine-grained concrete from both sides of the saw cut, i.e., the crack, cf. Figure 2.12 (left). However, due to the asymmetrical anchoring lengths the pullout takes place from only one side of the crack. Lorenz derived the bond stress versus slip relation (BSR) based on the force-versus-crack-opening relationship obtained from the experimental investigation; see Figure 2.12 (right). These findings can be used to calculate the end anchor length and the overlap length in textile-reinforced concrete.

In this work the test setup developed by Lorenz and Ortlepp [56] was chosen for multifilament-yarn pullout tests. Aside from simple specimen production and test execution, in this setup yarn pullout is secured by choosing a short embedding length on one side of the "crack". On the opposite side the anchoring of the yarn in the fine-grained concrete matrix proves to be best suited to reality and as precise as possible in determining the bonding properties of textile reinforcement in the fine-grained matrix. Moreover, the measured force-crack-opening-relationship can provide sufficient information to figure out the different influences of water-to-binder ratio as well as short fibres on the yarn-matrix bond properties, see Section 4.2.2 and Section 4.3.1.

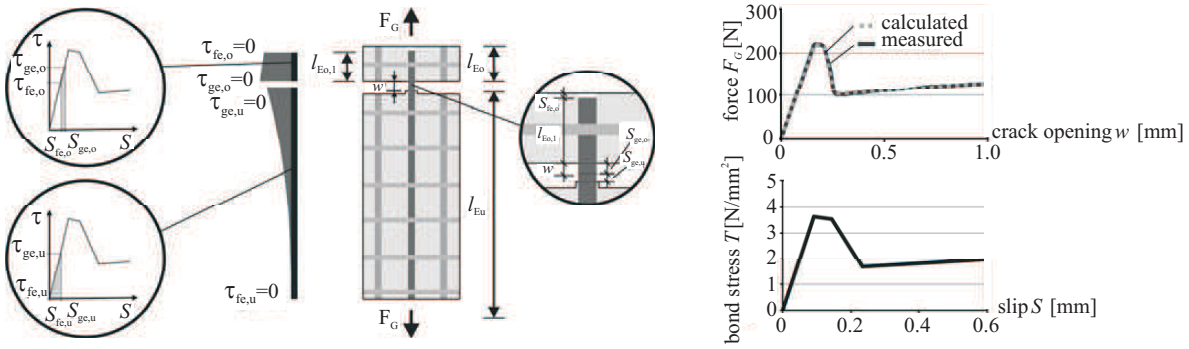

Figure 2.12: Distribution of bond stresses via the anchor length with representation of the activated areas of BSR (left), and measured and analytical force versus crack opening relation and the corresponding determined BSR (right) [56]

2.3 Concrete with short fibres

2.3.1 Effect of short fibres on fresh concrete properties

The addition of short fibres leads to a considerable reduction of workability, which is unfavourable in most cases, especially for practical applications. Researchers have noticed this effect with different types of short fibres. Soroushian and Bayasi [58] investigated this with three types of steel fibres: crimped, straight, and hooked. They observed that the inclusion of fibres decreased the workability of fresh concrete and that this effect was more pronounced for fibres with higher aspect ratios (length-to-diameter).

Wong [59] investigated the influence of different types of short fibres (steel fibres, polypropylene fibres and fibremesh) on the workability of concrete. The results obtained indicated that the consistency of fresh, fibre-reinforced concrete is influenced by the type of the fibres. While fine fibres reduced the workability considerably (reduction of slump value from 140 mm to 65 mm), based on slump measurments, only a slight reduction was recorded when thicker long-cut steel fibres were used; here a reduction of slump value from 140 mm to 105 mm.

Hinzen and Brameshuber in [60] described the reduction of workability by different types of short fibres. They investigated the effect of five different types of short fibres, i.e., different fibre diameters in five varied volume contents. Slump flow testing was used to determine the consistency of the concrete. Beside the conventional slump flow tests, a sieve test was developed to assess the penetrating ability of fine-grained concretes and to examine the influence of the different short fibre types on penetrating ability. It was found that while a steady decrease in workability with increasing fibre content is recorded, the fine-grained concrete spread is influenced to different degrees by the various fibre types.

2.3.2 Advantages of short fibres in hardened concrete

The cracking process in plain concrete under tensile loading can be divided into three stages. Initiation and development of micro-cracking over the whole volume of the material summarizes the first stage. In the second stage, the micro-cracks tend to concentrate in the weakest area and form a so-called “crack band” or “process zone”. The third stage corresponds to the formation of a macro-crack, when the tensile strength of the concrete is reached. In reaching this stage, the concrete fails in quasi-brittle fashion; i.e., a rapid softening of the concrete occurs if the test is performed in deformation-controlled regime, evidenced by a steep slope of the stress-deformation

curve. However, the stress transfer after material failure is, depending on test setup, specimen geometry, and material components, measurable and can be traced back mainly to crack bridging (Van Mier [61]) and interlocking (Duda [62]). The fracture process and the mechanics of the concrete has been investigated in detail by many researchers; see, for example Mechtcherine [15].

Discontinuous, randomly distributed fibres are added to concrete in order to mitigate the above-mentioned brittleness and in some instances to increase the tensile strength and strain capacity of the concrete. Concrete with short fibres fails completely only after the fibres break or are pulled out of the matrix. Whether the first or the second failure mechanism prevails depends upon a number of factors such as the fibres' tensile strength, their strain capacity, tensile strength of the matrix, the fibre bonding to the surrounding matrix, and others. The quality of the bond depends in turn on the fibre aspect ratio, fibre surface characteristics, and matrix properties.

There is a wide range of fibres which can be used to improve the mechanical properties of cementitious composites. Beside steel fibres, which have been the most common types of fibre used in concrete for some considerable time, glass, natural and synthetic fibres like polyethylene (PE), polypropylene (PP), polyvinyl alcohol (PVA), polyamides (PA), aramid, and carbon are becoming more attractive. The influence of fibres on the properties of concrete varies widely depending on the very different mechanical and geometrical properties of the fibres themselves. Incorporating fibres into the cement-based matrix has been found to improve several of its properties: toughness, ductility, tensile strength as well as impact and fatigue resistance; see, for example, Bentur and Midness [63], Jun and Stang [64], Mechtcherine et al. [65]. Although the usage of short carbon fibres in concrete is still rare, some research work on carbon-fibre-reinforced concrete has been conducted with regard to the fibre-matrix interface and the improvement of this type of fibre on some concrete properties, primarily cracking resistance and toughness. Moreover, investigations into flexural fatigue behaviour and the endurance limits of concretes reinforced with carbon fibres have been carried out; see for example, Suzuki et al. [66], Banthia and Sheng [67, 68], Sakai et al. [69] and Deng [70]. More information concerning definitions, properties, and parameters related to fibre-reinforced concrete and to its applications can be found, for example, in the state-of-the-art report on fibre-reinforced concrete prepared by ACI [71].

Short, fine, well distributed fibres bridge and arrest micro-cracks and, thus, limit their development. Therefore, the merging of micro-cracks is delayed by the presence of short fibres, and higher loads are needed to open and propagate these cracks. Said differently, the tensile strength of the composite can be improved. Short fibres can bridge macro-cracks as well. This leads to prevention of the brittle failure of concrete, i.e., enhancement of ductility, and in some cases even to strain-hardening behaviour depending on fibre type, fibre length, and fibre volume fraction. Rossi et al. [72] showed the mechanical action of short fibres in respect of micro- and macro-cracks. Barros et al. [73] performed a series of tests on both plain mortar and glass-fibre-reinforced concrete and clearly illustrated that the addition of short fibres leads to an increase in energy absorption capacity, tensile strength, and improvement in deformation capacity. They concluded that fibre orientation, which depends mainly on the mixing and production methods, has a pronounced influence on the tensile strength. Furthermore, the mechanism of pullout of the fibres bridging the crack is responsible for the increase in fracture energy in comparison to the plain matrix.

Many approaches have been developed by researchers in their efforts to understand the mechanics of the behaviour of short fibres in concrete or mortar both in the pre- and post-cracking states. Interface mechanics models and of fracture mechanics models were used for the most part. The interface mechanics approaches consider the composite to be a three-phase system depending on fibre properties, concrete properties, and the properties of fibre-matrix interface. Models using fracture mechanics deal with the energy needed for further crack development and fibre de-bonding from the matrix.

2.3.3 Orientation and distribution of fibres

The distribution and orientation of fibres play a very important role in affecting the mechanical properties of composites. In contrast to continuous fibres, where orientation and location are defined according to design requirements, cf. Figure 2.13 (left), the angle of inclination, and the distribution of short fibres can be random within the mixture. This type of discrete reinforcement is added to the mixture during the mixing phase, which leads to a "free" orientation and distribution of the fibres throughout the concrete body, as shown schematically in Figure 2.13 (right). Along with the gentle mixing of fibres further parameters should be considered in order to get a perfect dispersion of added short fibres over the entire volume of concrete and to prevent "hedgehog" formation: aggregate grain-size, fibre aspect ratio, fibre content, water content, etc.

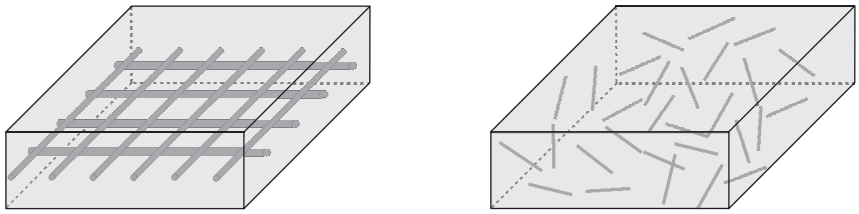

Figure 2.13: Schematic representation of two types of fibre reinforcement: bi-axial continuous fibres (left) and discontinuous randomly distributed fibres (right)

Fibre orientation is a very important issue because it determines the number of fibres bridging a crack, in turn distinctly influencing the mechanical performance of the concrete. The production technique chosen, the dimensions of the members, and the rheological properties of the fresh mix influence to a great extent the orientation of the fibres. In considering these effects, it is common to determine the fibre orientation factor, $\alpha_f \leq 1$ which is defined as the efficiency of fibre bridging; see Krenche [74].

The technique used to produce the element, i.e., the method of concrete placement and the equipment used, can affect the orientation of the fibres considerably. While the simple casting of concrete with fibres in the mold leads more or less to a random orientation of the fibres, the laminating process to be used in this work fosters a more uniform orientation of short fibres in the advantageous load-parallel direction; see Section 3.2.2. Figure 2.14 illustrates schematically the fibre orientation in the case of the lamination process and, for the sake of comparison, the case of 1D orientation, respectively. The fibre orientation factor in case of 1D orientation equals one ($\alpha_f = 1$).

In volumes whose dimensions considerably exceed the length of fibres, the fibre can be considered randomly oriented and the angles of inclination of the fibres range from zero to 90°. Li et al. [75] described 3D random orientation of fibre by presenting a mechanical model with fibres having

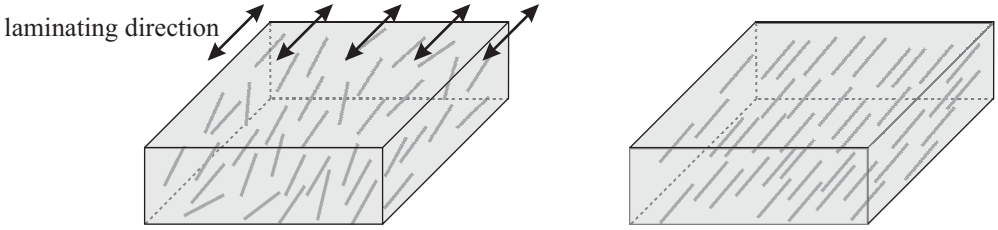

Figure 2.14: Schematic representation of the orientation of discontinuous fibres: due to laminating process (left) and biased 1D fibre orientation (right)

their ends lying on a hemispherical surface. However, the possibility of free orientation of the fibres is restricted by boundaries. The dimensions of the structural element or the thickness of concrete layer, contact with the formwork, and the finish of the exposed surface lead to constrained-random distribution, especially up to a distance equal to fibre length from the surface. Therefore, for elements which are restricted in geometry the fibre orientation varies in regions according to distance to the boundary surface and moving away from 3D and tends to approach 2D conditions, cf. Figure 2.15.

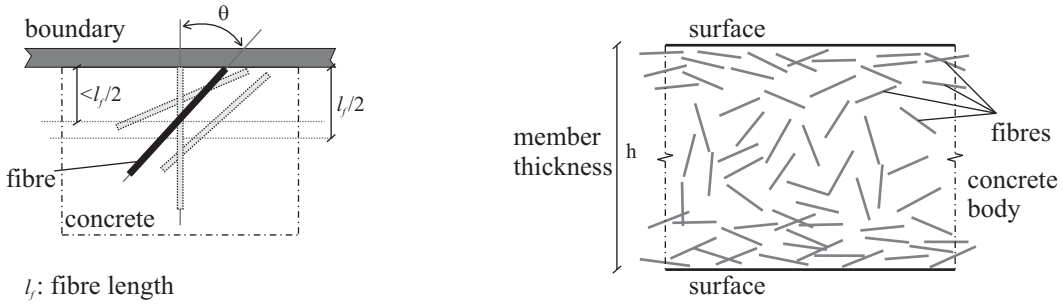

Figure 2.15: Effect of boundary on fibre inclination angle (left) and orientation of fibres along the section of specimen with two boundaries (right), adapted from [76]

Soroushian and Lee [76] showed the effects of boundaries on fibre orientation by comparing the determined fibre orientation factor from the measured number of fibres per unit area of the cracked section in different locations (categorized at top, middle, and bottom of specimen). Fifteen years later, experimental results obtained by Gettu et al. [77] indicated that the fibre orientation factor is variable along the cross-section and decreases gradually from the boundary to the center.

Based on the above-mentioned studies and some relevant previous investigations, for example Aveston and Kelly [78], it was concluded that the fibre orientation factor can be assumed constant ($\alpha_f = 0.5$) at a distance from the boundaries equal to or greater than the fibre length. Moving outward from the center of the element, the factor increases. At the surface, the factor becomes $2/\pi$ ($\alpha_f = 0.64$) because the out-of-plane fibre inclinations are hindered; cf. Figure 2.16 (left). In general, the fibre orientation factor is influenced by member thickness as shown in Figure 2.16 (right). More details and an extensive summary concerning the derivation of fibre orientation factor are presented by Lee et al. [79] and [80]. However, no information on fibre orientation factor in elements produced by laminating process is available in literature.

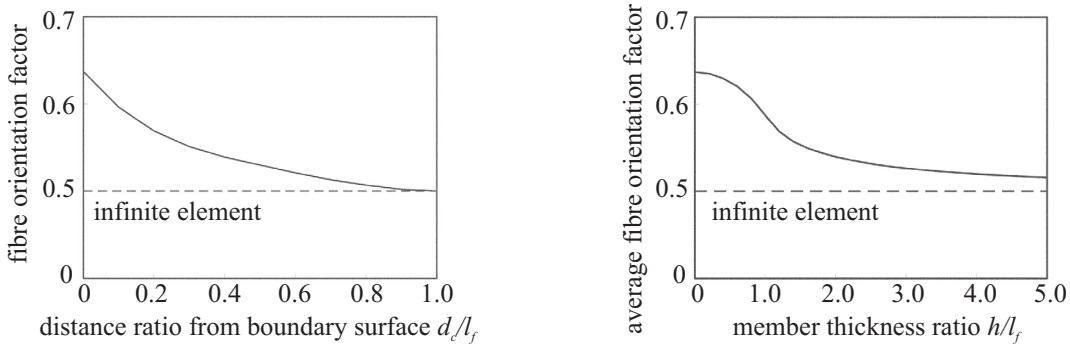

Figure 2.16: Variation of fibre orientation factor according to distance from boundary surface (left) and variation of fibre orientation factor with increasing member thickness (right) [80]; where: d_c: distance from boundary, l_f: fibre length, h: member thickness

.

In this investigation, the influence of the lamination technique used to produce the specimens on fibre orientation is considered. The use of this technique leads to an increase in the number of fibres crossing a crack, i.e., an increase of fibre orientation factor; see Section 5.3.3. The fibre orientation factor should be determined in order to estimate the number of fibres bridging a crack which is necessary to modelling the opening of one single crack; see Section 5.4.3.

2.3.4 Mechanisms of formation and propagation of cracks in fibre-reinforced concrete

Concrete usually exhibits a large number of pores, flaws, and micro-cracks even before subjection to any external load. These are considered to be defects in concrete and influence the mechanical performance of the material to a great extent. Many, if not all, of these "initial" defects emanate from segregation, excess water, restrained shrinkage, and/or thermal dilation. When load is applied, areas of stress concentration develop at the tips of the initial defects. Beside the development of the already existing defects, additional micro-cracks initiate due to increase in loading and align themselves to merge and form a macro-crack.

When fibres are added to cement-based materials, two additional phases should be considered. The first phase is the fibre itself. The second one is the interface transition zone (ITZ), i.e., the bond region between fibre and matrix, which influences significantly the overall mechanical performance of the composite. It has been shown that improving the density of the interface transition zone leads to a better fibre-matrix bond and, hence, a higher pullout load for the fibre; see for example Chang and Li [81]. Rasmussen [82] found that the development in strength of the ITZ is time-dependent and related to the development of C-S-H phases through hydration of cement. This phenomenon must be considered for the specimens used in the thesis at hand. All specimens must have the same curing time and all tests must be performed at the same specimen age; see Section 3.2.3.

Many investigations into the mechanics of fibre in concrete have been performed to understand the actual effects of fibres. Banthia and Sheng [68] showed that a considerable increase in strength, toughness, and stiffness of cement-based composites can be achieved by the addition of fibre reinforcement. Other studies showed that depending on fibre type, i.e., its length, stiffness, diameter, etc., the effect of fibre on mechanical behaviour varies in accordance with the composite status: before material cracking and post-cracking; see example Betterman et al. [83] and

Markovic et al. [84]. From this point, the term "before material cracking" indicates the stage prior to the formation of the first macro-crack.

In order to describe the mechanisms clearly, the action of fibres in cement-based materials is discussed in the following sub-chapters separately in these two stages: before the formation of the first macro-crack or pre-cracking, and after the formation of the first macro-crack or post-cracking.

2.3.4.1 Action of fibres in pre-cracking stage

Before any macro-crack is formed in the material, the load will be carried by both the fibre and the concrete matrix distributed according to their stiffness and volume content. This holds true for the case of a perfect bond between fibre and matrix. Otherwise, the part of load carried by the fibre is transferred from the matrix and depends mainly on the fibre-matrix bond quality. Whether the addition of fibres improves the tensile strength of the material or does not offer a substantial enhancement in strength when compared to the corresponding mixture without fibres has been investigated over many decades. The improvement in composite strength due to the addition of distributed short fibres depends not only on the tensile strain capacity of the matrix, strength and elastic modulus of fibre but also on the volume fraction of fibres, see for example Shah [85]. However, it should always be considered that the addition of short fibres in relatively large volumes could lead to poorer workability; see also Section 2.3.1), and therefore to increased porosity, and, hence, a decrease in strength.

Based on the shear-lag theory originally introduced by Cox [86], the influence of the modulus of elasticity of both fibre and matrix on the shear stress in the interface is analysed and presented by Löfgren [87]. As shown in Figure 2.17 (left), higher shear stresses in the interface are achieved due to high-modulus fibres. Moreover, a higher matrix modulus leads to greater shear stress in the interface and to an earlier fibre activation, i.e., the stress is induced earlier in the fibre; cf. Figure 2.17 (right). Löfgren showed that although this shear-lag model underestimates the very short fibres and neglects the effect of the interface transition zone, it provides valuable information on the influence of some parameters on the transfer of shear stress from matrix to fibre.

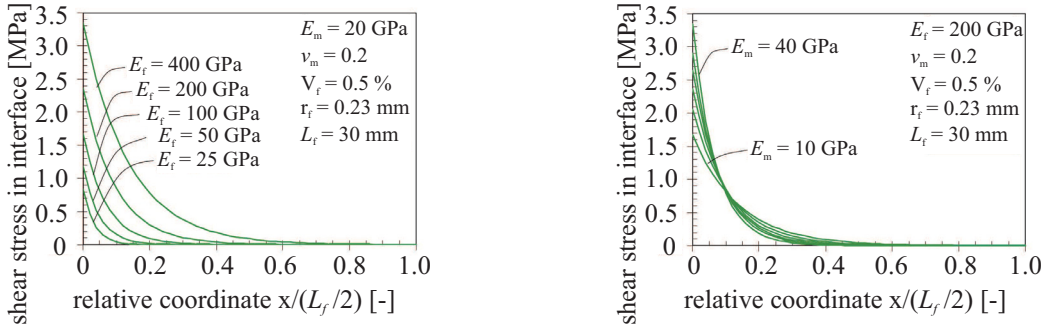

Figure 2.17: Influence of modulus of elasticity of fibre (left) and modulus of elasticity of matrix (right) on shear stress at the interface; where: E_m: matrix modulus, E_f: fibre modulus, L_f: fibre length, v_m: Poisson's ratio of matrix, r_f: radius of the fibre, V_f: fibre volume fraction; according to [87]

Nelson et al. [88] investigated the reinforcing effect of micro-fibres[1] in the frontal process zone ahead of a crack tip since it is there where first-crack strength is determined. The authors compared the fracture toughness of three specimens: a plain cement matrix, a composite characterized by the absence of micro-damage, and a composite with saturated micro-cracking in the frontal process zone. Five stages of composite behaviour were determined as shown in Figure 2.18: linear-elastic behaviour (Zone I); nonlinear deformation (Zone II); stable growth of the failure crack (Zone III); unstable growth of the failure crack (Zone IV); and Zone V, fibre bridging of the crack. They found that the fracture toughness of composite with micro-fibres was greater by 40 % than that of the plain matrix. This was traced back to the micro-fibres' effectively arresting the growth of micro-cracks and thereby delaying the formation of the failure crack.

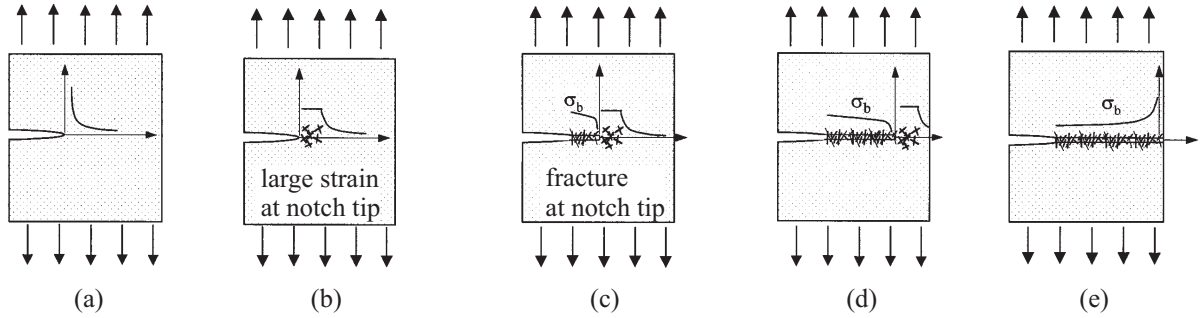

Figure 2.18: Stages of damage in process zone at crack tip: (a) Zone I: linear-elastic behaviour, (b) Zone II: micro-crack formation in frontal process zone, (c) Zone III: stable growth of crack; (d) Zone IV: unstable growth of failure crack, and (e) Zone V: fibre bridging of failure crack; according to Nelson et al. [88]

Lawler et al. [89] examined the effect of micro- and macro-fibres on the fracture process of mortar by monitoring crack development through the use of the Subregion Scanning Computer Vision Technique. While the pre-peak mechanical performance is improved due to the micro-fibres' hindering of the widening of micro-cracks, thus leading to higher strength and delaying the formation of macro-cracks, macro-fibres were effective in the enhancement of post-cracking behaviour. Furthermore, Lawler et al. mentioned that the smaller spacing between the fibres is the determining factor of the significant improvement in tensile strength.

2.3.4.2 Action of fibres in post-cracking stage

Unlike plain concrete, concrete with appropriate fibre reinforcement does not break in a brittle manner after initiation of the first crack crossing the concrete element. Aside from the improvement in the energy absorption shown by the area under the force-deformation curve, deformation capacity is distinctly improved. The tensile behaviour of cement-based composites reinforced with fibres after the formation of the first macro-crack in the matrix may be classified as either the softening or hardening; see Figure 2.19. For the softening regime a localized single crack determines post-cracking behaviour. Once the matrix cracks, the stress starts decreasing. The area under the force-deformation, indeed force-crack opening, curve is the fracture energy. With increasing fibre volume, materials exhibiting strain-hardening behaviour can be developed, characterized by the formation of multiple cracks. In this case, all cracks distributed along the

[1] fibres are deemed micro-fibres when the diameter is less than or equal to 30 μm according to [88] and less than 22 μm according to [89]

specimen contribute to the energy absorption by the composite and, thus, the term "work-to-fracture" is more meaningful than the term "fracture energy", which describes the energy needed for the complete development of just one macro-crack.

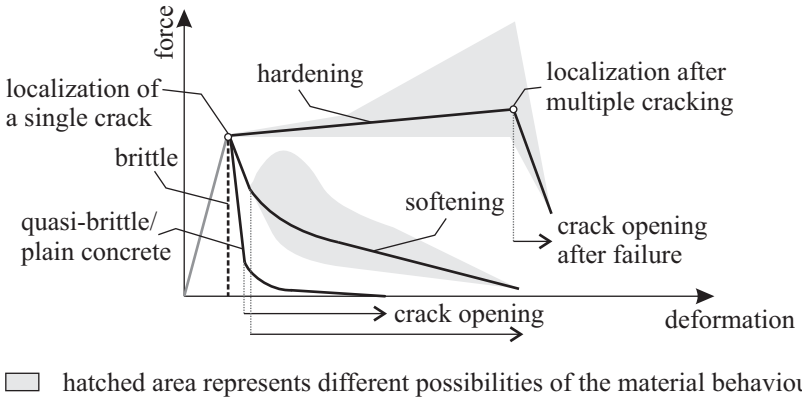

Figure 2.19: Schematic representation of tensile behaviour of cement-based materials: brittle material, plain concrete, composite materials with softening and hardening behaviour

The improvement in the post-cracking behaviour is generally due to crack-bridging. In addition to fibre reinforcements, short fibres, and multifilament-yarns, aggregates bridge cracks as well.

Aggregate bridging

The fracture process in plain concrete under uniaxial tensile load has been investigated by many researchers. In general, it has been shown that by increasing the load, more and more micro-cracks are initiated and developed in the weakened region and a fracture process zone is formed. The fracture process zone can also be defined as a concentration of many micro-cracks in one region. Subsequently, a macro-crack is developed and the softening of concrete starts. The descending branch of the load-deformation curve indicates stress transfer by crack-branching (Van Mier [61]) and friction or interlock of the crack surfaces (Duda [62]), see Figure 2.20. Finally, increasing deformation, i.e., crack opening, leads to complete failure.

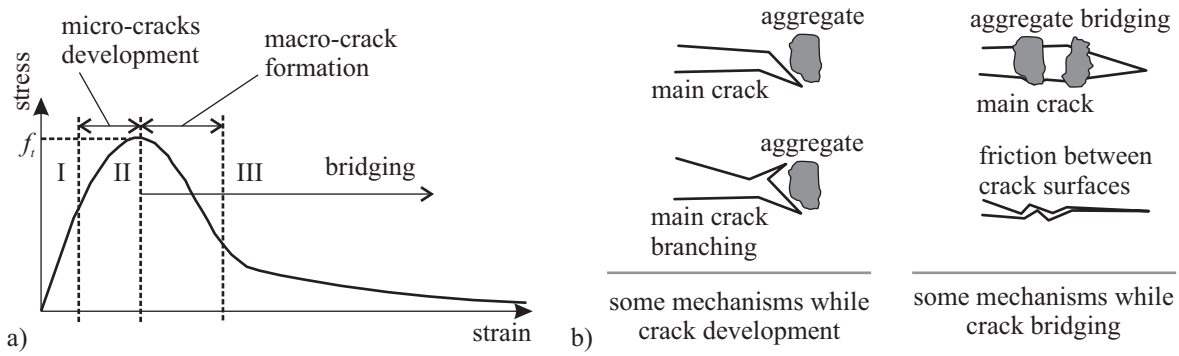

Figure 2.20: a) Sketch of stress-strain relation for plain concrete under tension based on Duda [62]: (I) micro-cracking, (II) merging of micro-crack and formation of fracture process zone (III) opening of macro-crack, and b) some mechanisms of crack propagation in plain concrete, adapted from Shah et al. [90]

Mechtcherine [91] studied the fracture mechanical behaviour of three types of concrete, i.e., high strength concrete, normal strength concrete, and normal strength concrete with higher ag-

gregate content, under tension in a detailed investigation of the fracture surface of the specimens under test. A direct correlation was found between the roughness of the fracture surfaces and the degree of concrete heterogeneity, which was proven crucial to the formation and propagation of cracks in concrete.

As mentioned in Section 2.2.2.2 the concrete used in this investigation is a fine-grained, cement-based concrete with a maximum grain size of 2 mm. This relatively small size of the aggregates limits their bridging ability and leads to a pronounced decrease in the effect of aggregate bridging comparing to that recorded in ordinary concrete. Brockmann [18] investigated the mechanical and fracture-mechanical properties of similar cement-based concrete mixtures and pointed out: "... it was shown that all fine grained concrete mixtures show a significantly less ductile fracture behaviour in comparison with ordinary concrete..." (see Brockmann [18], p. 163). Moreover, the high bridging performance of fibres and yarns, also at low strain levels, makes the contributions of aggregate bridging to the energy dissipation negligible in such systems.

Fibre bridging

The mechanical behaviour of fibres in concrete depends not only on their amount, distribution, and orientation but also on the properties of the individual fibre and its interaction with the matrix. In general, one of the two following failure mechanisms is expected to take place: fibre fracture or fibre pullout. Whether the first or the second failure dominates depends on many parameters:

- type of the fibre (single or bundle)
- tensile strength of the fibre
- surface characteristic of the fibre
- bond quality, i.e., mechanical properties of the interface between fibre and matrix
- angle of inclination of the fibre to crack surface
- loading rate, etc.

In addition to numerous experimental investigations on fibre pullout, a number of theoretical models have been developed to describe fibre pullout behaviour. It is generally accepted that the bond between fibre and surrounding matrix is the main criterion responsible of the stress transfer. Pullout behaviour is basically the result of de-bonding of a fibre from the surrounding matrix, followed by frictional slip. Two fundamental concepts of interface property characterization were used to describe de-bonding: the stress approach and the fracture-mechanical approach. In the stress approach, the de-bonding of fibre-matrix interface starts when the the interface shear stress exceeds the shear strength. For the fracture-mechanical approach, the de-bonding zone is considered to be a crack, and adequate energy must be supplied for further propagation, i.e., de-bonding. More details relevant to these two models including a comparison study of the load-versus-crack-length relationships predicted by the two approaches can be found in Stang et al. [92] and Li and Stang [93].

Fibre fracture takes place instead of fibre pullout when the fibre tensile strength is reached before the fibre is completely de-bonded. For fibres which are shorter than the critical length l_{crit} (see Equation 2.2; Kelly and Tyson [94]), the tensile stress transferred from the matrix to the fibre remains below the tensile strength of the fibre. Fibres with a length beyond the critical length

can be loaded in a composite to a higher stress level, which may exceed the fibre tensile strength and therefore lead to the fibre failure.

$$l_{crit} = \alpha \cdot \frac{f_{t,F}}{2\tau_m} \cdot d \tag{2.2}$$

where: α is the coefficient to consider crack position relative to the fibre half-length (> 1), $f_{t,F}$: strength of fibre, τ_m: average bond strength, d: fibre diameter.

Single fibre

The typical pullout response of a straight single fibre consists of three main parts, see Figure 2.21:

- Part I: the ascending part represents the increase in the interface shear bond stress. The slope of this part depends on the mechanical properties of the bond and the stiffness of the fibre.
- Part II: when the applied stress exceeds the bond strength, de-bonding in the interface takes place; this process develops gradually until full de-bonding occurs.
- Part III: depending on the interface properties, a sudden drop in the measured force-displacement curve (decrease in force) can be observed. From that moment, pullout starts while the interface forces of the de-bonded fibre are transferred by friction. The pullout load decreases with increasing slip, which is limited by the fibre's embedded length l_e. Furthermore, it was found that depending on the fibre type and interface properties, different relationships in this portion can be observed: constant friction, slip softening and slip hardening, as shown, for example, in the investigation on PVA fibres pullout tests performed by Redon et al. [95] and Boshoff et al. [96]

More details concerning the bonding mechanics of fibres in concrete are presented and discussed by Bentur et al. [97].

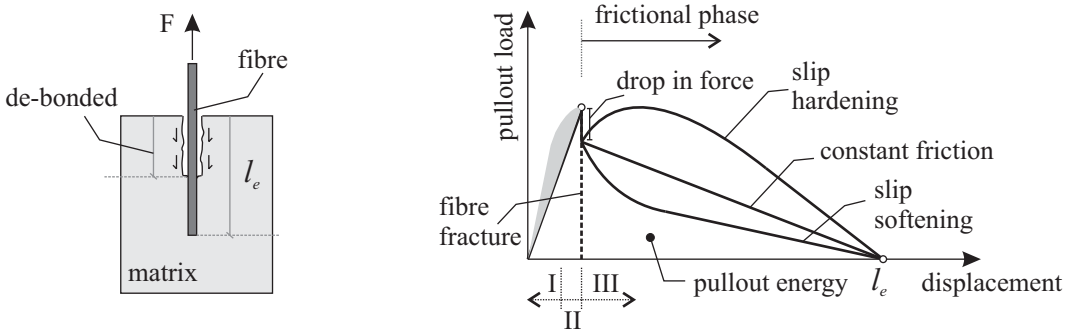

Figure 2.21: Schematic view of pullout of straight single fibre (left) adapted from Bentur et al. [97], and general shape of load-displacement response (right) adapted from Redon et al. [95]

However, single-fibre pullout tests are limited due to their sensitive setups and the small diameters of the fibres. Further parameters, such as the fibres' embedded lengths, fibre inclination and double-side de-bonding should be taken into account when the results of single-fibre pullout tests are used in the modelling of a single-crack, as used here in Section 5.4.3.

Fibre inclination
Pullout behaviour changes dramatically when the fibre is inclined to the crack plane. Three micro-mechanisms should be considered: matrix spalling, fibre de-bonding, and fibre bending. The force acting on the brittle matrix from the fibre may lead to a local failure, i.e., to matrix spalling due to the stress concentration at the exit point resulting from the change in direction of fibre pullout. Leung and Li [98] investigated different matrices with various stiffnesses to analyse the possibility of spalling in order to develop a micro-mechanical model for the determination of crack-bridging stress in random, brittle, fibre-reinforced composites.

The other two important micro-mechanisms, fibre de-bonding and fibre bending, depend mainly on the respective fibres' properties.

For inclined flexible, ductile fibres, the micro-mechanism which dominates pullout behaviour is the de-bonding component. Due to the change in the direction of fibre pullout, an additional force is provided near the fibre exit point, i.e., an increase in frictional resistance to pullout. This effect depends on the angle of inclination and the fibre-matrix interface properties and was incorporated into the calculation of pullout force by Li et al. [99] by using the Equation 2.3:

$$P(\phi) = P(\phi = 0) \cdot e^{f\phi} \tag{2.3}$$

Where $P(\phi)$ is the pullout force as a function of the fibre inclination ϕ, $P(\phi = 0)$ is the pullout force perpendicular to crack plane, indeed the matrix surface in the case of pullout tests, and f is a factor associated with the local friction between fibre and matrix at the fibre exit point (determined by 0.5 from pullout experiments under different inclinations by Kanda and Li [100]).

However, the effect of the angle of fibre inclination on increasing the possibility of fibre rupture must be considered. An increase in local friction leads to a lower fibre fracture load in comparison to that of aligned fibre. According to Kanda and Li [100] the fibre's load-carrying capacity is limited to a maximum value given in Equation 2.4:

$$P_{fu}(\phi) = P_{fu}(\phi = 0) \cdot e^{-f^{'}\phi} \tag{2.4}$$

Where $P_{fu}(\phi)$ is fibre's maximum load carrying capacity, $P_{fu}(\phi = 0)$ is the original load carrying capacity, i.e., for fibre pullout perpendicular to the crack plane, ϕ is fibre inclination in rad and $f^{'} = 0.3$ (parameter determined in [100]).

For stiff fibres, an additional force should be considered as a result of the bending of fibres, as the fibres will have to bend at the cracked surface. The effect of stiff fibre bending on bridging stress was studied experimentally by Katz and Li [101] for carbon fibres and cement matrix. The selected inclination angles were 15, 30, 45, 60 and 75°. The results obtained showed that increasing the inclination-angle-to-fracture surface leads to a decrease in the maximum bridging load. This can be explained by the brittleness of the carbon fibre. Zhang und Li [102] considered the effect of the bending of stiff, brittle fibres and performed an analytical study on the effect of fibre inclination angle on fibre-fracture load. It was found that fibre-fracture load is significantly reduced in comparison to the case of fibres with zero inclination angle.

Based on the descriptions above, it can be concluded that fibre inclination can lead to an increase in bridging force, but it can also lead to higher stress in the fibre due to bending and, therefore, higher fibre fracture potential, thus decreasing the number of fibres pulled out; see [102].

Fibre embedded length
Fibre embedded length influences both the pullout force and failure scenario.

Chaallal and Benmokrane [103] performed their experimental study to investigate the pullout behaviour and bond characteristics of glass-fibre rods embedded in concrete. In order to determine the optimal anchored length, they demonstrated the relation between embedded length and pullout force. It was found that the required pullout force increases by increasing the embedded length. When the embedded length becomes long enough, i.e., critical length, rupture under tension takes place instead of pullout from concrete. The analyses show an almost linear relationship between pullout force and embedded length, see Figure 2.22 (left).

Boshoff et al. [96] investigated the effect of the pullout rate on the mechanical response of the interface between the fibre and the matrix by means of single-fibre pullout tests. One important finding, among others, was that the probability of fibre rupture during pullout increased with an increase of the embedded length. Figure 2.22 (right) shows that the dependency of the probability of fibre fracture on the embedded length can be considered linear.

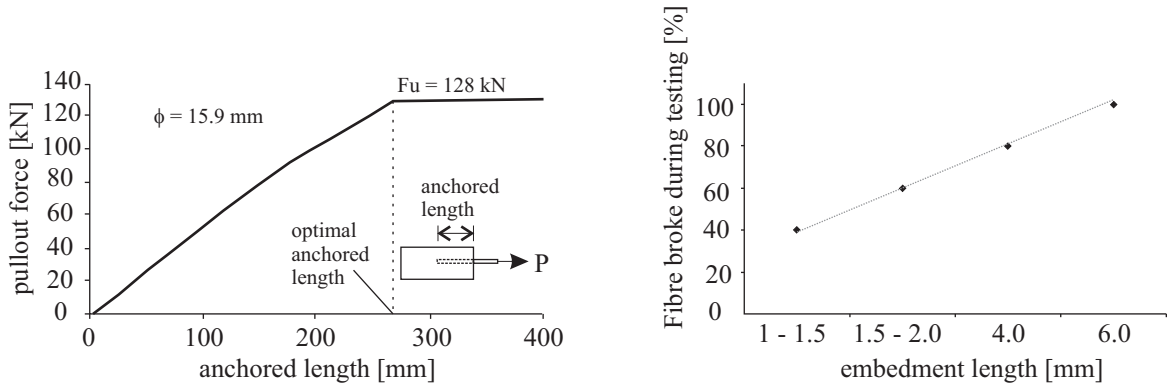

Figure 2.22: Pullout force versus the embedded length of a glass-fibre rod; based on [103] (left) and the relation between the percentage of the fibres that fracture during testing and embedded length; based on [96]

These two relationships will be considered for the extension of the pullout results obtained in the framework of this thesis since only one embedded length will be tested.

Fibre double-side de-bonding
Due to the limitation of pullout test setups, which enables testing of one-side pullout only, double-sided de-bonding should be considered when the pullout results are to be used for the description of concrete with short fibres; see Section 3.3.3. The necessity of considering this effect was presented by Wang et al. [104]. This is based on the notion that in reality the de-bonding and pullout of a fibre which is involved in crack bridging can occur from both sides of the crack.

The effect of fibre embedded length and fibre inclination on its pullout behaviour as well as double-sided de-bonding is taken into consideration in order to extend the pullout results of single-fibre pullout testing, which will be used to describe the formation and opening of one single crack, as presented in Section 5.4.3. Such extensions were applied earlier by Jun and Mechtcherine [105] to the pullout results of Polyvinyl Alcohol (PVA) fibres in order to model the behaviour of strain-hardening cement-based composites (SHCC) and a consistent results were obtained.

Fibre bundle

The failure of bundles of fibre has been also investigated. Bundled fibres usually consist of hundreds of filaments held together by means of a special polymer material, so-called sizing, applied to the filaments so that they remain bundled after mixing with concrete. The bundle of short fibres can be considered as a "short piece of strands". Thus, it possesses two different micro-structures: sleeve filaments with a direct bond to the surrounding matrix by means of hydration products and a core of poorly bonded filaments. The quality of the interface zone between the outer filaments and the surrounding matrix, the stress transfer between outer and inner filaments, and the penetration of the cement grains into the filaments depend mainly on the sizing treatment. More details concerning sizing can be found in IGARASHI and KAWAMURA [106]. They studied the influence of the effects of size of bundled fibres of glass and carbon on the microstructural features of the interface zone.

A complex, still not fully understood mechanism exists for fibre-to-matrix and fibre-to-fibre stress transfer. The effectiveness of this type of short fibre in the pre- and post-cracking stages depends very strongly not only on their strength, orientation, and deformability but also on their bonding. BARTOS [107] performed *in-situ* SEM tensile tests to understand the micro-fracture mechanics of the failure of glass strands bridging a crack in cement matrix. He showed that the type of fracture is affected by the bond, as illustrated in Figure 2.23: while the entire bundle of fibres, left in the figure, is almost completely pulled out due to the poor bond to the surrounding matrix, the outer filaments of the strand, as shown in the middle of the figure, may fracture, well bonded to the matrix, and the inner filaments slip and are pulled out, so-called "telescopic failure". BARTOS mentioned that this telescopic failure is desirable because of the resulting improvement in both strength and toughness of the composite. When the filaments within the strand are well bonded together and there is, additionally, very good fibre-matrix bonding, the strand fractures as a whole in brittle manner; see Figure 2.23 (strand on the right side of the image).

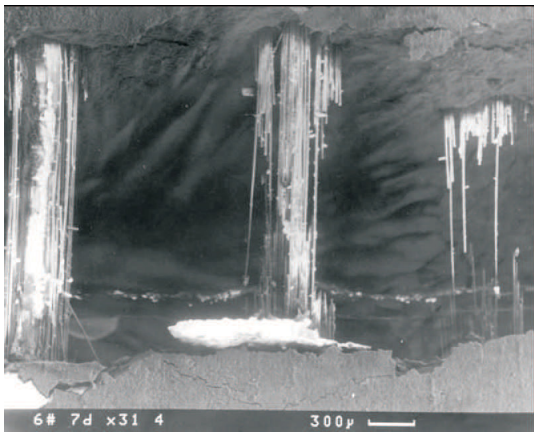

Figure 2.23: SEM image showing three different modes of failure of glass strands bridging a crack in cement matrix [107]

In the dissertation at hand, both pullout tests parallel to fibre axis as well as pullout tests of inclined fibres were performed on such bundles of fibres to investigate the influence of fibre orientation, see Section 4.4.2.

2.4 Rheological modelling

Crawley [108] mentioned that the "best" model is the one that simply and adequately describes a significant part of the variable response data. He proposed that:

- models should have as few parameters as possible;
- linear models should be preferred to non-linear models;
- experiments relying on few assumptions should be preferred to those relying on many;
- models should be pared down until they are minimally adequate;
- simple explanations should be preferred to the complex.

However, over-simplification is to be avoided as well, especially for complex composite materials.

The review of the literature shows that only very few physical models give reasonable descriptions of fracture mechanisms in concrete. It seems that the rheological models which use combinations of simple rheological elements are most appropriate for this purpose. The use of springs, friction blocks, strength and dashpot elements is helpful as it gives a physical feeling for the way a material might respond, rather than simply using an abstract mathematical expression. The four rheological basic elements are shown in Figure 2.24.

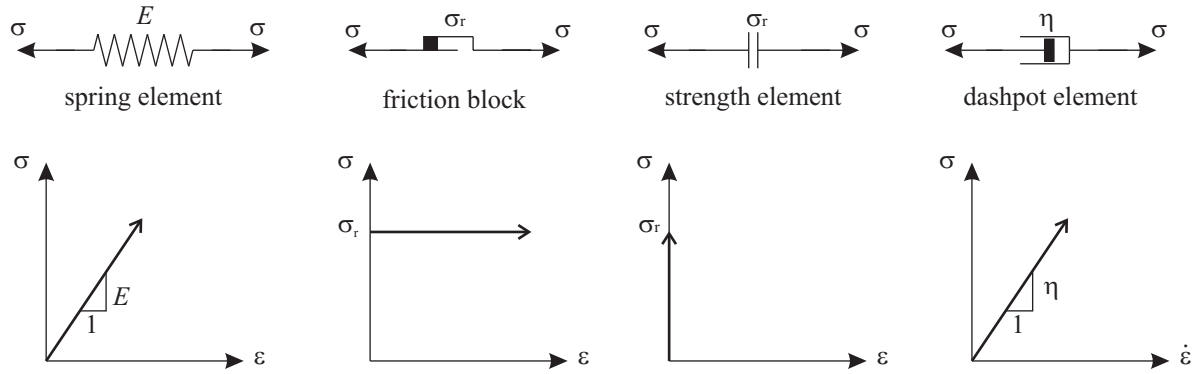

Figure 2.24: Rheological basic elements and corresponding responses

The linear-elastic behaviour of the spring element is described by Hook's law:

$$\epsilon = \frac{1}{E}\sigma \tag{2.5}$$

The friction block is used to represent the plastic behaviour and described by:

$$\epsilon = 0 \;\forall\; \sigma < \sigma_r \tag{2.6a}$$

$$\epsilon \neq 0 \;\forall\; \sigma = \sigma_r \tag{2.6b}$$

To represent the strength of a material, strength element can be used:

$$\begin{aligned} \epsilon &= 0 \;\forall\; \sigma \leq \sigma_r \\ element fail \;\; &\forall\; \sigma > \sigma_r \end{aligned} \tag{2.7}$$

The dashpot is used to describe the viscous deformation behaviour:

$$\dot{\epsilon} = \frac{1}{\eta}\sigma \tag{2.8}$$

These basic elements, with their assigned properties, can be combined in serial or parallel arrangements to build up the model. Descriptions of almost every possible deformation as well as fracture behaviour can be achieved by different possible combinations. In the following some examples are presented: A serial arrangement of a spring element with a friction block builds up the so-called **Prandtl-Reuss model**, which describes elastic-plastic behaviour. **Maxwell model** consists of a spring element and a dashpot in series. With this model creep response and stress relaxation can be represented. The outcome of a parallel arrangement of a spring element and a dashpot is the so-called **Kelvin (Voigt) model**, which represents visco-elastic behaviour. Serial arrangement of **Maxwell model** with **Kelvin (Voigt) model** leads to the creep model in concrete known as **Burgers model**, see in Figure 2.25. More details can be found, for example, in Kessler-Kramer [109].

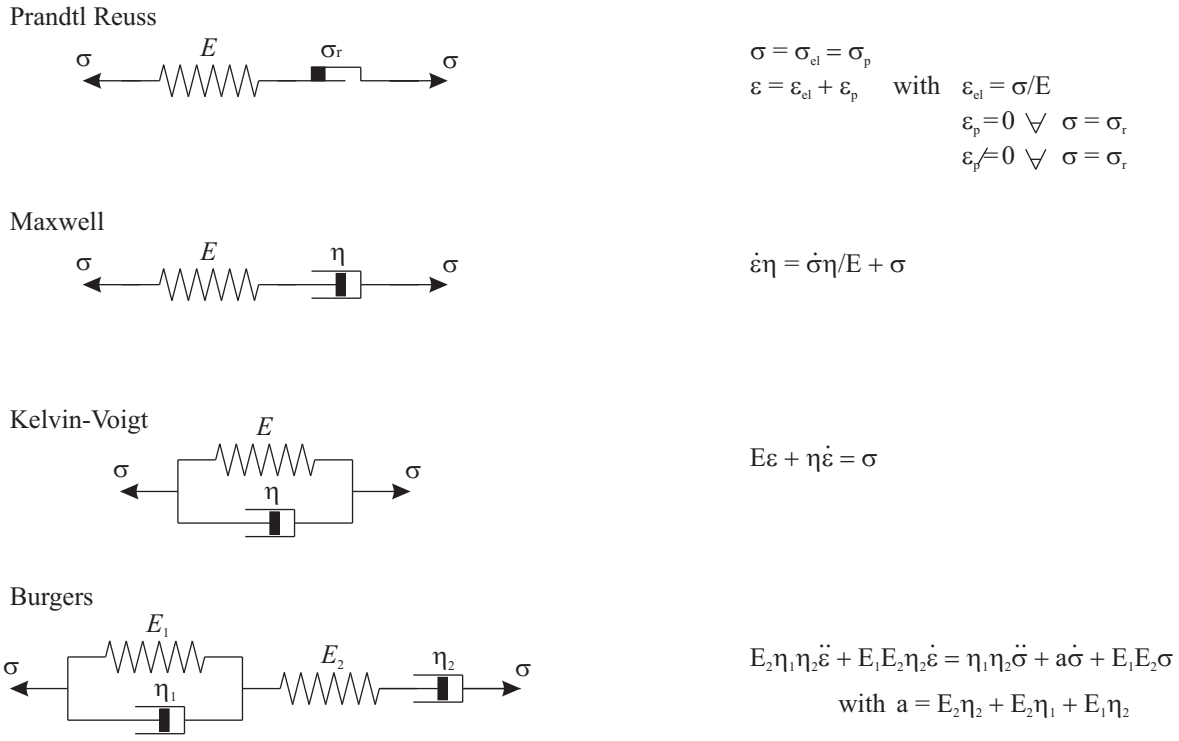

Figure 2.25: Some rheological models and the corresponding constitutive laws

Duda and König [110] used two rheological elements, springs and friction blocks, to developed a material model describing the behaviour of concrete under monotonic loading and under cyclic loading as well. Two groups of friction blocks (A and B) representing two load transferring mechanisms (adhesion between grain and matrix and friction between grain and matrix after cracking), respectively, were arranged in parallel. Springs were added to the friction blocks in order to extend the model for cyclic loading. Furthermore, the mechanism of dislocating, i.e., separation and then removal, of some particles from the crack surface while crack opening and the resulting prevention of surfaces from fitting into each other again should be considered. Therefore, the element group C was added to model this behaviour, as shown in Figure 2.26. Moreover, by using distribution functions to describe the number of active elements at actual crack width, the analytical relations were derived and the validity of the model was proven by comparing the material model with experimental results, as presented in [110].

A decade later, based on fracture-mechanical and phenomenological investigations Kessler-Kramer et al. [111] developed a new material law for concrete under cyclic tensile loading. Its

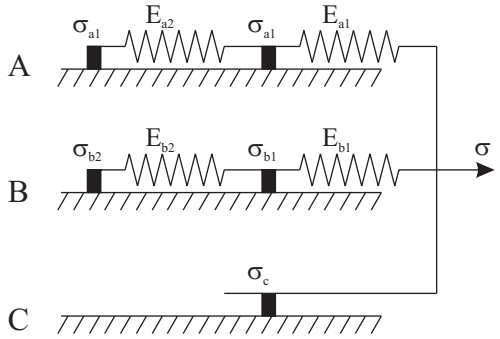

Figure 2.26: Material model of behaviour of concrete under monotonic and cyclic loading, developed by DUDA and KÖNIG [110]

constitutive relations were derived based on a rheological-statistical model consisting of simple rheological elements. The number of load cycles, time effects, and the heterogeneity of concrete were considered in this model by adequate combinations of springs, friction blocks and dashpots representing the elastic, frictional, and viscous deformation components, respectively. The selected basic model consists of two Kelvin-Voigt elements and three friction blocks, as shown in Figure 2.27[2]. The dashpots arranged parallel to the spring elements are to consider both the rate dependency of concrete and the effects due to load history. The complete model consists of n basic models arranged in parallel and the corresponding parameters (E, η and σ) are statistically distributed according to the Weibull distribution function. Details concerning the determination of model parameters and deriving the constitutive law can be found in [111] and [109]. Good agreement between experimental results and the results of numerical calculations indeed proved the validity of the model.

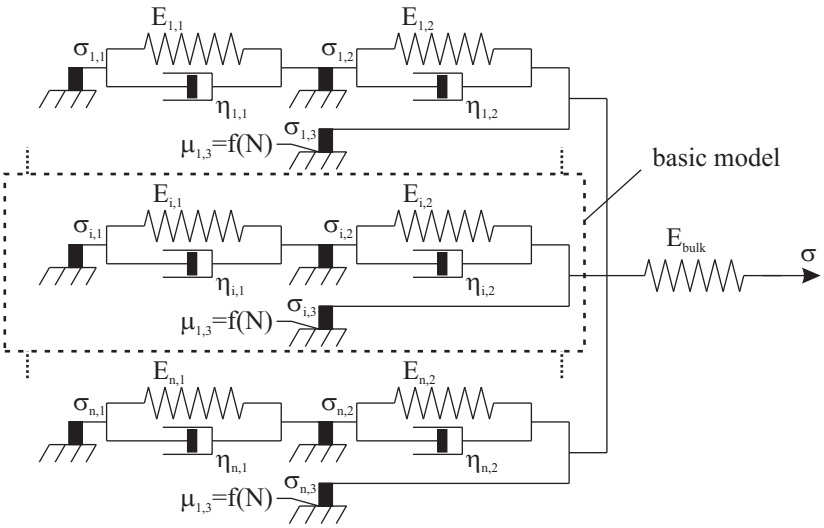

Figure 2.27: Rheological-statistical model describting of the fatigue behaviour of concrete under tensile loading, from [111]

Further rheological-statistical models have been developed to describe various aspects of fracture behaviour of concrete. MECHTCHERINE [15] developed an "advanced material law" for concrete subjected to thermal loads, describing the damage of concrete by increasing strains before and

[2] the associated friction coefficient $\mu_{i,3}$ is given as a function of the number of load cycles N to allow modelling the effect of loosened particles

after tensile strength is reached. Zheng et al. [112] presented a stochastic damage constitutive relationship for high-strength and high-performance concrete (HSHPC) subjected to uniaxial tension stress. However, no study on modelling the behaviour of composites with fibres using rheological elements is available in the literature. Based on the different bond and failure mechanisms of short fibres, just such a model will be developed in this thesis. The basics for this model are data obtained from and phenomena observed in single-fibre pullout tests. The model will be presented in **Chapter 5**.

2.5 Summary – Conclusions to the own work

In this chapter information obtained from literature and relevant to the content of this thesis regarding both materials textile-reinforced concrete (TRC) and concrete with short fibres has been presented and discussed.

First, the particular choice of TRC components regarding workability, some physical characteristics, i.e., penetration through and between the yarns, and durability were addressed. One of the matrix compositions developed at the Institute of Construction Materials at the Technische Universität Dresden in earlier studies was chosen for this investigation. In order to compare the actual mechanical behaviour with observations obtained from previous investigations, specific production technique, curing conditions and test setup were chosen to prepare the specimens of uniaxial tensile tests which constitute the core of the experimental program.

The characteristic behaviour of TRC under tension was presented with special attention to the course of stress-strain relationship. Various simplifications and idealisations of structure and specific behaviour of both the multifilament-yarn itself and the interface zone between the yarn and surrounding matrix were discussed with regard to developing different models describing the response of TRC under tension. Subsequently, attention was paid to various investigations, based mainly on pullout tests, carried out to check the validity of the models developed. A so-called double-side pullout test was chosen for the investigations at meso-level of observation in this thesis to understand the bond, stress transfer and pullout mechanisms of the material and to clarify the failure criteria caused by yarn pullout.

Crack-bridging mechanisms induced by fibres and the development of micro-cracks in a matrix which contains short fibres have been investigated extensively by many researchers. Information on single-fibre pullout behaviour was necessary to understand the crack bridging mechanisms. It was shown that detailed investigation on material micro-structure is required in order to describe the physical phenomena which govern the material failure.

The fibre orientation factor and boundary effects were investigated for elements with fibre distribution varies from 3D to 1D. No information on fibre orientation factor in the case of specimens produced by laminating techniques, i.e., with fibre orientation between 2D and 1D, more nearly 1D, was available. This point should be considered within the framework of this thesis.

Finally, rheological modelling by means of combination of simple rheological elements in conjunction with statistical functions were discussed. Currently available models deal with fracture behaviour of concrete without fibres. Since this type of model, by the use of rheological elements, gives a physical meaning and also better feeling for the material response, the author decided to use such approach for modelling fibre pullout behaviour, including possible fibre failure.

3 Experimental program

3.1 Materials

To investigate the mechanisms of interaction between textile reinforcement and short fibres and the joint action of such hybrid reinforcement in cement-based materials, a parameter study was set up. Three different types of short fibres, each with its own properties different to the other types, distributed in two different cement-based matrices, differentiated from one another by their water-to-binder ratios, were investigated **separately** and in **combination** with one type of textile reinforcement. Furthermore, two different degrees of textile reinforcements with varied numbers of of textile layers were investigated. The short fibres were added in two quantities, low and high, to vary the mechanical properties of the mixes. Mixtures with a low percentage of short fibre were tested without textile reinforcement and with a relatively high degree of textile reinforcement. A high percentage of short fibre WAS combined with a low degree of textile reinforcement, but testing was also conducted without the textile layers. In addition, plain matrix mixes and matrices with only textile reinforcement, of low and high degree, were tested.

It should be underlined here that these parameter combinations and the following particular choice of the raw materials were selected not to optimize the compounds or the choice of the components but to gain better insight into the specific working mechanisms of hybrid reinforcement.

3.1.1 Fine-grained cement-based matrix

Table 3.1 gives the compositions of the two finely grained concretes used in this study. The matrix compositions were chosen according to the results of previous investigations performed at the Institute of Construction Materials at the TU Dresden. It was found that matrices with a high content of ground, granulated blast furnace slag in the cement (CEM III) and the addition of pozzolans (fly ash and micro-silica) show favourable properties in respect of the durability of the glass fibre reinforcement as well as the bond between fibre and cementitious matrix (see Section 2.2.2.2). Furthermore, in order to match both the small diameter of the filaments and the small distance between reinforcement textile layers, the maximum aggregate diameter had to be small as well; see also Section 2.2.2.2. Quartzite sand 0-1 mm was used as aggregate.

Two mixtures, designated as M030 and M045, having water-to-binder ratios of 0.30 and 0.45, respectively, were used in the investigation described in the work at hand. Some superplasticizer with a basis of naphthalene-sulphonate was added in order to achieve sufficient flowability in the mixtures. The average slump flow value obtained with a small cone, in a mini-slump test with 15 strokes, was approximately 200 mm for both mixtures, measured based on DIN EN 1015-3; see also Figure 3.5 (left). It should mentioned here that an extra amount of superplasticizer was added to some of the mixtures with the addition of short fibres to achieve adequate workability, see Table 3.2.

Table 3.1: Compositions of both fine-grained cement-based matrices used in the investigation [kg/m^3]

Matrix	w/b	Cement CEM III B 32.5	Fly ash	Micro-silica suspension[a]	Quartzite sand 0-1 mm	Water	Superplasticizer
M030	0.30	632	265	101	947	234	11
M045	0.45	554	233	89	832	330	2

[a]Solid:water = 1:1

Table 3.2: Amount of extra superplasticizer added to the mixtures with the addition of short fibres [kg/m^3]

Matrix	Amount of the short fibres by volume	Dispersed glass fibres	Integral glass fibres	Carbon fibres
M030	0.5 %	2	0	4
	1.0 %	4	1	8
M045	0.5 %	0	0	3
	0.5 %	2	0	6

3.1.2 Continuous fibres – Textile reinforcement

One particular type of polymer-impregnated, biaxial fabric made of alkali-resistant (AR) glass was chosen as textile reinforcement for both the TRC specimens prepared for uniaxial tension tests as well as the specimens prepared for multifilament-yarn pullout tests. The impregnation degree of this type is 30 % as a mass proportion of the multifilament-yarn' material (AR glass). The density of the AR glass material used is 2.75 g/cm^3. As mentioned in Section 2.2.6.2, the impregnation is applied uniformly over the entire cross-section area of the yarn. However, previous investigations at the Institue of Construction Materials at the Technische Universität Dresden showed that the degree of impregnation is actually not uniform along the yarn. Some "weak spots" were detected, especially at the locations where the weft and warp threads cross each other. Both the weft and warp threads had a fineness of 2 * 640 tex[1]. The spacing between yarns was 7.2 mm, cf. Figure 3.1. The cross-section of the yarn is considered to be an ellipse, and the number of filaments is 3200. The average tensile strength of the yarns was approximately 1010 MPa, Young's modulus was 64.8 GPa, and strain capacity 2 %. More information regarding the structure of used type of textile, and many others, can be found in Hausding [113] and Eckers [114].

3.1.3 Short fibres

Short dispersed and short integral AR glass or carbon fibres, all having a length of 6 mm, were chosen as additional reinforcement for this investigation, see Figure 3.2. Two fibre contents of 0.5 % and 1.0 % by volume of concrete were used.

AR glass short fibres have been well known in the field of concrete research and application for many decades, having both high strength and relatively high stiffness; however, they are brittle. Carbon short fibres are more expensive currently, have very high strength and stiffness, and show also brittle behaviour. The usage of short carbon fibres in concrete is still seldom. Information concerning the research work on short fibres can be found in Section 2.3.2.

[1]tex = mass in g of 1 km yarn; tex = g/km

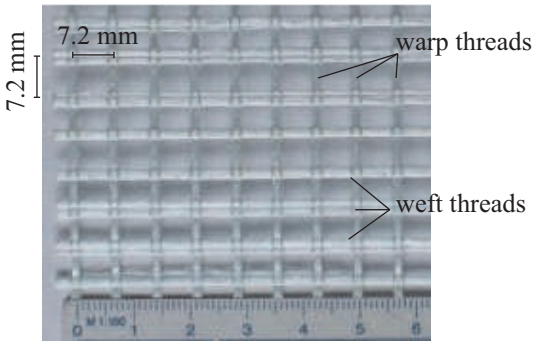

Figure 3.1: Textile reinforcement used in the investigation (AR glass)

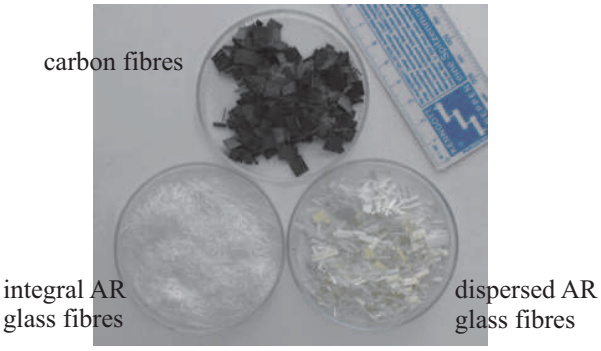

Figure 3.2: Short fibres used in the investigation

Table 3.3 gives the main properties of the selected short fibres. No information from the producer could be obtained about the sizing applied to these short fibres. Figure 3.3 provides ESEM images of the three types of short fibres used in this investigation.

Table 3.3: Types and properties of short fibres used in the investigation

Material	Type	Length [mm]	Diameter[a] [μm]	Density [g/cm^3]	Tensile strength [MPa]	Young´s modulus [MPa]
AR glass	Dispersed	6	20	2.68	1700	72000
AR glass	Integral	6	13	2.68	1700	72000
Carbon	Dispersed	6	7	1.70	3950	238000

[a]For integral fibre: diameter of individual filaments

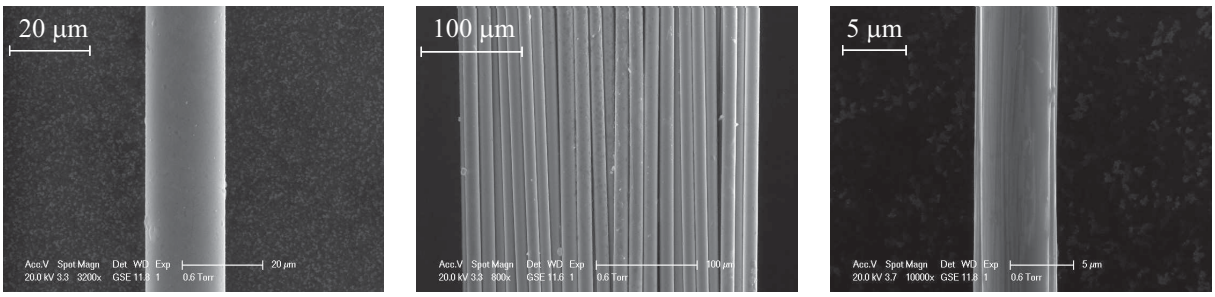

Figure 3.3: ESEM images of dispersed glass fibre (left), integral glass fibre (middle) and carbon fibre (right)

During the mixing of fine-grained concrete, or simply in water, short dispersed fibres act in such a manner as to distribute and spread themselves within the fresh matrix as thousands and millions of predominantly single filaments. Short integral fibres remain stuck together and act as short pieces of multifilament-yarn in the mixture as is illustrated in Figure 3.4.

3.2 Production of specimens

This section details the mixing and production procedures used in the preparation of specimens: TRC with and without the addition of short fibres as well as specimens with only short

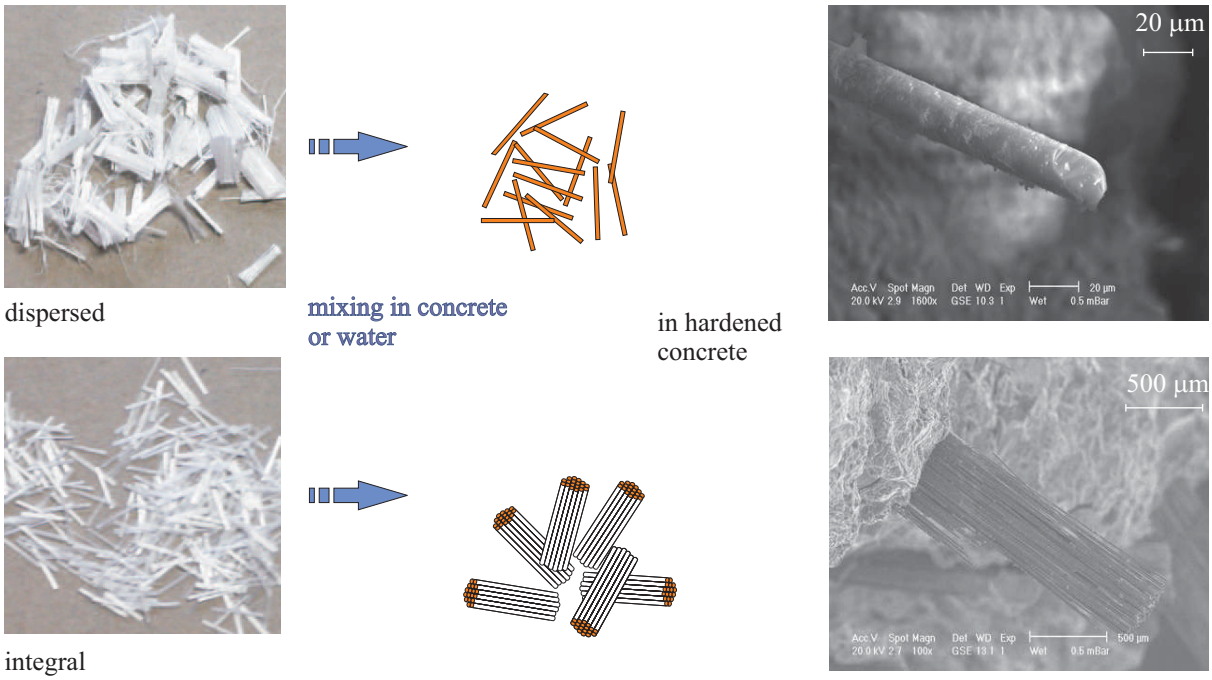

Figure 3.4: Graphic presentation of the condition of dispersed and integral fibres when mixed in concrete or water (left) and ESEM images of the AR glass fibres in hardened concrete (right)

fibres, i.e., specimens prepared for the investigation on the macro- and meso-level of observation.

3.2.1 Mixing procedure

A Hobart stand mixer HSM 30 Liter (50 Hz, 1.1 kW) was used to mix the matrix compositions in this investigation. The mixing steps with their corresponding duration and mixing speed used to for both matrices were carried out as follows; additional steps carried out for specimens with short fibres are written in *italic*):

- mixing of all dry fine-grained components, i.e. cement, fly ash and sand, together for 120 seconds with a low mixing speed level, 68 rotations/minute, in order to produce a homogeneous dry mix;
- addition of mixing water while continuously mixing over a period of approximately 10 seconds; mixing at low speed for another 110 seconds;
- addition of micro-silica suspension while continuously mixing at low speed over a period of approximately 10 seconds; continuation of mixing at low speed for another 50 seconds; mixing at high speed, 178 rotations/minute, for 60 seconds;
- stop in the mixing process for reintegrating possibly segregated fine materials at the bottom of the mixing container or on the mixing paddle, by scraping manually;
- mixing at high speed for 60 seconds while adding superplasticizer;
- *gradual manual addition of short fibres with a time duration of 60 seconds and extra amount of superplasticizer*;
- mixing at high speed for 60 seconds;

- completion of mixing of plain fine-grained concrete;
- *in case of the addition of short fibres a confirmation by means of a "touch-test" is necessary to ensure the desired uniform fibre distribution.*

A slump flow test with a small cone based on DIN EN 1015-3 was performed to confirm the consistency of the fresh mixtures with and without fibre addition. Mixtures without fibres which yielded a slump flow value of approximately 200 mm were considered to be adequate with respect to workability. Moreover, bleeding of water at matrix "cake" edges and segregation of components were, as well, checked.

The slump flow tests on the mixtures with the addition of short fibres showed lower slump flow values in comparison to mixtures without fibres. Therefore, visual inspection and manual checking, based mainly on experience and subjective assessment, were necessary to ensure that the mixtures were sufficiently workable. The criterion used here for judgment is the possibility of spreading the concrete on the textile reinforcement layers by means of a laminating technique explained in the next sub-chapter. As mentioned in the mixing steps, extra superplasticizer was used to improve the consistency of the mixtures with the addition of short fibres. The amounts of superplasticizer added are addressed in Table 3.2. Figure 3.5 shows clearly the effect of the addition of short fibres on the concrete cakes resulted from slump flow tests of four mixtures made with matrix M030: a) plain matrix, i.e., without short fibres, b) with the addition of 1.0 % by volume short integral glass fibres, c) with the addition of 1.0 % by volume short dispersed glass fibres and d) with the addition of 1.0 % by volume short carbon fibres. All other slump flow tests values and figures of concrete cake can be found in Appendix A.

3.2.2 Specimen fabrication

A completely enclosed plastic formwork was used for the production of specimens for the uniaxial tensile tests as well as for the multifilament-yarn pullout tests. The formwork consists of a rectangular ground plate, 550 mm long, 500 mm wide, and 15 mm thick, for three specimens and three covers, all shaped exactly to the foundation plate to ensure that the specimens had identical geometries; see Figure 3.6. The covers were 100 mm wide. After pouring the concrete and placing the textile reinforcement into the ground plate, as explained in the next paragraph, the covers were placed on the top and pressed to achieve a plate thickness of 12 mm. The excess material, fine-grained concrete, flowed through the remaining openings between the covers and could be removed. By using such a formwork and technique, consistent specimen quality and similar hydration conditions for both sides of the specimen were assured. Hence, curvatures due to different shrinkage at the top and bottom sides of the specimens could be avoided. The specimens were then cut from the plate with the given geometry according to the test setup. The cutting process was performed 3 days prior to testing.

Specimens for both uniaxial tensile tests and multifilament-yarn pullout tests were produced using the lamination technique. The laminating process began with the spreading of a thin concrete layer on the bottom of the mould. Then the first sheet of textile reinforcement was laid on this fresh concrete layer and afterward, gently, partially pressed in and smoothed. The complete embedding of the first textile layer took place during the application of the second concrete layer, cf. Figure 3.7. The thicknesses of the concrete layers depended on the desired number of textile layers. These production steps were repeated until all reinforcing layers were placed and incorporated into the finely grained concrete. It should underlined here that the mould was gently vibrated (frequency of 50 Hz) during the production process in order to ensure sufficient compacting as far as possible.

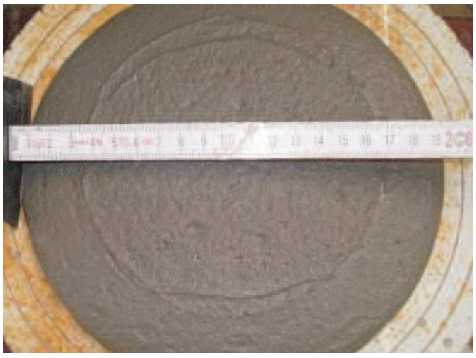

a) plain matrix M030
d = 195 mm

b) matrix M030 with 1.0 % short integral glass fibres
d = 195 mm

c) matrix M030 with 1.0 % short dispersed glass fibres
d = 165 mm

d) matrix M030 with 1.0 % short carbon fibres
d = 145 mm

Figure 3.5: Slump flow test with small cone of the mixtures: a) plain matrix, b) with the addition of 1.0 % short integral AR glass fibres, c) with the addition of 1.0 % short dispersed AR glass fibres and d) with the addition of 1.0 % short carbon fibres; matrix M030

The compacting process during the production of the specimens is of particular interest for mixtures with the addition of short fibre, after which the matrices lose some of their workability. This leads in turn to some worsening of the de-airing process.

3.2.3 Curing condition

Immediately after fabricating the specimens, the formwork was covered by PE foil. One curing condition was applied to all specimens. Due to the relatively long setting time, approximately 12 hours for the cement used (CEM III B 32.5, see Section 3.1.1) [16], the specimens were demoulded at a concrete age of 2 days. After demoulding, the specimens were stored in water until reaching an age of 7 days. Subsequently, the specimens were stored in a climate-controlled room at 20 °C and 65 % RH up to an age of 28 days, i.e., the testing age of all specimens used in this investigation.

Figure 3.6: Mould in use (left), mould overfilled by the materials after compacting (middle) and large plate after demoulding (right); the dashed lines indicate the geometry of specimens to be cut from the plate

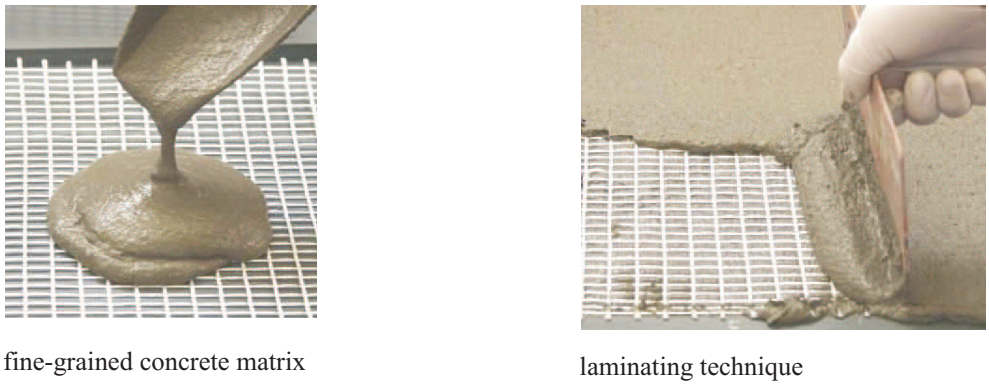

fine-grained concrete matrix

laminating technique

Figure 3.7: Lamination technique: complete embedding of a textile reinforcement layer by the application of the next concrete layer

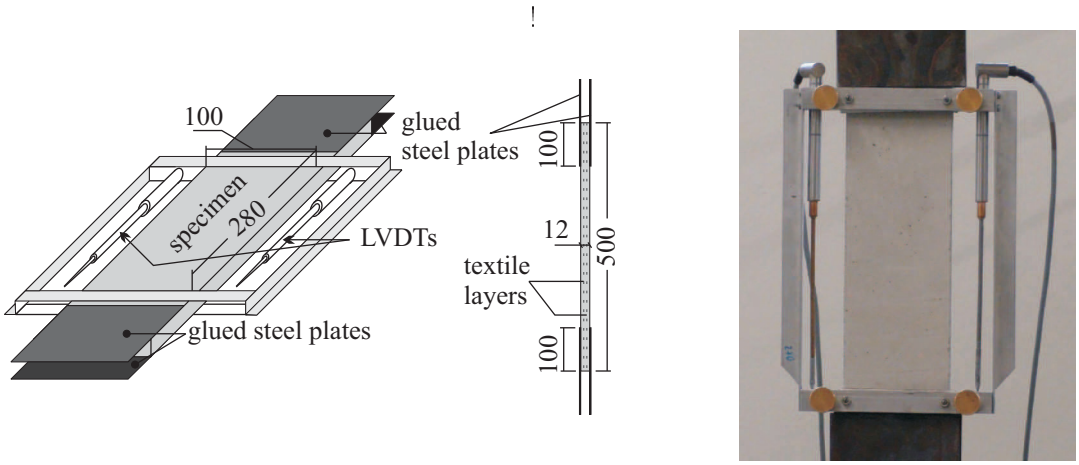

Figure 3.8: Schematic view of specimen geometry and setup used in uniaxial tension tests on rectangular plates (left) and TRC plate during testing (right)

3.3 Experimental methods and parameters combination

Uniaxial tension tests carried out on thin, narrow plates constitute the core of the experimental program. Multifilament-yarn and single-fibre pullout tests were performed to provide more insight into the bonding behaviour between the multifilament yarns or short fibres and the surrounding fine-grained matrix, respectively.

The following section presents information on the test methods applied in this work to investigate the materials as composites and as individual components at the macro-, meso- and micro-levels of observation. First, the geometry and preparation of specimens are introduced. Subsequently, an overview of the setup and testing procedures is given.

3.3.1 Uniaxial tensile tests – Macro-level

In addition to the TRC specimens, which were reinforced with either 2 or 4 layers of textile reinforcement, and still further, both with and without the addition of short fibres, a series of specimens made of plain, finely grained concrete matrix and another series consisting of concrete reinforced only with short fibres, i.e., without textile reinforcement, were tested at this level of observation.

Three specimens were cut from the plate, which was produced as explained in Section 3.2.2. All specimens subjected to tensile loading were of the same dimensions, 500 mm long, 100 mm wide and 12 mm thick; cf. Figure 3.6 (right) and Figure 3.8 (left).

One day before testing, the specimens were taken from the climate-controlled room; see Section 3.2.3. Steel plates of 4 mm thickness were glued to the surfaces of the area, 100 mm square, symmetrically at both ends of the specimen; cf. Figure 3.8. Before gluing the steel plates to the concrete, the surface of the concrete in these areas was roughened and the resulting loosened cement particles and dust were removed. Highly viscous epoxy resin consisting of two components was used as the adhesive. The gluing of the steel plates and the subsequent hardening were achieved with a fixing device in order to ensure accurate positioning. The specimens with their steel plates were mounted and centered such that they were free of constraining forces, i.e., with zero-stress, to the hydraulic jaws of the testing machine.

A dynamic hydraulic testing machine, Instron 8501, was used for these tests. The machine has a maximum loading capacity of 100 kN and an actuator range of 250 mm.

The load was transferred to the specimens via the above-mentioned, non-rotatable steel plates. Such non-rotatable boundaries configuration was used to ensure to the extent possible a uniform strain distribution over the specimen's cross-section during the experiment. The tests were performed with a controlled deformation rate of 0.5 mm/min. Deformation was measured by two linear variable differential transformers (LVDTs) which had a gauge length of 280 mm and were fixed to the specimens as displayed schematically in Figure 3.8.

Table 3.4 gives an overview of the experimental program performed using uniaxial tensile tests.

Table 3.4: Experimental program for uniaxial tensile tests

Type of specimens	Number of specimens	Parameters									
		Matrix		Textile reinforcement		Short fibres (% by volume)					
						Glass dispersed		Glass integral		Carbon	
		M030	M045	2 layers	4 layers	0.5	1.0	0.5	1.0	0.5	1.0
Plain concrete	3	x									
	3		x								
Concrete with only textile reinforcement	3	x		x							
	3	x			x						
	3		x	x							
	3		x		x						
Concrete with only short fibres	3	x				x					
	3	x					x				
	3	x						x			
	3	x							x		
	3	x								x	
	3	x									x
	3		x			x					
	3		x				x				
	3		x					x			
	3		x						x		
	3		x							x	
	3		x								x
Concrete with hybrid reinforcement	3	x		x			x				
	3	x		x					x		
	3	x		x							x
	3		x	x			x				
	3		x	x					x		
	3		x	x							x
	3	x			x	x					
	3	x			x			x			
	3	x			x					x	
	3		x		x	x					
	3		x		x			x			
	3		x		x					x	

3.3.2 Multifilament-yarn pullout tests – Meso-level

With the formation and development of cracks in the matrix, textile reinforcement and short fibres begin to dominate the behaviour of the material through their crack-bridging ability and the stress transfer across the cracks. In order to come to a better understanding of crack-bridging mechanisms and stress transfer in this stage, multifilament-yarn pullout tests and single-fibre pullout tests were necessary, as shown in the conception of testing plan presented in Figure 1.3. Specimens were made with both matrices M030 and M045 (see Table 3.1) with and without the addition of short fibres.

Rectangular specimens of 200 mm length, 70 mm width, and 12 mm thickness were cut from the plates produced and cured in the same manner as those for the uniaxial tensile tests; see Section 3.2.2 and Section 3.2.3. However, for these tests only one layer of textile was used as reinforcement.

The test setup was designed by Krueger et al. [57] and further developed by Lorenz and Ortlepp [115]. The upper anchoring area was determined by the specific arrangement of a "must"-crack position, or breaking area, visible as a saw cut on both sides, cf. Figure 3.9. In the notched cross-section only one multifilament-yarn is still intact and, with some surrounding finely grained concrete, connects the two parts of the specimen to each other. The embedded length of the yarn, i.e., anchoring length, considered in the evaluation of the test results is indicated as l_e in Figure 3.9 and determined by an additional saw cut below the clamp. The displacement-controlled pullout test was carried out using the hydraulic testing machine ZWICK Z250/SW5A with a strain rate of 1 mm/min. The "crack opening" at the predetermined breaking area was measured by external clip gauges DD1, cf. Figure 3.9 (right). More details concerning this test setup and evaluation methodology are given by Lorenz and Ortlepp in [56] and Lorenz [116].

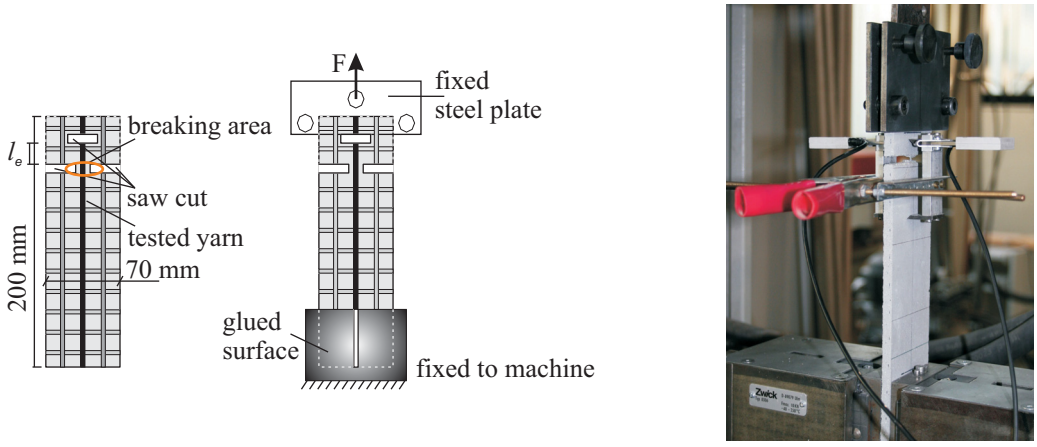

Figure 3.9: Schematic view of specimen geometry and setup used in multifilament-yarn pullout tests (left) and a specimen during testing (right); adopted from [56]

Table 3.5 gives an overview of the experiments performed on meso-level.

3.3.3 Single-fibre pullout tests – Micro-level

As already mentioned in the previous Section 3.3.2 and shown in Figure 1.3, single-fibre pullout tests, along with the multifilament-yarn pullout tests, were highly important in clarifying the mechanisms leading to the various effects of the differing regimes of enhancement on the material's mechanical performance.

Between the two most common basic setups for testing single-fibre pullout behaviour, the test setup according to Kabele et al. [117] was adopted for the investigation within this thesis instead of the alternative test setup presented by Katz and Li [118]. The choice of this particular experimental setup was based on the information presented by Jun [119]. Further details on the method used including information regarding the improvements introduced are explained in the following section.

This test is quite sensitive with respect to specimen preparation as well as, of course, to the testing itself. The diameter and the brittleness of the fibres limit to a great extent the feasibility of such tests. Pullout experiments of short integral AR glass fibres were performed both parallel to its axis and with an inclination. In the case of short dispersed AR glass fibres, pullout tests only parallel to the fibre axis were possible. Specimens made with both matrices M030 and M045 (see Table 3.1) were tested. No pullout tests could be performed with single carbon fibres. Another test setup and a more sensitive testing machine are required to carry out such tests because of the very fine diameter of carbon fibre (7 μm); cf. Table 3.3 and Figure 3.3.

To prepare the specimens for the pullout tests parallel to fibre axis, the short fibre was inserted into a hollow medical cannula with a blunt tip. The position of the fibre was fixed with wax when an embedded length of approximately 3 mm, half the length of the short glass fibre, was reached. Subsequently, the free length out of the cannula, i.e., embedded length, was measured precisely by the use of pictures made by a high resolution camera, as shown in Figure 3.10. A frame with a number of prepared cannulae was fixed to the mould. Finally, the matrix was added and gently compacted until the ends of the cannulae lay 1 mm beneath the matrix surface. The specimen had a cylindrical shape with a diameter of 10 mm and height of 15 mm.

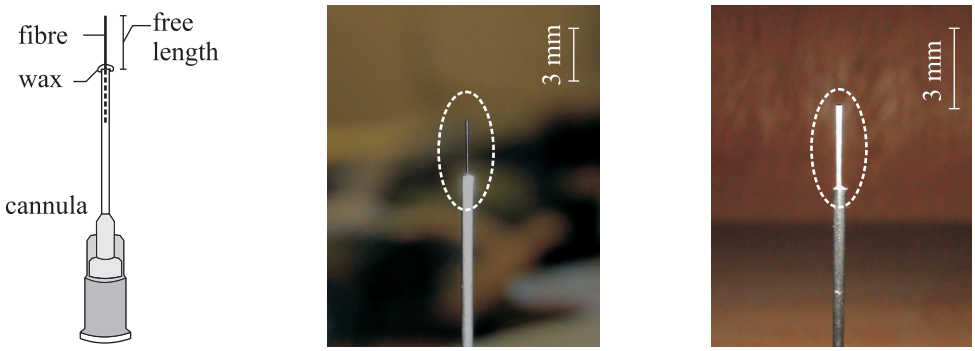

Figure 3.10: Preparation of specimens for fibre pullout tests; schematic detail of fixed fibre (left), cannula with a single dispersed glass fibre (middle) and cannula with an integral glass fibre (right)

To produce the specimens for pullout of inclined fibres a frame with inclined holes (45° in this investigation, see also Section 4.4.2.2) was used. The moulds with the attached cannulae for both type of tests are shown in Figure 3.11.

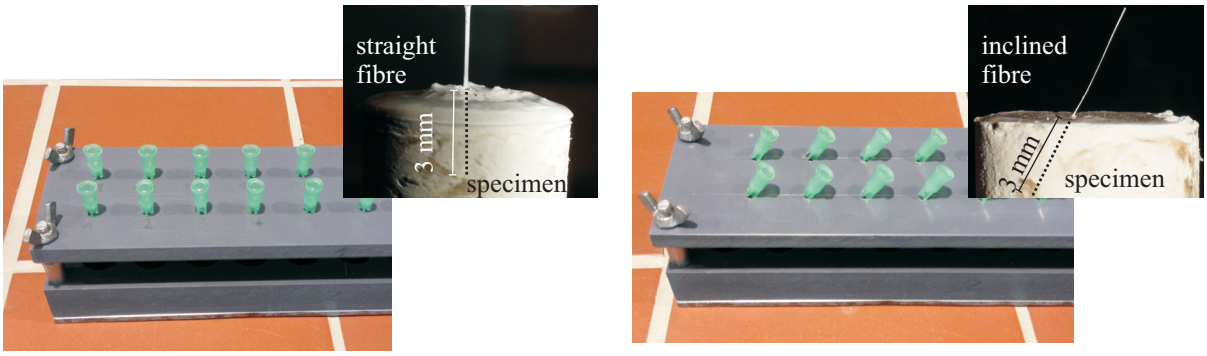

Figure 3.11: Filled moulds with attached cannulae and specimens after demoulding for: Pullout parallel to fibre axis (left) and pullout of inclined fibre (right)

The specimens were demoulded at an age of 2 days, up to an age of 7 days sealed in foil, and then stored in a climate-controlled room at 20 °C and RH 65 % up to a testing age of 28 days. It is worth pointing out here that the matrix cylinders were removed from the mould with a high degree of care. Moreover, since the bond between wax and fibre was much weaker than the bond between fibre and matrix, the fibre-matrix interface was not damaged when the cannulae were pulled out.

For testing, the specimen was fixed to the clamps, and the fibre was glued using a commercially available fast adhesive for metals and plastic materials, to the upper mounting plate of the testing machine as shown in Figure 3.12. The mechanical testing machine Zwick 1445 was used for the tests where the load was measured using a 10 N load cell. The tests were performed with a controlled deformation rate of 0.01 mm/s. Deformations were measured by means of the displacement of the machine cross-head. Further details on this testing setup can be found in Jun and Mechtcherine [120] and Jun [119].

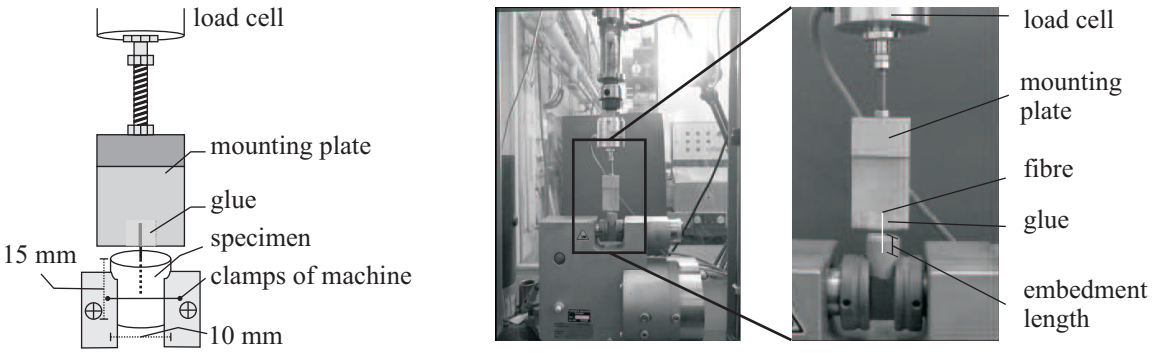

Figure 3.12: Schematic view of test setup used for single-fibre pullout tests (left) and a specimen during testing (right); the case of pullout parallel to fibre axis

Table 3.6 gives an overview of the experimental program performed using single-fibre pullout tests.

Table 3.5: Experimental program for multifilament-yarn pullout tests

Number of	Matrix		Without short	With short fibres (1.0 % by volume)		
specimens	M030	M045	fibres	Glass dispersed	Glass integral	Carbon
3	x		x			
3	x			x		
3	x				x	
3	x					x
3		x	x			
3		x		x		
3		x			x	
3		x				x

Table 3.6: Experimental program for single-fibre pullout tests

Type of pullout	Number of	Matrix		Type of short fibre	
test	tests	M030	M045	Glass dispersed	Glass integral
Parallel to	10	x		x	
fibre axis	10		x	x	
	13	x			x
	31		x		x
Inclined fibre	15	x			x
	16		x		x

4 Experimental results and discussion

In this chapter the experimental results gained from the tests performed at the macro-, meso- and micro-levels of observation are presented and discussed.

First, the results obtained from the tests performed at macro-level of observation are presented. Uniaxial tension tests on thin, narrow plates made of TRC with and without the addition of short fibres constitute the core of the experimental program. Special attention is directed at the course of the stress-strain relationship, crack pattern development, energy dissipation and failure behaviour.

Based on the phenomena observed in the results of the uniaxial tension tests, further systematic investigation was necessary to gain better insight into the specific working mechanisms of such hybrid fibre reinforcement. First, the effects of water-to-binder ratio on the bond and fracture behaviour of fibres are revealed based on results of multifilament-yarn and short-fibre pullout tests. Subsequently, the effect of short fibres on the bond behaviour between multifilament-yarns and the surrounding fine-grained matrix is investigated; the different aspects of enhancement due to the addition of short fibres depending on their type and orientation are treated as well.

Furthermore, the findings of visual inspections of the specimens' surfaces and microscopic investigations of the fracture surfaces and the interface zones between fibre and matrix are used to clarify the fracture behaviour and provide insights into the various failure mechanisms arising in the tests.

4.1 Behaviour of the TRC with short fibres under uniaxial tension

4.1.1 General effects of the addition of short fibres on TRC behaviour under tension

To form a first impression of the influence of the addition of short fibres on TRC behaviour under tension, four different series with regard to the degree of reinforcement were tested: 2 layers of textile, a low degree of textile reinforcement; 4 layers of textile, a high degree of textile reinforcement; 2 layers of textile with the addition of 1.0 % by volume of short fibres, a high percentage of short fibres; and 4 layers of textile with the addition of 0.5 % by volume of short fibres, a low percentage of short fibres. Figure 4.1 shows representative stress-strain curves obtained from uniaxial tensile testing on the specimens with and without the addition of short dispersed glass, integral glass, and dispersed carbon fibres for both matrices M030 and M045. Despite the relatively low percentage of short fibres added to specimens reinforced with 4 layers of textile reinforcement, a considerable increase in the tensile stress at low strain levels could be observed. This improvement was highest due to the addition of short carbon fibres in comparison to the results obtained with reference TRC plates: here a factor of approximately 2 was achieved for the values of first-crack stress. The performance of TRC specimens with short dispersed glass fibres came in second best at low strain. In the tests on TRC with short integral glass fibres only

moderate improvement could be recorded. These observations were valid for the results obtained from both matrices. With respect to the tensile strength and strain capacity of the composite, the addition of short fibres did not provide any improvement, but in most cases rather some decrease, in particular when the matrix with a higher water-to-binder ratio M045 (w/b=0.45) was used. All stress-strain curves obtained from specimens reinforced with 4 layers of textile with and without the addition of short fibres are presented in Appendix B.

More pronounced improvement on the entire stress-strain course of TRC was observed when short fibres were added in relatively high percentage, i.e., 1.0 % by volume, to specimens reinforced with 2 layers of textile reinforcement, cf. Figure 4.1. While the first-crack stress was significantly increased in all specimens with added short fibres for both matrices M030 and M045, the tensile strength of the composite was improved as well in almost all specimens.

Summarizing, it is obvious from the curves that the addition of short fibres leads to an increase in the load-bearing capacity of TRC at small deformations more effectively than doubling the degree of textile reinforcement. This observation reveals an important advantage in using short fibres as an extra reinforcement to textile-reinforced concrete (Section 1.1).

Based on this general overview, the focus in the following is directed to the results obtained from plates reinforced with 2 layers of textile and 1.0 % by volume of short fibres, since this combination seems to be efficient and also promising with respect of clarification of mechanisms behind the observed changes in composite behaviour.

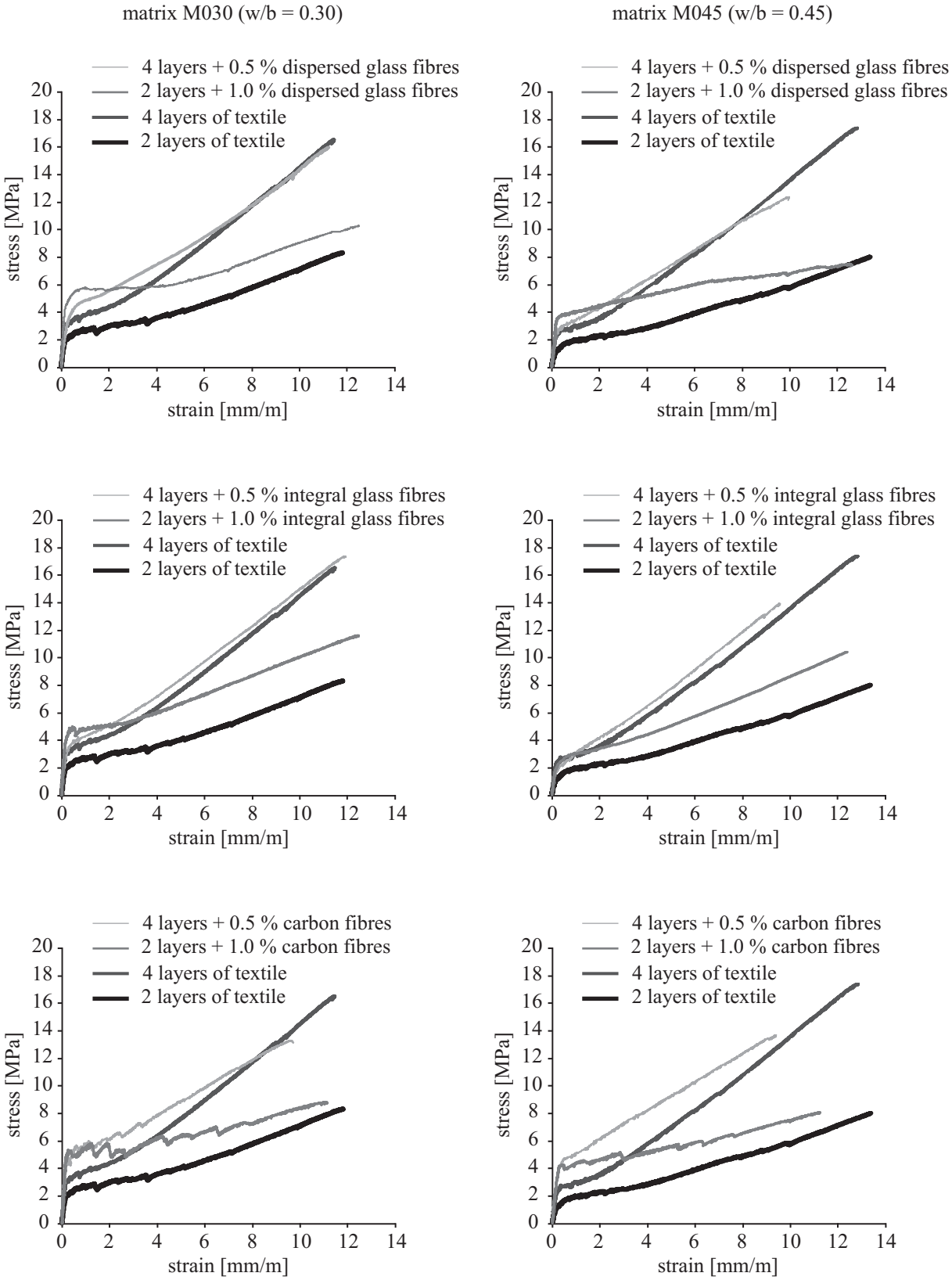

Figure 4.1: Effect of the addition of short dispersed glass (above), integral glass (middle) and carbon fibres (below) on the behaviour of TRC plates subjected to tensile loading made with the matrix M030 (left) and M045 (right), respectively; representative curves

4.1.2 Influence of short fibre on the behaviour of crack-free TRC – First-crack stress

Figure 4.2 shows the stress-strain curves obtained from uniaxial tension tests performed on TRC specimens reinforced with 2 layers of textile both with and without the addition of short fibres. For both matrices M030 and M045, a very significant effect on first-crack stress of TRC under tension was observed due to the addition of all three types of short fibres used. First-crack stress was defined as stress level at which the first "jump" in the measured curve associated with the formation of the first macro-crack on specimen's surface became apparent. The values of the first-crack stress are given in Table 4.1.

It is clear from the table and the diagrams that short dispersed glass fibres were generally more efficient in increasing first-crack stress in TRC than the integral glass fibres. For the specimens made of the matrix M030 (water-to-binder ratio of 0.3), the improvement was nearly the same. The value of the first-crack stress increased by factor of 2.4 and 2.2 due to the addition of dispersed and integral glass fibres, respectively. The difference in effect was much more pronounced for the TRC with M045 matrix (w/b = 0.45). While an increase by a factor of approximately 3 was achieved when dispersed glass fibres were added, the value of the first-crack stress was doubled in TRC specimens with integral glass fibres, cf. Figure 4.2 and Table 4.1.

Even more distinct enhancements in the first-crack stress of TRC were achieved due to the addition of short carbon fibres. Here, increase by factors of 2.6 and nearly 4 was recorded for specimens made with matrix M030 and M045, respectively.

Table 4.1: Mechanical performance of TRC plates, 2 layers of textile, with and without the addition of 1.0 % by volume of short dispersed glass, integral glass and dispersed carbon fibres

Specimen with 2 layers of textile		First-crack stress [MPa]	Tensile strength [MPa]	Work-to-fracture [kN mm]	Strain capacity [mm/m]
		Average value (standard deviation)			
M030	Without short fibres	1.92 (0.37)	8.34 (0.33)	20.14 (0.91)	11.82 (0.47)
	+ 1.0 % dispersed glass	4.65 (0.21)	9.69 (0.53)	28.88 (1.90)	12.61 (0.93)
	+ 1.0 % integral glass	4.20 (0.06)	10.77 (0.73)	27.45 (2.12)	11.56 (0.42)
	+ 1.0 % dispersed carbon	5.04 (0.37)	8.81 (0.34)	27.03 (1.41)	11.05 (0.42)
M045	Without short fibres	1.17 (0.14)	7.25 (0.21)	18.49 (3.38)	11.96 (0.81)
	+ 1.0 % dispersed glass	3.46 (0.06)	7.46 (0.22)	20.50 (4.59)	10.73 (1.65)
	+ 1.0 % integral glass	2.39 (0.69)	9.49 (1.01)	21.16 (1.36)	11.78 (0.53)
	+ 1.0 % dispersed carbon	4.48 (0.27)	8.09 (0.11)	23.26 (3.37)	11.12 (0.35)

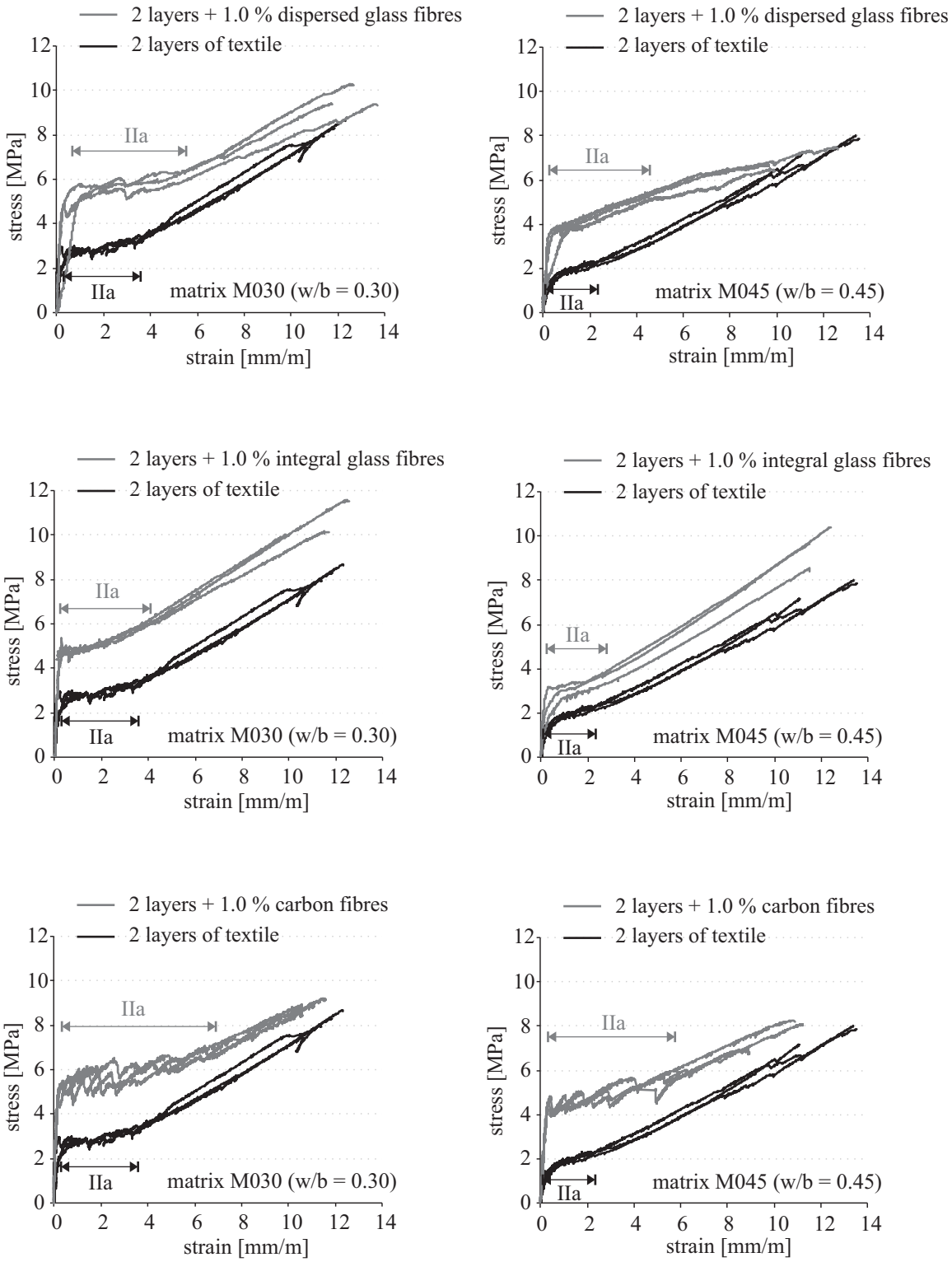

Figure 4.2: Effect of the addition of short dispersed glass (above), integral glass (middle) and carbon fibres (below) on the behaviour of TRC plates (2 layers of textile) subjected to tensile loading made with the matrix M030 (left) and M045 (right), repectively

Furthermore, the addition of short fibres led to a significant increase in stiffness of the composite, i.e., slope of the stress-strain curve in state I (cf. Figure 2.4). In order to illustrate this effect better, representative stress-strain curves were chosen and compared to each other. Extractions of the curves at very low strain levels, as presented in Figure 4.3, show that the slope of these parts of the curves, where the behaviour is nearly linear-elastic, is much steeper for the curves obtained from TRC specimens with the addition of short fibres. It is remarkable that the stiffness increased by approximately factor 2 due to the addition of short fibres, i.e., to a much higher extent than could be expected based on the theory of composite materials for the given concentration of short fibres. This observation is valid for both matrices.

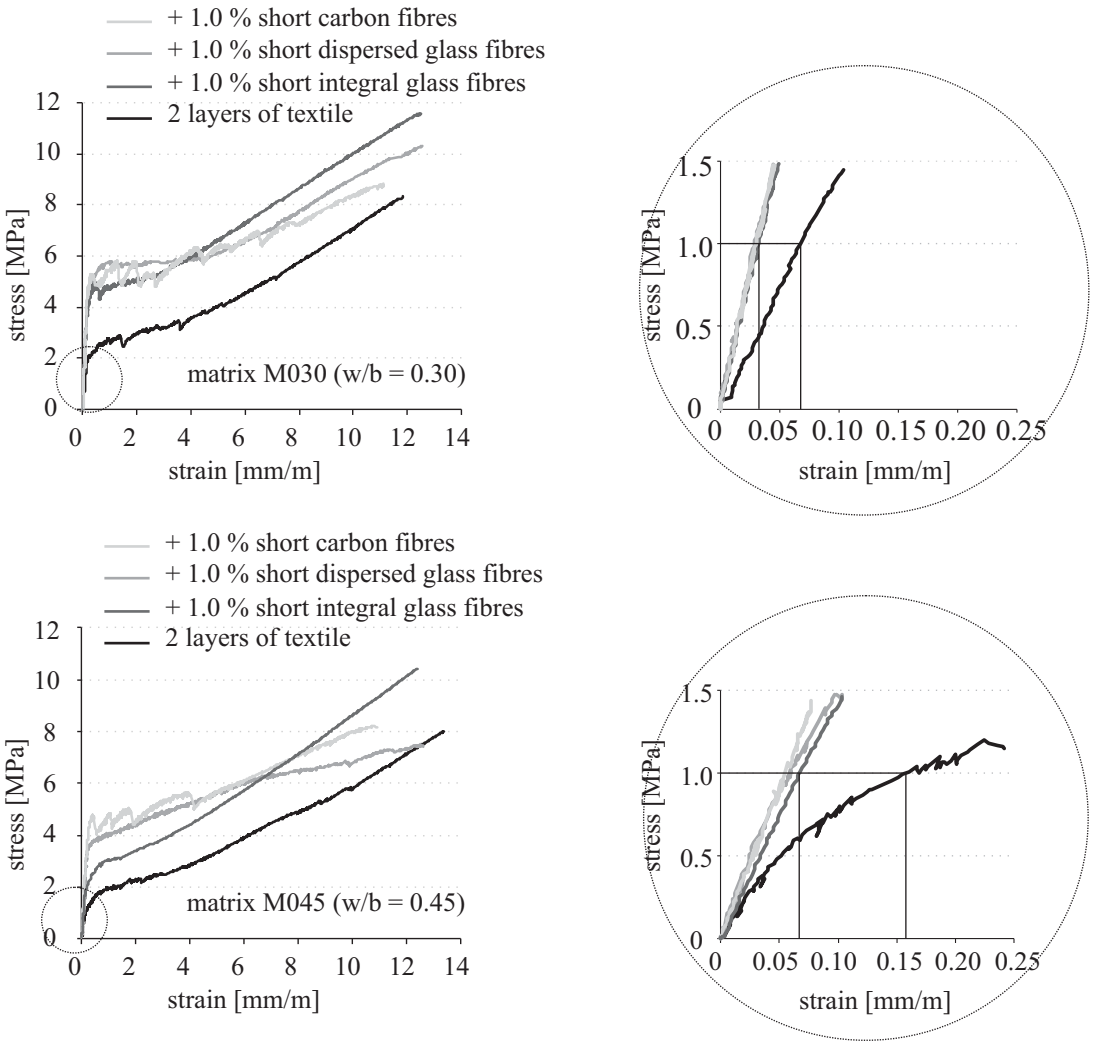

Figure 4.3: Effect of addition of short dispersed glass, integral glass and carbon fibres on slope of crack-free state of TRC plates subjected to tensile loading; M030 (above) and M045 (below)

4.1.3 Influence of short fibres on crack formation and crack pattern

The addition of short fibres led to the expansion of the strain region where multiple cracks form (state IIa, cf. Figure 2.4). This hold true for all parameters combinations with both matrices, see Figure 4.2. As shown in the curves and pointed out with the help of the double-arrows, the effect of integral glass fibres is less pronounced than the other two types of dispersed fibres (glass or carbon). This expansion was particularly pronounced in the case of the TRC with short

carbon fibres: The width of this region, i.e., strain span, more than doubled for the TRC made both with M030 and M045 matrices, see Figure 4.2.

The observation of the specimens' surfaces showed that this widening resulted from the formation of larger numbers of cracks. To emphasize, observably for the same strain level the TRC specimens with short fibre, especially when dispersed, always exhibited a higher number of cracks and a smaller crack distance in comparison to the TRC specimens without short fibre. Figure 4.4 shows examples of crack patterns observed at a strain level of approximately 10 mm/m formed on the surface of specimens reinforced with 2 layers of textile with and without the addition of short integral glass, dispersed glass and carbon fibres. In case of TRC specimens with the addition of short carbon fibres (and due to the large amount of fibres), the cracks on the surface were hardly recognizable to a digital camera even with high resolution. It can be also traced back to the dark color of the specimen coming from the fibre, cf. Figure 4.4. Different crack patterns for other parameters combinations are presented in Appendix C.

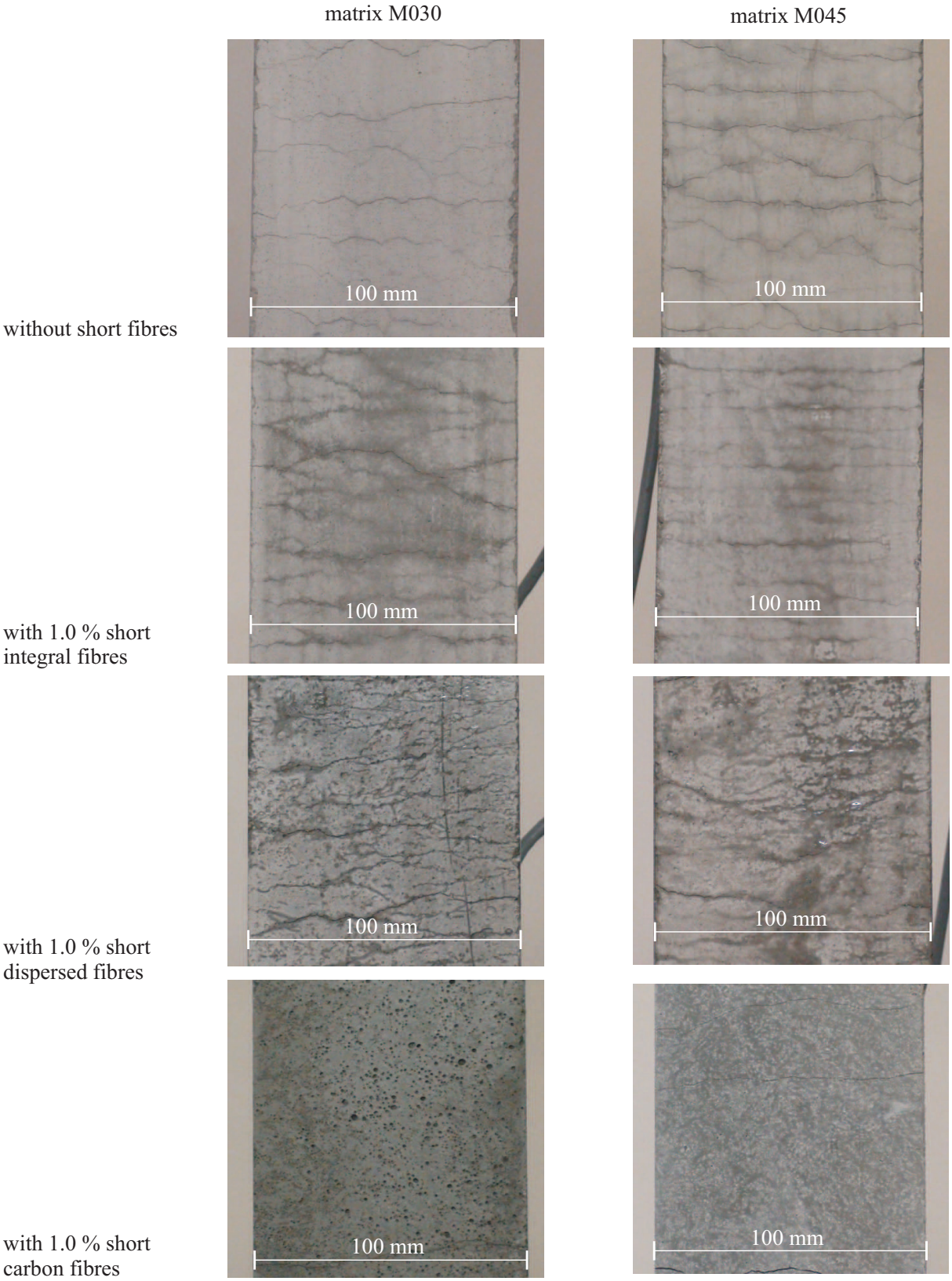

Figure 4.4: Effect of short integral glass, dispersed glass and carbon fibres on crack patterns on specimen' surface; TRC plates (two layers of textile) with matrix M030 (left) and M045 (right) at strain level of approximately 10 mm/m

4.1.4 Influence on short fibres on tensile strength and energy dissipation

The positive influence of short fibres on the mechanical performance of TRC was clearly noticeable along the entire course of stress-strain curves. However, with increasing stress and strain levels, the advantage of the addition of short dispersed fibre began to diminish, so that only a very moderate increase in the tensile strength of the composite could be recorded due to the addition of short dispersed fibres. Similar tendencies were obtained for TRC specimens made with both matrices, M030 and M045. The addition of short, dispersed glass and carbon fibres led to an increase in tensile strength of 1.35 and 0.47 MPa, respectively, for the TRC specimens made with matrix M030. An average increase by 0.21 MPa for TRC plates with short dispersed glass fibres and 0.84 MPa for those with short carbon fibres was recorded for specimens made of the matrix M045, cf. Table 4.1. At the moment of TRC failure the stress-strain curves for the plates with added short dispersed fibres and for the specimen without short fibres approached each other closely, cf. Figure 4.2. This phenomenon arises most likely out of an increase in the number of ruptured short fibres, corresponding to increasing stress level and progressive crack opening. In contrast, integral fibres remain active up to relatively high strain levels. The tensile strength of the composite was significantly enhanced by the addition of short integral fibres. An average increase of the tensile strength value by more than 2.4 MPa and 2.2 MPa was achieved due to the addition of short integral glass fibres to TRC plates made with matrices M030 and M045, respectively.

Moreover, since the stress-strain curves for TRC with short fibre are always above the corresponding curves for TRC without short fibre, it can be concluded that the area under the stress-strain curve, i.e. the energy dissipated when TRC with short fibres is subjected to tensile loading, increases noticeably in comparison to TRC without short fibres. The increase of the work-to-fracture due to the addition of short fibres to the TRC made of the matrix M030 was relatively high: approximately 44 %, 36 %, and 34 % due to the addition of short dispersed glass, integral glass and carbon fibres, resectively. The increase in the work-to-fracture was less pronounced for specimens made with the matrix M045: 11 % for TRC specimens with short dispersed glass fibres, 14 % for those with short integral fibres and 26 % for TRC specimens with short carbon fibres; cf. Table 4.1.

As a measure of energy absorption the term “work-to-fracture” is purposefully used in this thesis instead of the common terms used in describing the mechanical characteristics of fracture, i.e., ’fracture toughness’ or ’fracture energy’. The values of this parameter were determined by the area under the complete force-deformation curves. The reason for this choice of terminology is because of the formation of multiple cracks in the case of TRC, where all contribute to energy absorption by the composite. Work-to-fracture thus strongly depends on the specimens’ length, which is not the case if fracture toughness or fracture energy is under consideration. The latter two characterise the mechanical behaviour of material fracture with only one macroscopic crack. The reader should note that although only one visible crack was formed in the specimens made of plain matrix or concrete matrix reinforced with short fibres (no textile reinforcement), work-to-fracture was still chosen as a characteristic to describe the fracture behaviour of these materials (see Table 4.3 in Section 4.1.2), so that the results obtained from the tests on specimens with and without textile reinforcement could be compared directly.

In order to illustrate the effect of short fibres on work-to-fracture more clearly, Figure 4.5 shows the increase of the energy dissipation as the hatched area between representative curves for TRC with and without dispersed carbon fibres. It can be observed from these curves that a particularly dramatic improvement with respect to energy dissipation can be asserted at relatively small strain

levels (up to 4 mm/m). This region of moderate strains is of particular interest with respect to the structural design.

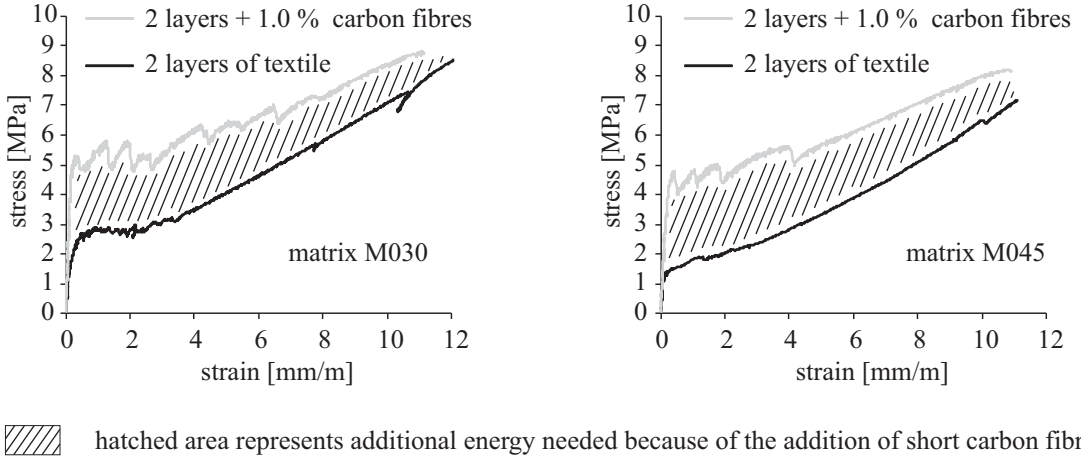

Figure 4.5: Increase in energy dissipation due to the addition of short fibre; the diagrams show characteristic stress-strain curves of TRC with and without the addition of short carbon fibre for specimens made with the matrices M030 (left) and M045 (right)

4.1.5 Discussion of the test results obtained from TRC specimens with and without short fibres

The improvement in the level of first-crack stress of TRC due to the addition of short fibres as observed in the tensile tests on plate specimens (see Section 4.1.2) can be likely ascribed to four main mechanisms:

- The bridging of micro-cracks by fine, well distributed short fibres inhibits the growth of such cracks and subsequently the forming of the first macro-crack. Thus, higher stress is needed to induce the transition from micro-cracking to macro-cracking.
- Well distributed short fibres arrest the extension of micro-cracks to other micro-cracks and thus hinder their merging and uniting to form a macro-crack.
- The addition of short fibres reduces the shrinkage of the matrix and, hence, reduces the resulting internal damage in the finely grained concrete. Additionally, short fibres arrest micro-cracks which develop due to shrinkage (cf. also the previous two points). This might be one of the explanations of the increase in stiffness due to the addition of short fibres (cf. Figure 4.3). However, deeper investigation of this mechanism should be performed in order to provide relevant details concerning this phenomena.
- As a consequence of the addition of short fibres, the overall degree of reinforcement increases. Since the strength and stiffness of these fibre reinforcements are considerably higher than those of the corresponding material parameters of the matrix, the strength of the crack-free composite, i.e., the first-crack stress value, must – according to the theory of composite materials – increase with an increasing degree of fibre reinforcement, provided that the bond between fibre and matrix is good.

In comparison to short integral fibres, short dispersed fibres have proven themselves to be significantly more efficient with regard to the increase of first-crack stress, see Figure 4.2 and

Table 4.1. This can be traced back to the notion that dispersed fibres are much more numerous and much more finely distributed in the matrix and, thus, better able to bridge both micro-cracks and very fine defects. In contrast, the integral fibres appear as pronounced "concentrations" of mono-filaments at particular spots, which limits their bridging capability, see Figure 4.6.

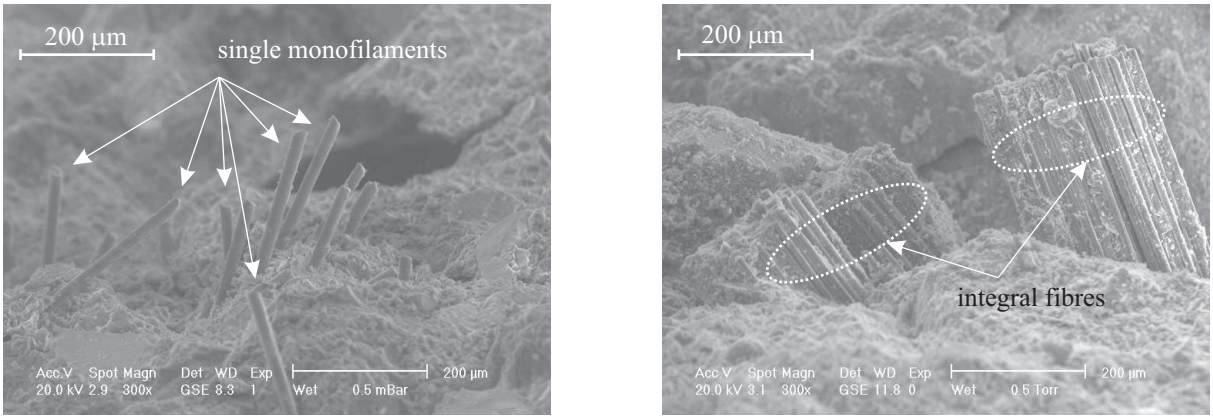

Figure 4.6: Microscopic images of the fracture surfaces of TRC with addition of short dispersed (left) and short integral (right) glass fibres to the matrix M030

Moreover, according to the results shown in Figure 4.2 and Table 4.1, a more pronounced enhancement in first-crack stress was achieved by the addition of carbon fibres. The explanation may be quite straightforward since carbon fibre has both a higher tensile strength and greater stiffness in comparison to AR glass fibre. In addition, short carbon fibre has a smaller diameter as compared to the short glass fibre (nearly one-third, cf. Table 3.3 and Figure 3.3 in Section 3.1.3). For the same amount (by volume) of fibres, the smaller diameter means a larger quantity of short fibres and thus much finer distribution over the volume of the matrix and larger matrix-fibre bond surface area. Thus, the carbon fibre used in this study is likely to influence all four of the above-suggested mechanisms for enhanced first-crack stress positively, and to a higher extent than the AR glass fibre. The superior behaviour of carbon fibres might be even more pronounced if carbon fibres would exhibit similarly effective bonds to cement-based matrices as glass fibres exhibit; see as an example Scheffler et al. [47].

Results showed, as well, that short dispersed fibres (glass and carbon) are more effective in improving the behaviour of TRC at relatively low strain levels (up to approximately 4 mm/m) than short integral fibres. The small diameter of short dispersed fibres and their marked slenderness help to establish a very good bond to the matrix, which in turn helps already in activating the dispersed fibre by the growth of the tiniest defects, while short integral fibres have a relatively large diameter, and herewith a lower surface-to-cross-section ratio. At low deformations or crack openings only sleeve (outer) filaments of the integral fibres are activated. The core (inner) filaments become active only at higher deformations, especially when the outer filaments start to fail and the pullout of inner filaments can be observed.

The visual inspection of the TRC specimens' surfaces showed that the expansion of the strain region where multiple cracks form can be traced back to a higher number of cracks in the specimens with short fibres. Four possible mechanisms can be assumed to be fundamental to such behaviour:

- Reaching higher first-crack stress levels in the tests on the TRC specimens with the addition of short fibre leads to the formation of a greater number of micro-cracks over the entire specimen volume or length, even prior to development of the first macro-crack. Beginning with first-crack stress, macro-cracks develop from these micro-cracks. A greater number of finely distributed micro-cracks offers more nuclei for macro-cracks formation, leading to more pronounced multiple cracking.

- The formation of a macro-crack results in a decrease in matrix stress in the vicinity of the crack. The next crack may not form at a distance below a threshold value; cf. Figure 4.7 (left). Bridging macro-cracks with short fibres causes additional stress transfer over fine macro-cracks. This results in a less pronounced relaxation of the matrix in the cracks' vicinity, as schematically shown in Figure 4.7 (right). The next crack may, therefore, form at a smaller distance from an existing crack; thus more pronounced multiple cracking can develop.

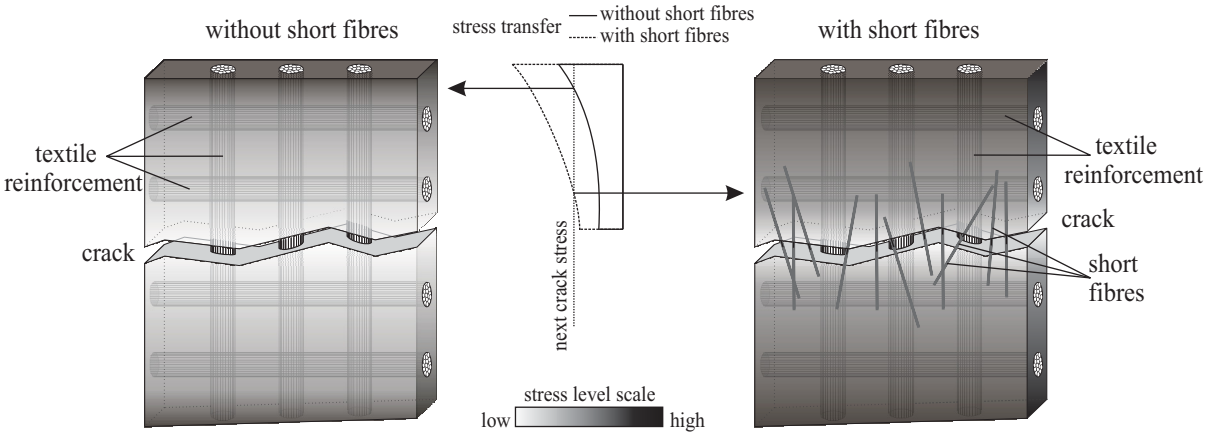

Figure 4.7: Stress distribution in the matrix in the vicinity of a macro-crack in TRC without short fibres (left) and with the addition of short fibres (right)

- As it is shown in Figure 4.2 the formation of these multiple-cracks for TRC specimens with short fibres took place at higher stress levels than those for TRC without short fibres. Moreover, the number of cracks is higher and the cracks are finer in the specimens with short fibres, cf. Figure 4.4. These could be due to extra improvement in bond between multifilament-yarn and surrounding matrix when short fibres are added.

- Previous investigations on TRC without the addition of short fibre (e.g., Butler et al. [21]) showed that the bond between filaments and cementitious matrix is non-uniform over the length of yarn. The hydration products form adhesive cross-links between matrix and filament, as shown in Figure 4.8 (left). The bonding properties of the cross-links depend on the characteristics of the hydration products, which are influenced by the matrix, the filament-sizing, and the condition and duration of hydration. Details on the cross-link model are given by Butler et al. [51]. It is assumed at this stage of the investigation that short fibres can improve the bond between multifilament yarn and surrounding matrix by means of new, additional cross-links. By their random dispersion in the matrix and their positioning on the yarn surface, short fibres provide extra connecting points to the surrounding matrix. This leads to better yarn-matrix bonding and less matrix relaxation in the vicinity of the crack, and so more and finer cracks will form. Figure 4.8 (right) presents this schematically. This phenomenon is discussed in more details in Section 4.3.1.

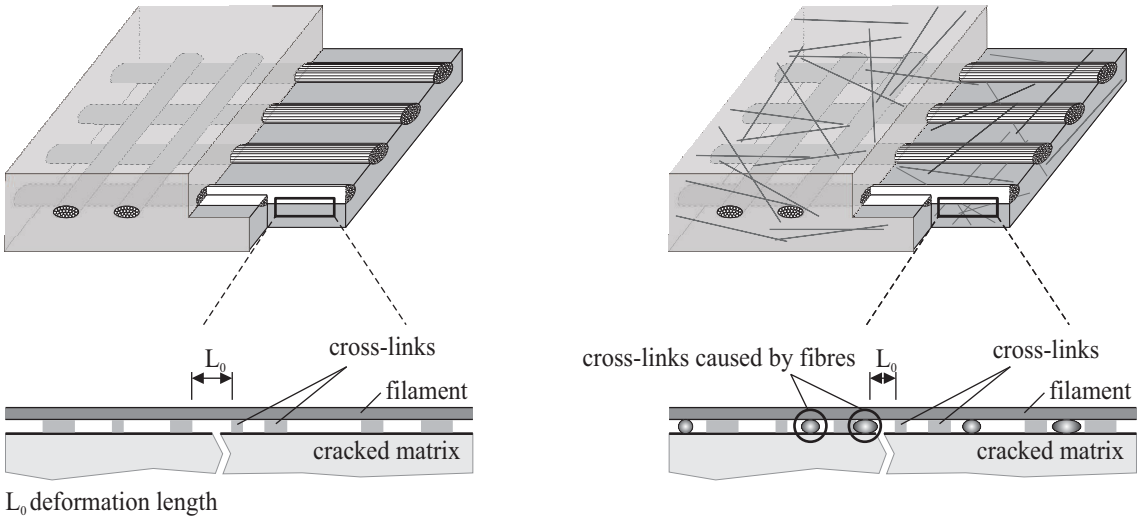

Figure 4.8: Cross-link model for TRC: without short fibres (left) and with short fibres (right)

The failure probability of short dispersed fibres increases steadily with increased loading and crack opening. It appears that the great majority, if not all, of the dispersed fibres fail long before the tensile strength of the composite is reached. In contrast, integral fibres remain "active" at high deformations, which explains the increase in the tensile strength of the composite when short integral glass fibres are added to TRC, see Table 4.1.

By comparing the results obtained from both matrices it can be noticed that while higher first-crack stresses and tensile strength values were achieved when matrix M030 (w/b = 0.30) was used, the enhancement due to the addition of short fibres was mostly more pronounced in the specimens made with matrix M045 (w/b = 0.45).

At this stage due to the quite wide range of parameter combinations, the need for further experiments becomes evident for an understanding of the mechanisms and in providing explanations of the phenomena observed in the uniaxial tensile tests.

Better understanding of crack-bridging mechanisms, stress transfer, bond behaviour between short fibres and finely grained concrete as well as between yarn surface and the surrounding matrix was necessary. Moreover, information regarding the effect of individual parameters was of high importance to provide detailed insights into the various failure mechanisms observed in the experiments.

In order to gain more and better insight into the specific material behaviour of the finely grained concrete with such hybrid reinforcement, in addition to uniaxial tension tests, seen as tests at the macro-level of observation, on plates reinforced with only short fibres, tests at meso- and micro-level of observation, specifically, multifilament-yarn and single-fibre pullout tests, respectively, were performed. The purpose was to provide deeper knowledge on the effect of water-to-binder ratio on the bond and fracture of fibres, the mechanisms in the joint action of short fibre and textile reinforcement and on the effect of short fibre orientation on the fracture behaviour.

It is worthy of note here that: (1) although only one macro-crack is formed in the specimens made of plain concrete or concrete with short fibres, these uniaxial tensile tests are considered as tests at the macro-level of observation, and (2) multifilament-yarn pullout tests are considered

as tests at the meso-level of observation, even though they deal with the pullout of only one multifilament-yarn.

4.2 Contribution of the components of TRC to its behaviour under uniaxial tensile loading

4.2.1 Uniaxial tensile tests – Effect of w/b on macro-level

At the macro-level of observation, experimental investigation using uniaxial tension tests performed on thin, narrow plates unreinforced (plain matrix) and reinforced by: (a) only textile reinforcement, (b) only short fibres and (c) hybrid reinforcement, i.e., textile reinforcement with the addition of short fibres, were carried out. These tests were performed using two different matrices M030 and M045 with water-to-binder ratio of 0.30 and 0.45, respectively.

4.2.1.1 Finely grained concrete – Plain matrix

As expected, because of its high water-to-binder ratio in comparison to matrix M030, matrix M045 exhibited lower strength under tension and compression and lower values of Young's modulus and strain capacity. Table 4.2 gives the mechanical properties for both concretes under investigation. Compressive strength was measured according to DIN 18555 [121]. The tensile strength values for both matrices are below the values which could be expected on the basis of the measured compressive strength values according to, for example, the FIB Model Code [122]. However, the unusually slender shape and great length of the specimens used for the tension tests, micro-cracking due to shrinkage, and some eccentricity during testing should be taken into account. These come together with the brittleness of fine-grained concrete to high sensitivities to possible fine defects and subsequently to a considerable reduction in strength. The relatively low values of Young's modulus result from the absence of large aggregates and a relatively low fine aggregate content, but also probably from shrinkage micro-cracks. Figure 4.9 shows the typical stress-strain curves of both matrices obtained by uniaxial tensile tests. Microscopic investigations of plain concrete showed some difference in the matrix structure, as well. While a more "dense and compact" internal structure was observed for matrix M030, see (Figure 4.10 (left), microscopic images taken the from matrix with the higher water-to-binder ratio, M045, showed a relatively loose micro-structure, cf. Figure 4.10 (right).

Table 4.2: Mechanical properties of finely grained concretes

Concrete	Compressive strength [MPa]	Tensile strength [MPa]	Strain capacity [mm/m]	Young's modulus [MPa]
	Average value (standard deviation)			
M030	62.3 (1.2)	2.16 (0.28)	0.11 (0.01)	18910 (1940)
M045	36.1 (1.0)	1.74 (0.14)	0.10 (0.01)	16790 (270)

4.2.1.2 Specimens with textile reinforcement

The results obtained from specimens with textile reinforcement are already shown in Section 4.1, Figure 4.2. However, the results in this section are illustrated in a different way in order to show the influence of the matrix quality, namely of the water-to-binder ratio, more clearly.

Figure 4.11 shows representative stress-strain curves obtained from uniaxial tension tests performed on TRC plates with and without the addition of short dispersed glass, integral glass, and carbon fibres. The influence of w/b on the stress-strain behaviour of TRC with and without the addition of short fibres is quite obvious since the curves obtained from specimens made with

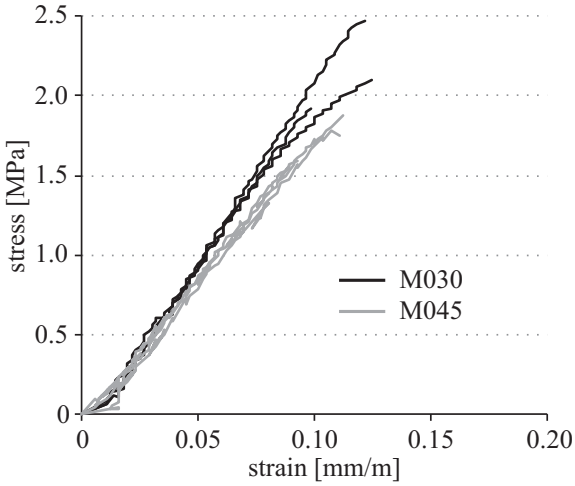

Figure 4.9: Stress-strain curves determined in uniaxial tensile tests for both matrices M030 and M045

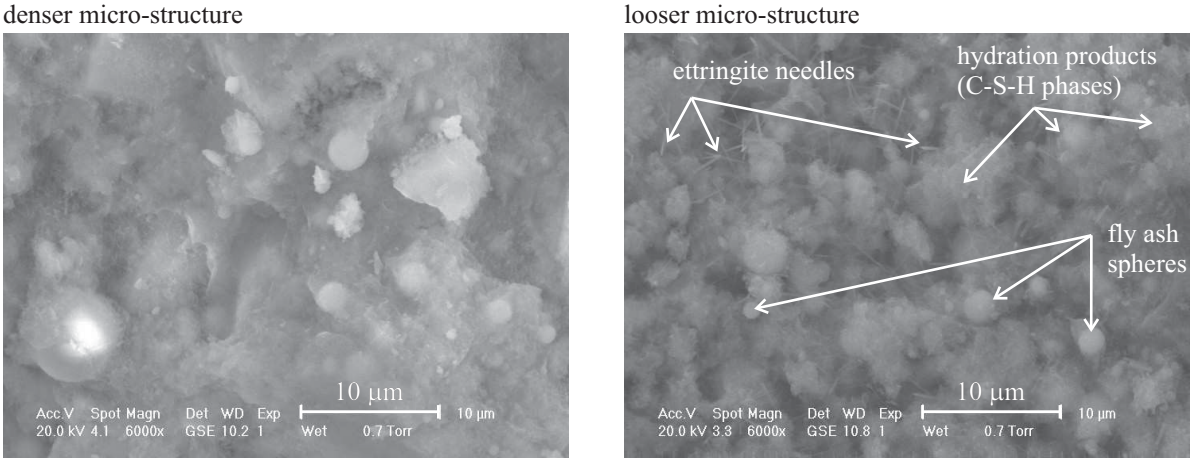

Figure 4.10: ESEM images of micro-structure of both plain matrices: M030 (left) and M045 (right)

matrix M030 are always above those from specimens made with matrix M045. The relatively low water-to-binder ratio of matrix M030 leads to a significant increase in the slope of state I, the crack-free state for all parameter combinations. This finding is obviously traceable to the better fibre-matrix bond when matrix M030 is used. Deeper discussion is presented in Section 4.2.1.3 and Section 4.2.3. The higher stress level over the entire course and the enhancement of tensile strength indicate a higher crack-bridging capability, i.e., higher stress transfer, resulted from the good fibre bond at both sides of the crack when matrix M030 is used, see also Section 4.2.2. Furthermore, it can be observed from the curves that the degree of enhancement of the TRC behaviour resulted from the addition of short fibres varies depending on the matrix used (cf. Table 4.1). This phenomenon is discussed in Section 4.3.

4.2.1.3 Specimens reinforced by short fibres only

Figures 4.12 and 4.13 present the results of uniaxial tension tests performed on rectangular plates without textile reinforcement. The curves were obtained for the matrices M030 and M045 with and without the addition of two different proportions, 0.5 % and 1.0 % by volume, of short dispersed AR glass and carbon fibres. Additionally, the results for plain matrix are plotted as

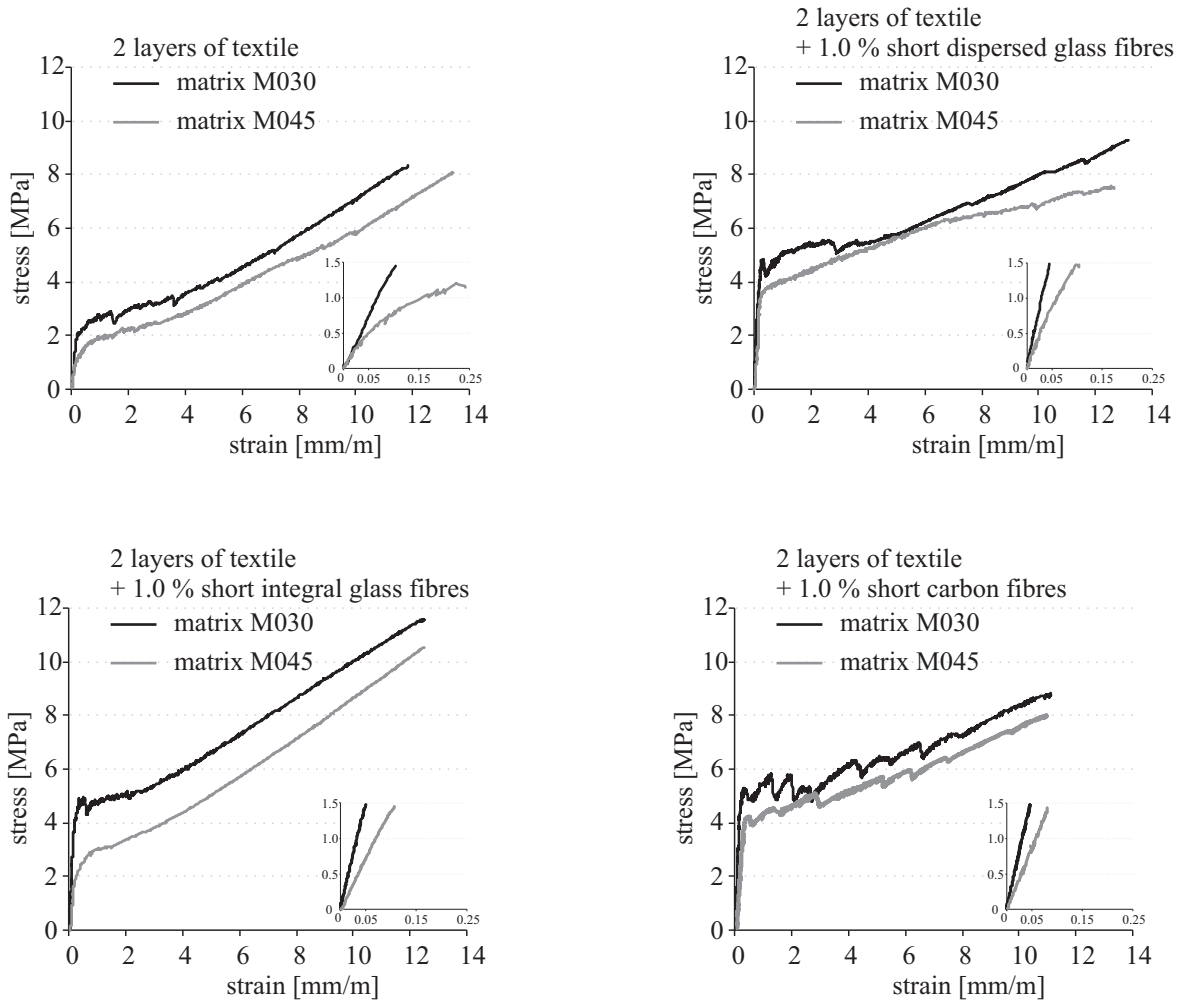

Figure 4.11: Effect of water-to-binder ratio on the stress-strain behaviour of TRC with and without the addition of short dispersed glass, integral glass and carbon fibres; representative curves

a reference. The presentation and discussion of the tests performed on specimens reinforced by short integral glass fibres can be found in Section 4.4.1. For the specimens made with matrix M030 and reinforced with short fibre, a considerable increase in tensile strength could be observed in comparison to the specimens without fibres. This holds true for both types of short fibres used, but it is more obvious in the case of carbon fibre: The value increased by factor of 1.5 due to the addition of glass fibres and up to a factor of 2.7 for the specimens with the addition of 1.0 % of carbon fibres; see Table 4.3. In contrast, only a relatively moderate improvement in tensile strength, by a factor of 1.4, was recorded for the specimens made with the matrix M045 due to the addition of carbon fibre. In the case of the addition of glass fibre still less improvement could be noted, see Table 4.3.

These findings can be traced back to the effect of w/b on the quality of the fibre-matrix bond; clearly the denser matrix M030 is more conducive to better bonding than the matrix M045 with a higher water-to-binder ratio. This means that the fibre embedded in the matrix M030 can contribute to a great extent to the bearing of stress in the ascending branch of the stress-strain curve. This provides as well an explanation of the pronounced difference in stiffness before the formation of the first crack between specimens made with matrix M030 and M045

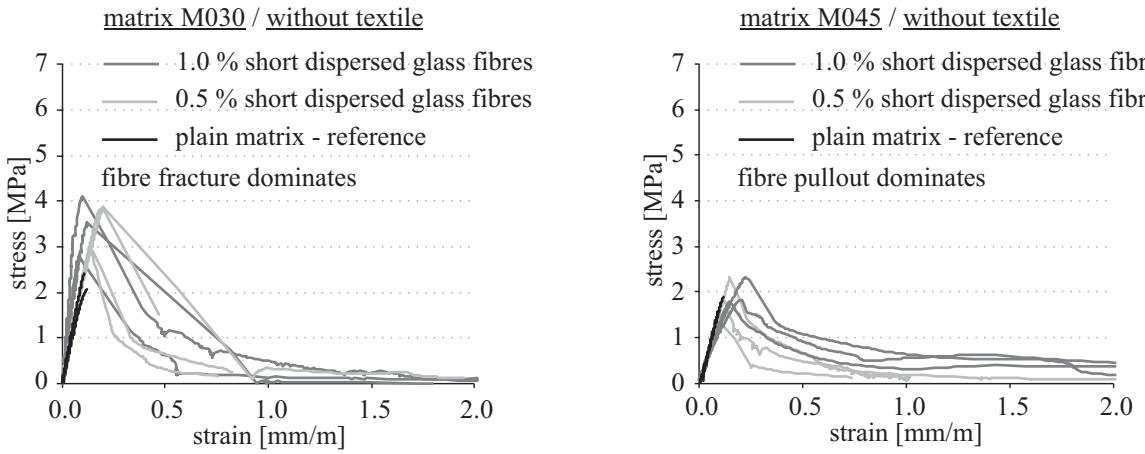

Figure 4.12: Results of tension tests on plates reinforced with 1.0 % by volume of short dispersed glass fibres for the specimens made with matrix M030 (left) and M045 (right)

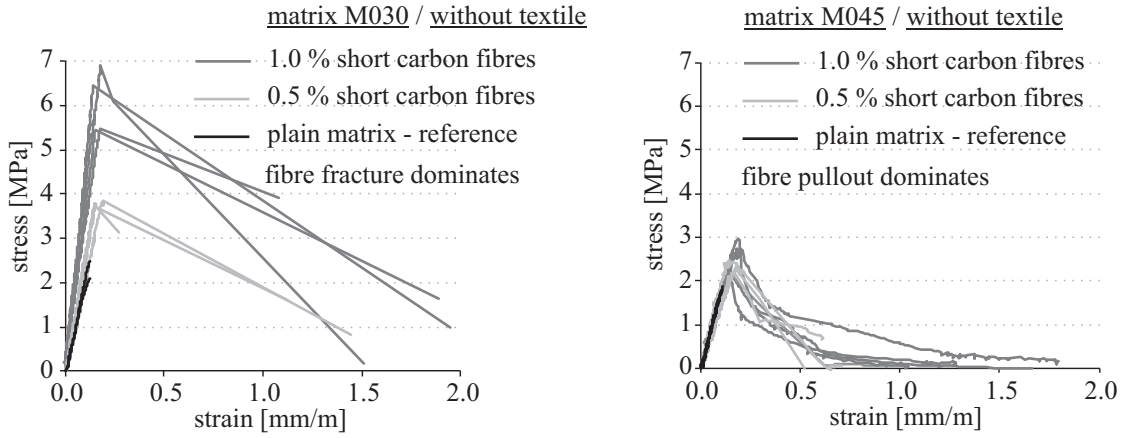

Figure 4.13: Results of tension tests on plates reinforced by 1.0 % by volume of short dispersed carbon fibres for the specimens made with matrix M030 (left) and M045 (right)

in comparison to the moderate difference for the reference specimens without short fibres, cf. Figure 4.9.

The extent of this contribution is limited by the tensile strength of the fibre and the fibre content. The very high tensile strength and high stiffness of the carbon fibres, with the good fibre-matrix bond provided when the matrix M030 is used, explain to a great extent the more pronounced enhancement when these fibres are added (Figure 4.13 left) in comparison to short glass fibres. As is explained later in this section, the weak fibre-matrix bond and the resulting defects in the micro-structure when the matrix M045 is used limit this improvement, even when short carbon fibres are added (Figure 4.13 right). Furthermore, the distribution and orientation of short fibre are also of high importance from the perspective of the findings presented; see also Section 4.4.

It should be also kept in mind that with increasing content of short fibre the workability becomes worse and that such concrete was likely to have more voids due to entrapped air; see also Section 3.2.1 and Section 3.2.2. Density values of both matrices with and without the addition of 1.0 % by volume of short fibres were measured in order to proof the resulting higher porosity when short fibres are added. Table 4.4 confirms the lower density values of the mixtures with the addition of short fibre in comparision with those obtained from mixtures without short fibres.

Table 4.3: Mechanical characteristics of concrete specimens with and without the addition of 0.5 % and 1.0 % by volume of short dispersed glass and carbon fibres (no textile reinforcement)

Matrix	Fibre reinforcement	Tensile strength [MPa]	Strain at tensile strength [mm/m]	Young's modulus [MPa]	Work-to-fracture [kN mm]
		Average value (standard deviation)			
M030	–	2.16 (0.28)	0.11 (0.01)	18910 (1940)	0.04 (0.01)[a]
	+ 0.5 % dispersed glass	3.41 (0.53)	0.16 (0.04)	21770 (820)	0.54 (0.26)
	+ 1.0 % dispersed glass	3.41 (0.76)	0.15 (0.06)	37500 (5000)	0.52 (0.16)
	+ 0.5 % dispersed carbon	3.82 (0.09)	0.16 (0.03)	23720 (2600)	1.17 (0.05)[b]
	+ 1.0 % dispersed carbon	5.84 (0.48)	0.17 (0.04)	40260 (5300)	2.06 (0.30)[b]
M045	–	1.75 (0.14)	0.10 (0.01)	16790 (270)	0.03 (0.01)[a]
	+ 0.5 % dispersed glass	1.82 (0.50)	0.12 (0.02)	15150 (1870)	0.21 (0.08)
	+ 1.0 % dispersed glass	1.98 (0.30)	0.18 (0.04)	12720 (1430)	0.49 (0.09)
	+ 0.5 % dispersed carbon	2.43 (0.20)	0.15 (0.02)	15270 (1800)	0.34 (0.07)
	+ 1.0 % dispersed carbon	2.46 (0.38)	0.16 (0.02)	16180 (1100)	0.32 (0.10)

[a] No softening could be observed, see Figure 4.9; therefore, only the area under the ascending branch of the force-displacement curve was used to calculate work-to-fracture

[b] The behaviour in the softening regime was not stable; therefore, softening branch was considered to be linear

This holds true for both matrices M030 and M045. For increased additions of fibre it is more difficult to achieve an even fibre distribution over the volume of the matrix. These aspects explain to some degree the fact that increasing the content of fibres beyond 0.5 % by volume did not improve the tensile strength of the composite; see also Table 4.3. This does not hold true for the specimens made with matrix M030 when the content of carbon fibres was increased to 1.0 % by volume; here an enhancement in the tensile strength by factor of 1.5 was achieved due to the increase of carbon fibre from 0.5 % to 1.0 % by volume, cf. Table 4.3. This might be a result of the distinct efficiency of the combination of such very high-strength fibres with an effective bond to the surrounding matrix.

The stiffness of the composites was improved when matrix M030 was used, cf. Figure 4.12 (left) and Figure 4.13 (left), most probably due to the good fibre-matrix bond and mitigation of the development of micro-cracks due to shrinkage. The average value of Young's modulus was improved by a factor of 1.25 due to the addition of 0.5 % by volume of short fibres and approximately by a factor of 2 for the specimens with the addition of 1.0 % by volume short fibres, cf. Table 4.3. This holds true for both dispersed glass and carbon fibres. In contrast, fibres with weak bonds to the matrix can be considered as defects, which leads, most likely in concert with extra air voids, even to some decrease in matrix stiffness, as shown in Figure 4.12 (right). The average value of Young's modulus of specimens made with matrix M045 decreased from 16790 MPa to 15150 MPa and 12720 MPa due to the addition of 0.5 % and 1.0 % by volume of glass dispersed fibres, respectively. This was less pronounced when carbon fibres were added

to the matrix M045. Table 4.3 substantiates these findings quantitatively; here the values of tensile strength and the corresponding strain values can be compared for the different parameter combinations.

Table 4.4: Density of the matrices M030 and M045 both with and without the addition of 1.0 % by volume of various types of short fibres

Type of specimens	Density [g/cm^3]	
	Average value (standard deviation)	
	Matrix M030	Matrix M045
Plain matrix	2.039 (0.009)	1.945 (0.006)
With 0.5 % short integral glass fibres	2.018 (0.004)	1.919 (0.003)
With 1.0 % short integral glass fibres	2.011 (0.009)	1.904 (0.003)
With 0.5 % short dispersed carbon fibres	1.950 (0.012)	1.880 (0.011)
With 1.0 % short dispersed carbon fibres	1.928 (0.005)	1.843 (0.003)
With 0.5 % short dispersed glass fibres	1.940 (0.009)	1.855 (0.006)
With 1.0 % short dispersed glass fibres	1.923 (0.010)	1.813 (0.009)

The water-to-binder ratio of the matrix, i.e., the quality of fibre-matrix bond, together with the type of used short fibres determine the behaviour after the formation of the first macro-crack.

The shapes of the descending branches of the stress-strain relationships measured for the compositions based on the matrix M030 indicate that most of the fibres fail at a stress level corresponding to the tensile strength of the composite. Almost no stress transfer can occur afterward; there is sudden, brittle failure, see Figures 4.12 (left) and 4.13 (left). Optical investigation of the fracture surfaces confirms the hypothesis that such behaviour is due to the failure of the great majority of fibres. In contrast, for matrix M045 pronounced fibre pullout behaviour was observed with only moderate fibre fracture, cf. Figures 4.12 (right) and 4.13 (right), obviously due to the weaker matrix-fibre bond resulting from a higher water-to-binder ratio. Accordingly, the contribution of the fibres to the stress-bearing of the composite prior to crack opening is very moderate. However, the descending branches show a much more stable course, i.e., a gradual decrease in stress level with increasing strain, or actually, crack opening, in comparison to the curves obtained for the specimens made with the matrix M030 (cf. Figures 4.12 and 4.13). In the latter case, the apparent linear descending branch does not show real material behaviour but results from the abrupt failure and related difficulties in the steering of the test and data recording. The optical investigation of the fracture surfaces confirms these findings. The very few numbers of fibres observed on the fracture surface when the matrix with a relatively low water-to-binder ratio (w/b = 0.30) is used indicates the strong bond between matrix and fibre, and so, no pullout of fibres can be observed, i.e., the fibres break, cf. Figure 4.14 (left). With w/b = 0.45 pullout of the fibres dominates the behaviour, the result of a weaker matrix-fibre bonding, and a considerable number of unruptured fibres could be observed on the fracture surface as a result of fibre pullout as shown in Figure 4.14 (right).

It should be noted that for specimens made with matrix M030 and the addition of carbon fibres only one stress-to-strain value could be measured in the softening regime. This is explained by the brittleness of the material, the high specimen length, and the resulting, well-known snap-back effect. Hence, the softening branches for these specimens were approximated as linear, cf. Figure 4.13 (left). The author is aware that such estimations of the descending branch and the resulting work-to-fracture values are very vague and likely overestimated, but he decided that it

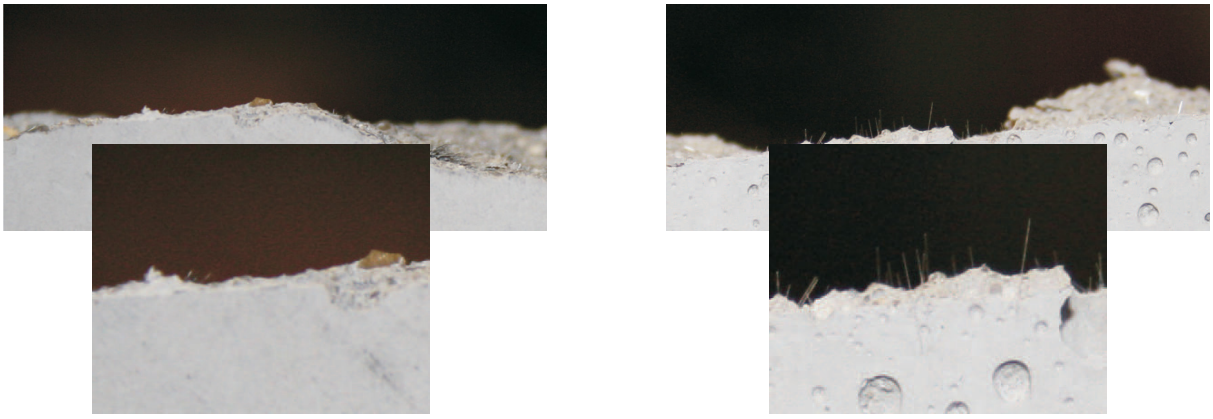

Figure 4.14: Fracture surfaces of plates with addition of short dispersed glass fibres: matrices M030 (left) and M045 (right)

is still meaningful to use these estimations at least for very rough comparisons of the softening behaviour of the types of TRC under investigation.

4.2.2 Multifilament-yarn pullout tests – Effect of w/b on meso-level

The influence of water-to-binder ratio on the pullout behaviour of multifilament-yarns is illustrated in Figure 4.15. For the peak points the values of force and displacement at the peak load were used, while for the final points the force values at a displacement of 0.5 mm were recorded. Since no significant influence was noticeable with large deformations, only the force values up to a displacement of 0.5 mm were taken. It is clear from the curves that a higher pullout force was needed when matrix M030 was used in comparison to that achieved for matrix M045, see also Table 4.5. This holds true for both cases, with and without the addition of short dispersed glass fibres. An increase in the average pullout force of approximately 46 % was achieved for the specimens without the addition of short fibres. The increase was less pronounced for the specimens with the addition of 1.0 % short dispersed glass fibres; approximately 12 %, see Table 4.5. As can be noticed from the values, the difference became considerably smaller for the matrices with short fibres. The discussion of this phenomenon may be found in Section 4.3.1. The presentation and discussion of the multifilament-yarn pullout tests on specimens reinforced with other types of short fibres can be found in that section as well.

Microscopic investigations of the multifilament yarns' surfaces were performed to explain the influence of water-to-binder ratio on the bond between the matrix and yarn surface. ESEM images show a very dense microstructure of the bonding area between the yarn and the matrix M030; a nearly uniform layer of hydration products (C-S-H phases) covers the yarn's surface, indicating a good bond, cf. Figure 4.16 (right). This is not the case when matrix M045 is used; here, hydration products do not cover the yarns' surfaces completely, but only on some areas, with wide gaps between the "islands" of hydration products, cf. Figure 4.16 (left).

4.2.3 Single-fibre pullout tests – Effect of w/b on micro-level

The single-fibre pullout tests, regarded as micro-level tests, confirm the findings presented in the previous sections. Brittle failure of fibres dominated behaviour when matrix M030 was used. Typically, a vertical drop in the force-displacement curves due to fibre breakage was observed after the relatively high ultimate force (up to 0.8 N) was reached, see Figure 4.17 (left). This

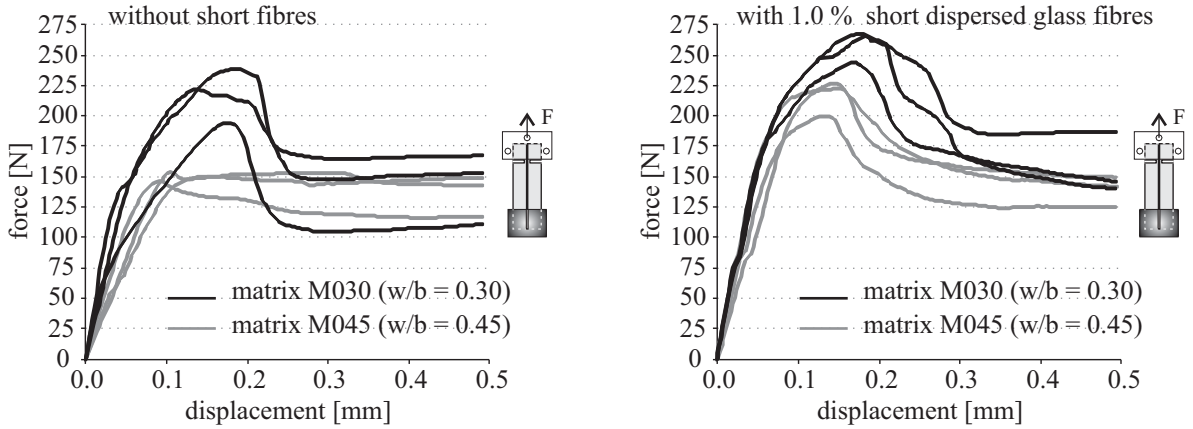

Figure 4.15: Results of multifilament-yarn pullout tests with matrices M030 and M045 without (left) and with (right) the addition of 1.0 % short dispersed glass fibres

Table 4.5: Ultimate force of multifilament-yarn pullout tests for both matrices with and without the addition of various short fibres

Type of specimen	Matrix	Ultimate pullout force [N]	Displacement at ultimate pullout force [mm]
		Average value (standard deviation)	
Without short fibres	M030	215.4 (22.1)	0.17 (0.03)
	M045	147.6 (3.20)	0.19 (0.11)
With 1.0 % dispersed glass fibres	M030	240.5 (26.1)	0.17 (0.02)
	M045	214.0 (14.0)	0.15 (0.01)
With 1.0 % integral glass fibres	M030	360.9 (92.4)	0.12 (0.03)
	M045	266.7 (64.4)	0.15 (0.05)
With 1.0 % dispersed carbon fibres	M030	283.2 (50.2)	0.15 (0.04)
	M045	233.8 (41.9)	0.08 (0.02)

relatively high ultimate force at fibre failure pointed to the good matrix-fibre bond when matrix M030 was used. The ultimate pullout force of the fibres embedded into matrix M045 was much lower; the maximum value reached was approximately 0.3 N. Most of the fibres provided force-displacement relationships with a pronounced softening branch, which indicated fibre pullout, cf. Figure 4.17 (right). The results presented above are valid for the specimens made with the short dispersed glass fibres. Due to their very fine diameter (7 μm) no pullout tests with single carbon fibres were carried out. The results for the pullout of integral glass fibre will be presented in Section 4.4.2.

These results, obtained on the micro-level of observation, show the influence of water-to-binder ratio on the bond between the matrix and single short fibres directly. They agree well with the results obtained from specimens reinforced by short fibres only, at the macro-level of observation; see Figures 4.12 and 4.13.

To corroborate this, the specimens of single-fibre pullout tests were carefully split in the middle and investigated using ESEM. In most of the specimens made with the matrix M030, a part of

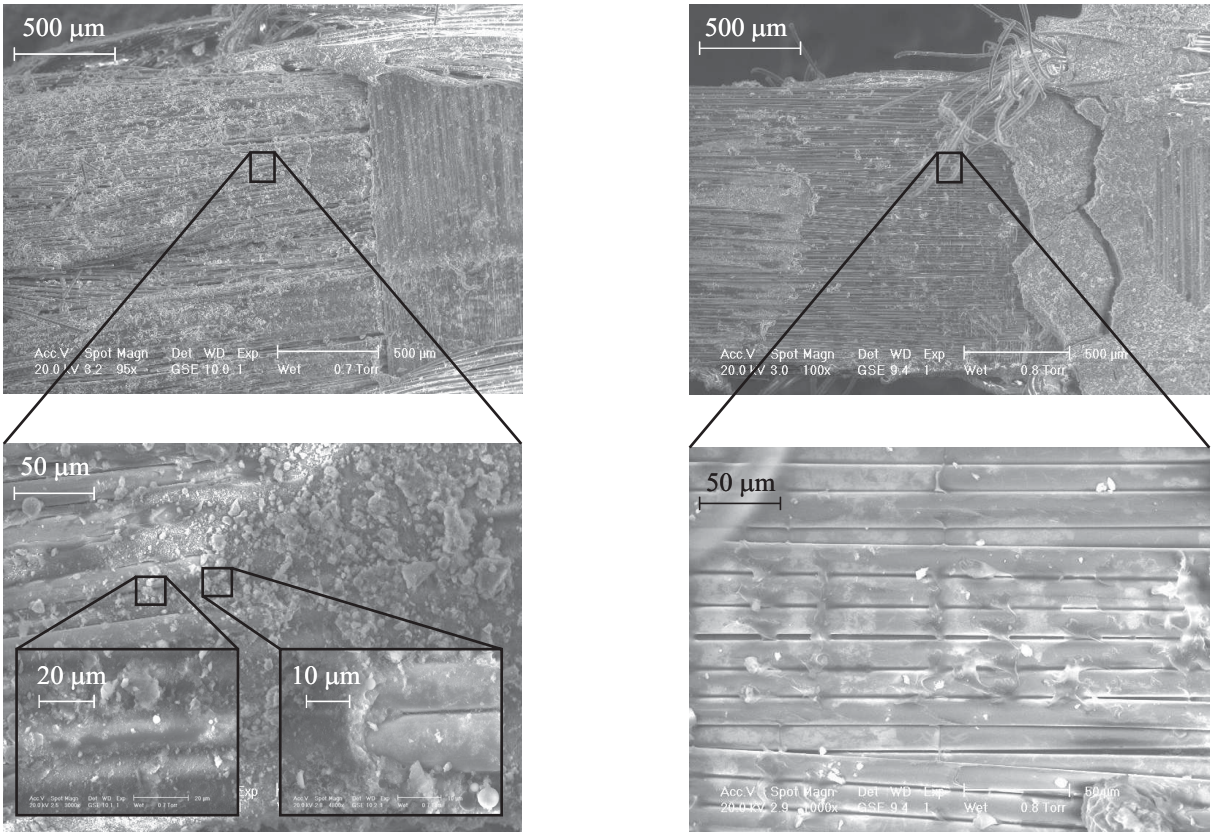

Figure 4.16: ESEM images on multifilament-yarn surfaces in matrix M030 (left) and M045 (right) without short fibres

the fibre was found, i.e., the part remained in the specimen after fibre breakage, see Figure 4.18 (left). In contrast, the empty fibre canal in the cases when matrix M045 was used indicated complete fibre pullout, see Figure 4.18 (right).

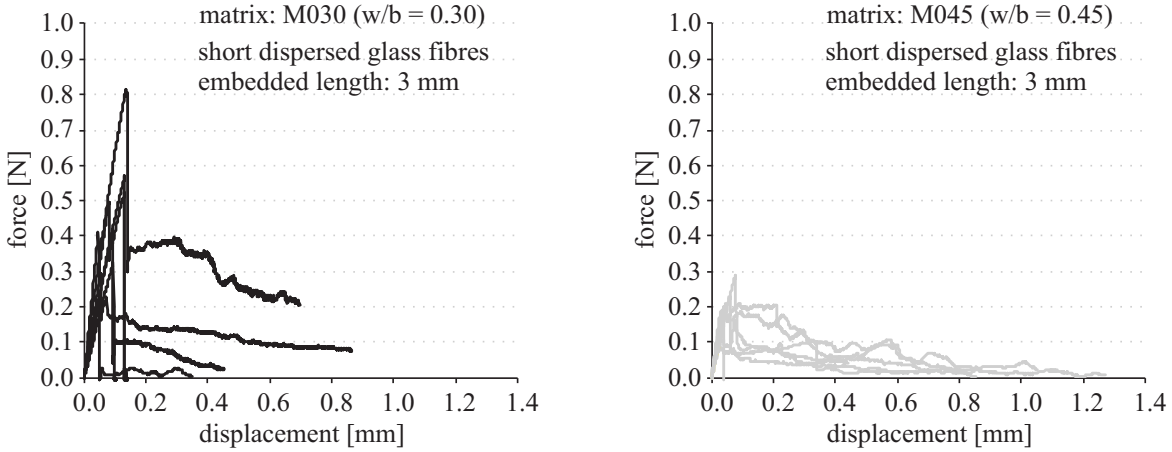

Figure 4.17: Force-displacement curves obtained from the single dispersed glass fibre pullout tests with matrices M030 (left) and M045 (right)

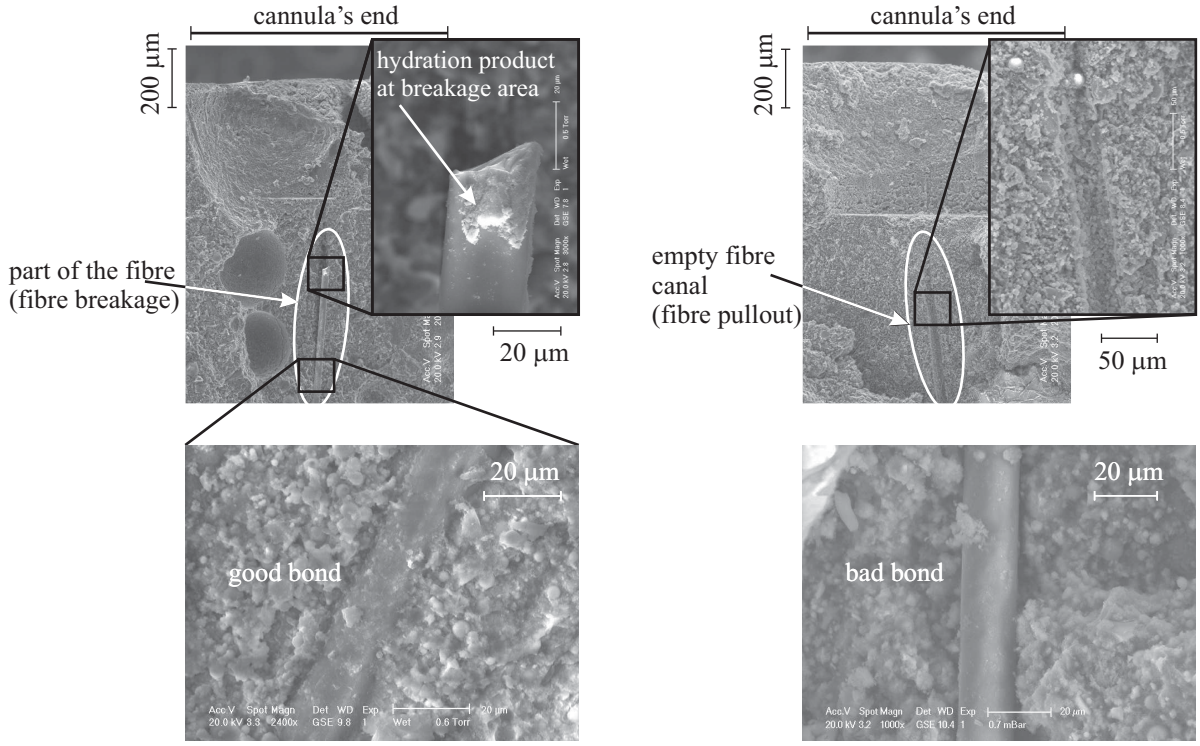

Figure 4.18: ESEM images of split specimens of single dispersed glass fibre pullout tests with matrix M030 (left) and M045 (right)

4.3 Effect of short fibre on yarn-matrix bond

As shown in Section 2.2.6, the bond between filament and cementitious matrix is non-uniform by means of randomly distributed hydration products, see also Figure 2.8 (left). The bond properties between the fibre surface (multifilament-yarn or single fibre) and the surrounding matrix depend on the characteristics of the hydration products, i.e., adhesive cross-links. These cross-links are responsible for the bond and their intensity influences bond quality. The higher the number of adhesive cross-links on the yarn surface, the stronger the bond to the surrounding matrix. In order to grasp the influence of the addition of short fibres on the bond between multifilament-yarn and the surrounding matrix, deeper investigation on the matrix-fibre interface was necessary. The results of this investigation are presented in this section.

4.3.1 Multifilament-yarn pullout tests – Effect of short fibres on meso-level

In order to understand the influence of the short fibre on the bond between multifilament yarns and the surrounding matrix, investigations into the pullout behaviour of multifilament yarns were performed by using the pullout tests described in Section 3.3.2.

Here it is worth pointing out that prior to starting the tests, a crack was initiated through the notched cross-section, cf. Figure 3.9, and a smooth rotational twist was performed at that junction to break short fibres crossing the crack and, thus, minimize their influence on the bridging of the crack, as cf. Figure 4.19; specially when integral fibres were used, which indeed could not be completely broken due to the "smooth twist".

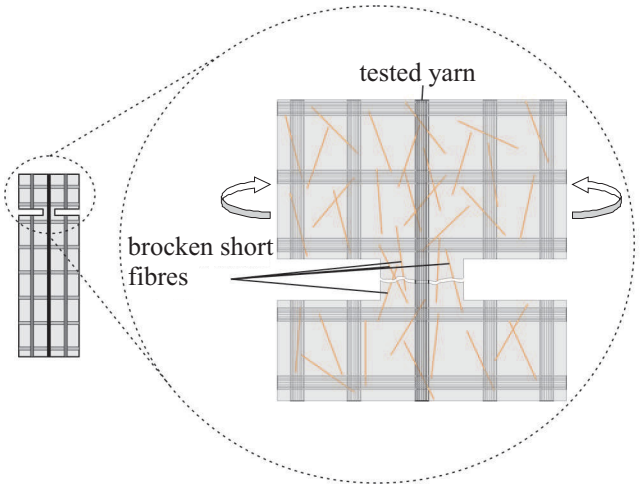

Figure 4.19: A smooth rotational twist at the breaking area to minimize the crack-bridging due to short fibres

Figures 4.20, 4.21 and 4.22 show force-displacement curves obtained for specimens made with the matrices M030 and M045 and the addition of 1.0 % of short dispersed glass, integral glass, and carbon fibres, respectively. Obviously, the addition of short fibres led to a considerably higher ultimate pullout force, which indicated a better bond between yarn and matrix for all investigated parameter combinations; see also Table 4.5.

The increase in the ultimate pullout force was reasonable when short dispersed glass fibres were used: 45 % for the specimens made with the matrix M045 and only approximately 11 % for the specimens made with the matrix M030, cf. Figure 4.20. As shown in Figure 4.22 and listed in

Table 4.5 the addition of short carbon fibres lead to a more distinct increase in ultimate pullout force. Increase in the average pullout force by more than 55 % was achieved for the specimens made with matrix M045 and 30 % for those with matrix M030. With the addition of short integral glass fibres the increase in the average values was much more pronounced, independent of the matrix used, M030 or M045: 67 % when matrix M030 is used and up to 80 % for the specimens made with the matrix M045, cf. Figure 4.21 and Table 4.5.

It is noteworthy that the displacements measured at reaching the ultimate force decreased slightly due to the addition of short, dispersed glass fibre, and more dramatically where short integral glass and dispersed carbon fibre were used. The influence of the addition of short fibres was much less noticeable with large deformations: For displacements of 0.5 mm only little differences could be observed between the courses of the curves for various parameter combinations.

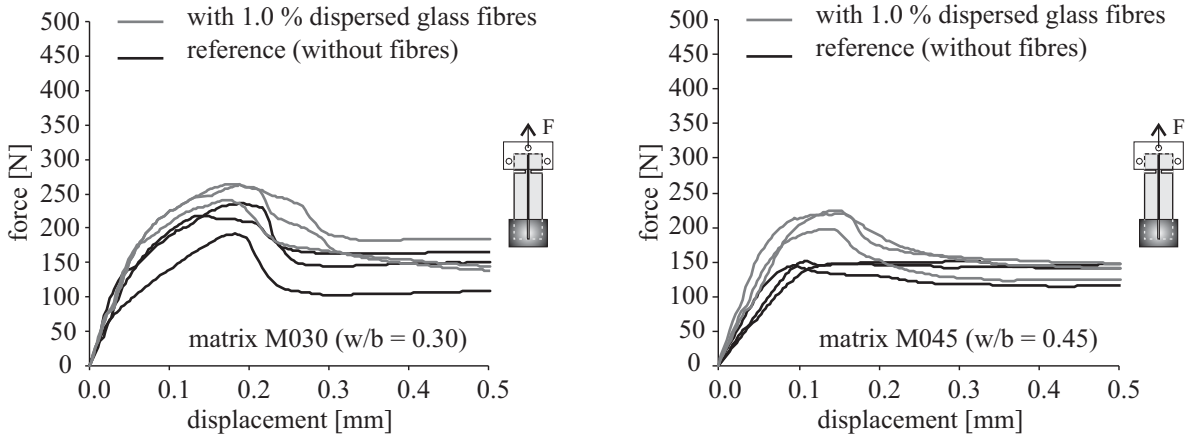

Figure 4.20: Results of multifilament-yarn pullout tests made with and without the addition of 1.0 % short dispersed glass fibres and with the matrix M030 (left) and matrix M045 (right)

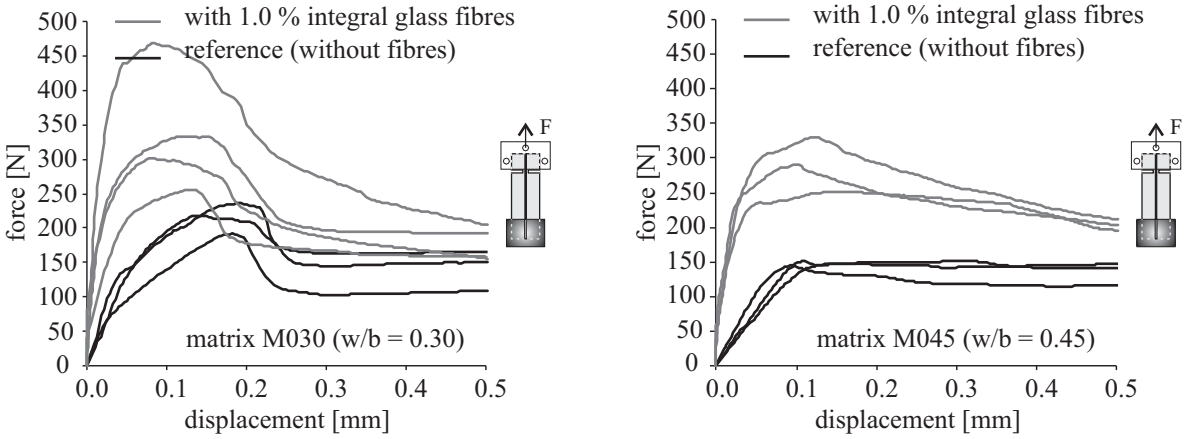

Figure 4.21: Results of multifilament-yarn pullout tests made with and without the addition of 1.0 % short integral glass fibres and with the matrix M030 (left) and matrix M045 (right)

The hypothesis illustrated in Figure 4.8, that the addition of short fibres improves the strength of the bond between the multifilament-yarns and matrix can be one of the straightforward explanations of the results obtained in these tests.

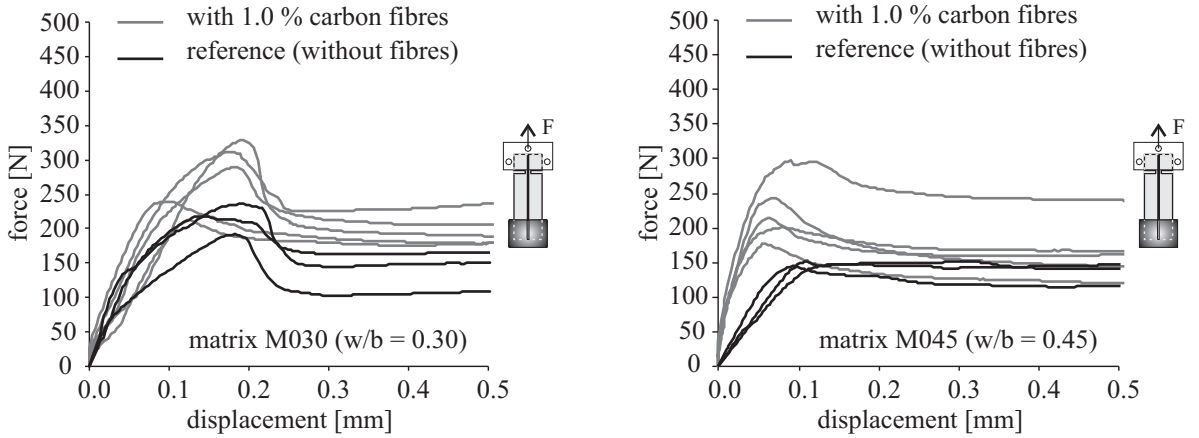

Figure 4.22: Results of multifilament-yarn pullout tests made with and without the addition of 1.0 % short carbon fibres and with the matrix M030 (left) and matrix M045 (right)

The microscopic investigations on the multifilament-yarns' surfaces of the tested specimen showed that short fibres can indeed improve the bond between multifilament-yarn and the surrounding matrix by means of new, additional cross-links. Extra connecting points to the surrounding matrix are provided by short fibres by their random dispersion in the matrix and their positioning on the yarn surface. Figures 4.23 and 4.24 illustrate experimental evidence that such cross-links in connection with short dispersed glass fibres indeed exist. While images presented in Figure 4.23 are of multifilament-yarns in the matrix M030, Figure 4.24 shows the ESEM images of cross-links on yarns' surface in the matrix M045.

The effect of "strengthening" the bond by additional cross-links must be more pronounced in the case of the matrix M045 since fibres have here more opportunitiy on the multifilament-yarn surface to "close the gaps" in comparison to the very dense microstructure of the bonding area between the yarn and the surrounding matrix M030, cf. Figure 4.16 in Section 4.2.2. This gives a direct explanation of the higher increase in pullout forces for specimens made with the matrix M045 in comparison to those obtained from specimens made with the matrix M030.

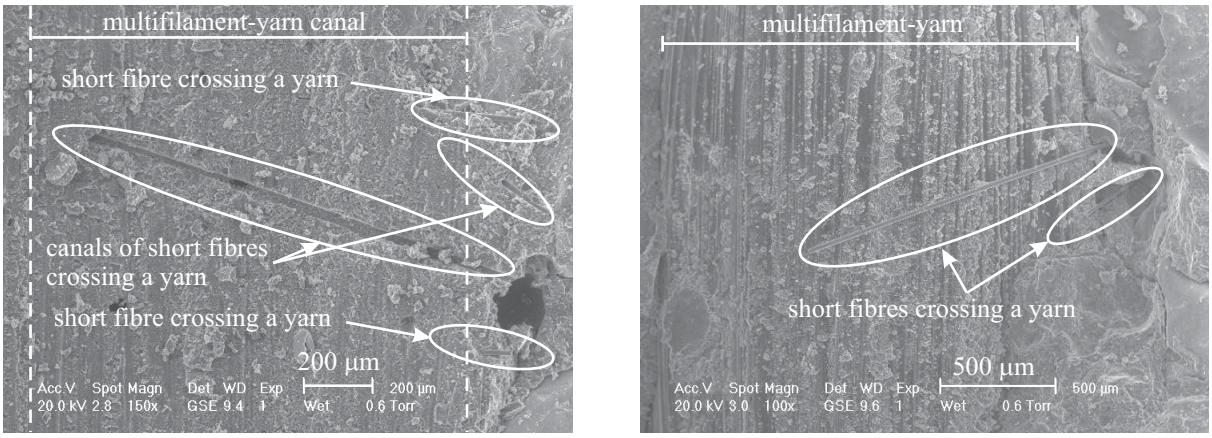

Figure 4.23: ESEM images of multifilament-yarn in the matrix M030 (w/b = 0.30) with the addition of short dispersed glass fibres

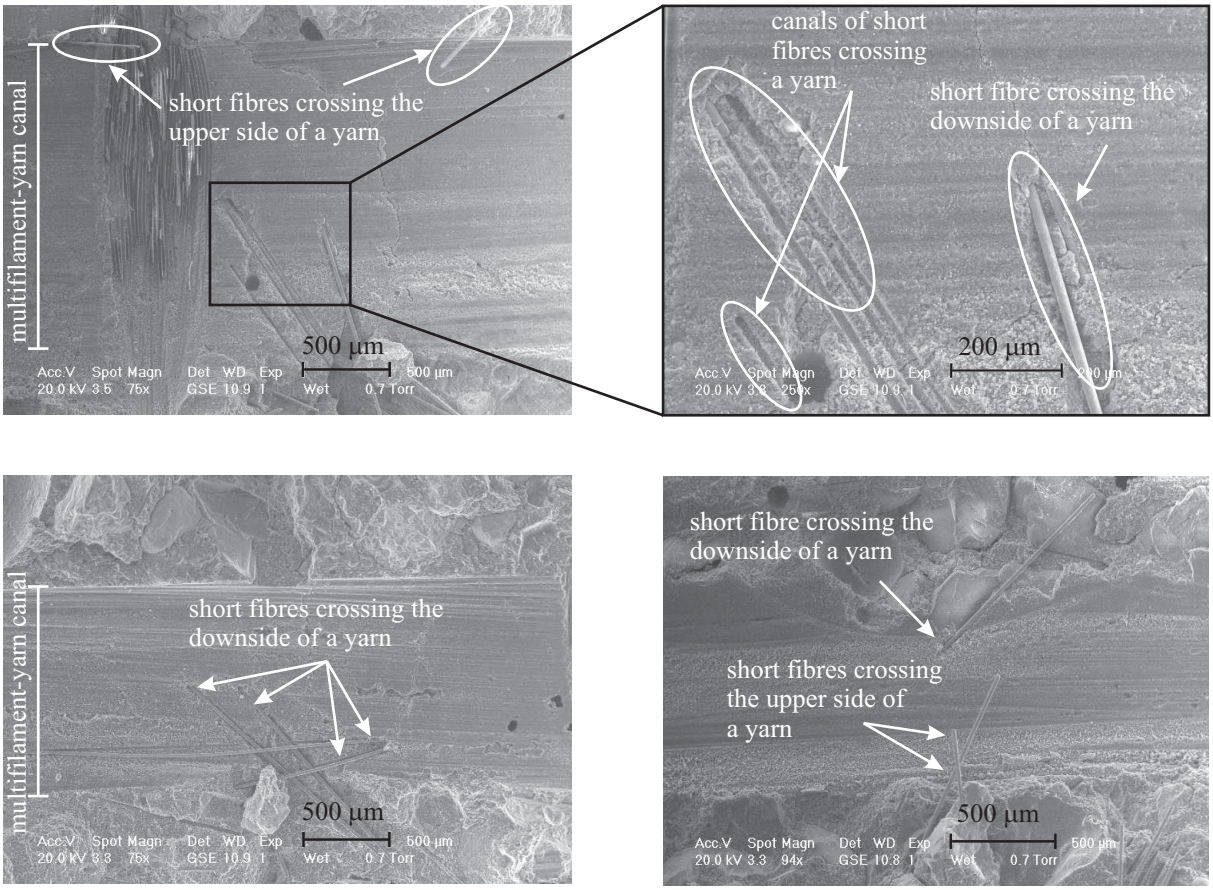

Figure 4.24: ESEM images of multifilament-yarn in the matrix M045 (w/b = 0.45) with the addition of short dispersed glass fibres

Similar findings were noted in the observations made for the specimens with the addition of short carbon fibres, cf. Figure 4.25. However, higher density of these cross-links made by carbon fibres was observed in comparison with those due to short dispersed glass fibres. This can traced back to their larger quantity (for the same amount by volume; here 1.0 % by volume) resulted from the smaller diameter of carbon fibres. Having more adhesive cross-links between matrix and filaments leads to better bonding, and thus a higher pullout force is needed. This might be an explanation of the higher pullout-force obtained from the specimens with the addition of short carbon fibres, cf. Figure 4.22 and Table 4.5.

Furthermore, the measured increase in bond strength due to the addition of short integral glass fibre was even more pronounced; cf. Figure 4.21 and Table 4.5. Microscopic investigations on the multifilament yarns' surfaces were performed as well to explain this phenomenon. ESEM images show that short integral fibres provide bigger and likely stronger cross-links between the yarn surface and the surrounding matrix than dispersed fibres because of their larger size and, thus, stronger anchoring in the surrounding matrix, as shown in Figure 4.26 (left) and Figure 4.26 (right) for specimens made with matrices M030 and M045, respectively.

Figure 4.27 illustrates schematically the arguably deciding mechanism leading to this improvement using the cross-link model.

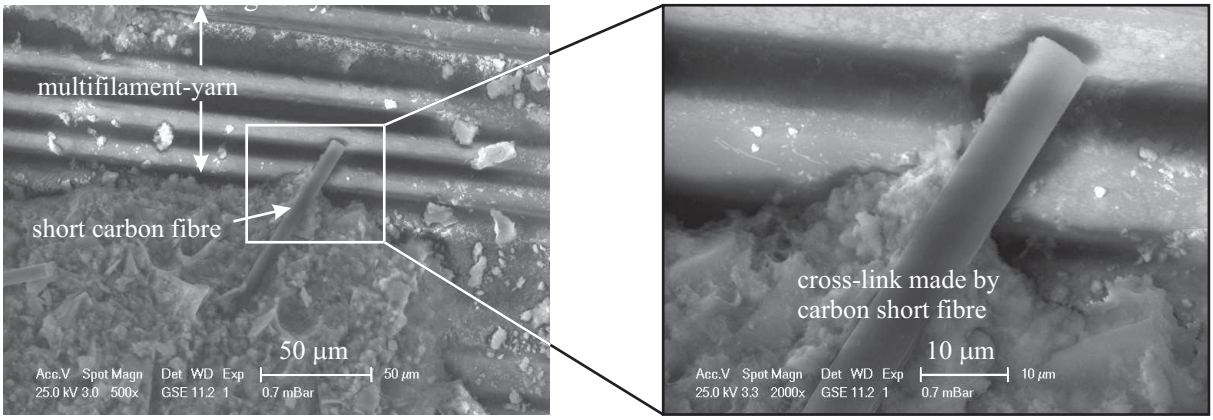

Figure 4.25: "Cross-link" between multifilament-yarn and matrix caused by a short carbon fibre

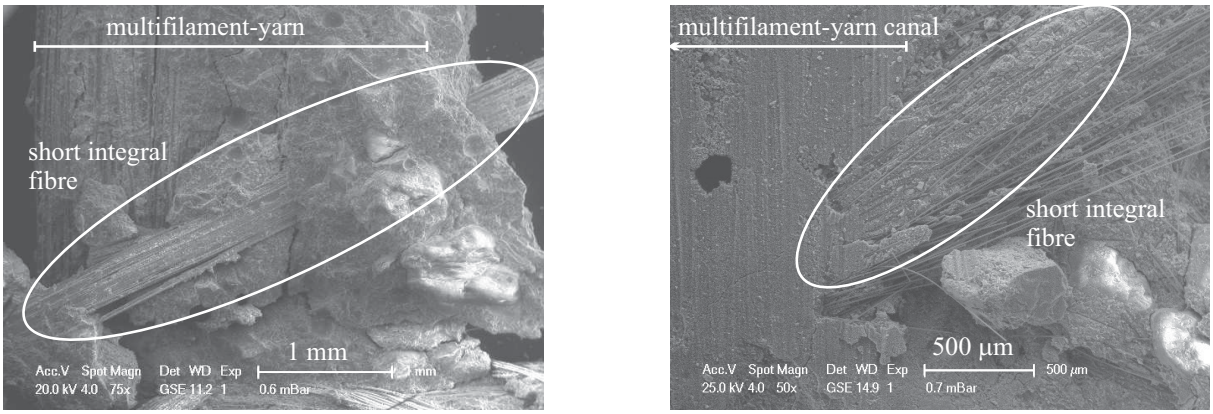

Figure 4.26: ESEM images of multifilament-yarn with the addition of short integral glass fibres in the matrix M030 (left) and matrix M045 (right)

In addition, microscopic investigation of fracture surfaces by means of ESEM showed that short fibres are frequently linked to multifilament yarns. This was frequently observed in the specimens with the addition of short dispersed glass fibres (Figure 4.28) and to a higher degree when short carbon fibres were added; cf. Figure 4.29. This can be traced back to the small diameter of short dispersed glass and carbon fibres, high stiffness and their marked slenderness which help to "needle" in the multifilament-yarn and link to the surrounding matrix. This might improve the bond between textile and matrix, thereby leading to higher pullout-forces in the specimens with the addition of short fibres. This finding can be added to the four mechanisms mentioned and discussed in Section 4.1, which treats multiple crack formation. In contrast to short dispersed fibres, no linkage of integral glass fibre to multifilament-yarn was observed.

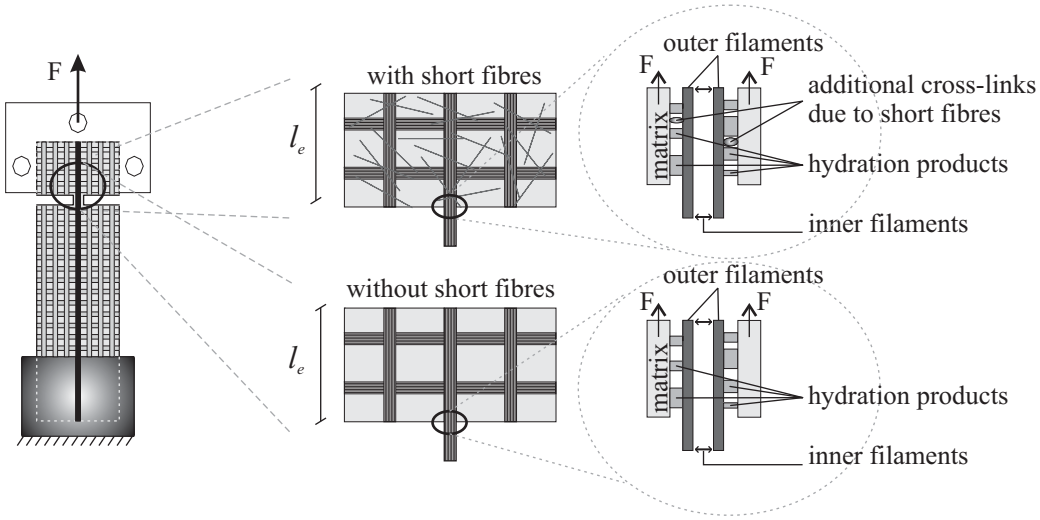

Figure 4.27: Bond mechanisms in the multifilament-yarn pullout tests

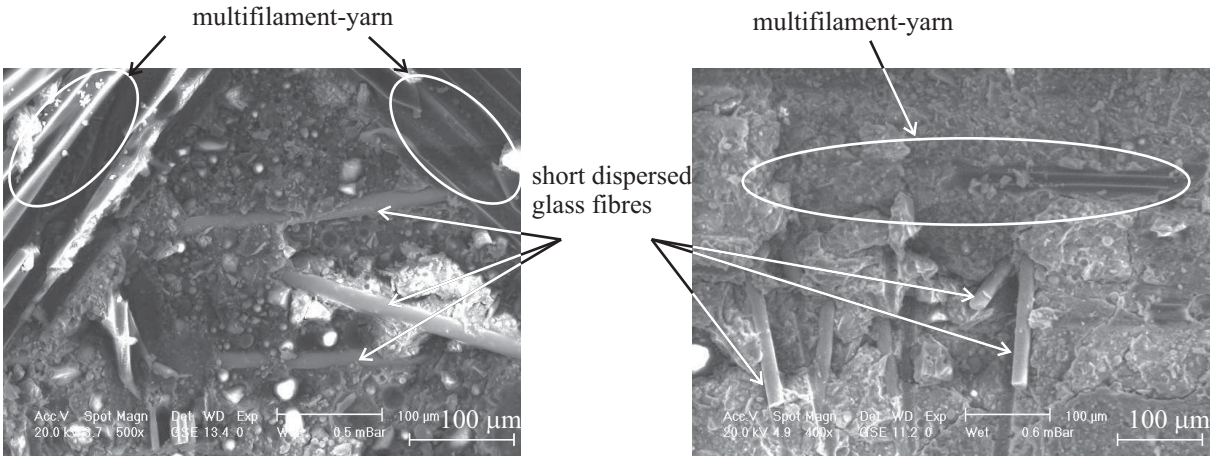

Figure 4.28: Short dispersed glass fibres linked to multifilament-yarn of a textile layer

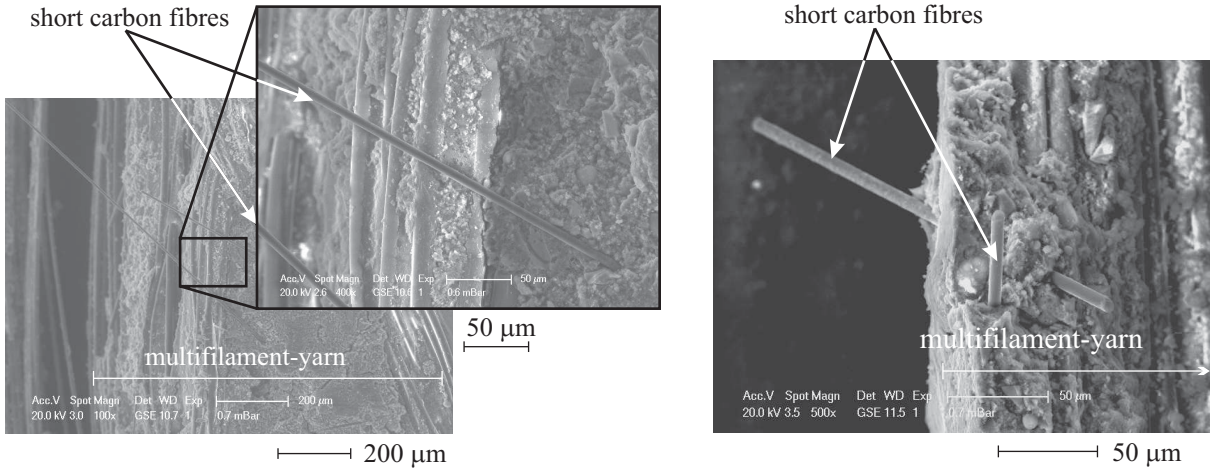

Figure 4.29: Short carbon fibres linked to multifilament-yarns of a textile layer

4.4 Effect of short fibres' type and orientation

As it was shown briefly in Section 2.3.3, orientation of fibres in concrete is a very important issue due to its distinct influence on the mechanical performance of the composite. The angle of inclination of a fibre in a cementitious matrix influences to a great extent its pullout resistance, as has been shown experimentally by several researchers, for example, [99]. In other words, the orientation of a fibre to load direction and to the crack surface influence its load bearing capacity, i.e., its efficiency in crack-bridging.

As an outgrowth of the technique used to produce the specimens in this study, i.e., the laminating process, a specific, preferable orientation of short fibre can be expected; see Section 3.2.2. The influence of such orientation of short fibres on their crack-bridging capability must be investigated. Furthermore, depending on the type of short fibre crack-bridging capacity can be widely differing. This aspect must be also clarified.

For this purpose, series of uniaxial tensile tests on specimens reinforced by short fibres only and single-fibre pullout tests, considered as tests at the macro- and micro-levels of observation, respectively, were performed. The results of this investigation are presented in this section.

4.4.1 Uniaxial tensile tests – Effect of fibre type on macro-level

Figures 4.30 and 4.31 present the results of uniaxial tensile tests performed on rectangular plates without textile reinforcement. The stress-strain curves were obtained for both matrices M030 and M045 with and without the addition of 1.0 % by volume of short dispersed or integral glass fibres. The stress-strain curves for both plain matrices are presented separately in Figure 4.9 and discussed in Section 4.2.1.1.

The addition of short fibres has widely differing effects on the mechanical behaviour of the matrix, depending on the type of fibre and properties of the matrix. For the specimens made of matrix M030 and reinforced with short fibres, a considerable increase in tensile strength and stiffness, i.e., steeper slope of the curve, could be observed in comparison to the specimens without fibres. The increase in tensile strength was particularly pronounced in the case of the addition of short integral glass fibres, cf. Table 4.6. The stress-strain relationship remained linear nearly up to the reaching of maximum stress level; cf. Figure 4.30 (right). In contrast, the corresponding stress-strain curves for specimens with the addition of short dispersed glass fibres deviated from a linear course at low stresses already, long before reaching maximum stress values; see the extracted part in Figure 4.30 (left). This nonlinearity can only result from micro-cracking, and it is obvious that so much micro-cracking must activate the fibres at an earlier stage of loading, which would lead already to failure of a part of the short dispersed, mono-filament, fibres at relatively low stress levels. Similar tendencies were observed for the specimens made with the matrix M045. These specimens showed a pronounced improvement in the tensile strength due to the addition of the integral fibres, whilst in the case of the addition of the dispersed fibres a considerably lower increase could be noted, see Figure 4.31 and Table 4.6. Furthermore, some decrease in stiffness was recorded for specimens made with matrix M045 due to the addition of short fibres.

As illustrated in Figure 4.30 (right), one of the specimens with the addition of short integral glass fibres exhibited an incompatible tensile strength value compared to those obtained from the other two specimens. This can be traced back to the great length and unusual slenderness of the

specimens, which may lead to a high sensitivity to early defects and, therefore, to such "atypical" values. These values were excluded from the statistical evaluation.

Table 4.6: Mechanical characteristics of specimens with and without the addition of 1.0 % by volume of short dispersed or integral glass fibres (no textile reinforcement)

Matrix material	Reinforcement with short fibres	Tensile strength [MPa]	Strain at tensile strength [mm/m]	Work-to-fracture [kN mm]
		Average value (standard deviation)		
M030	–	2.16 (0.28)	0.11 (0.01)	0.04 (0.01)
	+ 1.0 % dispersed glass	3.41 (0.76)	0.15 (0.06)	0.52 (0.16)
	+ 1.0 % integral glass	4.22 (-)	0.17 (0.03)	0.85 (0.18)
M045	–	1.75 (0.14)	0.10 (0.01)	0.03 (0.01)
	+ 1.0 % dispersed glass	1.98 (0.30)	0.18 (0.04)	0.49 (0.09)
	+ 1.0 % integral glass	2.42 (0.68)	0.18 (0.06)	0.63 (0.23)

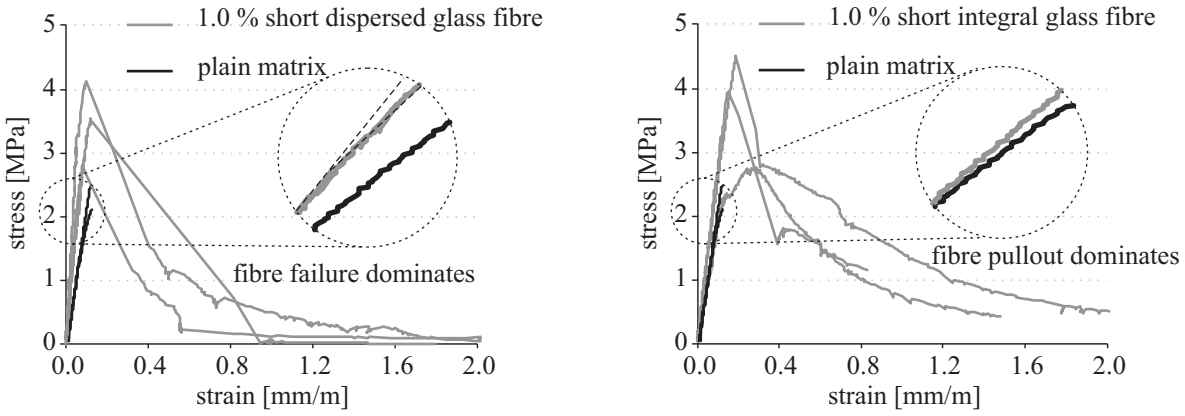

Figure 4.30: Results of uniaxial tension tests on plates made with matrix M030 (w/b = 0.30) and reinforced with 1.0 % by volume of short dispersed glass fibres (left) and short integral glass fibres (right)

These findings are obviously traceable to the effect of the water-to-binder ratio on the quality of the fibre-matrix bond; see also Section 4.2. Clearly the denser matrix M030 (w/b = 0.30) is more conducive to better bonding than the matrix with a higher water-to-binder ratio M045 (w/b = 0.45), Figure 4.18 in Section 4.2.3. This means that the fibre embedded in matrix M030 can contribute to a great extent to the bearing of tensile stresses in the ascending branch of the stress-strain curve. The stiffness of the composite where matrix M030 was used was also improved, most probably due to the good fibre-matrix bond. Fibres with weak bonds to the matrix can be considered as defects which, together with some extra air voids resulting from a relatively high proportion of short fibres and, hence, poor de-airing, most likely lead to some decrease in matrix stiffness as shown in Figure 4.31 for specimens with 1.0 % dispersed fibres in matrix M045.

Depending on the matrix used, the descending portion of the curves of specimens with the addition of dispersed fibres indicates that a considerable number of mono-filament glass fibres have been broken (Figure 4.30 left) and pulled out (Figure 4.31 left) in the tests with matrix M030 and M045, respectively. With increasing crack opening the load-bearing capacity of the dispersed glass fibres decreases significantly. In contrast, for specimens with the addition of

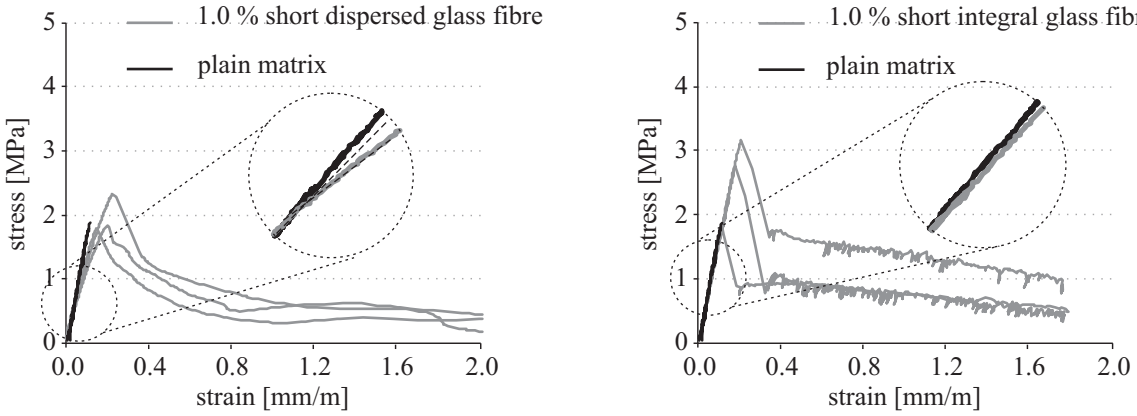

Figure 4.31: Results of uniaxial tension tests on plates made with matrix M045 (w/b = 0.45) and reinforced with 1.0 % by volume of short dispersed glass fibres (left) and short integral glass fibres (right)

integral glass fibres the descending branch showed a much more stable course at a relatively high stress level after the initial snap-back and indicated a good crack-bridging ability, cf. Figure 4.30 (right) and Figure 4.31 (right), which is obviously better than that of the dispersed fibres.

In comparison with the results obtained from specimens with hybrid reinforcement, i.e., textile reinforcement and short fibres, the results obtained from specimens containing short fibre only (no textile layers) showed that the action of short fibres can be very different in the absence of textile reinforcement. The matrix with short integral fibres showed – other than in the experiments with hybrid reinforcements, cf. Section 4.1.2 – a more pronounced improvement in first-crack stress than that achieved by the matrix with the addition of dispersed fibres. This is actually the only macro-crack as well, cf. Figure 4.30 and Figure 4.31. Here, the first-crack stress is equal to the tensile strength of the composite. This observation was accompanied by a deviation from the linear course of the stress-strain curve long before reaching the maximum stress value when short dispersed fibres were used. This early non-linearity is related to the early development of micro-cracking, which likely results from a higher number of air voids and other micro-defects in the mixtures with the addition of short, dispersed fibres. Because of the larger quantity of dispersed fibres for the same given volume and their larger specific surface area, these fibres lead to some loss of the workability and, therefore, worsening in the de-airing process. This effect is more pronounced in the case of dispersed fibres in comparison to the integral fibres. Table 4.7 confirms this conclusion by the measured density values of the matrix due to the addition of short fibres: The density decreases with fibre addition due to the resulting higher porosity.

Furthermore, it should be underscored here that the presence of textile reinforcement layers leads to a more uniform orientation of short fibres in the advantageous load-parallel direction, particularly due to the laminating process used for the TRC production, as it was also in this study; see Section 3.2.2. In that case, when fibres are oriented in the load-parallel direction, the dispersed fibres act more efficiently with respect to increasing first-crack stress than do integral fibres. Dispersed fibres are likely to influence the four suggested mechanisms responsible for enhancement first-crack stress (cf. Section 4.1.5) more positively than integral fibres; this is mentioned and discussed in Section 4.1. In contrast, in the specimens without textile reinforcement the fibre orientation is more random, which means that more fibres may be unfavourably inclined to

Table 4.7: Density of the matrices M030 and M045 both with and without the addition of short dispersed and integral glass fibres, based on Table 4.4 in Section 4.2.1.3

Type of specimens	Density [g/cm^3]	
	Average value (standard deviation)	
	Matrix M030	Matrix M045
Plain matrix	2.039 (0.009)	1.945 (0.006)
With 1.0 % short integral glass fibres	2.011 (0.009)	1.904 (0.003)
With 1.0 % short dispersed glass fibres	1.923 (0.010)	1.813 (0.009)

the crack plane. In this case, integral inclined fibres are much more effective in crack-bridging than the dispersed fibre. Inclined dispersed fibres fail easily, even with relatively small crack openings because brittle glass can not sustain the high curvatures at crack's edge, cf. Figure 4.32 (left). The situation is less dramatic when integral fibres are used, as also observed in the pullout tests on inclined integral fibres; see Section 4.4.2.2. Figure 4.32 (right) shows schematically the force-displacement response and the different states of the pullout of inclined integral fibre. At high force levels de-bonding and partial pullout of fibre, associated with crack opening, occur while some (mainly sleeve filaments) fail. However, the core filaments remain intact and can transfer tensile forces. The force transfer across the crack continues in the softening regime, which results basically from the pullout of the core filaments and further failure of individual mono-filaments.

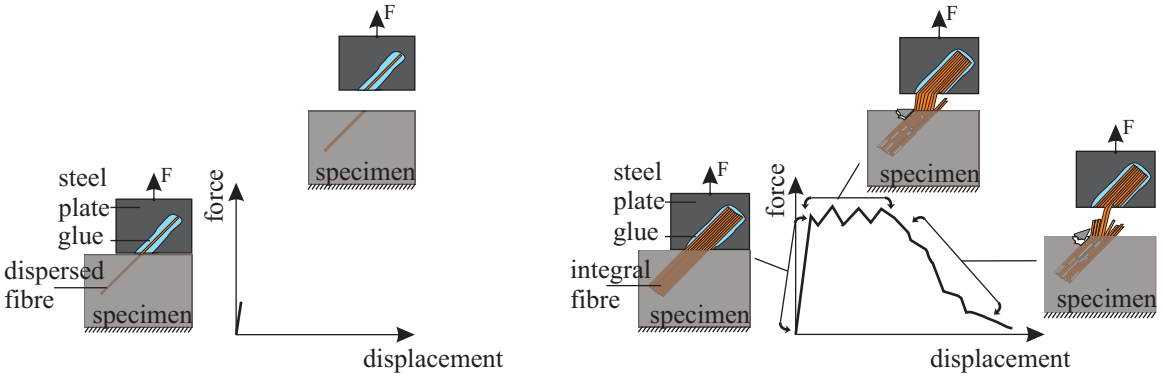

Figure 4.32: Schematic view of crack-bridging action of inclined short dispersed fibre (left) and short integral fibre (right)

4.4.2 Single-fibre pullout tests – Effect of fibre type and orientation on micro-level

As short fibres are aligned nearly randomly within the matrix, only very few fibres are oriented parallel to the direction of the applied tensile load. The great majority of fibres are oriented at different angles to the crack surface and, therefore, to the direction of the pull-out. Single-fibre pullout tests parallel to the fibre axis as well as tests with a given angle of inclination were performed in order to gain a better understanding of the crack-bridging behaviour and various failure mechanisms observed in the experiments presented in the previous section.

4.4.2.1 Single-fibre pullout parallel to the fibre axis

Figures 4.33 and 4.34 show force-displacement curves obtained from single dispersed and integral fibres embedded into the matrices M030 and M045, respectively. Brittle failure of the fibres dominated when dispersed glass fibres were tested in the matrix M030. A vertical drop in the force-displacement curves due to fibre breakage was observed after the ultimate force was reached, cf. Figure 4.33 (left). The ultimate force attained by the pullout of integral fibre embedded in the matrix M030 under the pullout test was more than 10 times higher; see Table 4.8. Only very few of the integral fibres failed in a brittle manner; most of them provided force-displacement relationships with a pronounced softening branch, which indicates a gradual fibre pullout or a gradual failure, cf. Figure 4.33 (right). The resulting diagrams for the matrix M045 are presented in Figure 4.34. Due to a weaker bond, much lower ultimate force values were reached, cf. Table 4.8. While the trend to the failure of dispersed fibres was less pronounced in comparison to the tests with the matrix M030, no fibre failure but only pullout in case of integral fibres was observed, see Figure 4.34 (right) and Table 4.8.

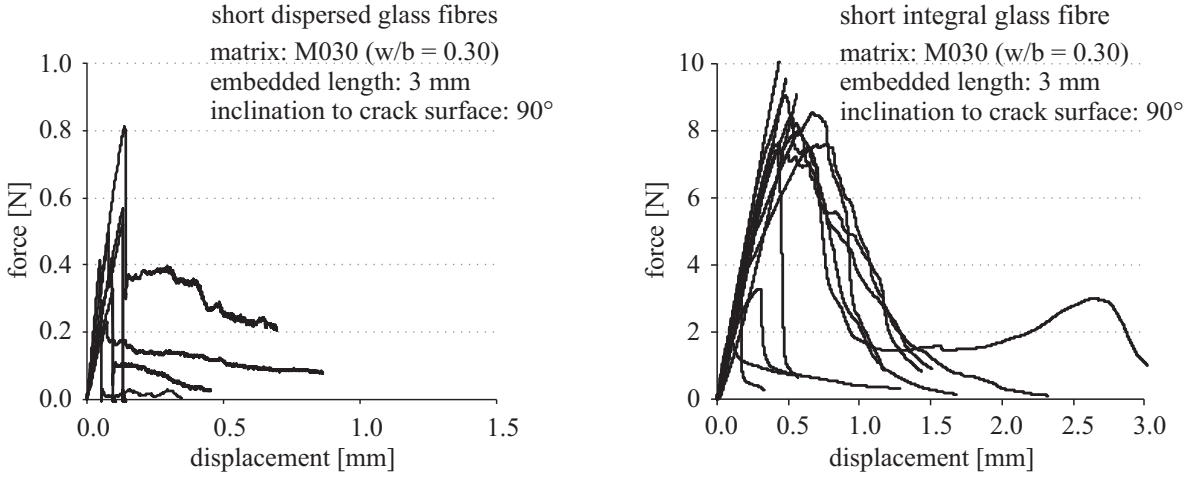

Figure 4.33: Force-displacement curves obtained from single-fibre pullout tests with the matrix M030 for dispersed glass fibres (left) and integral glass fibres (right)

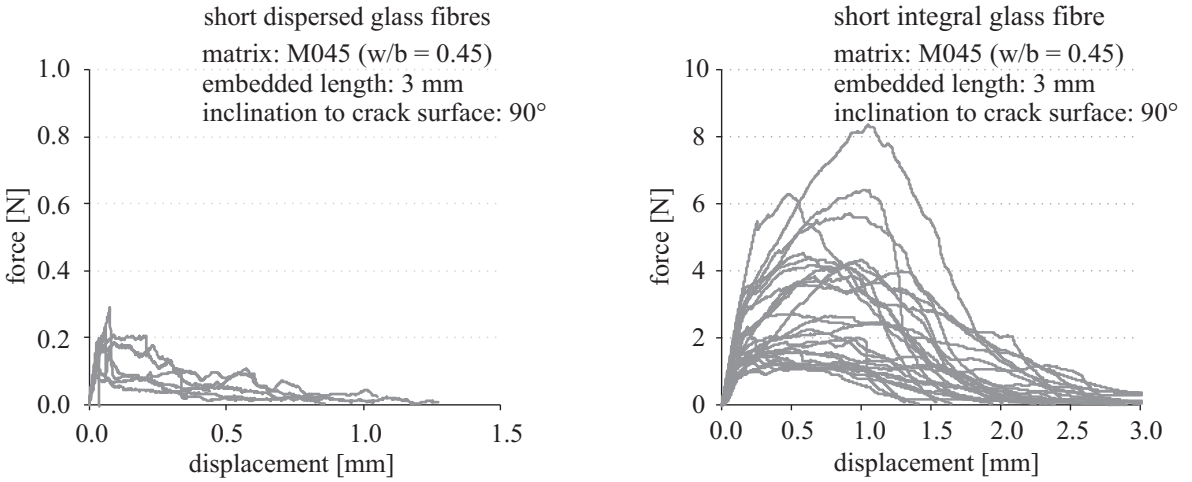

Figure 4.34: Force-displacement curves obtained from single-fibre pullout tests with the matrix M045 for dispersed glass fibres (left) and integral glass fibres (right)

Table 4.8: Evaluation of the results of pullout tests performed on single dispersed and integral glass fibres

Type of fibre			Matrix M030	Matrix M045
Dispersed fibre	Number of all tested fibres		10	10
	Broken fibres	Number of fibres	7	3
		Max./min./average force value [N]	0.57/0.07/0.37	0.20/0.13/0.17
		Max./min./average displacement at the ultimate force [mm]	0.13/0.01/0.06	0.04/0.03/0.04
	Pullout fibres	Number of fibres	3	7
		Max./min./average force value [N]	0.81/0.29/0.51	0.29/0.10/0.18
		Max./min./average displacement at the ultimate force [mm]	0.13/0.05/0.08	0.08/0.02/0.05
		Max./min./average displacement at the force equal to 0 [mm]	0.86/0.45/0.67	1.27/0.45/0.89
Integral fibre	Number of all tested fibres		13	31
	Intact fibres force $\geq$ 10 N	Number of fibres	3	–
		Max./min./average displacement at the ultimate force [mm]	0.56/0.44/0.49	
	Broken fibres	Number of fibres	2	–
		Max./min./average force value [N]	7.42/2.96/5.19	–
		Max./min./average displacement at the ultimate force [mm]	0.4/0.17/0.28	
	Pullout fibres	Number of fibres	8	31
		Max./min./average force value [N]	9.05/1.95/6.80	8.35/0.40/2.95
		Max./min./average displacement at the ultimate force [mm]	0.76/0.11/0.48	1.36/0.21/0.67
		Max./min./average energy absorbed [Nmm] (standard deviation)	8.64/0.54/5.23 (2.86)	10.9/0.56/3.81 (2.51)

4.4.2.2 Pullout of inclined fibres

In this investigation three representative angles were considered from among all possible cases, as shown in Figure 4.35:

- Plane fibres, 0°, i.e., fibres are oriented parallel to the crack surface; this type represents all fibres oriented to the crack surface at angles between 0° and 30°. These fibres are considered as non-bridging fibres, i.e., the contribution of these fibres to the stress bearing capacity of the matrix is neglected.
- Straight fibres, 90°, i.e. fibres are oriented parallel to the load direction; this type represents all fibres oriented to the crack surface at angles between 60° and 90°. The results of pullout tests on such fibres are shown in the previous Section 4.4.2.1.
- Inclined fibres, 45°; this type represents all fibres oriented to the crack surface at angles between 30° and 60°.

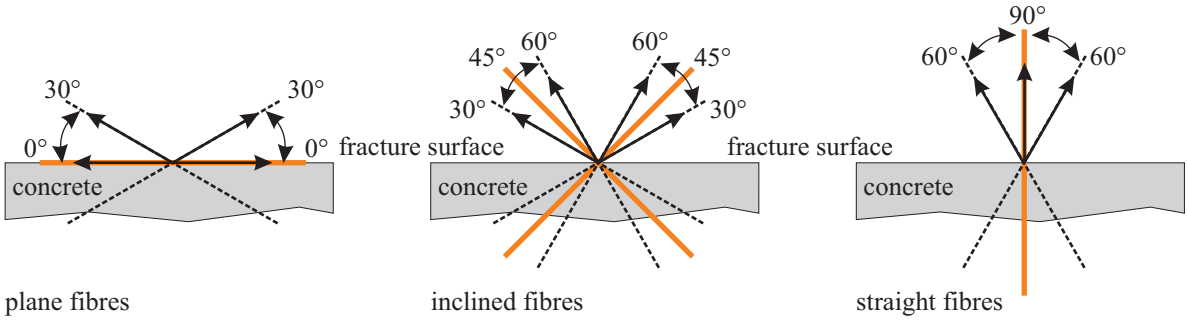

Figure 4.35: Classification of the fibre orientation in respect of the fracture surface

As mentioned in Section 3.3.3 it was not possible to perform pullout tests on inclined, dispersed type fibres due to the difficulties in the handling of the very fine glass or carbon filaments; hence, the study is limited to the short integral glass fibre. Figure 4.36 shows the large scatter in the results obtained from fibre pullout tests with the angle of 45° for both matrices M030 and M045. The results vary significantly, although the fibres had the identical embedded length of 3 mm. In some cases barely measurable pullout behaviour was recorded, in other cases the maximum load cell capacity was reached before the fibre failed; see Table 4.9. While the measured maximum pullout forces were in the same range as in the corresponding pullout tests parallel to the fibres' longitudinal axes, the displacement at peak force was larger by approximately a factor of two in the experiments with inclined fibres, cf. Tables 4.8 and 4.9.

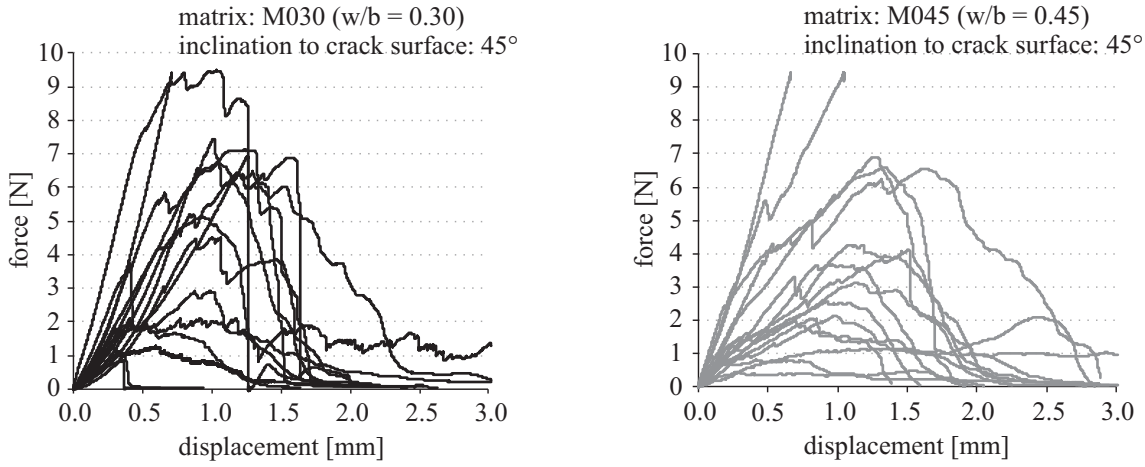

Figure 4.36: Force-displacement curves obtained from pullout tests on single inclined integral glass fibre embedded into the matrices M030 (left) and M045 (right)

Fibre failure mode depends very strongly on its bond quality to the surrounding matrix. This effect was discussed in Section 4.2.3. Regardless, a strong bond is formed when matrix M030 (w/b = 0.30) is used; results presented in Figure 4.33 showed explicitly that fibre fracture or fibre pullout dominated the behaviour depending on fibre type, dispersed or integral, respectively. To corroborate this, the specimens of single-fibre pullout tests were carefully split in the middle and investigated using ESEM. In most of the specimens with short, dispersed fibre, and made with the matrix M030, part of the fibre was found, i.e., the part after fibre breakage, cf. Figure 4.18 (left). In contrast, in the pullout tests with integral fibre only the sleeve filaments, well bonded to surrounding matrix, failed, while the middle-hollow indicates that the core filaments were pulled out, cf. Figure 4.37.

Table 4.9: Evaluation of the results of pullout tests performed on single inclined integral glass fibre

Type of fibre			Matrix M030	Matrix M045
Integral fibre	Number of all tested fibres		15	16
	Intact fibres force $\geq$ 10 N	Number of fibres	1	2
		Max./min./average displacement at ultimate force [mm]	0.71	1.05/0.66/0.85
	Broken fibres	Number of fibres	–	–
	Pullout fibres	Number of fibres	14	14
		Max./min./average force value [N]	9.40/1.06/4.68	6.90/0.45/3.31
		Max./min./average displacement at ultimate force [mm]	1.25/0.27/0.78	1.60/0.20/1.00

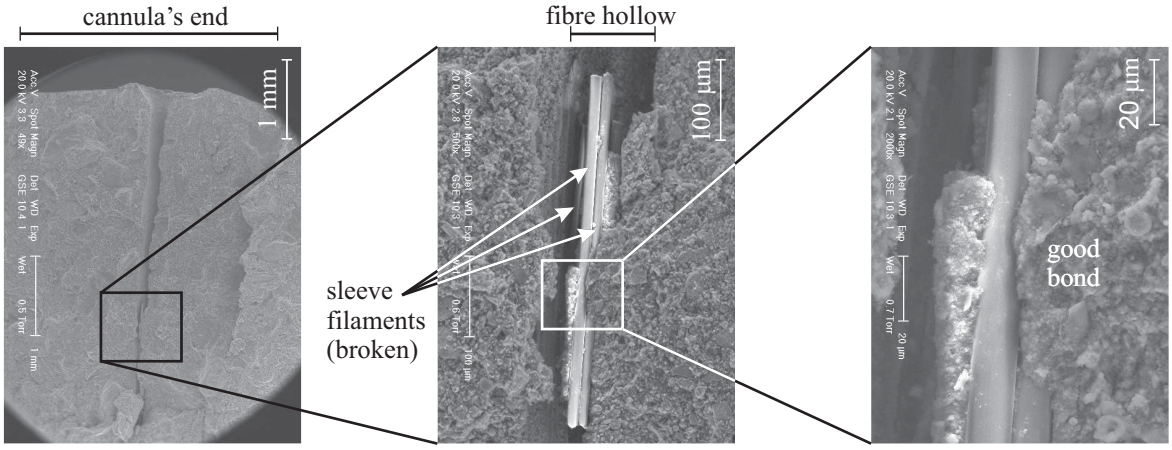

Figure 4.37: ESEM images of split specimens of single integral glass fibre pullout tests with matrix M030

The pullout tests performed on inclined integral fibres yielded a very large scatter of the results, cf. Figure 4.36. This scattering can be at least partly explained by different arrangements of the solid particles in the vicinity of the fibre. Figure 4.38 shows three characteristic curves representing three different modes of failure as well as the corresponding micro-photographs of the specimens. Figure 4.38 (above) shows a tightly fixed fibre; there is no space in the vicinity of the fibre. Two particles clamp the fibre between them. The loading cell capacity was not high enough to complete the test, which means that neither breakage nor pullout of the fibre could be achieved. In contrast, a relatively large void adjacent to the fibre edge is presented in Figure 4.38 (middle); much space in the fibre's vicinity allowed the fibre to be pulled out with very little resistance (low maximum force). Finally, the case shown in Figure 4.38 (below) represents the typical case of a uniform particle arrangement around the fibre. This arrangement led to the breakage of some outer filaments and the pullout of the majority of inner filaments. This mode of fracture is the preferred one.

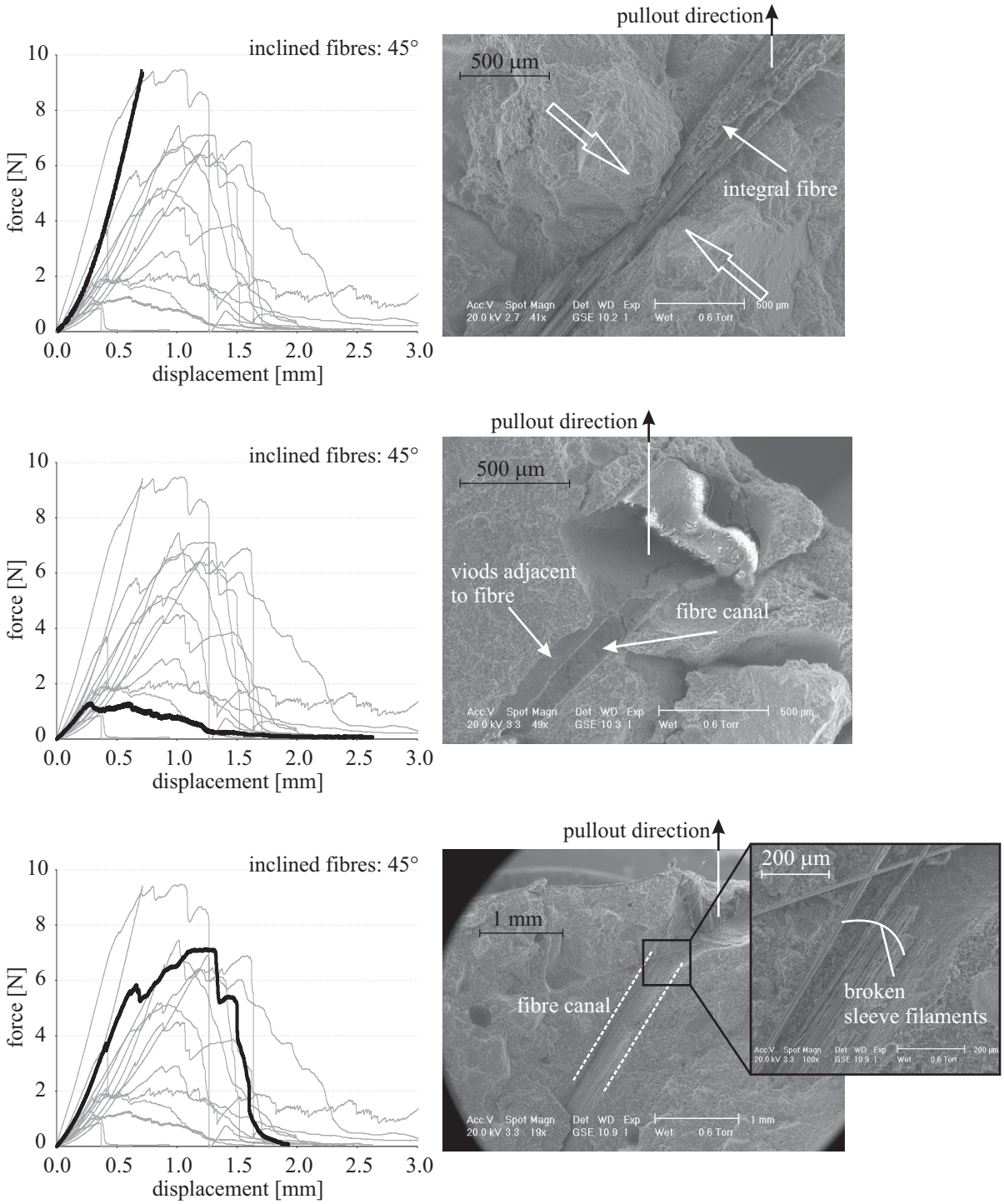

Figure 4.38: Three characteristic curves obtained from the single-fibre pullout tests performed on inclined integral glass fibres and the corresponding ESEM images: completely fixed fibre (above), easily pulled-out fibre (middle), and typical fibre pullout response (below)

4.5 Summary

This chapter presented the results of the experiments performed on the textile-reinforced concrete with and without short fibre as well as their constituents. First, deformation-controlled, uniaxial tensile tests were carried out on the composite material. The tests showed the positive effects of adding short dispersed glass, integral glass, and dispersed carbon fibres on the mechanical performance of TRC under tensile loading: increase in first-crack stress, formation of a greater number and, thus, finer cracks, and increased tensile strength in the composite. The first-crack stress value of TRC specimens increased by approximately three times due to the addition of 1.0 % by volume of short dispersed glass fibres. This was even more distinct in the case of the short carbon fibres, nearly by a factor of 4 for specimens made of the matrix with the higher water-to-binder ratio (M045: w/b = 0.45). While dispersed fibre were found to be more effective than integral fibres with respect to the formation of higher number of cracks, finer cracks, and finer crack patterns, integral glass fibres had more pronounced positive effects on both tensile strength and work-to-fracture of the composite. Moreover, it was found that the range of the effect of short fibres on TRC behaviour depends on fibre type. While the advantage of the addition of short dispersed fibre began to fade at relatively high strain levels, integral fibres improved the load bearing capacity of the TRC over the entire strain range, right up to failure.

A multi-scale investigation program was developed in order to gain more and better insight into the specific material behaviour of the finely grained concrete with such hybrid reinforcement. For this purpose uniaxial tension tests on plates made of plain concrete matrix and concrete matrix reinforced with only short fibres were performed. Furthermore, multifilament-yarn and single-fibre pullout tests were carried out to gain a better understanding of bonding properties and crack-bridging behaviour.

Depending on the water-to-binder ratio of the matrix, various qualities of matrix-fibre bond were observed. Results obtained from specimens reinforced only with short fibres showed that the fibre embedded in the matrix with low water-to-binder ratio (good bond) could contribute to a great extent to the bearing of stresses, which led to increase in strength and stiffness of the composite. On the contrary, decrease in matrix stiffness was recorded due to the weak fibre-matrix bond. This phenomenon was observed for specimens made with the matrix with high water-to-binder ration due to the addition of short dispersed glass and carbon fibres. The fibres in this case can be considered as defects with respect to stiffness. However, this does not hold true with regard to the tensile strength value which was increased due to the addition of short fibres.

Furthermore, short fibres improved the bond between multifilament-yarn and the surrounding matrix. By their random positioning on the yarn's surface; short fibres built new "special" adhesive cross-links which provided extra connecting points to the surrounding matrix. This effect differed depending on fibre type. Because of their relatively larger size, short integral fibres provided a larger and stronger anchoring into the surrounding matrix than those provided by short dispersed glass or carbon fibres by means of new adhesive cross-link. In addition, it was found that short fibres are frequently linked to multifilament yarns. Due to their marked slenderness which help to "needle" in the multifilament-yarn, short dispersed glass fibres and to a higher degree short dispersed carbon fibres may provide additional links between textile and matrix, thereby improving bond quality.

Widely differing effects of the addition of short fibres on the mechanical behaviour of the matrix in the absence of textile reinforcement were observed: Short integral fibres led to a more pronounced increase in tensile strength of the matrix than was reached due to the addition of short, dispersed fibres. This was explained by the higher effectiveness of integral inclined fibres in crack-bridging than that of dispersed inclined fibres.

5 Rheological-statistical model

5.1 Introduction

In the foregoing chapters, a multi-scale investigation program and its results are presented and discussed. The findings at different levels of observation were brought together, i.e., results obtained at the macro-level of observation could be described based on the findings on the meso- and micro-levels.

The purpose of developing the model presented in this chapter was to make a first step towards a sound analytical description of the specific mechanisms which steer the mechanical behaviour of concrete with hybrid reinforcement. It should enable a better understanding of the characteristic phenomena observed in the experiments. At this stage the model is designed to serve as a support tool for theoretical considerations, but not for practical applications. However, prospectively the model could be further developed to serve the purpose of material design with adequate predicting capacity.

The model was derived based on the results and phenomena observed in the experiments performed on single-fibre pullout tests and in the related microscopic investigation and then extended to a description of TRC with short fibres. The concept of the multi-scale modelling approach is illustrated in Figure 5.1. It should be emphasized here that at this stage the model as developed takes into consideration only dispersed short fibres. Additional mechanisms involved in the behaviour of integral fibres are not considered.

5.2 Modelling at micro-level of observation – Single fibre

The failure behaviour of a single-fibre results from different bond mechanisms as discussed in Section 4.2.3. Since bond behaviour was studied using single-fibre pullout tests, it is meaningful to use the same arrangement for developing a model.

Microscopic investigation showed that the bond between fibre and cementitious matrix is nonuniform over the length of the fibre, see Figure 5.2 (left). Hydration products form adhesive cross-links between matrix and filament. The bonding properties of these cross-links depend on the characteristics of the hydration products, which are influenced by the composition of the matrix and also the surface properties of the fibre. Figure 5.2 (right) represents a simple physical description of the above mentioned phenomenon.

Based on this assumption, rheological-statistical model to describe fibre-matrix interaction has been developed, Figure 5.3. This model should consider the properties of both the interface between fibre and matrix and those of the fibre.

This model consists of simple rheological elements like springs and friction blocks representing the elastic and plastic frictional deformation, respectively. The fibre itself is represented by a given number (i) of serially arranged springs. The maximum bearing load and the length of each spring element are F_{Si} and l_i, respectively. The stiffness of each spring element is given by

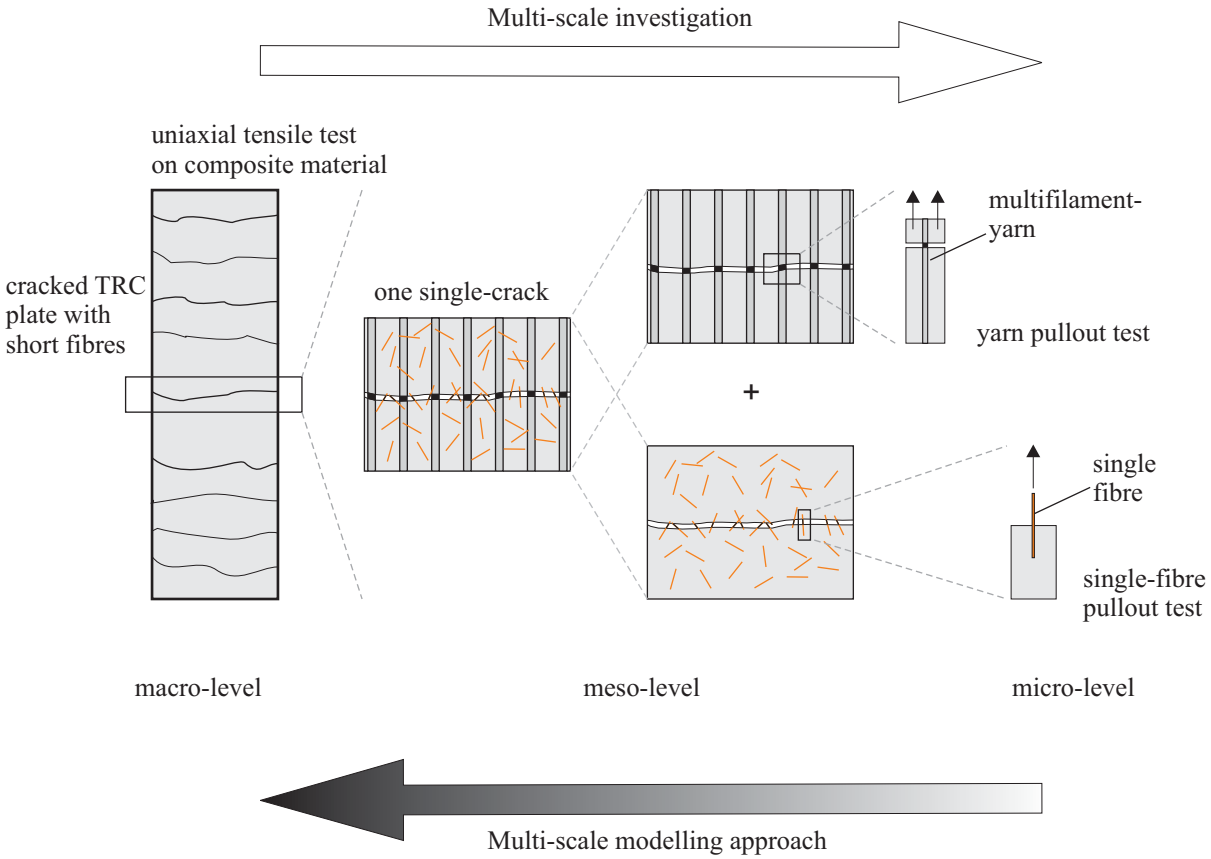

Figure 5.1: Schematic view of the concept of the multi-scale modelling approach used in this investigation in order to consider the contribution of individual components of the composite to the overall mechanical behaviour of TRC with short fibres

$S_i = \frac{E_i \cdot A_i}{l_i}$, where E_i is the the elastic modulus and A_i is the cross sectional area of the fibre. Each spring element represents a segment of fibre between two cross-links. Therefore, the number of springs is defined by the number of cross-links, cf. Figure 5.3. In order to distinguish among the springs later in the explanation, each spring element is labeled according to its stiffness, e. g., spring S_i.

A parallel arrangement of one spring element and one friction block (friction load $F_{cf,i}$) is used to describe the behaviour of one cross-link i, cf. Figure 5.4 (left). The stiffness of these spring elements is very high in order to represent the nearly non-deformable cross-links. Due to such high stiffness of the cross-links and their load-bearing capacity, only a part of the load is transferred through the fibre beyond the first to the following cross-links, so that a number of cross-links along the interface are activated. Theoretically, the de-bonding process might be started at any location along the interface due to cross-link breakage, but since the force acting on the first cross-link is the greatest, the failure starting with first cross-link to crack surface is the most realistic scenario.

Since the very low deformation capacity of cross-links leads to a dramatic decrease in load transferred to the fibre end, it is assumed in this model that the cross-links will be activated one after another starting from the first to crack the surface and gradually move toward the fibre end. For this purpose and also to simplify the mathematical description of the model, the stiff spring element used to describe the elastic behaviour of a cross-link is replaced by a strength

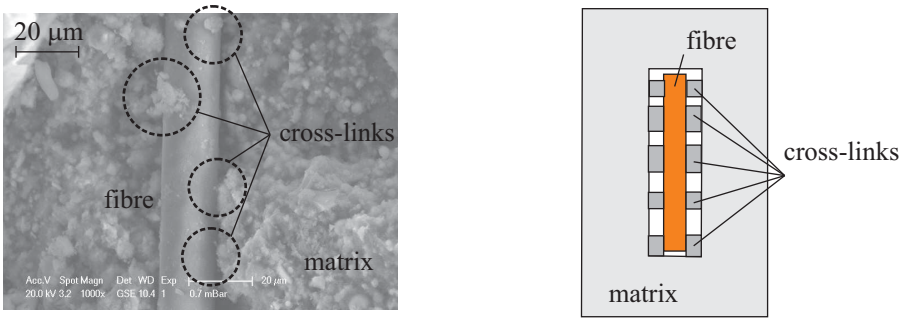

Figure 5.2: ESEM image of AR glass filaments bonded to a cementitious matrix with the different positions of cross-links (left) and the corresponding physical description (right)

element with a critical load $F_{cb,i}$; cf. Figure 5.4 (right). By replacing the spring elements, the applied load can be transferred further only after the failure of the activated strength element, i.e., the cross-links will be activated successively.

The critical load ($F_{cb,i}$) of the strength element is the load at which the de-bonding at the corresponding cross-link takes place. Simultaneously with the failure of the strength element the friction element is activated with a frictional load $F_{cf,i} \leq F_{cb,i}$. The parallel arrangement of these two elements ensures that friction starts only after de-bonding.

As illustrated in Figure 5.3 the applied load is transferred via cross-links to the surrounding matrix. In the model, the currently activated cross-link is indicated by index n: $n \in [2, ..., N]$ where index N is used to identify the last cross-link in the system.

In the model it is assumed that:

- $A_i = A = const$ and $E_i = E = const$.
- The friction load remains constant for the entire displacement $w_{c,i}$ which represents the distance between the corresponding cross-link and crack surface along the fibre axis. e.g. by reaching the displacement $w_{c,3}$, the cross-link 3 leaves the fibre canal and becomes "friction-free".
- Fibre exhibits linear-elastic behaviour.
- The distance between crack surface and the first cross-link is greater than zero ($w_{c,1} > 0$).

As mentioned above and discussed in Section 4.2.3, the fibre failure mode, i.e., fibre fracture or fibre pullout, depends to a great extent on the bonding properties between the fibre and the surrounding matrix. Fibre fracture dominates the behaviour when the bond is strong, i.e., fibre breakage takes place when fibre strength is reached before bond strength. Fibre pullout starts when all cross-links fail, i.e., complete de-bonding occurs. This takes place when the fibre strength is higher than the bond strength.

In the following, these two scenarios will be discussed separately based on the rheological-statistical model presented in Figure 5.3.

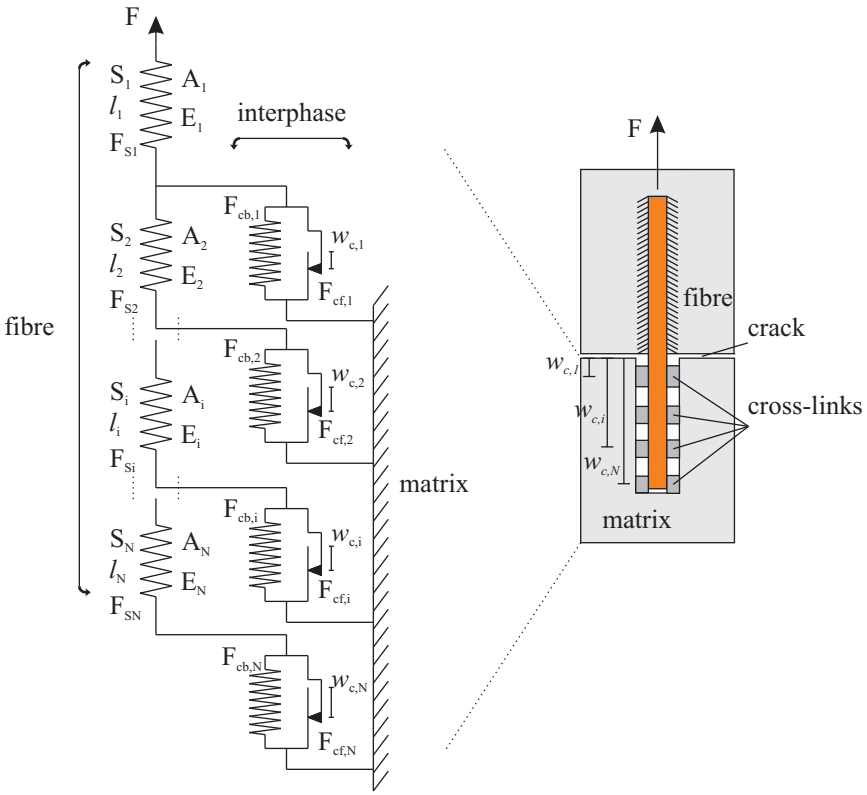

Figure 5.3: Rheological model of single-fibre pullout tests

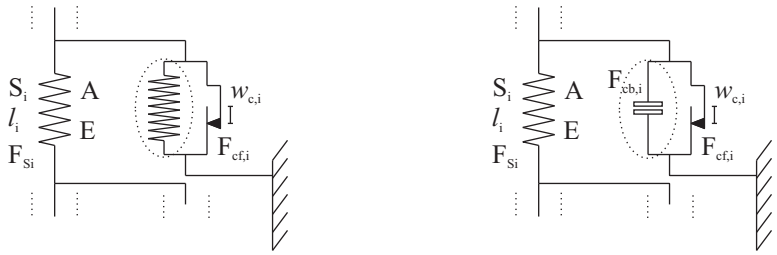

Figure 5.4: Simplification of cross-link model: Replacement of a stiff spring element (left) by a strength element (right)

5.2.1 Fibre fracture

Fracture of fibre takes place when the maximum bearing load of the fibre is reached. This may occur under one of the following two scenarios:

1. The fibre breaks while all cross-links remain intact, i.e., fibre remains completely bonded to the matrix. This scenario results from exceeding the strain capacity of the fibre due to crack opening prior to the failure of the first cross-link $F_{fra} = F_{S_1} < F_{cb,1}$. Here, the fibre response is linear elastic and the fracture is brittle; cf. Figure 5.5, which is described by Equation 5.1.

$$\begin{aligned} \forall F_{fra} &= F_{S1} < F_{cb,1} \\ \Delta l_{fra} &= \frac{F_{fra}}{C_1} \end{aligned} \tag{5.1}$$

Where: F_{fra} is the load value at which the fibre fractures, i.e. the load value at which the deformation capacity of the fibre Δl_{fra} is reached.

It should be mentioned that the stiffness of the whole system, which results from the respective stiffness of the activated springs, will be indicated by C.

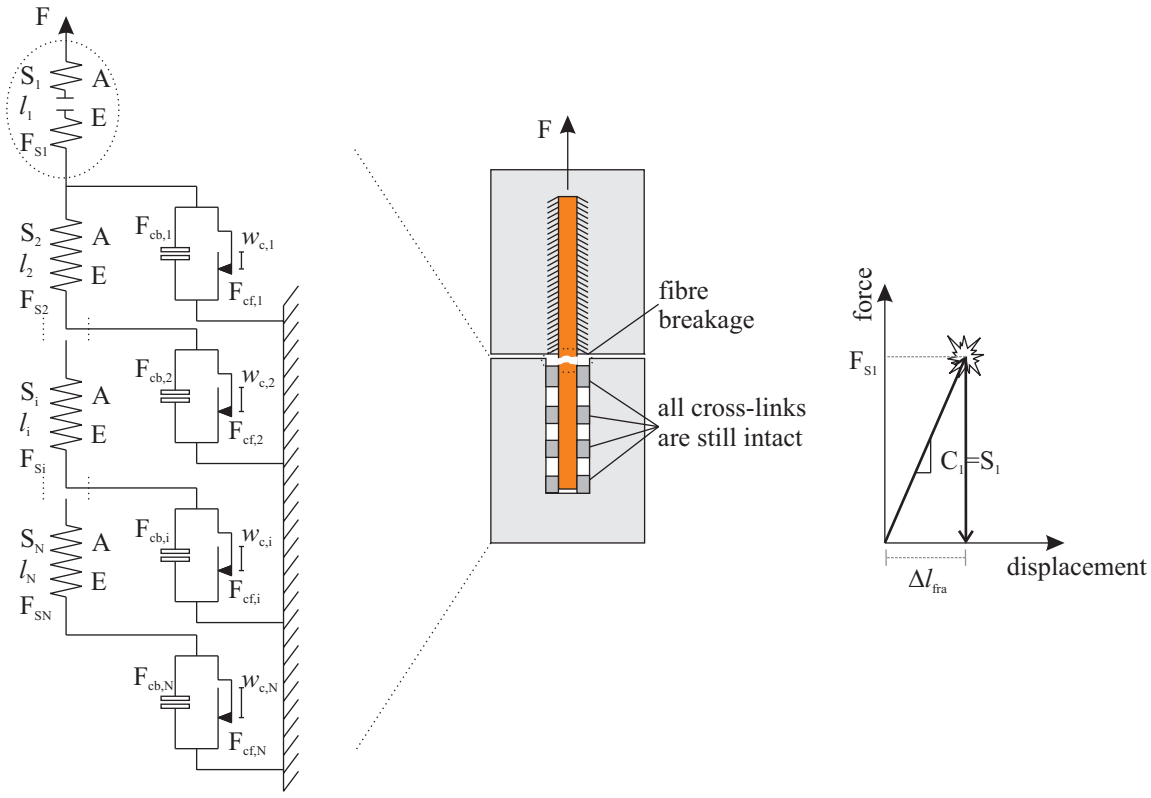

Figure 5.5: Fibre fracture after linear-elastic response, the fibre remains completely bonded

2. Fibre fracture occurs after the failure of some, but not all, cross-links, i.e., the fibre is not completely de-bonded. In this scenario, the sum of the maximum load borne by at least one cross-link and the frictional forces of all previous, already broken, cross-links is higher than the load-bearing capacity of the fibre $F_{cb,i} < F_{fra} < (F_{cb,n} + \sum_{i=1}^{i=n-1} F_{cf,i})$, where $i \in [1, ..., n-1]$. By increasing the applied load, the cross-links fail successively, starting from the crack surface and continuing toward the fibre end. Each strength element fails in turn when its critical load $F_{cb,i}$ is reached. The breakage of a strength element leads to the activation of both its parallel-arranged friction element and the corresponding spring element which, hence, leads to load transfer to the next strength element. This can be physically explained as follows: The frictional action of a cross-link starts immediately after its failure, leading to a load transfer to the next cross-link through the fibre. The activation of a new segment of the fibre is represented in the model by the activation of the next serially arranged spring element. Since the "working" part of the fibre becomes longer, the stiffness of the system decreases. This type of behaviour is called "elastic-plastic with hardening - multi yield"; cf. Figure 5.8.

   The breakage of the first strength element leads to a drop in force in the cross-link from $F_{cb,1}$ to $F_{cf,1}$ and to an immediate activation of the parallel-arranged friction block, indeed with a constant friction load $F_{cf,1}$), the second spring element (spring S_2), and through it also of the second cross-link. At this moment, the difference in load $F_{cb,1} - F_{cf,1}$ begins

being passed to spring S_2, which leads to a mutual sequential relaxation and stretch in both springs S_1 and S_2, respectively, restoring equilibrium in node 1; cf. Figure 5.6. As a result of the increased fibre length for the given displacement, a drop in load is observed.

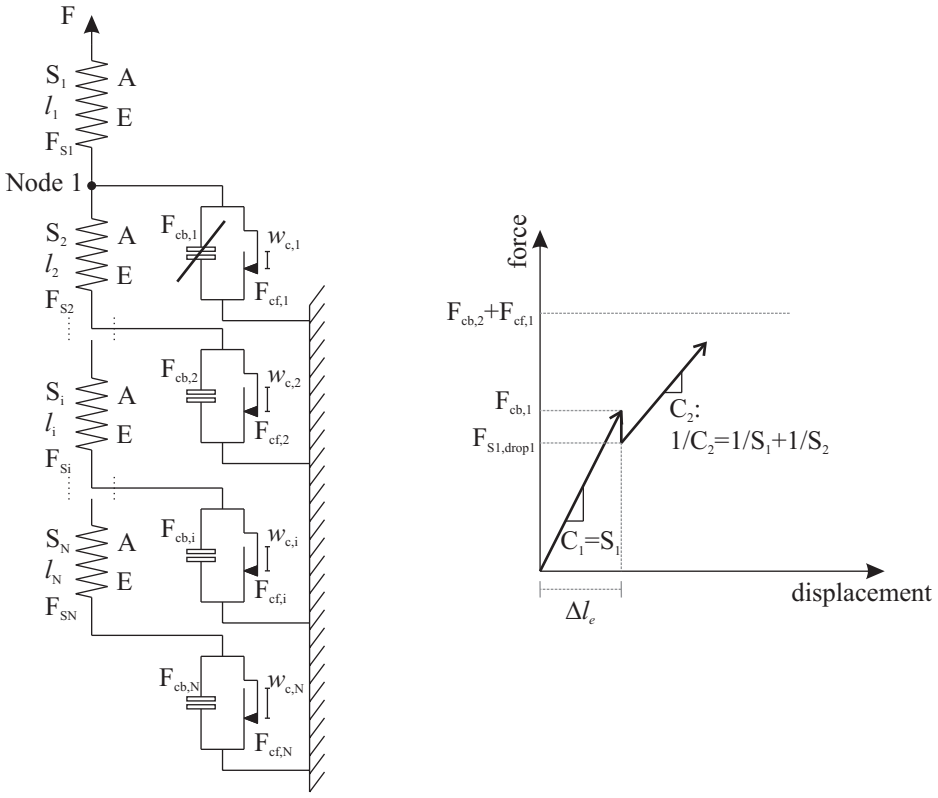

Figure 5.6: Drop in stress resulting from breakage of the first cross-link

The system is in balance again when the force in spring S_1 reaches the value $F_{S_1,drop1}$, cf. Figure 5.6. The index "$S_1, drop1$" is used to indicate the force in spring S_1 after the first drop, i.e., the breakage of the first cross-link. This force is given in Equation 5.2. It should be emphasized that this equation is valid under the above mentioned assumptions, i.e., $A_i = A = const$ and $E_i = E = const$.

$$F_{S1,drop1} = F_{cb,1} \cdot \frac{l_1}{l_1 + l_2} + F_{cf,1} \cdot \frac{l_2}{l_1 + l_2} \tag{5.2}$$

The second strength element fails when the applied force reaches a value of $F_{cb,2} + F_{cf,1}$. Subsequently, the system restores equilibrium again in both node 1 and node 2, and second drop in force occurs, cf. Figure 5.7.

The resulting $F_{S_1,drop2}$ can be calculated based on the properties of the five elements connected to nodes 1 and 2, cf. Figure 5.7. Basically the deformation in spring S_2, which results from the force drop after the failure of the strength element $F_{cb,2}$ and stretching of the activated spring S_3, should be derived first, i.e., the shifting of node 2. The shifting of node 2, based on properties of spring S_1 and spring S_2, leads subsequently to a shift of node 1. Based on the equilibrium relationships in node 1, the corresponding deformation in spring S_1 can be derived as well. The drop in force due to the failure of the second cross-link can be given by Equation 5.3:

$$F_{S1,drop2} = S_1 \cdot (\Delta l_1 - \Delta l_{1,3}) \tag{5.3}$$

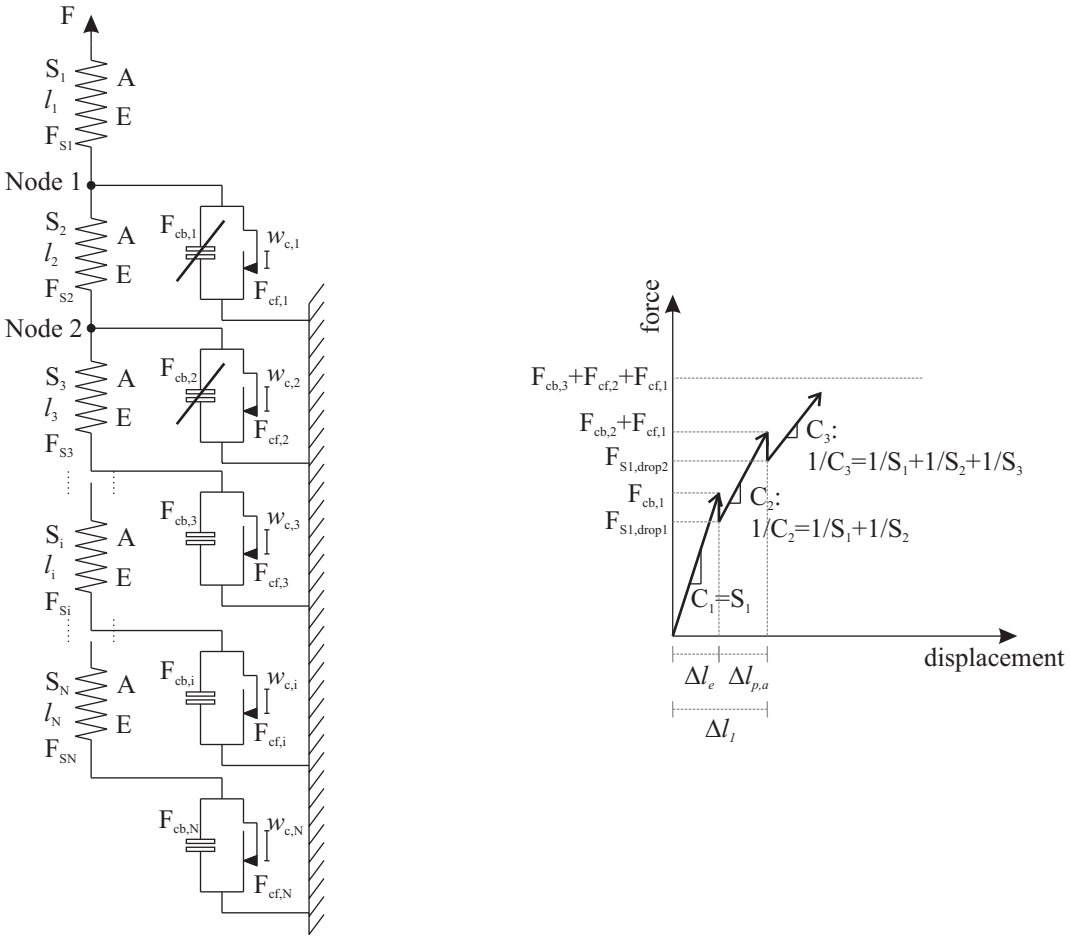

Figure 5.7: Drop in stress resulting from the breakage of the second cross-link

Where:
Δl_1: The deformation of spring S_1 just before the failure of the second force element:

$$\Delta l_1 = \Delta l_e + \Delta l_{p,a} = \frac{F_{cb,1}}{S_1} + (\frac{1}{S_1} + \frac{1}{S_2}) \cdot F_{cb,2} + \frac{1}{S_1} \cdot (F_{cf,1} - F_{cb,1})$$

Δl_e: Deformation in spring S_1 when the critical load $F_{cb,1}$ is reached

$\Delta l_{p,a}$: The deformation recorded between the breakage of the first and the second cross-link

$\Delta l_{1,3}$: The deformation of spring S_1 resulting from the failure of the second force element and the activation of spring S_3. This deformation can be calculated as:

$$\Delta l_{1,3} = \frac{l_2}{S1 \cdot (l_2 - l_1)} \cdot [\frac{(F_{cb,1} - F_{cf,1})}{l_1 + l_2} \cdot (l_2 - l_1 + \frac{l_3 \cdot l_1}{l_2 + l_3}) - F_{cf,2} \cdot \frac{l_3}{l_2 + l_3} - F_{cf,1}]$$

The same procedures can be followed to derive the next drops which may result from the failure of further strength elements. However, the mathematics would be more complicated due to the increase in number of the nodes and elements involved.

It can be generalized that the new activated cross-link n fails when the applied load value reaches the sum of its strength $F_{cb,n}$ and the frictional forces of all previous, already broken, cross-links; see Equation 5.4.

$$F = F_{cb,n} + \sum_{i=1}^{i=n-1} F_{cf,i} \tag{5.4}$$

After the breakage of each cross-link a drop in load may develop. The resulting load-displacement curve is presented in Figure 5.8, which describes one possible scenario where the fibre fails at the last activated cross-link.

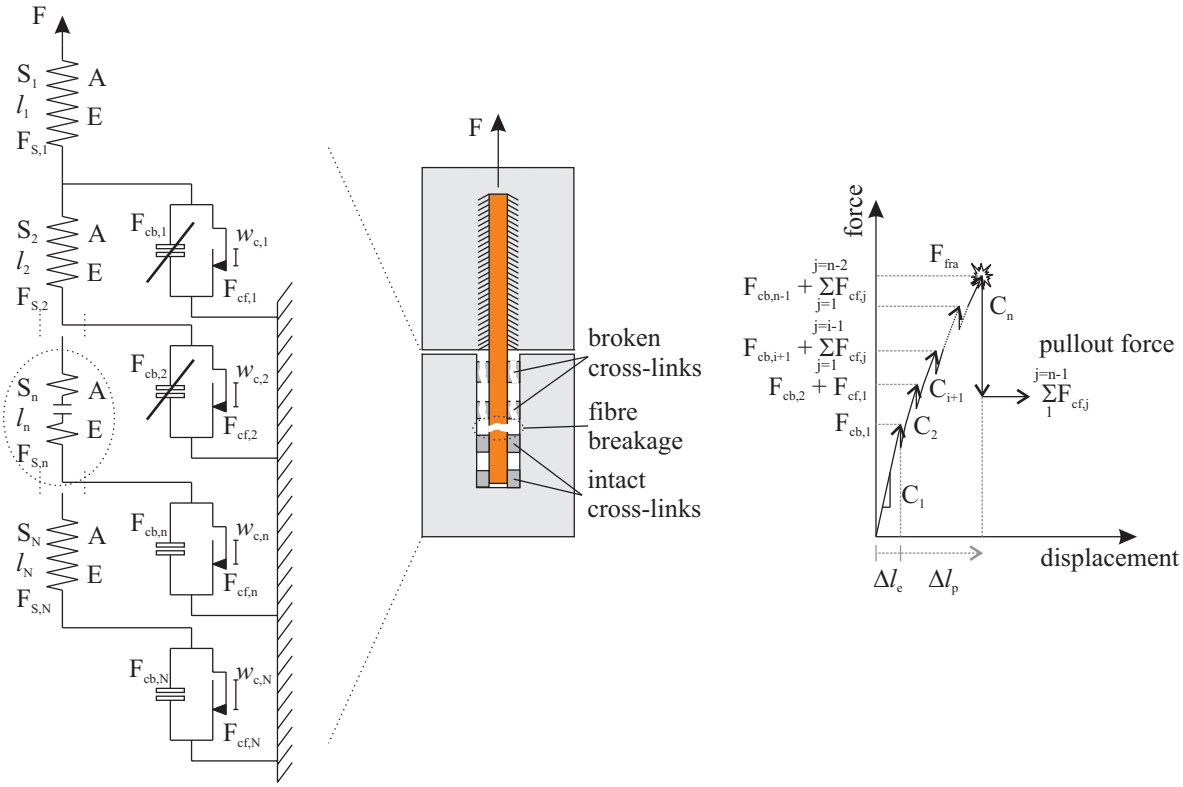

Figure 5.8: Fibre fracture after an elastic-plastic response due to the sequential breakage of cross-links, the fibre is not completely de-bonded

According to this scenario the fibre fractures when the sum of strength value of the newly activated cross-link n and the frictional forces of all previous, already broken, cross-links is higher than the maximum load bearing capacity of the fibre, i.e., when the strength of one of the spring elements is reached, $F_{fra} = F_{Si}$. Having a new spring element after the failure

of each cross-link, i.e., activation of a new segment of fibre, leads to a gradual decrease in the stiffness of the system. This behaviour can be described in Equation 5.5:

$$
\begin{aligned}
&\Delta l = \Delta l_e + \Delta l_p \\
&\forall F < F_{cb,1} \\
&\Delta l_e = \frac{F_{cb,1}}{C1} \\
&\Delta l_e : \ Deformation\ in\ spring\ S1\ when\ the\ critical\ load\ F_{cb,1}\ is\ reached, \\
&i.e.\ deformation\ of\ the\ fibre\ at\ the\ breakage\ of\ the\ first\ cross-link. \\
&\forall F_{cb,1} \leq F < F_{cb,n} \\
&\Delta l_p = \sum_{i=1}^{i=n-2} \frac{F_{cb,i+1} + F_{cf,i} - F_{S1,drop''i''}}{C_{i+1}} + \frac{F_{fra} - F_{S1,drop''n-1''}}{C_n} \\
&where: \ \frac{1}{C_n} = \sum_{i=1}^{i=n} \frac{1}{Si}
\end{aligned}
\tag{5.5}
$$

After fibre fracture pullout starts. The de-bonded part of the fibre is pulled out with a load equal to the sum of the frictional forces of all broken cross-links $\sum_{j=1}^{j=n-1} F_{cf,j}$, cf. Figure 5.8. More details concerning fibre pullout may be found in Section 5.2.2.

It should be underlined here that, by considering the force distribution, the highest probability of fibre failure is at the crack surface, where the force is represented according to Equation 5.4. Figure 5.9 illustrates schematically the force distribution along the fibre axis before the breakage of cross-link n. $F_{current,n}$ is the force in cross-link n before its breakage, i.e., $F_{current,n} < F_{cb,n}$.

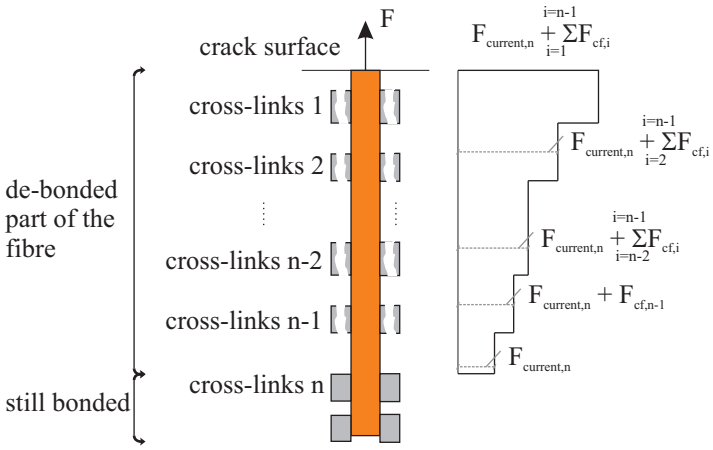

Figure 5.9: Force distribution along fibre axis; partially de-bonded fibre

It is still probable that the fracture of the fibre occurs directly at a strong cross-link due to the stress concentration at its location. However, since the strength of the fibre varies along its axis, i.e., the strength of the spring elements is not constant $F_{Si} \neq const$, the fracture of the fibre is possible at any location along the de-bonded length. Possible damage of the fibre, which resulted from the breakage of cross-links during partial pullout, could lead to the fibre fracture in this damaged area. Figure 5.10 illustrates a possible scenario where the fibre fractures between the first and the second cross-link. Here the pullout force is just

the frictional force of the first cross-link. However, this phenomenon is not investigated fully in the current model.

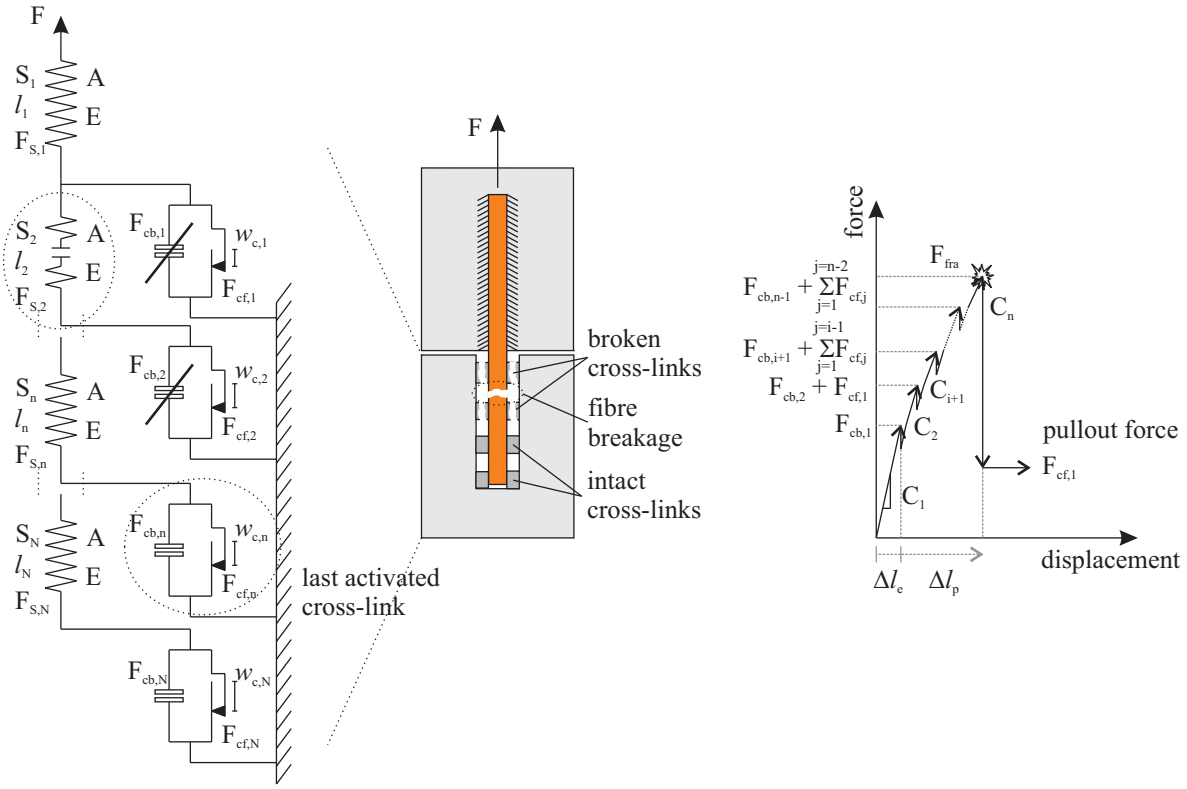

Figure 5.10: Another scenario of fibre fracture after an elastic-plastic response, the fibre fractures at a location between the first and the second cross-link

5.2.2 Fibre pullout

Fibre pullout starts after complete de-bonding along the interface between the fibre and matrix, i.e., after the breaking of all cross-links responsible for the bond between fibre and surrounding matrix. De-bonding of the fibre is complete after the failure of the last cross-link N at which the load increases up to: $F_{cb,N} + \sum_{i=1}^{i=N-1} F_{cf,i}$. At the moment of breakage of the last cross-link, a drop in stress takes place and the force decreases suddenly to the level $\sum_{i=1}^{i=n} F_{cf,i}$, cf. Figure 5.11.

The displacement capacity of each friction element is limited by the value $w_{c,i}$ which represents the distance between the corresponding cross-link i and crack surface. The force of friction due to pullout of the fibre decreases gradually as a result of the sequential exiting of cross-links from the fibre canal due to crack opening, as shown schematically in Figure 5.12 (left). The descending pullout branch can be described by the graded curve based on the different displacement capacities of the friction blocks, cf. Figure 5.12 (right). By exceeding the displacement capacity of each cross-link $w_{c,i}$, the total pullout force decreases by the value associated with the corresponding failed friction block $F_{cf,i}$. This process continues with further crack opening and the friction blocks fail one after the other while frictional force decreases gradually. The friction decreases to zero when the crack opening reaches the value of $w_{c,N}$ and the last cross-link leaves the fibre canal, cf. Figure 5.12 (right).

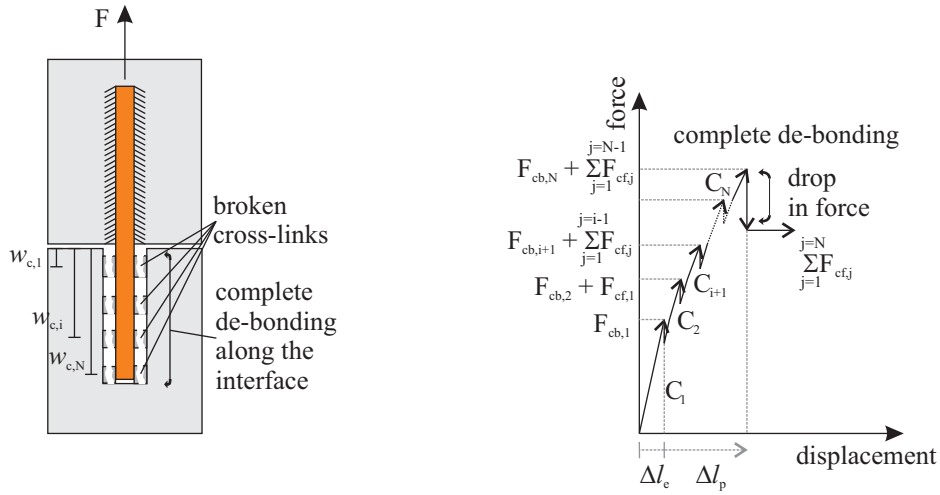

Figure 5.11: Fibre de-bonding

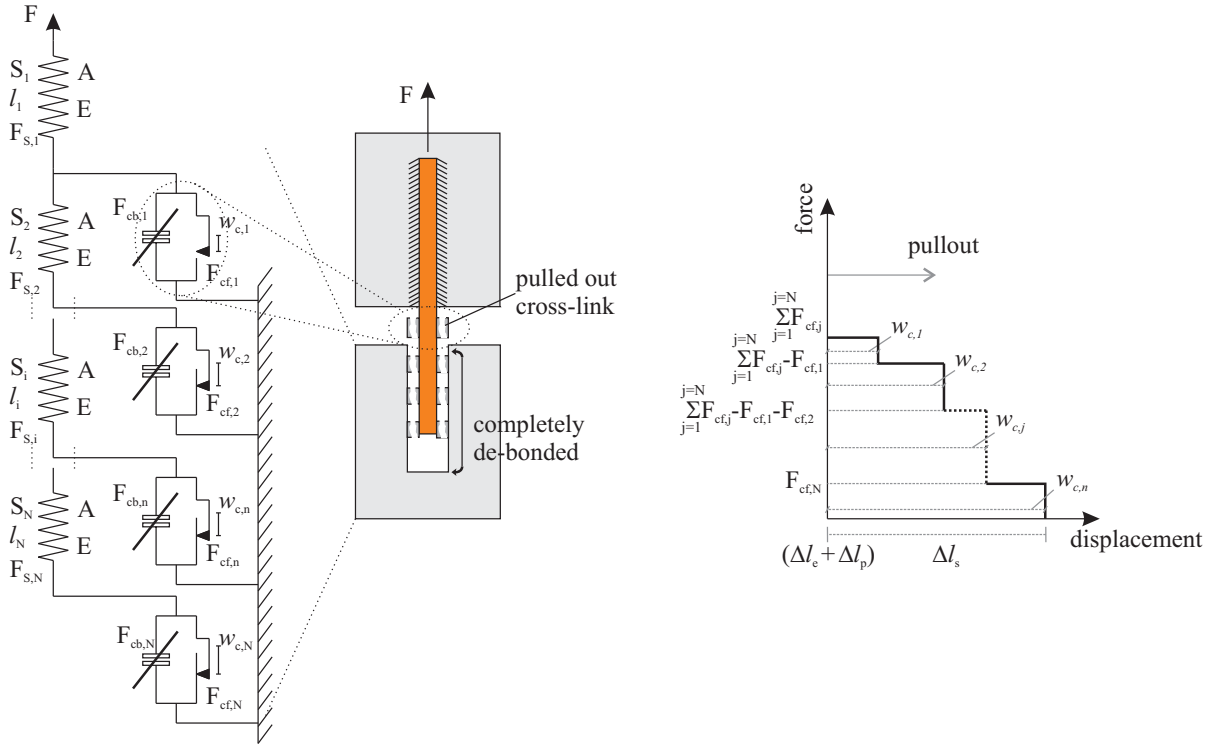

Figure 5.12: The failure of first friction element due to exit of the corresponding cross-link from the fibre canal (left) and a simplified, graded curve describing the softening branch of the force-displacement relationship (right)

5.3 Statistical study of fibre distribution and orientation at fracture surface – Meso-level

5.3.1 Introduction

Three main parameters relevant to the crack-bridging capacity of fibres should be considered when the fracture surface is investigated: fibre embedded length, fibre orientation, and number of fibres. These parameters are also needed as input values for the multi-scale model presented in this chapter.

The investigation of short fibres at fracture surfaces of specimens with textile reinforcement layers was relatively complex and confusing due to the high numbers of fibres resulting from the multifilament-yarns and short fibres. This being so, it was decided to investigate the short fibres on fracture surfaces from specimens reinforced only by short fibres. As mentioned in Section 4.2.1.3, only a low number of short fibres could be observed on the fracture surface when the matrix with low water-to-binder ratio (M030) was used in comparison to the considerable number of fibres observed on the fracture surface of specimens made with matrix M045 (w/b = 0.45), cf. Figure 4.14. For a statistical study, it makes more sense to investigate the fracture surface with high numbers of fibres, i.e., specimens made with matrix M045. Moreover, since no experimental results of pullout tests on single carbon fibres were available, and since therefore the data basis for modelling was missing here, no statistical studies could be performed on short carbon fibres.

Based on the above description, the statistical study is limited to matrix M045, water-to-binder ratio of 0.45, and two types of short fibres: integral glass and dispersed glass fibres. In order to include the influence of the lamination technique used to produce the specimens with textile and hybrid reinforcement for purposes of this dissertation, an additional series of specimens reinforced with short fibres only, 3 specimens with each type of short fibre, were produced for the statistical study using laminating technique. These specimens were produced by pouring the concrete with short fibres in batches and spreading it using the lamination technique. The same curing conditions mentioned in Section 3.2.3 were applied for these specimens. The mechanical behaviour of these specimens was not considered.

A watchmaker's eyepiece and an optical microscope with a high resolution camera were used to investigate the condition of fracture surfaces. The results obtained from this investigation and their statistical evaluation are described in the following sections.

5.3.2 Fibre embedded length

To find an appropriate function to describe the probability distribution of fibre embedded lengths a considerable number of fibres at fracture surfaces from different specimens were investigated and the lengths of the fibres were recorded. The statistical calculations were performed using the commercial software RStudio [123].

Because of the nearly random orientation of fibres within the matrix, the great majority of fibres are oriented at different angles to the crack surface. For both types of short fibres, three angles were considered to represent all possible cases:

- 90° for all fibres oriented to the crack surface at angles between 60° and 90°
- 45° for all fibres oriented to the crack surface at angles between 30° and 60°

- fibres oriented at angles between 0° and 30° were counted and considered as non-bridging fibres; accordingly no statistical study of fibre embedded length was performed for these fibres.

The theory of Weibull was chosen to describe the probability distribution function of the fibres' embedded lengths, see Equation 5.6. This choice was based on previous investigations by other researchers where the Weibull distribution function was proposed for modelling the fibre length distribution and was shown to be effective in describing fibre length density distribution for short glass fibre reinforced polypropylene, e.g., Chin et al. [124] and for short fibre reinforced polymers, e.g., Fu and Lauke [125].

$$f(l_a) = \frac{\beta}{\eta}\left(\frac{l_a-\gamma}{\eta}\right)^{\beta-1} e^{-\left(\frac{l_a-\gamma}{\eta}\right)^{\beta}} \tag{5.6}$$

Where: $f(l_a) > 0$
l_a: Embedded length
β: Shape parameter
η: Scale parameter
γ: Location parameter.

Short dispersed glass fibres in matrix M045

Because of the very small diameter of short dispersed glass fibres, only 20 μm, an optical microscope with a high resolution camera was used to investigate this type of fibres. Approximately 2500 dispersed fibres at six fracture surfaces ($\approx$ 400 fibres per surface) from three different specimens, i.e., three final cracks, were randomly chosen and investigated.

It should be mentioned here that the expression "fibres bridging the crack" means the fibres measured on both fracture surfaces obtained after complete opening of a crack.

While the lengths of the fibres varied between 47 μm and approximately 2800 μm for fibres with angle 90° to the crack surface, for those with angle 45° to the crack surface the fibre length range was between 100 μm and 2400 μm.

For the histograms, 14 and 12 classes were determined for fibres with the angle 90° and 45° to crack surface, respectively. A class width of 0.2 mm was chosen. Since the data are made up of positive numbers, the first class was made to go from 0 to 0.2 mm. The parameters for the distribution function of fibres with angle of 90° to the crack surface were determined by:

β: 1.485
η: 760.7
γ: 0.

and for fibres with angle 45° to the crack surface:

β: 1.360
η: 782.9
γ: 0.

Figure 5.13 shows the density functions representing the distribution of fibre embedded lengths of dispersed glass fibres in matrix M045.

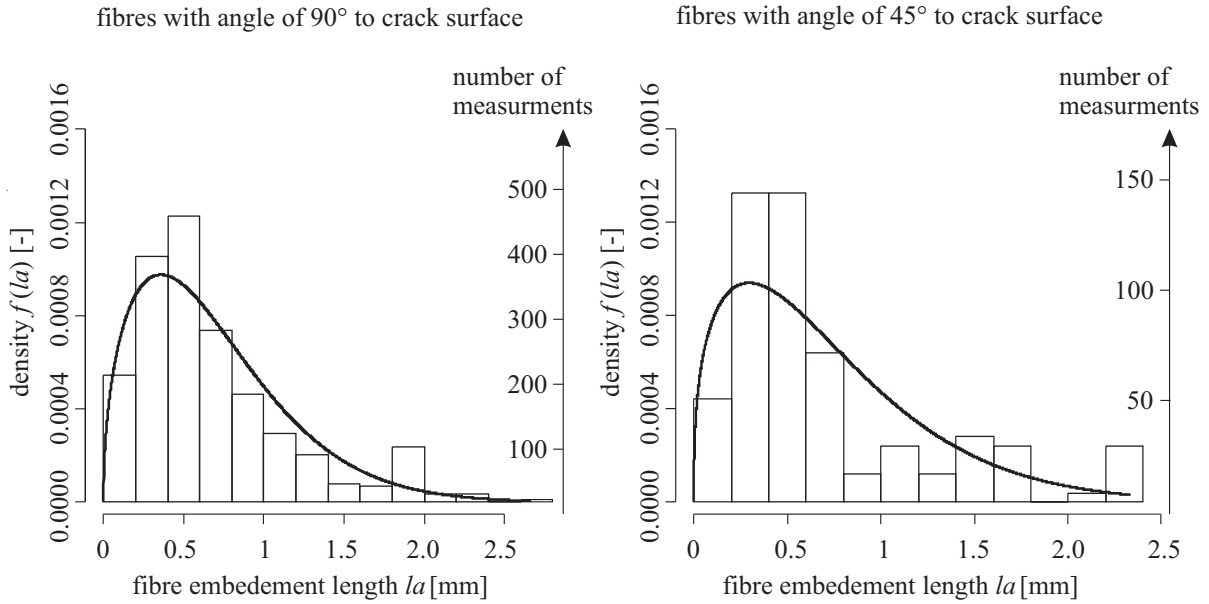

Figure 5.13: Distribution of embedement length of dispersed fibres with angle 90° (left) and 45° (right) to crack surface

Short integral glass fibres in matrix M045

As observed in the single-fibre pullout tests performed on short integral glass fibres, all tested fibres showed complete pullout and a softening branch up to 3 mm, which was the chosen fibre embedded length in the tests; see Figure 4.34 (right) and Table 4.8 for pullout parallel to fibre axis and in Figure 4.36 (right) and Table 4.9 for the pullout of inclined fibres. Based on these findings, the fibres measured and investigated at the fracture surface represent indeed all fibres bridging the crack with a fibre embedded length which is equal to the measured length.

Approximately 750 integral fibres for three different completely opened cracks (i.e., six fracture surfaces with $\approx$ 125 fibres per surface) from three different specimens were investigated. A watchmaker's eyepiece and a ruler with a scale in millimeters were used for this purpose. To simplify the measurements the values of fibre lengths were rounded to the values: 1.0, 1.5, 2.0, 2.5 and 3.0 mm.

For the data of these fibres, 5 classes were determined for the histograms of both fibres with angles 90° and 45° to the crack surface. Here, the first class was made to start from 1.

Figure 5.14 (left) and (right) show histograms and the density functions represent the distribution of fibre embedded lengths for integral fibres with angle 90° and 45° to the crack surface, respectively.

The parameters for the Weibull distribution functions were determined for fibres with 90° by:

β: 3.792
η: 2.228
γ: 0

and for fibres with angle of 45° to crack surface by:

β: 3.513
η: 2.414
γ: 0

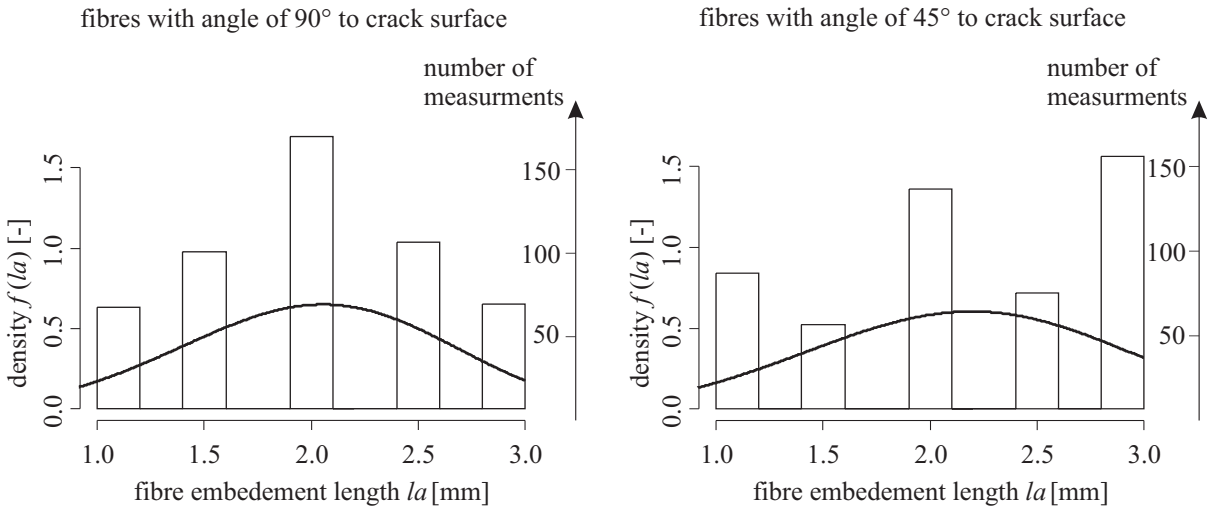

Figure 5.14: Distribution of embedded lengths of integral fibres with angles of 90° (left) and 45° (right) to the crack surface

As it is shown in Figure 5.13, the chosen Weibull distribution function is indeed appropriate to describe the density distribution of the embedded lengths of short dispersed glass fibres. This choice was less effective for the density distribution of short integral glass fibres, cf. Figure 5.14. Here another distribution function might be more fitting. However, the small number of classes used in this investigaton does not enable a more comprehensive statistical evaluation.

5.3.3 Orientation and number of fibres

Generally, the fibre inclination angles with respect to cracks in a concrete matrix are randomly distributed. Random orientation of fibres in a 3D, infinite element can be illustrated as a sphere with a probability density for the fibre inclination angle expressed as a sine function, as shown in [75]. However, the dimensions of a specimen or structure member influence fibre orientation greatly. The possibility of free orientation of fibres is restricted by boundaries, see also Section 2.3.3. The boundary effect leads to the orientation of fibres moving from 3D towards 2D conditions.

The production technique used to produce the specimens, the laminating process used in this investigation, and the finishing of surfaces influence fibre orientation further and give an additional push to the nearly 2D-oriented fibres in a plane to towards a unidirectional alignment, i.e., the direction of laminating which is parallel to the loading direction.

Short dispersed fibres and matrix M045

Because of the very small diameter of dispersed glass fibres (20 μm) and, therefore, their very dense concentration at the fracture surface, it was not possible to investigate their orientation in same manner as was done for short integral fibres; see next section. For this reason, a certain number of fibres were investigated from randomly chosen areas at the bottom, middle, and top sides of both fracture surfaces of a completely opened crack on one specimen, 50 fibres from each location. What is meant by "bottom" and "top" sides of the fracture surface are respectively the sides of the specimens at the ground plate of the mold and the sides where the covers of the mold were placed; see Section 3.2.2). The results show that the number of fibres at angle of 90° to the crack surface are much higher than those with angle of 45° to the crack surface, cf. Figure 5.15. This holds true for all fibres chosen, independent of the location at the crack surface. This could be traced back both to the boundaries, i.e., slender specimens, and to the specimens' production technique, lamination. Furthermore, the results show that the number of fibres with an angle of 90° to the crack surface at the bottom side of the specimen is higher than the number of these fibres at the middle and top of the specimen, cf. Figure 5.15. This pronounced difference can be traced back to the procedure of specimen fabrication where the first "batch" of concrete at the bottom of the mould is exposed to more vibration and orientation throughout the entire period of fabrication.

The fibre orientation factor is used to describe these effects by determining the number of fibres crossing a crack surface. The fibre orientation factor is estimated based on Equation 5.7 according to [75].

$$n_f = \alpha_f . A_c . \frac{V_f}{A_f} \tag{5.7}$$

Where:
n_f: Number of fibres
α_f: Orientation factor

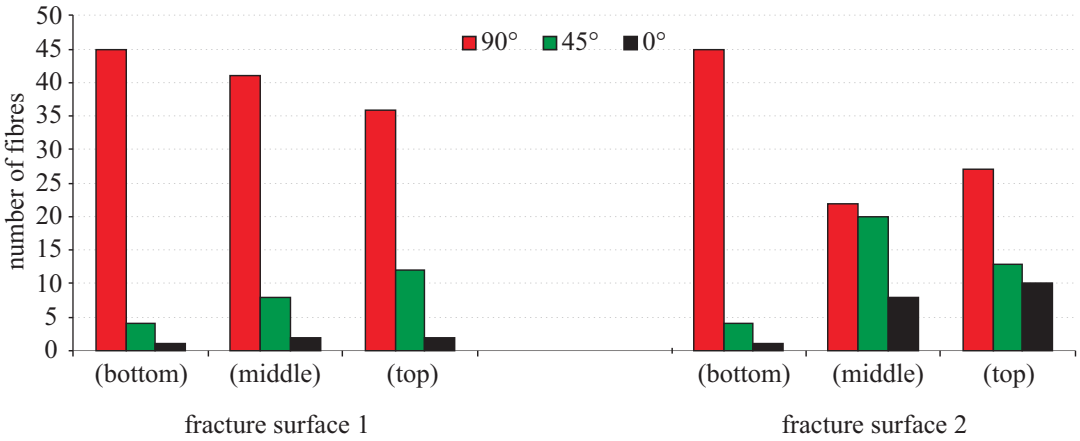

Figure 5.15: Variation of fibre orientation in three different locations at fracture surface along the specimen hight

A_c: Cross-sectional area (unit cross-sectional area)
V_f: Volume fraction of fibre
A_f: Cross-sectional area of one fibre.

The orientation factor takes into account the randomness of fibres in their orientation with respect to the tensile direction. As discussed in Section 2.3.3, the fibre orientation factor is influenced by surrounding boundaries, member thickness, and distance from the surface. For a three-dimensional case with a random orientation of fibres, the value of the orientation factor can be considered as $\alpha_f = 0.5$. If the fibres are oriented in 2D random orientation the factor becomes $\alpha_f = 0.64$, see Lee et al. [79] and [80]. However, no information on the influence of the lamination technique on fibre orientation factor is available in the literature.

In order to describe this effect, the cross-sectional area of one specimen, i.e., the fracture surface of a completely opened crack, was divided in two main regions:

- central region, where only two parallel boundary surfaces influence the orientation of the fibres
- side regions, where three boundaries influence the orientation of the fibres.

The number of fibres in randomly chosen areas (unit area of 2 mm x 2 mm) from these regions were counted and the fibre orientation factors were determined using Equation 5.7. Three unit areas per side region and six in the central region were specified at the bottom, middle and top of the fracture surface height, see Figure 5.16. Due to the large number of fibres in the cross section and their dense distribution, the dimensions of the tested area were set relatively small in order to obtain a more accurate count. Since it is essential to consider the exact number of fibres in a given specific area to determine the fibre orientation factor, the approach used here is different to that used in investigating fibre orientation along the specimen height, leading to Figure 5.15.

While the fibre orientation factor in side regions was very high (approximately $\alpha_f = 0.8$), in central regions it varied between $\alpha_f = 0.75$ for the areas at boundary surface and $\alpha_f = 0.62$ in the center of the specimen, as is schematically illustrated in Figure 5.16.

It should be mentioned here that the fibre investigated on the fracture surface do not include those which failed before de-bonding and pullout. In order to consider these fibres, the recorded

number was multiplied by 1.40 to get the total number of fibres bridging the corresponding cross sectional area. This factor was derived based on the pullout tests performed on dispersed fibres embedded into matrix M045, cf. Table 4.8 in Section 4.4.2.1: In these tests 30 % of fibres failed. Actually these tests are only for fibres with angle of 90° to the crack surface. However, the author decided it is still meaningful to use the factor 1.4 to get the total number of fibres since no information is available regarding the percentage of failed fibres when tested with inclination to the crack surface.

For the purpose of modelling, the fibre orientation factor of ($\alpha_f = 0.62$) is chosen for the whole cross-section; see Section 4.1.3. This choice was taken only in order to include the influence of the lamination technique. No boundary effect is considered in the model.

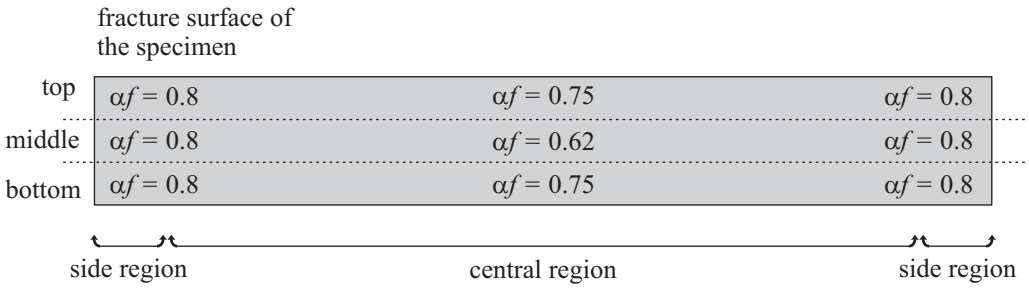

Figure 5.16: Variation of fibre orientation factor according to distance from boundary surface in a specimen produced using lamination technique

Short integral fibres in matrix M045

In order to show the influence of boundaries and the laminating process on the orientation of integral fibres, the fracture surface of one specimen was divided into 13 fields along its width; each area had a section of approximately 7.7 mm x 12 mm, cf. Figure 5.17 (above). The fibres in each area were counted by visual inspection and classified in three categories: angles of 90°, 45°, and 0° to the crack surface, similar to the process presented in the previous subsection. The total number of fibres in each field is the sum of the number of fibres of opposing areas on both sides of the crack. Figure 5.17 (below) presents the number of fibres of the three categories into each field. It can be noted from the figure that the concentration of fibres with angle of 90° to the crack surface is much higher at the specimens' sides, fields 1, 2, 12 and 13, than at the middle of specimen, fields 6, 7 and 8; the former had approximately double amount of fibres. This can be traced back to the greater boundary effect at the specimen sides, three surfaces. Moreover, the number of fibres with an angle of 90° to the crack surface is higher than that of fibres with an angle of 45° to the crack surface along the entire width; cf. Figure 5.17. This could be a result of the lamination technique used to produce the specimens. It can be also noticed from the figure that the total number of fibres of all orientations is higher in the fields at specimen sides than that in the middle of the specimen. No direct explanations for this observation can be given yet.

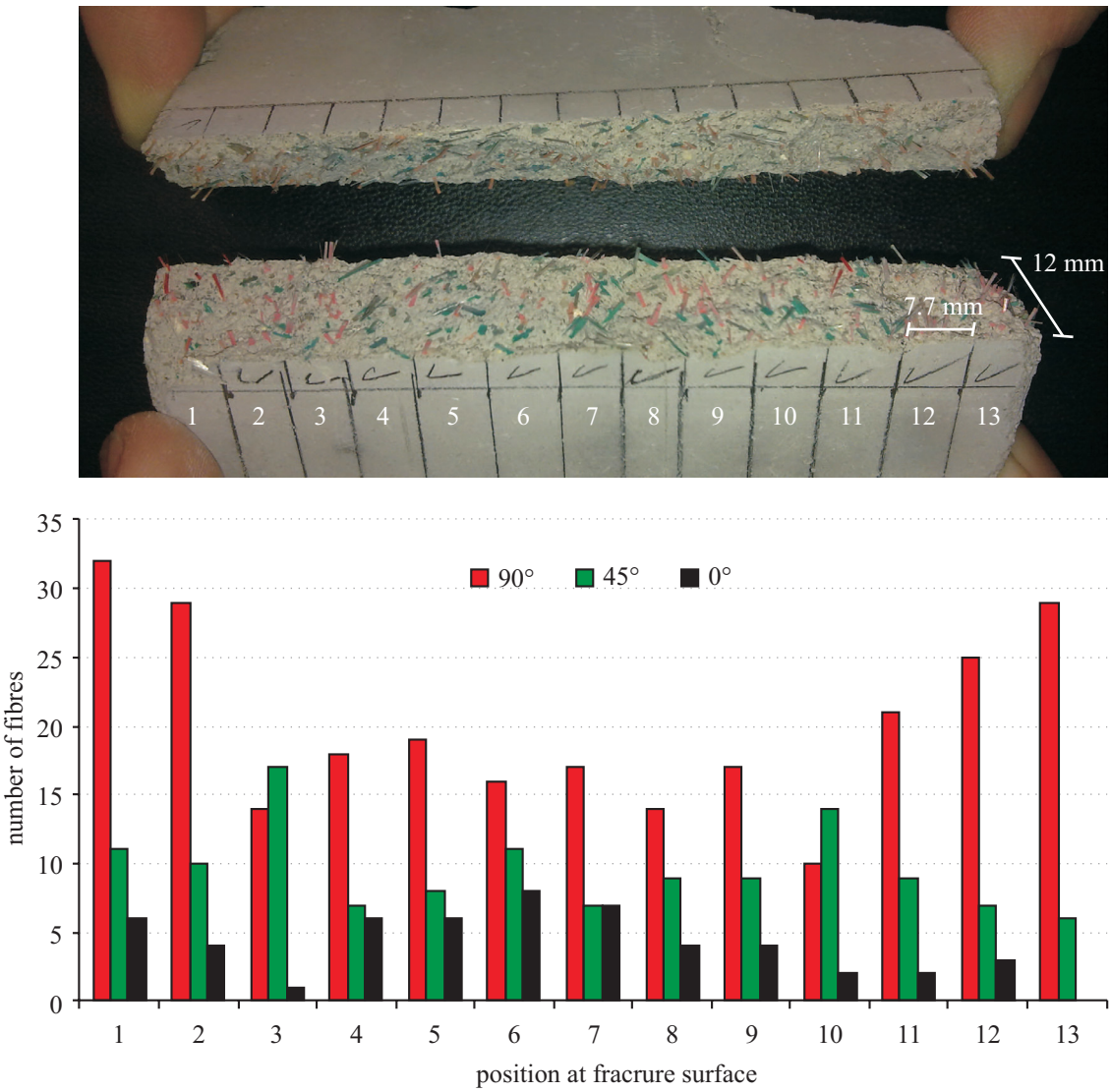

Figure 5.17: Fracture surface of a specimen reinforced with 1.0 % by volume short integral glass fibres (above) and the number of fibres counted along the specimen width (below)

5.4 Multi-scale modelling approach

5.4.1 Introduction

In this subchapter, multi-scale modelling approach for TRC with added short fibres and subjected to deformation-controlled tensile loading is described according to the concept given in Figure 1.3. In particular, the mathematical expressions for the description of fibre pullout were derived first. The force-displacement relations obtained were derived based on the rheological-statistical model presented in Section 5.2 and considered the decisive physical phenomena observed in experiments performed at the micro-level of observation. This step is performed using the commercially available software Excel.

Subsequently, the joint action of fibres involved in crack bridging action could be modelled and the corresponding relationship at the meso-level of observation was derived. The interconnection of several cracks and the uncracked matrix whilst considering the effect of multifilament-yarns on crack-bridging finally resulted in the description of TRC with short fibres behaviour under tensile loading, behaviour at the macro-level of observation. The derivation of mathematical relations at the meso- and macro-levels of observation was performed using the commercial software MATLAB.

5.4.2 Mathematical description of single-fibre pullout response – Micro-level

As described in Section 4.2.3, the fibre failure mode, either fibre fracture or fibre pullout, depends on the bond between the matrix and the single short fibre. The model presented in Section 5.2 considers these phenomena and reproduces the pullout responses depending on the characteristics of the cross-links and the fibre.

The results of single-fibre pullout tests performed on short dispersed glass fibres embedded in matrix M045 (w/b = 0.45), cf. Figure 4.34 (left) and Table 4.8 were chosen as reference. The experimental curves were described using defined points determined by characteristic values based on the failure mode. While one additional point, except for the point of origin, is needed to describe fibre fracture, two additional points are needed in order to describe the scenario of fibre pullout. The values of the displacement and the force at which the fibre fails are the characteristic values for the fibre fracture scenario. This extra point is valid also for the fibre pullout scenario. The displacement and force equal to zero at the point where the fibre is fully pulled out are the characteristic values used to determine the second point for the pullout scenario. The average values given in Table 5.1 were chosen to determine these characteristic points. However, as described in Section 5.2.1, the behaviour between the point of origin and the point at ultimate force is not necessarily linear, but might be elastic-plastic with hardening due to the sequential de-bonding process. This can also be observed by extracting the ascending branch of the force-displacement curves at very low strain levels obtained from pullout tests performed on single-fibres, as presented in Figure 5.18 (left). In order to show this effect in a better way, four representative curves were chosen from the group of curves, see Figure 5.18 (right). Based on this, the course between these points is schematically described by a hatched area to refer to the various possibilities of the shape of the relation, as shown in Figure 5.19.

In order to obtain some single-fibre pullout responses from the model, assumptions of the model parameters need to be made. The suggested values of the model parameters were proposed based on microscopic investigations of fibre surfaces, the statement of the number and location of the cross-links, and a study of the ascending branch of force-displacement curves obtained

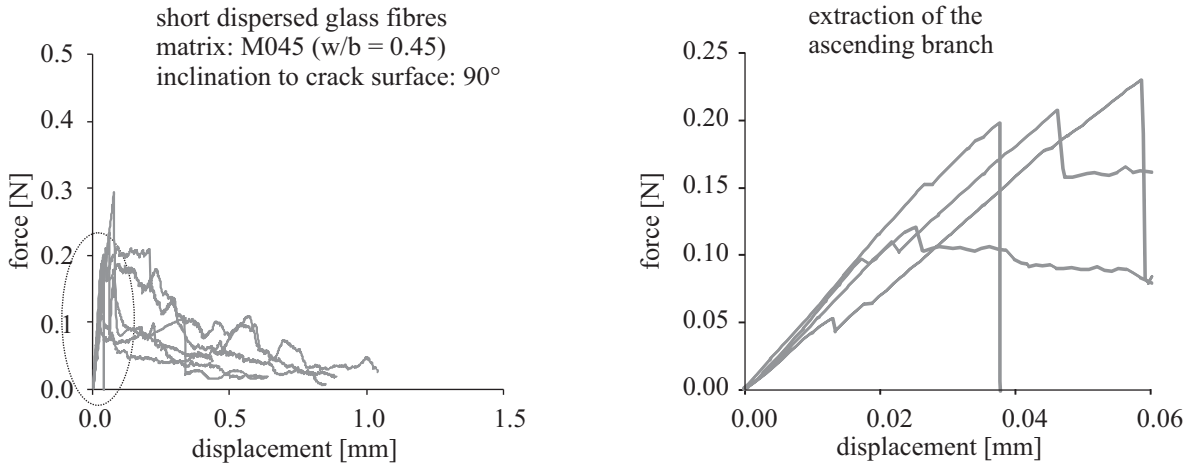

Figure 5.18: Non-linearity of the ascending branch of force-displacement curves obtained from pullout tests performed on short dispersed glass fibres embedded in matrix M045

Table 5.1: Evaluation of pullout tests results performed on short dispersed glass fibres embedded in matrix M045 with respect to response modes; according to Table 4.8

Type of fibre			Matrix M045
Dispersed fibre	Number of tested fibres		10
	Broken fibres	Number of fibres	3
		Max./min./average ultimate force value [N]	0.20/0.13/0.17
		Max./min./average displacement at the ultimate force [mm]	0.04/0.03/0.04
	Pullout fibres	Number of fibres	7
		Max./min./average ultimate force value [N]	0.29/0.10/0.18
		Max./min./average displacement at the ultimate force [mm]	0.08/0.02/0.05
		Max./min./average displacement at the force equal to 0 [mm]	1.27/0.45/0.89

from experimental tests, i.e., determination of the strength and stiffness of the spring elements. It should be highlighted here that due to the vague evaluation of positions and number of cross-links, as shown for example in Figure 5.2, the determination of the parameters was a rough estimation procedure, and some simplification had to be done. It must be stressed here that the model can and should be updated when future investigations to provide experimental values for the parameters. The parameters are assumed as follows: the number of cross-links and springs $i = 10$, distance between cross-links $w = 0.3$ mm, bond strength of a cros-link $F_{cb,i} = 0.0184$ N, friction force of a cross-link $F_{cf,i} = 0.0184$ N, stiffness of a spring element $S_i = 28$ N/mm and the maximum bearing load of the fibre $F_{fra} = 0.165$ N in case of fibre fracture and $F_{fra} > 0.184$ N in case of fibre pullout. In order to simplify the mathematical calculations, it was assumed that the force of each strength element is equal to the friction force of the parallel-arranged friction element, i.e., each cross-link possesses a friction force equal to its bond strength $F_{cb,i} = F_{cf,i}$. Based on this assumption, no drops in stress due to the breakage of cross-links were observed. Moreover, the distance between the first cross-link and the crack surface is equal to the distances between cross-links.

The condition that the maximum bearable load of the fibre is reached before the breakage of all cross-links should be fulfilled to get the response of fibre fracture ($F_{fra} < F_{cb,n} + \sum_{i=1}^{i=n-1} F_{cf,i}$). Figure 5.19 gives an example of a generated force-displacement curve ending with the fibre fracture.

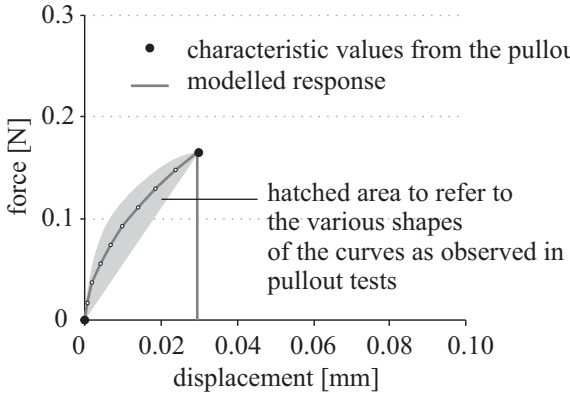

Figure 5.19: Force-displacement curve of fibre fracture; comparison of behaviours obtained from single-fibre pullout experiments and modelled behaviour

In the case of fibre pullout, two characteristic points were needed to represent the behaviour from the experiments, cf. Table 5.1. The first part of the modelled curve is completed with the complete de-bonding of the fibre, i.e., all cross-links are broken, but the fibre is not ($F_{fra} > F_{cb,N} + \sum_{i=1}^{i=N-1} F_{cf,i}$); see also Section 5.2.2. The second part is a result of the sequential leaving of cross-links from the fibre canal. Figure 5.20 shows an example of the response for the case of fibre pullout.

As is shown in Figure 5.20 (left), the measured maximum displacement during pullout test of approximately 1 mm is much less than the embedded length of 3 mm. This phenomenon was observed in all tests performed on dispersed glass fibres embedded into matrices M045 or even M030, cf. Figure 4.17. A possible explanation of this is that the friction capacity decreases pronouncedly during the pullout process. The cross-links themselves may be damaged due to their friction along the fibre canal. The term "progressive damage of friction capacity" can be used to describe this effect. Such observations were also found in the literature for another types of fibres, e.g., Jun [119] and Boshoff et al. [96] for pullout tests performed on single polyvinylalcohol (PVA) fibres. This is an important phenomenon that requires further investigation.

Since it is assumed in the model that the friction force of each cross-link remains constant along the entire distance to the crack surface, the maximum pullout displacement obtained from the model is equal to the embedded length, or actually, to the initial distance of the last cross-link from the crack surface, cf. Figure 5.20 (left). However, the deviation between the modelled and the experimental softening branch can be minimized by the use of reduction coefficient, cf. Figure 5.20 (right).

The steep initial part of the descending branch for a number of experimental curves; cf. Figure 5.18 (left) is due to the drop in force just before starting the pullout process. This can occur in the case of fibre failure before complete de-bonding or in that of fibre pullout; see the explanation of this phenomenon in Section 5.2. The difference in the precipitousness of the drop may depend on the location at which the fibre fractures; this is discussed in the section mentioned and illustrated schematically in Figures 5.8 and 5.10. Figure 5.21 shows the results obtained from

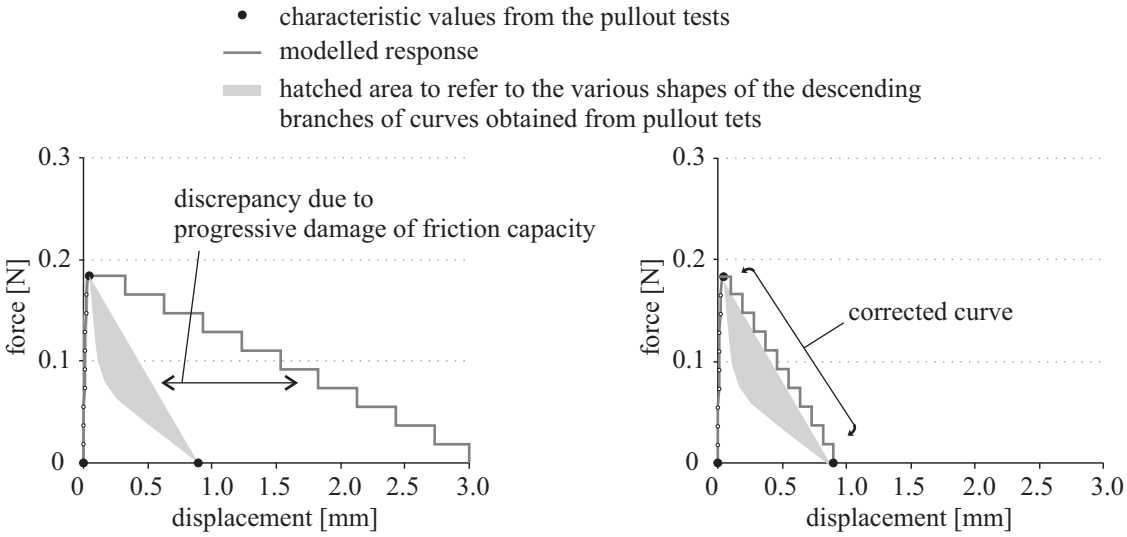

Figure 5.20: Force-displacement curve of fibre pullout; comparison of behaviours obtained from single-fibre pullout experiments and modelled behaviour before (left) and after (right) the use of a reduction coefficient for pullout displacement

the model in the case of fibre failure just before the complete de-bonding and the fibre fractures at a location in the middle of its embeddedment length.

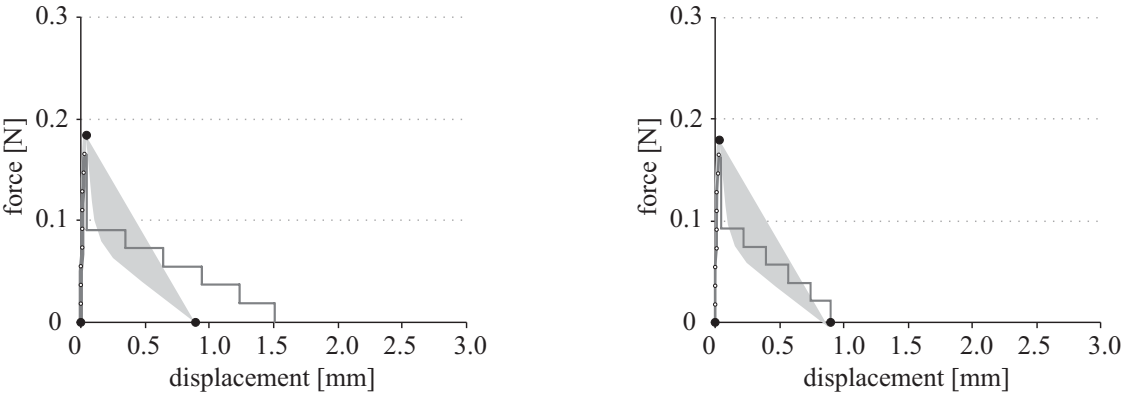

Figure 5.21: Force-displacement curve of pullout of a part of the fibre before it is completely de-bonded, breaking at the middle of the embedded length; before (left) and after (right) the use of a reduction coefficient for pullout displacement

It should be mentioned here that the above-modelled responses obtained reproduce the experimental results of single-fibre pullout tests parallel to its axis with one particular embedded length. No additional effects, as those of embedded length, fibre inclination, and double-sided de-bonding, are included in the model yet. These parameters are incorporated into the model in the next Section 5.4.3.

5.4.3 Mathematical description of single crack behaviour – Meso-level

Since short fibres are nearly randomly distributed and orientated in the matrix, the influences of fibre embedded lengths, fibre inclinations and the effect of double-sided de-bonding should

be included in the pullout responses used to describe the formation and opening of each single crack.

It must be stressed here that the assumptions presented below are perhaps very vague and daring; however, they are needed to present the entire modelling concept. When future test series provide the needed experimental data, the model can and should be updated.

As described in Section 2.3.4.2 both the ultimate force and failure scenario depend on the embedded length. This effect will be included based on the observation found in the literature, in particular [103] and [96].

The ultimate forces obtained from single-fibre pullout tests with an embedded length of 3 mm are presented in Table 5.1. Starting with these values and assuming a linear relation between the ultimate force and the embedded length as shown in Figure 5.22 (left) the pullout or fracture forces of two further embedded lengths, 1 mm and 2 mm, were estimated.

In order to estimate the relationship between embedded length and the failure scenario, an extra series of single-fibre pullout tests with different embedded lengths was needed. The new data should provide the percentage of fibres which rupture or pull out in pullout tests. Due to the difficulties in the handling of the very fine glass filament, test series with 1 mm or 2 mm embedded length could hardly be performed in an appropriate manner within the framework of this dissertation. Thus, an extra test series with 5 mm embedded length was performed. 7 specimens were tested: 3 fibres fractured and 4 failed in the pullout scenario; 42.8 % of fibres fractured in the tests. The value of the percentage of broken fibres obtained from these tests was used together with the corresponding value obtained from tests with 3 mm embedded length by means of a linear extrapolation to find out the percentage values at embedded lengths of 1 mm and 2 mm, cf. Figure 5.22 (right). However, as shown in the figure, this linear regression cannot be absolutely correct, since it yields a non-zero value for zero embedded length.

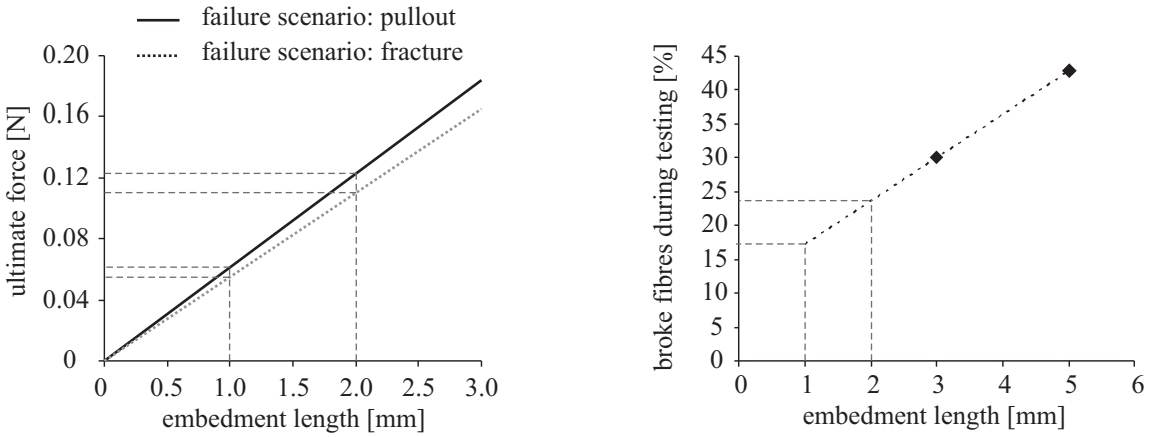

Figure 5.22: Relationships between embedded length and ultimate force (left) and the percentage of fibres broken during testing (right)

Figures 5.23 and 5.24 show the generated responses for the embedment lengths of 2 mm and 1 mm, respectively, divided into two groups according to the particular failure scenario.

The effect of fibre inclination was considered according to the approach presented by Katz and Li [101]; see Section 2.3.4.2. They derived the pullout force of inclined fibres depending on the pullout results obtained in the direction perpendicular to the matrix surface. It has been found that inclined fibres possess a higher bridging capacity in comparison to the fibres positioned

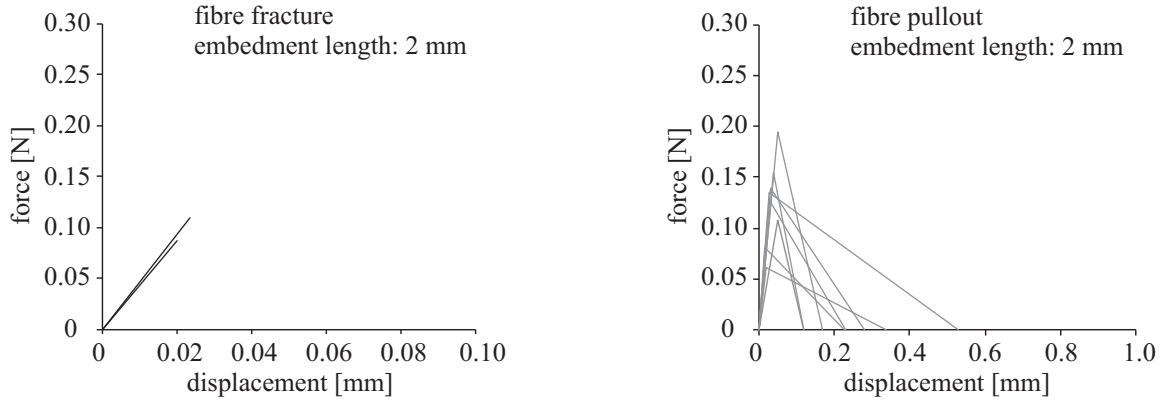

Figure 5.23: Generated single-fibre pullout responses for fibre embedded to a length of 2 mm; fibres fracture (left) and fibre pullout (right)

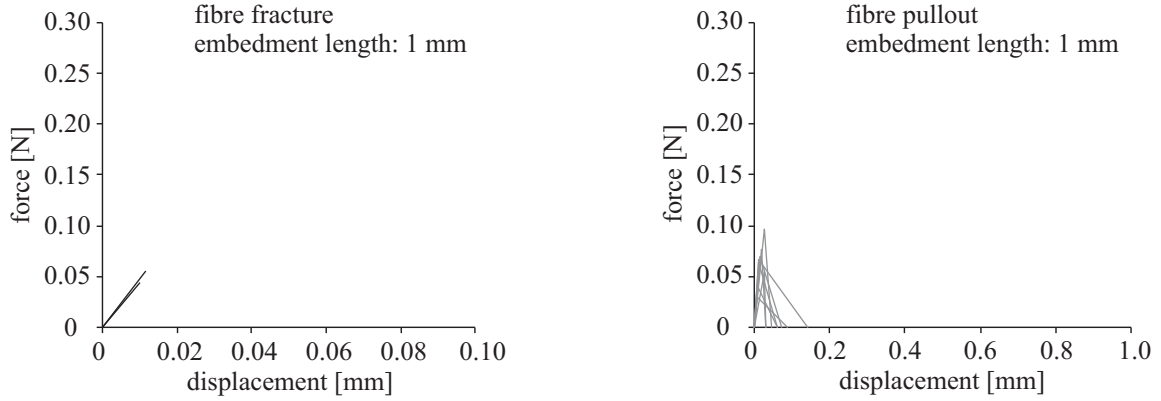

Figure 5.24: Generated single-fibre pullout responses for fibre embedded to a length of 1 mm; fibres fracture (left) and fibre pullout (right)

perpendicular to the matrix surface, i.e., there was an increase in bridging force due to the mechanisms of additional friction and bending at the exit point of the fibre. On the other hand, due to the high stress concentration at the exit point, inclined fibres tend to fail at lower stress levels, i.e., inclined fibres exhibit lower ultimate fracture loads, even in the case of ductile fibre as used in the study by Katz and Li [101].

Short fibre can be partially or fully de-bonded from both sides of the crack. As pullout tests describe only single-side fibre de-bonding (see Section 3.3.3), the pullout behaviour should be extended regarding the effect of double-side de-bonding. In considering this phenomenon, the pullout displacement before the failure is localized at one fibre end, has to be multiplied by 2 when the pullout results are used as a basis for describing the behaviour of single-crack bridging. The softening branch has then only to be shifted to a new origin at a higher displacement, while its slope remains the same.

Based on the pullout responses extended for considering specific phenomena as described above, the behaviour of the material at the meso-level of observation, i.e., the formation of one single-crack, can be derived.

It is assumed that the crack is formed through the entire cross-section. It should be mentioned here that the contribution of aggregates to crack-bridging is neglected due to their relatively

small size (maximum 1 mm) and the high bridging performance of fibres; cf. Section 2.3.4.2. Furthermore, it is assumed that one fibre can bridge only one crack. Theoretically the newly developed crack is not necessarily bridged by fibres fully bonded in the matrix, but some of them might be de-bonded and being pulled out already as a result of opening of an earlier crack in the vicinity of the crack under consideration. However, based on the observation of the specimens' surfaces, the above assumption is realistic since the crack spacing is in most cases larger than fibre length (6 mm), cf. Figure 4.4 in Section 4.1.3.

In order to limit computation time, fibre responses are generated only for a representative unit crack plane area of 1 cm^2. The number of bridging fibres for a cross-sectional area can be estimated using Equation 5.7 according to [75]. For the material under study, and due to the influence of the lamination technique used to produce the specimens in this investigation, on fibre orientation, the fibre orientation factor of $\alpha_f = 0.62$ is used to derive the number of bridging fibres. Details on the fibre orientation factor can be found in Section 2.3.3 and Section 5.3.3. The substitution to Equation 5.7 is given below in Equation 5.8:

$$n_f = 0.62 \cdot 1 \cdot \frac{0.01}{\pi \cdot (0.001)^2} = 1975 \; [fibres/cm^2] \tag{5.8}$$

A stress-displacement curve giving a characteristic material response at this level of observation can be derived by adding the force contributions of all fibres bridging the crack using the following Equation 5.9 and Equation 5.10:

$$P = b \cdot \sum_{i=1}^{n} F_i(\delta_i) \tag{5.9}$$

Where: P is the crack bridging force, b is the proportion between the actual and unit cross-sectional area, F_i is the carrying force of i^{th} fibre as a function of displacement δ_i, and n is the number of fibres bridging the unit cross-sectional area of the crack plane.

And:

$$\sigma = \frac{P}{A} \tag{5.10}$$

Where: σ is tensile stress and A is the actual cross-sectional area.

Figure 5.25 (left) shows a representative, modelled stress-displacement relationship obtained using the procedure described above. The relationship provided by the model agrees well, both quantitatively and qualitatively, with the curves obtained experimentally from specimens made with matrix M045 (w/b = 0.45) and reinforced with 1.0 % by volume short dispersed glass fibres. It should be mentioned here that the modelled single-crack behaviour presented describes the opening of a crack which propagates through the entire cross-section, starting at stress levels equal to zero, i.e., stress levels lower than those typically associated with crack formation. The experimental curves present the complete behaviour, including both the formation and the opening of single crack. Therefore, for a more exact comparison, an experimental curve with only that part of stress-crack opening relation, i.e., after exceeding the particular first-crack stress, is relevant to direct verification of the modelled curve. Such experiments were not included in the scope of this thesis. Moreover, the differences in the slope of the ascending branch of the curve before reaching the ultimate stress value can be traced back to the uniaxial tensile test setup used in this investigation, see Section 3.3.1. Although only one macroscopic crack was formed in the specimens made of concrete matrix with short fibres, the deformation was measured by two

linear variable differential transformers (LVDTs) with a gauge length of 280 mm. The "gentle sloping" of the experimental curves might result from the relatively large gauge length used in the tests. Typically, for material fracture with one visible macro-crack, the crack opening is measured directly at both crack faces. The choice of this test setup is because of the formation of multiple cracks in the case of TRC so that the results obtained from the tests on specimens with and without textile reinforcement could be compared directly, especially for the work-to-fracture measurements, see details in Section 4.1.4.

However, correction of the experimental curve can be done by subtracting the linear-elastic deformations from the curve. Comparison between the modelled curve and the corrected experimental curve is presented in Figure 5.25 (right).

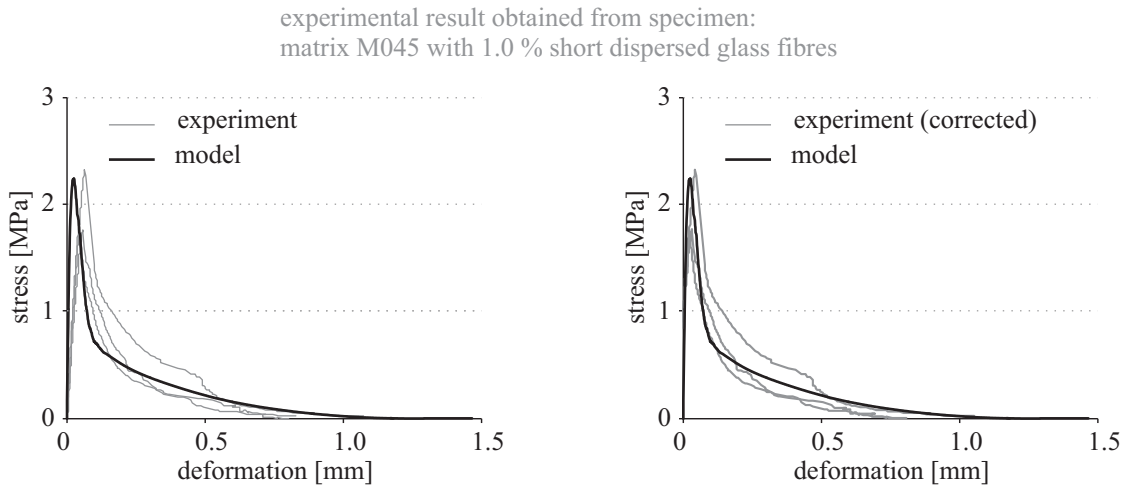

Figure 5.25: Comparison of a modelled stress-deformation relationship for the opening of one single-crack (bold line) and experimental results (thin line) (left), and after subtracting the linear-elastic deformations from the experimental curve (right)

In order to show the influence of lamination technique on the enhancement of bridging capacity, due to the increase in number of fibres bridging the crack, the modelling process was repeated under the assumption of a 3D random distribution of fibres. For this purpose, the number of fibres was determined using Equation 5.7 and a fibre orientation factor of $\alpha_f = 0.5$. Figure 5.26 (left) and (right) presents a comparison of the modelled responses obtained when the specimens produced with the lamination technique and when the fibres are randomly distributed, respectively. Since the model generates a new curve, i.e., new shapes of stress-crack opening relations, every time it runs, five different responses are presented for each case. It can be noted from the curves that an increase in the ultimate stress by approximately 30 % was achieved due to the use of the lamination technique.

5.4.4 Mathematical description of the TRC behaviour at macro-level

The concept followed for the modelling approach of the TRC behaviour at the macro-level of observation considers separately the three characteristic regions of the overall behaviour of textile reinforced concrete with short fibres: crack-free state (state I), multiple cracking region (state IIa) and crack-widening region (state IIb), see Section 2.2.5.

For modelling purposes, the behaviour of the crack-free matrix in state I, i.e. the behaviour before the formation of the first macro-crack, is considered to be linear-elastic. First-crack stress values and related strains obtained from experiments performed on TRC specimens made with

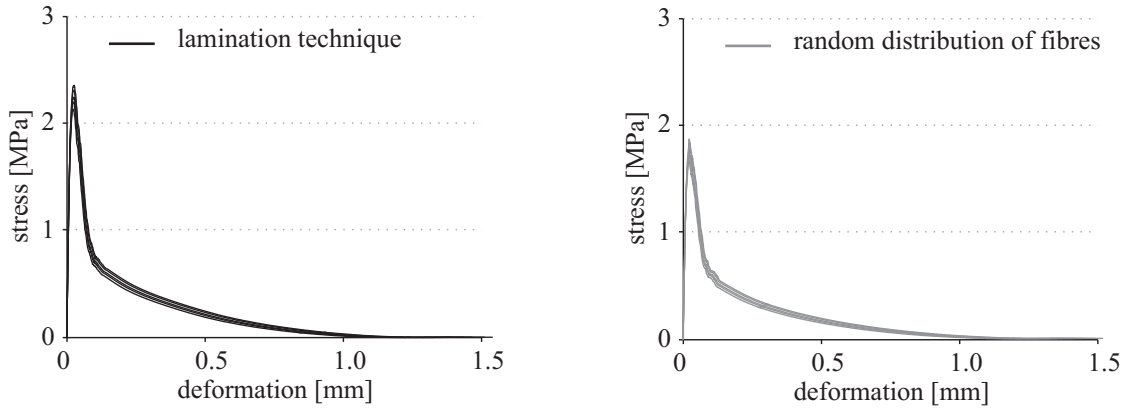

Figure 5.26: Comparison of modelled tensile behaviour considering a fibre distribution associated with the lamination technique (left) and random distribution of fibres (right)

matrix M045 with the addition of short dispersed glass fibres under tensile loading were used for the modelling. The values were varied based on the average values and standard deviation (Table 5.2) using the normal distribution function.

Table 5.2: Characteristic values of state I and state IIb

Characteristic values	average	standard deviation
First-crack stress [MPa]	3.46	0.05
First-crack strain [mm/m]	0.30	0.05
Tensile strength [MPa]	7.46	0.22
Strain capacity [mm/m]	10.73	1.65
Slope of the curve in state IIb [-]	0.25	0.04

The same procedure was used for modelling of state IIb. The values of tensile strength, strain capacity and the slope of the ascending branch were used as characteristic values and were randomly generated using normal distribution based on the average and standard deviation values provided by experimental results; see Table 5.2.

Obviously, the description of both regions of the stress-strain curve, i.e. I und IIb, are straightforward and do not enable predicting the mechanical response of TRC. In future work, these regions should be described based on the properties of the matrix, textile reinforcement and short fibres and under consideration of the interaction between these material constituents.

The modelling approach of the curve region associated with the formation of multiple cracks, i.e., state IIa, is based on the assumption that the deformations result from individual contributions of serially interconnected cracks and the contribution of the crack-free matrix. With the opening of the first crack, both short fibres and textile reinforcement yarns crossing the crack are activated. Therefore, the tensile stresses through the cracked cross-section are transmitted by both the short and the continuous fibres. Since the specimens' have been tested under deformation-controlled tensile loading, the deformation just before and just after crack opening is nearly the same. The overall deformation of the specimen is the sum of the deformation in the crack-free matrix and the crack openings. The first crack is formed when first-crack stress is reached. As a result of the steady deformation increment, deformation control, the overall tensile stress in the system drops with the opening of the first crack. The sudden drop in stress is completed when the forces in

both the crack (bridging force) and the crack-free matrix become equal. Subsequently, the stress begins to rise again with increasing deformation of the specimen. Simultaneously, the opening process of the newly formed crack continues contributing to the overall deformation. The high load carrying capacity of yarns and fibres bridging the crack leads to an increase in the overall stress until the matrix strength in the second weakest cross-section is reached and the new second crack appears and the stress drops again due to the new crack's opening, similar to the situation after the formation of the first crack.

The modelled stress-deformation relation for the opening of one single crack bridged by short fibres and a representative curve obtained from multifilament-yarn pullout test with matrix M045 with the addition of 1.0 % by volume short dispersed glass fibres, cf. Figure 4.20 (right), were used to calculate the tensile stresses transferred across through the cracks. In respect of modelling following steps were performed:

- The response (stress values) of a single crack bridged by short fibres was varied between 90 and 110 % of the original modelled response. The additional responses were generated within this range using the uniform probability distribution.
- Stress-deformation relation representing the response of one single crack bridged by yarns only was derived from the force-displacement course obtained from the multifilament-yarn pullout test. For this, the pullout force was multiplied by 13 (the number of yarns crossing the crack from one textile reinforcement layer) and then multiplied by 2 (2 layers of the textile reinforcement). Subsequently, the force was divided by the cross-sectional area of the entire specimen to obtain the corresponding stress values. These values were varied between 90 and 110 % of the original derived values. The uniform distribution function was used in this case, as well. The author is aware that these values do not represent correctly the opening of single crack bridged by textile yarns since the used results are obtained from pullout tests with a short embedment length. In future work, the action of continuous yarns should be considered.

The model presented does not predict the number of cracks. In the experimentation the last crack is formed when the bridging force of both short fibre and multifilament-yarns (resulted from yarn/matrix bond) is lower than the matrix strength at the next weakest cross-section, i.e. little bond and therefore no new cracks. The system is then saturated with cracks. The determination of maximum stresses for each crack as well as the stress-deformation behaviour of individual cracks are generated randomly using uniform probability distribution. The end of state IIa and beginning of state IIb is determined by the intersection of the two separately modelled branches.

Figure 5.27 shows an example of modelled textile-reinforced concrete with short fibres under tensile loading together with a representative stress-strain curve obtained from experiments under uniaxial deformation-controlled loading. Since the model generates the characteristic values of states I and IIb and the particular shapes of stress-deformation relations within the given ranges randomly and anew every time it runs, each generated overall stress-strain response is slightly different.

The stress-strain relation provided by the model agrees well, both quantitatively and qualitatively, with the curve obtained experimentally. However, the modeling curves representing state IIa posses fewer "jumps" but are of greater magnitude associated with the formation of each new crack. Such behaviour can be traced back to the larger opening of each modelled crack

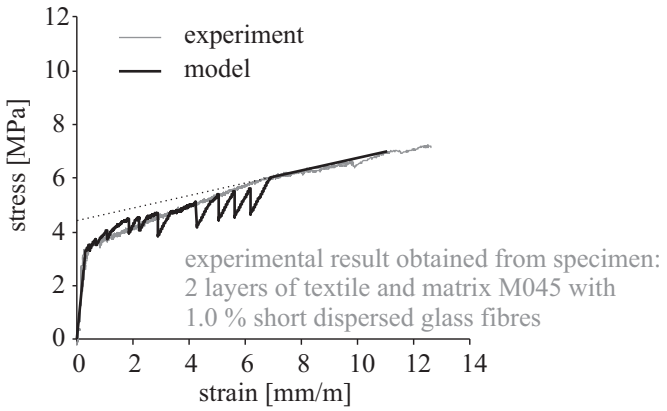

Figure 5.27: Comparison of the modelled stress-strain relation for textile-reinforced concrete with short fibres under tensile loading (black) and experimental results (gray)

in comparison to those occurring in the experiments. This phenomenon probably results from the "gentle", inclined, shape of the ascending branch before reaching the maximum stress in the stress-deformation relation used to describe the behaviour of each single crack bridged by short fibres. This might be due to the additional deformations measured using the testing machine for single-fibre pullout tests, where the deformations were measured by means of the displacement of the machine cross-head, see Section 3.3.3. An additional explanation for this phenomenon may be the relatively short embedded length of multifilament-yarn in yarn pullout tests. Having a continuous multifilament-yarn in tensile tests leads to a less inclined, steeper stress-deformation response before reaching the peak. The steeper responses of these two relations would mean a much earlier activation of both short fibres and yarns bridging the crack and, therefore, the required bridging stress is reached at much lower deformation. This would result in a higher number of cracks, greater crack density, and smaller "jumps" in magnitude and therefore lead to better correspondence of the modelled to the experimental curves.

6 Conclusions and outlook

6.1 Conclusions

6.1.1 Introduction

This thesis describes the mechanisms inherent in the joint action of short fibres and continuous fibres in high-performance, cement-based composites. The effects of adding different types of short fibres (dispersed AR glass, integral AR glass and carbon fibres) on the strength, deformation, and failure behaviour of textile-reinforced concrete (TRC) subjected to tensile loading were investigated. Experiments on different levels of observation were performed. While uniaxial tension tests on specimens made of TRC constituted the core of the experimental programme, multifilament-yarn and single-fibre pullout tests were carried out to provide detailed insights into the various bond and failure mechanisms. Subsequently, the mathematical descriptions of TRC with short fibres under deformation controlled tensile loading conditions were derived based on a multi-scale rheological-statistical modelling approach. These descriptions resulted basically from information obtained from the micro-mechanical experiments, especially from the single-fibre pullout tests.

Results obtained from experiments on different levels of observation, the relevant microscopic investigations and the model developed contribute to the understanding of the physical phenomena determining TRC behaviour with the addition of short fibres under tensile loading.

6.1.2 Experimental multi-level investigation

The stress-strain curves resulting from uniaxial tension testing demonstrated clearly the positive influence of all types of short fibre on the mechanical performance of TRC. Multifilament-yarn and single-fibre pullout tests were performed to clarify the mechanisms leading to the differing enhancements on the mechanical performance of TRC under tension. Moreover, the various effects of the short fibres in the absence of textile reinforcement was investigated and discussed. The morphology of the matrix-fibre interface was studied using an environmental scanning electron microscope, which provided some explanation of the phenomena observed. Based on the findings from the experimental investigations the following conclusions could be drawn:

- First-crack stress in TRC specimens increases significantly due to the addition of short fibres; the degree of this enhancement depends on the type of the fibre. Dispersed fibres were found to be more efficient in increasing first-crack stress values when compared to integral fibres.
- Expansion of the strain region, where multiple cracks form, was observed for the stress-strain curves for TRC with added short fibres. The visual inspection of the specimens' surfaces showed a higher number of cracks and finer crack patterns for given strain levels in the cases when short fibres were added to TRC.

- Depending on fibre type, the positive effects of the addition of short fibres on both tensile strength and work-to-fracture of the composite were found to vary significantly. The advantage of the addition of short, dispersed fibre began to fade at high strain levels and, therefore, the effect on the tensile strength of the composite was very moderate or not observed at all. Integral fibres improved the load bearing capacity of the TRC over the entire strain range, right up to failure. This resulted in more pronounced positive effects on both tensile strength and work-to-fracture of the composite.
- The water-to-binder ratio of the matrix influenced bond quality between fibre and matrix, i.e., various degrees of matrix-fibre bond were observed. As a result, the mechanical behaviour of the composite varied with w/b: While the good bond of the fibre embedded in a matrix with a low water-to-binder ratio leads to increase in stiffness and strength of the composite, fibres with weak bonding can be considered as defects with respect to stiffness.
- Short fibres improved the bond between multifilament-yarns and the surrounding matrix. By their random positioning on the yarn's surface, short fibres built new adhesive cross-links which provided extra connecting points to the surrounding matrix. Furthermore, because of their relatively larger size, short integral fibres provided a larger and stronger anchoring into the surrounding matrix than those provided by short dispersed fibres.
- Widely differing effects of the addition of short fibres on the mechanical behaviour of the matrix in the absence of textile reinforcement were observed. Short integral fibres led to a more pronounced increase in tensile strength of the matrix than that was reached due to the addition of short, dispersed fibres. This was explained by the higher effectiveness of integral inclined fibres in crack-bridging than the dispersed fibre. Because of the early activation and the failure of many dispersed fibres at an early stage in loading and due to the relatively large number of micro-cracks in the mixture with dispersed fibres, the corresponding stress-strain curves deviated from a linear course long before reaching the maximum stress value. In contrast, the stress-strain relationship of specimens with the addition of short integral fibres remained linear nearly up to the maximum stress level.

6.1.3 Modelling

The thesis further derives the mathematical description for TRC with the addition of short fibres under deformation-controlled tensile loading. These relationships were developed on the basis of a multi-scale modelling approach which considers the determined mechanisms and the physical phenomena observed in experimental investigations.

Based on the experimental results on the micro-scale, using single-fibre pullout tests, a physically based rheological model consisting of simple rheological elements was developed. This helped in analyzing in some depth the bond and failure mechanisms in the fibre-matrix interface. Special attention was paid to the gradual de-bonding process and the resulting force-displacement branch. The model adequately reproduced both relevant fibre failure scenarios: fibre fracture and fibre pullout.

By means of statistical procedures the combination of these models led to description of the stress-crack opening behaviour of an individual crack bridged by the given number of short fibres. Fibre embedded length, fibre inclination, and the influence of double-side de-bonding were considered main parameters.

The stress-strain relation for TRC with short fibres subjected to tensile loading was then derived. The concept followed at the macro-level of observation was modelling separately the three main

regions of the characteristic stress-strain curve. The regions of crack-free material and crack-widening were considered linear. Based on the corresponding characteristic values of each region and by the use of the normal distribution function, the behaviour in these states were described. The behaviour of the multiple cracking region was derived by considering an increasing number of cracks in serial interconnection and the contribution of the uncracked matrix in between. The stress transfer, i.e., bridging stress, across the crack was determined based on the contribution of both short fibres and multifilament-yarns. Behaviour of individual cracks was adjusted by varying the number of bridging fibres in different cracks and by varying the yarn bridging stress according to range observed in the pullout experiments.

The predicted responses provided by the model as developed were compared with experimental results obtained from the tests. The experimental and predicted curves were found to be in good agreement at all levels of observation.

6.2 Outlook

The following topics can be considered as options for the continuation of research work presented in this thesis.

The rheological-model developed to describe the failure behaviour of single-fibres is based mainly on interface properties by means of adhesive cross-links, i.e., hydration products. No specific knowledge regarding the exact mechanical properties of these cross-links is available. Furthermore, the limited information on the distribution and intensity of these cross-links on the fibre surface leads to less accuracy in estimating their number. Therefore, a thoroughgoing detailed investigation on interfaces in fibre-reinforced cement-based matrices can lead to more reasonable assumptions in respect of the model's parameters.

The assumption that the friction capacity of each cross-link remains constant along the distance between the corresponding cross-link and the crack surface leads to pullout behaviour with a linear softening branch and displacement equal to fibre embedded length. This is inconsistent with the pullout displacements observed in the tests. The fact that cross-links might be damaged during the pullout process could be considered. The integration of this phenomenon in the model would lead to a better agreement between the experimental and modelled pullout curves. The progressive damage of cross-links should be then described by an adequate function.

The model presented in this thesis considers the case of dispersed fibres. Due to their very different impact on TRC behaviour under tensile loading, it is meaningful to extend the model for the case of integral fibres, i.e., fibre bundles. The model should consider the interaction between core and sleeve filaments and the resulting telescopic failure. Such a model would help to understand the mechanisms leading to the improvement in tensile strength and work-to-fracture of TRC when this type of fibres is added.

The short fibres investigated in the framework of this thesis are brittle fibres. Different effects on TRC behaviour under tensile loading could be expected when ductile fibres were added. PVA (polyvenylalcohol fibres), for example, are not as expensive as carbon fibres and show good performance with regard to mechanical properties which distinguish ductile behaviour. This kind of fibre is used, for example, in Strain-Hardening Cement-based Composites (SHCC) and they perform impressively. The investigation of this type of short fibre would be very interesting and constitute a significant scientific supplement to the thesis at hand.

Bibliography

[1] Brameshuber, W. (ed.): *Textile reinforced concrete - State of the art report of RILEM technical committee 201-TRC.* Aachen, Germany : RILEM Publications S.A.R.L., 2006 (Report 36)

[2] Butler, M.; Lieboldt, M.; Mechtcherine, V.: Application of textile-reinforced concrete (TRC) for structural strengthening and in prefabrication. In: *Advances in Cement-Based Materials.* CRC Press, 2009. – ISSN 978–0–415–87637–7, S. 127–136

[3] Mechtcherine, V.: Novel cement-based composites for the strengthening and repair of concrete structures. In: *Construction and Building Materials* 41 (2013), Nr. 0, S. 365–373

[4] Jesse, F.: *Tragverhalten von Filamentgarnen in zementgebundener Matrix*, Technische Universität Dresden - Institut für Massivbau, PhD Thesis, 2004

[5] Andrade Silva, F. de; Butler, M.; Mechtcherine, V.; Zhu, D.; Mobasher, B.: Strain rate effect on the tensile behaviour of textile-reinforced concrete under static and dynamic loading. In: *Materials Science and Engineering: A* 528 (2011), Nr. 3, S. 1727–1734. – ISSN 0921–5093

[6] Mechtcherine, V.; Lieboldt, M.: Permeation of water and gases through cracked textile reinforced concrete. In: *Cement and Concrete Composites* 33 (2011), Nr. 7, S. 725–734. – ISSN 0958–9465

[7] Lieboldt, M.; Mechtcherine, V.: Capillary transport of water through textile-reinforced concrete applied in repairing and/or strengthening cracked {RC} structures. In: *Cement and Concrete Research* 52 (2013), Nr. 0, S. 53–62

[8] Lieboldt, M.: *Transport von Flüssigkeiten und Gasen in Textilbeton*, Technische Universität Dresden, Institut für Baustoffe, PhD Thesis, 2012

[9] Colombo, I.; Colombo, M.; Magri, A.; Zani, G.; Prisco, M.: Tensile behavior of textile: Influence of multilayer reinforcement. In: Parra-Montesinos, G. J. (Hrsg.); Reinhardt, H. W. (Hrsg.); Naaman, A. E. (Hrsg.): *High Performance Fiber Reinforced Cement Composites 6* Bd. 2. Springer Netherlands, 2012, S. 463–470

[10] Butler, M.; Hempel, R.; Schiekel, M.: The Influence of short glass fibres on the working capacity of textile reinforced concrete. In: J. Hegger, W. B. (Hrsg.); Will, N. (Hrsg.): *ICTRC'2006 - 1st International RILEM Conference on Textile Reinforced Concrete*, RILEM Publications SARL, 2006, S. 45–54

[11] Hinzen, M.; Brameshuber, W.: Influence of short fibers on strength, ductility and crack development of Textile Reinforced Concrete. In: Parra-Montesinos, G. J. (Hrsg.); Reinhardt, H. W. (Hrsg.); Naaman, A. E. (Hrsg.): *High Performance Fiber Reinforced Cement Composites 5.* RILEM Publications S.A.R.L., 2007 (RILEM Proceedings PRO 53), S. 105–112

[12] Korb, S.: *Untersuchungen zum Zugtragverhalten hochduktiler Faserbetone mit zusätzlicher Textilbewehrung*, Technische Universität Kaiserslautern, PhD Thesis, 2010

[13] Wittmann, F. H.: Structure of concrete with respect to crack formation. In: Wittmann, F. H. (Hrsg.): *Fracture Mechanics of Concrete*, Elsevier Science Publishers B.V., Amsterdam, 1983, S. 43–74

[14] Snyder, K.; Clifton, J.: Measures of air void spacing. In: *Proceedings of the International Conference on Building Materials*, Hochschule für Architektur und Bauwesen, Weimar, 1994, S. 155–157

[15] Mechtcherine, V.: *Bruchmechanische und fraktologische Untersuchungen zur Rissausbreitung in Beton*, Universität Karlsruhe (TH), PhD Thesis, 2000

[16] Stark, J.; Wicht, B.: *Zement und Kalk - Der Baustoff als Werkstoff*. Birkhäuser Verlag, Basel, 2000

[17] *Kapitel* 7: Industrieprodukte. In: Plank, J.; Stephan, D.; Hirsch, C.: *Bauchemie*. 5. Wiley-VCH Verlag GmbH & Co. KGaA, Weinheim, 2004 (Chemische Technik, Prozesse und Produkte), S. 1–137

[18] Brockmann, T.: *Mechanical and fracture mechanical properties of fine grained concrete for textile reinforced composites*, RWTH Aachen, PhD Thesis, 2005

[19] Butler, M.: *Dauerhaftigkeit von Verbundwerkstoffen aus zementgebundenen Matrices und alkaliresistenten Glasfaser-Multifilamentgarnen*, Technischen Universität Dresden - Institut für Baustoffe, PhD Thesis, 2009

[20] Majumdar, A. J.; Laws, V.: *Glass Fibre Reinforced Cement*. BPS Professional Books Division of Blackwell Scientific Publications Ltd, 1991. – 192 S.

[21] Butler, M.; Mechtcherine, V.; Hempel, S.: Durability of textile reinforced concrete made with AR glass fibre: effect of the matrix composition. In: *Materials and Structures* 43 (2010), S. 1351–1368. – ISSN 1359–5997

[22] Mechtcherine, V.: Towards a durability framework for structural elements and structures made of or strengthened with high-performance fibre-reinforced composites. In: *Construction and Building Materials* 31 (2012), S. 94–104. – ISSN 0950–0618

[23] Langlois, V.; Fiorio, B.; Beaucour, A.-L.; Cabrillac, R.; Gouvenot, D.: Experimental study of the mechanical behavior of continuous glass and carbon yarn-reinforced mortars. In: *Construction and Building Materials* 21 (2007), Nr. 1, S. 198–210. – ISSN 0950–0618

[24] Schorn, H.; Butler, M.; Hempel, R.; Schiekel, M.: Untersuchungen zur Dauerhaftigkeit von alkaliresistenten Glasfilamentgarnen in zementgebundenen Matrices. In: Curbach, M. (Hrsg.): *Proc. 2nd Colloquium on Textile Reinforced Structures (CTRS2)*, Dresden: Sonderforschungsbereich 528; Technische Universität Dresden, 2003, S. 77–90

[25] Schorn, H.; Hempel, R.; Weise, S.: Grundlagen für die Gefüge- und Verbundoptimierung der Matrices von textilbewehrten Betonen. In: *Arbeits- und Ergebnisbericht für die Periode II/1999-I/2002 zum SFB 528*. Technische Universität Dresden, 2001, S. 72–120

[26] Orlowsky, J.: *Zur Dauerhaftigkeit von AR-Glasbewehrung in Textilbeton*, RWTH Aachen, PhD Thesis, 2004

[27] Katz, A.; Li, V. C.; Kazmer, A.: Bond properties of carbon fibres in cementitious matrix. In: *Journal of Materials in Civil Engineering* 7 (1995), Nr. 2, S. 125–128

[28] Rieger, C.; Mier, J. G.: Pullout of microfibers from hardened cement paste. In: vanZijl, G. (Hrsg.); Boshoff, W. (Hrsg.): *Proc. of the International Conference on Advanced Concrete Materials*, 2009, S. 67–73

[29] Rieger, C.: *Micro-fibre cement pullout tests, uniaxial tensile tests and material scaling*, ETH Zurich, PhD Thesis, 2010

[30] Brameshuber, W.; Brockmann, T.: Development and optimisation of cementitious matrices for textile reinforced elements. In: *Proceedings of the 12th International Congress of the International Glassfibre Reinforced Concrete Association*, London: Concrete Society, 2001, S. 237–249

[31] Zorn, H.: Alkaliresistente Glasfasern: Von der Herstellung bis zur Anwendung. In: Curbach, M. (Hrsg.): *Proc. 2nd Colloquium on Textile Reinforced Structures (CTRS2)*, Dresden: Sonderforschungsbereich 528; Technische Universität Dresden, 2003, S. 1 – 14

[32] *Kapitel* Textiles. In: Gries, T.; Roye, A.; Offermann, P.; Peled, A.: *Textile Reinforced Concrete - State-of-the-Art Report of RILEM TC 201-TRC*. RILEM Publications SARL, 2006, S. 11–27

[33] Mott, R.; Brameshuber, W.; Hartung, I.; Dilger, K.: Production Methods for Textile-Reinforced Concrete. In: *American Concrete Institute* 260 (2009), S. 105–124

[34] Richter, M.: *Entwicklung mechanischer Modelle zur analytischen Beschreibung der Materialeigenschaften von textilbewehrtem Feinbeton*, Technische Universität Dresden, PhD Thesis, 2005

[35] Hartig, J.; Haeussler-Combe, U.; Schicktanz, K.: Influence of bond properties on the tensile behaviour of Textile Reinforced Concrete. In: *Cement and Concrete Composites* 30 (2008), Nr. 10, S. 898–906. – ISSN 0958–9465

[36] Weiland, S.: *Interaktion von Betonstahl und textiler Bewehrung bei der Biegeverstärkung mit textilbewehrtem Beton*, Technische Universität Dresden, PhD Thesis, 2009

[37] Ohno, S.; Hannant, D. J.: Modeling the stress-strain response of continuous fibre reinforced cement composites. In: *ACI Materials Journal* 91 (1994), S. 306–312

[38] Jesse, F.; Curbach, M.: Strength of continuous AR-glass fibre reinforcement of cementitious composites. In: Naaman, A. E. (Hrsg.); Reinhardt, H. W. (Hrsg.): *International Workshop High Performance Fiber Reinforced Cement Composites*, RILEM Publications SARL, 2003, S. 337–348

[39] Zastrau, B.; Richter, M.; Lepenies, I. G.: On the analytical solution of pullout phenomena in textile reinforced concrete. In: *Journal of Engineering Materials and Technology* 125 (2003), S. 38–43

[40] Lorenz, E.; Ortlepp, R.; Hausding, J.; Cherif, C.: Effizienzsteigerung von Textilbeton durch Einsatz textiler Bewehrungen nach dem erweiterten Naehwirkverfahren. In: *Beton- und Stahlbetonbau* 106 (2011), Nr. 1, S. 21–30

[41] Moeller, B.; Graf, W.; Hoffmann, A.; Sickert, J.-U.; Steinigen, F.: Textile reinforced concrete structures under uncertain dynamic loading processes. In: Motasoares, C. (Hrsg.); Martins, J. (Hrsg.); Rodrigues, H. (Hrsg.); Ambrasio, J. (Hrsg.); Pina, C. (Hrsg.); Motasoares, C. (Hrsg.); Pereira, E. (Hrsg.); Folgado, J. (Hrsg.): *III European Conference on Computational Mechanics*. Springer Netherlands, 2006, S. 750–750

[42] Kang, B.-G.: Analysis of Textile Reinforced Concrete at the Micro-level. In: Yoo, S.-D. (Hrsg.): *EKC2008 Proceedings of the EU-Korea Conference on Science and Technology* Bd. 124. Springer Berlin Heidelberg, 2008, S. 179–189

[43] Orlowsky, J.; Raupach, M.: Einfluss der Umgebungsbedingungen auf die Dauerstandfestigkeit von Textilbeton. In: *35. Tagung des DVM-Arbeitskreises Bruchvorgänge*. Berlin: Deutscher Verband für Materialforschung und -prüfung, 2003, S. 325–334

[44] Chudoba, R.; Vorechovsky, M.; Konrad, M.; Jerabek, J.: TRC-Specimens modeled as a chian of cracks bridged by bundles. In: Konsta-Gdoutos, M. (Hrsg.): *Measuring, Monitoring and Modeling Concrete Properties*. Springer, Netherlands, 2006, S. 777–783

[45] Hartig, J.; Jesse, F.; Schicktanz, K.; Haeussler-Combe, U.: Influence of experimental setups on the apparent uniaxial tensile load-bearing capacity of Textile Reinforced Concrete specimens. In: *Materials and Structures* 45 (2012), Nr. 3, S. 433–446

[46] Scheffler, C.; Gao, S.; Plonka, R.; Mäder, E.; Hempel, S.; Butler, M.; Mechtcherine, V.: Interphase modification of alkali-resistant glass fibres and carbon fibres for textile reinforced concrete I: Fibre properties and durability. In: *Composites Science and Technology* 69 (2009), Nr. 3-4, S. 531–538. – ISSN 0266–3538

[47] Scheffler, C.; Gao, S.; Plonka, R.; Maeder, E.; Hempel, S.; Butler, M.; Mechtcherine, V.: Interphase modification of alkali-resistant glass fibres and carbon fibres for textile reinforced concrete II: Water adsorption and composite interphases. In: *Composites Science and Technology* 69 (2009), Nr. 7-8, S. 905–912. – ISSN 0266–3538

[48] Lepenies, I. G.: *Zur hierarchischen und simultanen Multi-Skalen-Analysen von Textilbeton*, Technische Universität Dresden, PhD Thesis, 2007

[49] Zastrau, B.; Lepenies, I.; Richter, M.: Zur Entwicklung einer Materialbeschreibung von Textilbeton mit Anwendung repräsentativer Volumenelemente. In: Curbach, M. (Hrsg.): *Proc. 2nd Colloquium on Textile Reinforced Structures (CTRS2)*, Dresden: Sonderforschungsbereich 528; Technische Universität Dresden, 2003, S. 387–398

[50] Schorn, H.: An adhesive cross-linkage model for textile reinforcement in concrete. In: Zingoni, A. (Hrsg.): *Proc. of the Second International Conference on Structural Engineering, Mechanics and Computation SEMC*, (CD-ROM), 2004, S. 1563–1567

[51] Butler, M.; Hempel, S.; Mechtcherine, V.: Modelling of ageing effects on crack-bridging behaviour of AR-glass multifilament yarns embedded in cement-based matrix. In: *Cement and Concrete Research* 41 (2011), Nr. 4, S. 403–411. – ISSN 0008–8846

[52] Lepenies, I.; Meyer; Schorn, H.; Zastrau, B.: Modeling of load transfer behavior of AR-glass-rovings in textile reinforced concrete. In: *ACI Materials: Thin fiber and textile reinforced cementitious systems* SP-244-7 CD-ROM (2007), S. 109–123

[53] Banholzer, B.: Bond of a strand in a cementitious matrix. In: *Materials and Structures* 39 (2006), S. 1015–1028

[54] Banholzer, B.: *Bond behaviour of a multi-filament yarn embedded in a cementitious matrix*, RWTH Aachen, PhD Thesis, 2004

[55] Soranakom, C.; Mobasher, B.: Geometrical and mechanical aspects of fabric bonding and pullout in cement composites. In: *Materials and Structures* 42 (2009), S. 765–777

[56] Lorenz, E.; Ortlepp, R.: Bond behavior of textile reinforcements - Development of a pull-out test and modeling of the respective bond versus slip relation. In: Parra-Montesinos, G. J. (Hrsg.); Reinhardt, H. W. (Hrsg.); Naaman, A. E. (Hrsg.): *High Performance Fiber Reinforced Cement Composites 6* Bd. 2. Springer, Netherlands, 2012, S. 479–486

[57] Krüger, M.; Reinhardt, H.-W.; Fichtlscherer, M.: Bond behaviour of textile reinforcement in reinforced and prestressed concrete. In: *Otto-Graf-Journal* 12 (2001), S. 33–50

[58] Soroushian, P.; Bayasi, Z.: Fiber Type Effects on the Performance of Steel Fiber Reinforced Concrete. In: *ACI Materials Journal* 88 (1991), Nr. 2, S. 129–134

[59] Wong, C.: *Use of short fibres in structural concrete to enhance mechanical properties*, University of Southern Queensland, PhD Thesis, 2004

[60] Hinzen, M.; Brameshuber, W.: Influence of matrix composition and short fibres on the workability of fine grained fibre concrete. In: Brameshuber, W. (Hrsg.): *International RILEM Conference on Material Science*, RILEM Publications SARL, 2010, S. 131–140

[61] Mier, J. V.: Mode I fracture of concrete: Discontinuous crack growth and crack interface grain bridging. In: *Cement and Concrete Research* 21 (1991), Nr. 1, S. 1–15. – ISSN 0008–8846

[62] Duda, H.: *Bruchmechanisches Verhalten von Beton unter monotoner und zyklischer Zugbeanspruchung*. Berlin : Beuth Verlag, 1991 (Heft 419). – 60 S.

[63] Bentur, A.; Mindess, S.: *Fibre reinforced cementitious composites*. Taylor & Francis, 2006 (Modern Concrete Technology Series). – ISBN 9780415250481

[64] Jun, Z.; Stang, H.: Fatigue performance in flexure of fiber reinforced concrete. In: *ACI Materials Journal* 95 (1998), Nr. 1, S. 58–67

[65] Mechtcherine, V.; Millon, O.; Butler, M.; Thoma, K.: Mechanical behaviour of strain hardening cement-based composites under impact loading. In: *Cement and Concrete Composites* 33 (2011), Nr. 1, S. 1–11. – ISSN 0958–9465

[66] Suzuki, T.; Miyajima, T.; Sakai, M.: The role of the fiber/matrix interface in the first matrix cracking of fiber-reinforced brittle-matrix composites. In: *Composites Science and Technology* 51 (1994), Nr. 2, S. 283–289. – ISSN 0266–3538

[67] Banthia, N.; Moncef, A.; Sheng, J.: Uniaxial tensile response of cement composites reinforced with high volume fractions of carbon, steel, and polypropylene micro-fibers. In: *ACI Special Publication* 146 (1994), S. 43–68

[68] Banthia, N.; Sheng, J.: Fracture toughness of micro-fiber reinforced cement composites. In: *Cement and Concrete Composites* 18 (1996), Nr. 4, S. 251–269. – ISSN 0958–9465

[69] Sakai, M.; Matsuyama, R.; Miyajima, T.: The pull-out and failure of a fiber bundle in a carbon fiber reinforced carbon matrix composite. In: *Carbon* 38 (2000), S. 2123–2131

[70] Deng, Z.: The fracture and fatigue performance in flexure of carbon fiber reinforced concrete. In: *Cement and Concrete Composites* 27 (2005), Nr. 1, S. 131–140. – ISSN 0958–9465

[71] ACI-544: State-of-the-Art Report on Fibre Reinforced Concrete / American Concrete Institute, ACI 544 1R-96 (Reapproved 2002). 1996. – Forschungsbericht. – 66 S.

[72] Rossi, P.; Acker, P.; Malier, Y.: Effect of steel fibres at two different stages: The material and the structure. In: *Materials and Structures* 20 (1987), S. 436–439

[73] Barros, J. A. O.; Figueiras, J. A.; Veen, C. D. V.: Tensile behaviour of glass fibre reinforced concrete. In: Gomez, J. S. (Hrsg.); Branco, F. (Hrsg.); Brito, F. D. (Hrsg.); Cirne, J. S. (Hrsg.); Cruz, A. C. D. (Hrsg.): *Proc. of the 10th International Conference on Experimental Mechanics: Recent Advances in Experimental Mechanics* Bd. 2, 1994, S. 1073–1080

[74] Krenchel, H.: *Fibre Reinforcement*. Copenhagen: Akademisk Forlag, 1964. – 159 S.

[75] Li, V. C.; Wang, Y.; Backer, S.: A micromechanical model of tension-softening and bridging toughening of short random fiber reinforced brittle matrix composites. In: *Journal of the Mechanics and Physics of Solids* 39 (1991), Nr. 5, S. 607–625. – ISSN 0022–5096

[76] Soroushian, P.; Lee, C.-D.: Distribution and orientation of fibers in steel fiber reinforced concrete. In: *ACI Materials Journal* 87 (1990), Nr. 5, S. 433–439

[77] Gettu, R.; Gardner, D.; Saldivar, H.; Barragan, B.: Study of the distribution and orientation of fibers in SFRC specimens. In: *Materials and Structures* 38 (2005), S. 31–37

[78] Aveston, J.; Kelly, A.: Theory of multiple fracture of fibrous composites. In: *Journal of Materials Science* 8 (1973), S. 352–362

[79] Lee, S.-C.; Cho, J.-Y.; Vecchio, F. J.: Diverse embedment model for steel fibre-reinforced concrete in tension: Model development. In: *ACI Materials Journal* 108 (2011), Nr. 5, S. 516–525

[80] Lee, S.-C.; Cho, J.-Y.; Vecchio, F. J.: Diverse embedment model for steel fibre-reinforced concrete in tension: Model verification. In: *ACI Materials Journal* 108 (2011), Nr. 5, S. 526–535

[81] Chan, Y.-W.; Li, V. C.: Effects of transition zone densification on fiber/cement paste bond strength improvement. In: *Advanced Cement Based Materials* 5 (1997), Nr. 1, S. 8–17. – ISSN 1065–7355

[82] Rasmussen, T. V.: *Time dependent interfacial parameters in cementitious composite materials*, Technical University of Denmark, Department of Structural Engineering and Materials, PhD Thesis, 1997. – 170 S

[83] Betterman, L.; Ouyang, C.; Shah, S.: Fiber-matrix interaction in microfiber-reinforced mortar. In: *Advanced Cement Based Materials* 2 (1995), Nr. 2, S. 53 – 61. – ISSN 1065–7355

[84] Markovic, I.; Walraven, J.; Mier, J. van: Tensile behaviour of high performance hybrid fibre concrete. In: Li, V. (Hrsg.); Leung, C. (Hrsg.); Willam, K. (Hrsg.); Billington, S. (Hrsg.): *Proc. of the 5th International Conference on Fracture Mechanics of Concrete and Concrete Structures (FraMCoS-5)* Bd. 2, 2004, S. 1113–1120

[85] Shah, S. P.: Do fibers increase the tensile strength of cement-based matrix? In: *ACI Materials Journal* 88 (1992), Nr. 6, S. 595–602

[86] Cox, H. L.: The elasticity and strength of paper and other fibrous materials. In: *British Journal of Applied Physics* 3 (1952), Nr. 3, S. 72–79

[87] Löfgren, I.: *Fibre-reinforced concrete for industrial construction – a fracture mechanics approach to material testing and structural analysis*, Chalmers University of Technology - Department of Civil and Environmental Engineering, Structural Engineering, PhD Thesis, 2005

[88] Nelson, P. K.; Li, V. C.; Kamada, T.: Fracture toughness of microfiber reinforced cement composites. In: *Journal of Materials in Civil Engineering* 14 (2002), Nr. 5, S. 384–391

[89] Lawler, J.; Wilhelm, T.; Zampini, D.; Shah, S.: Fracture processes of hybrid fiber-reinforced mortar. In: *Materials and Structures* 36 (2003), S. 197–208

[90] Shah, S. P.; Swartz, S. E.; Ouyang, C.: *Fracture mechanics of concrete: Applications of fracture mechanics to concrete, rock, and other brittle materials.* New York : John Wiley and Sons, 1995. – 552 S.

[91] Mechtcherine, V.: Fracture mechanical behavior of concrete and the condition of its fracture surface. In: *Cement and Concrete Research* 39 (2009), Nr. 7, S. 620–628. – ISSN 0008–8846

[92] Stang, H.; Li, Z.; Shah, S.: Pullout problem: Stress versus fracture mechanical approach. In: *Journal of Engineering Mechanics* 116 (1990), Nr. 10, S. 2136–2150

[93] Li, V. C.; Stang, H.: Interface property characterization and strengthening mechanisms in fiber reinforced cement based composites. In: *Advanced Cement Based Materials* 6 (1997), Nr. 1, S. 1–20. – ISSN 1065–7355

[94] Kelly, A.; Tyson, W.: Tensile properties of fibre-reinforced metals: Copper/tungsten and copper/molybdenum. In: *Journal of the Mechanics and Physics of Solids* 13 (1965), Nr. 6, S. 329–350

[95] Redon, C.; Li, V.; Wu, C.; Hoshiro, H.; Saito, T.; Ogawa: Measuring and modifying interface properties of PVA fibers in ECC matrix. In: *Journal of Materials in Civil Engineering* 13 (2001), Nr. 6, S. 399–406

[96] Boshoff, W. P.; Mechtcherine, V.; Zijl, G. P.: Characterising the time-dependant behaviour on the single fibre level of SHCC: Part 2: The rate effects on fibre pull-out tests. In: *Cement and Concrete Research* 39 (2009), Nr. 9, S. 787–797. – ISSN 0008–8846

[97] Bentur, A.; Wu, S. T.; Banthia, N.; Baggott, R.; Hansen, W.; Katz, A.; Leung, C. K. Y.; Li, V.; Mobasher, B.; Naaman, A. E.; Soroushian, R. R. P.; Stang, H.; Taerwe, L.: Fiber-Matrix Interfaces. In: Naaman, A. (Hrsg.); Reinhardt, H. (Hrsg.): *RILEM proc. High Performance Fiber Reinforced Cementitious Composites* Bd. 31, RILEM, 1996, S. 143–192

[98] Leung, C. K. Y.; Li, V. C.: Effect of fiber inclination on crack bridging stress in brittle fiber reinforced brittle matrix composites. In: *Journal of the Mechanics and Physics of Solids* 40 (1992), Nr. 6, S. 1333–1362

[99] Li, V.; Wang, Y.; Backer, S.: Effect of inclining angle, bundling and surface treatment on synthetic fibre pull-out from a cement matrix. In: *Composites* 21 (1990), Nr. 2, S. 132–140. – ISSN 0010–4361

[100] Kanda, T.; Li, V. C.: Interface Property and Apparent Strength of High-Strength Hydrophilic Fiber in Cement Matrix. In: *Journal of Materials in Civil Engineering* 10 (1998), Nr. 1, S. 5–13

[101] Katz, A.; Li, V. C.: Inclination angle effect of carbon fibers in cementitious composites. In: *Journal of Engineering Mechanics* 121 (1995), Nr. 12, S. 1340–1348

[102] Zhang, J.; Li, V. C.: Effect of inclination angle on fiber rupture load in fiber reinforced cementitious composites. In: *Composites Science and Technology* 62 (2002), Nr. 6, S. 775–781. – ISSN 0266–3538

[103] Chaallal, O.; Benmokrane, B.: Pullout and bond of glass-fibre rods embedded in concrete and cement grout. In: *Materials and Structures* 26 (1993), S. 167–175

[104] Wang, Y.; Li, V. C.; Backer, S.: Modelling of fibre pull-out from a cement matrix. In: *International Journal of Cement Composites and Lightweight Concrete* 10 (1988), Nr. 3, S. 143–149. – ISSN 0262–5075

[105] Jun, P.; Mechtcherine, V.: Behaviour of Strain-hardening Cement-based Composites (SHCC) under monotonic and cyclic tensile loading: Part 2 - Modelling. In: *Cement and Concrete Composites* 32 (2010), Nr. 10, S. 810–818. – ISSN 0958–9465

[106] Igarashi, S.; Kawamura, M.: Effects of a size in bundled fibers on the interfacial zone between the fibers and the cement paste matrix. In: *Cement and Concrete Research* 24 (1994), Nr. 4, S. 695–703. – ISSN 0008–8846

[107] Bartos, P.: Enviromentally active GRC: Towards better appearance of concrete and a reduction of air-pollution in urban environment. In: *Nanotechnology in construction (scientific Internet-journal)* 2 (2011), S. 24–39

[108] Crawley, M. J.: *Statistical Computing: An introduction to data analysis using S-Plus*. Wiley, 2002. – 761 S. – ISBN 9780471560401

[109] Kessler-Kramer, C.: *Zugtragverhalten von Beton unter Ermüdungsbeanspruchung*, Universität Karlsruhe (TH), PhD Thesis, 2002

[110] Duda, H.; Konig, G.: Rheological material model for the stress-crack-width relation of concrete under monotonic and cyclic tension. In: *ACI Materials Journal* 88 (1991), Nr. 3, S. 278–287

[111] Kessler-Kramer, C.; Mechtcherine, V.; Müller, H.: Testing and modeling the behavior of concrete under cyclic tensile loading. In: Li, V. (Hrsg.); Leung, C. (Hrsg.); Willam, K. (Hrsg.); Billington, S. (Hrsg.): *Proc. of the 5th International Conference on Fracture Mechanics of Concrete and Concrete Structures (FraMCoS-5)* Bd. 2, 2004, S. 995–1004

[112] Zheng, S. S.; Tao, Q. L.; Liu, B.; Xie, M.; Hu, Y.: Study on stochastic damage constitutive relation for HSHPC material subjected to uniaxial tension stress. In: *Advanced Materials Research* 374-377 (2011), S. 2570–2573

[113] Hausding, J.: *Multiaxiale Gelege auf Basis derKettenwirktechnik - Technologie für Mehrschichtverbunde mit variabler Lagenanordnung*, Technische Universität Dresden - Institut für Textilmaschinen und Textile Hochleistungswerkstofftechnik, PhD Thesis, 2010

[114] Eckers, V.: *Multiskalenanalyse gitterartiger Textilstrukturen für textilbewehrten Beton*, RWTH Aachen, PhD Thesis, 2010

[115] Lorenz, E.; Ortlepp, R.: Berechnungsalgorithmus zur Bestimmung der Verankerungslänge der textilen Bewehrung in der Feinbetonmatrix. In: Curbach, M. (Hrsg.); Jesse, F. (Hrsg.): *Textile Reinforced Structures : Proc. of the 4th Colloquium on Textile Reinforced Structures (CTRS4) und zur 1. Anwendertagung* SFB 528, Technische Universität Dresden, 2009, S. 491–502

[116] Lorenz, E.: End anchorage and overlapping of textile reinforcements in textile reinforced concrete. In: Müller, H. S. (Hrsg.); Haist, M. (Hrsg.); Acosta, F. (Hrsg.): *Proc. of the 9th fib International PhD Symposium in Civil Engineering* Karlsruhe Institute of Technology (KIT)„ KIT Scientific Publishing, Karlsruhe, 2012, S. 685–690

[117] Kabele, P.; Novak, L.; Nemecek, J.; Kopecky, L.: Effects of chemical exposure on bond between synthetic fiber and cementitious matrix. In: Hegger, J. (Hrsg.); Brameshuber, W. (Hrsg.); Will, N. (Hrsg.): *ICTRC'2006 - 1st International RILEM Conference on Textile Reinforced Concrete*, RILEM Publications SARL, 2006, S. 91–99

[118] Katz, A.; Li, V. C.: A special technique for determining the bond strength of micro-fibres in cement matrix by pullout test. In: *Journal of Materials Science Letters* 15 (1996), S. 1821–1823

[119] Jun, P.: *Behaviour of Strain-hardening Cement-based Composites (SHCC) under monotonic and cyclic tensile loading*, Technische Universität Dresden - Institut für Baustoffe, PhD Thesis, 2010

[120] Jun, P.; Mechtcherine, V.: Behaviour of Strain-hardening Cement-based Composites (SHCC) under monotonic and cyclic tensile loading: Part 1 - Experimental investigations. In: *Cement and Concrete Composites* 32 (2010), Nr. 10, S. 801–809. – ISSN 0958–9465

[121] Norm: *Testing of mortars with mineral binders; general, sampling, test mortar.* 1982

[122] Béton (fib), F. I. (ed.): *fib Model Code for Concrete Structures 2010.* 2010. Ernst & Sohn, 2013. – 434 S.

[123] *http://www.rstudio.com/.* : *http://www.rstudio.com/*

[124] Chin, W.-K.; Liu, H.-T.; Lee, Y.-D.: Effects of fiber length and orientation distribution on the elastic modulus of short fiber reinforced thermoplastics. In: *Polymer Composites* 9 (1988), Nr. 1, S. 27–35

[125] Fu, S.-Y.; Lauke, B.: Effects of fiber length and fiber orientation distributions on the tensile strength of short-fiber-reinforced polymers. In: *Composites Science and Technology* 56 (1996), Nr. 10, S. 1179–1190

A Appendix – Slump flow tests

a)

matrix M030 with 0.5 % short
integral glass fibres
d = 195 mm

b)

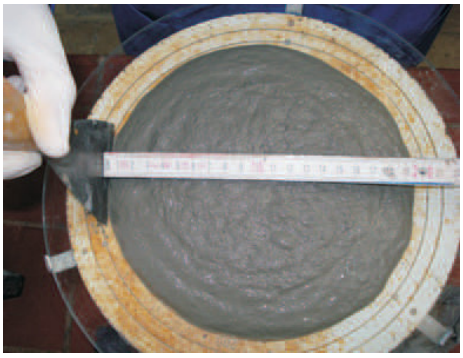

matrix M030 with 0.5 % short
dispersed glass fibres
d = 195 mm

c)

matrix M030 with 0.5 % short
carbon fibres
d = 145 mm

Figure A.1: Slump flow test with small cone of the matrix M030 a) with the addition of 0.5 % short integral AR glass fibres, b) with the addition of 0.5 % short dispersed AR glass fibres and c) with the addition of 0.5 % short carbon fibres

a)

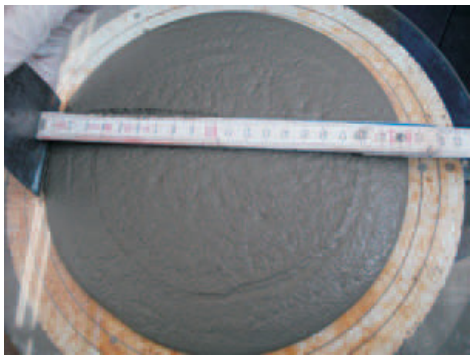

plain matrix M045
d = 205 mm

b)

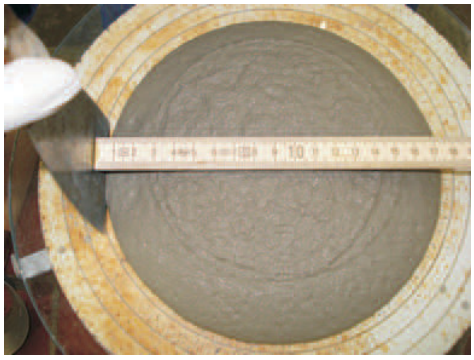

matrix M045 with 0.5 % short
integral glass fibres
d = 175 mm

c)

matrix M045 with 0.5 % short
dispersed glass fibres
d = 175 mm

d)

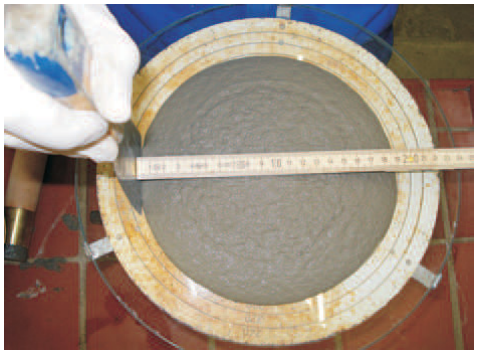

matrix M045 with 1.0 % short
integral glass fibres
d = 180 mm

e)

matrix M045 with 1.0 % short
dispersed glass fibres
d = 175 mm

Figure A.2: Slump flow test with small cone of the matrix M045 a) plain matrix b) with the addition of 0.5 % short integral AR glass fibres, c) with the addition of 0.5 % short dispersed AR glass fibres d) with the addition of 1.0 % short integral AR glass fibres, e) with the addition of 1.0 % short dispersed AR glass fibres

B Appendix – Results of uniaxial tensile tests (4 layers of textile with and without short fibres)

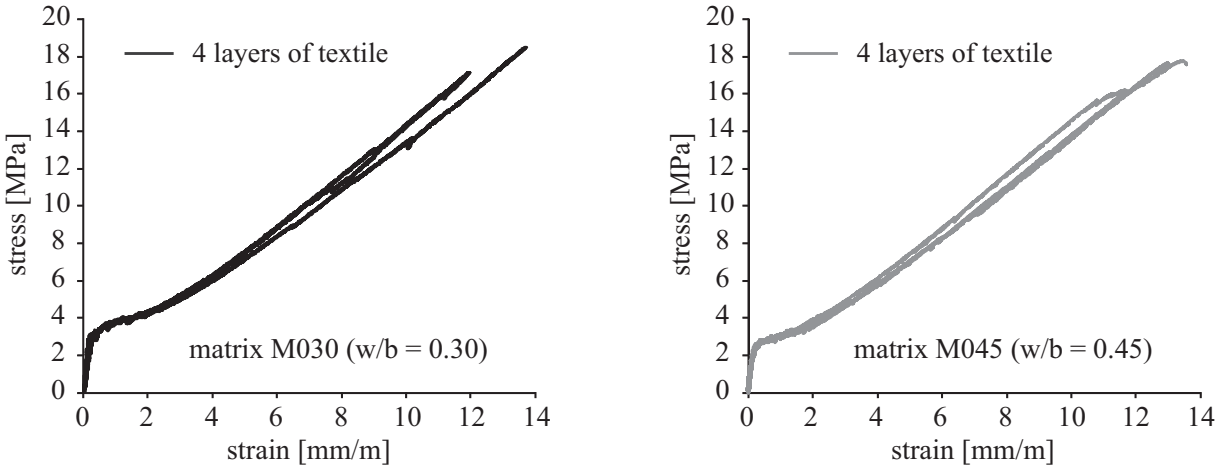

Figure B.1: Stress-strain curves determined in uniaxial tensile tests on specimens reinforced with 4 layers of textile made with the matrix M030 (left) and M045 (right)

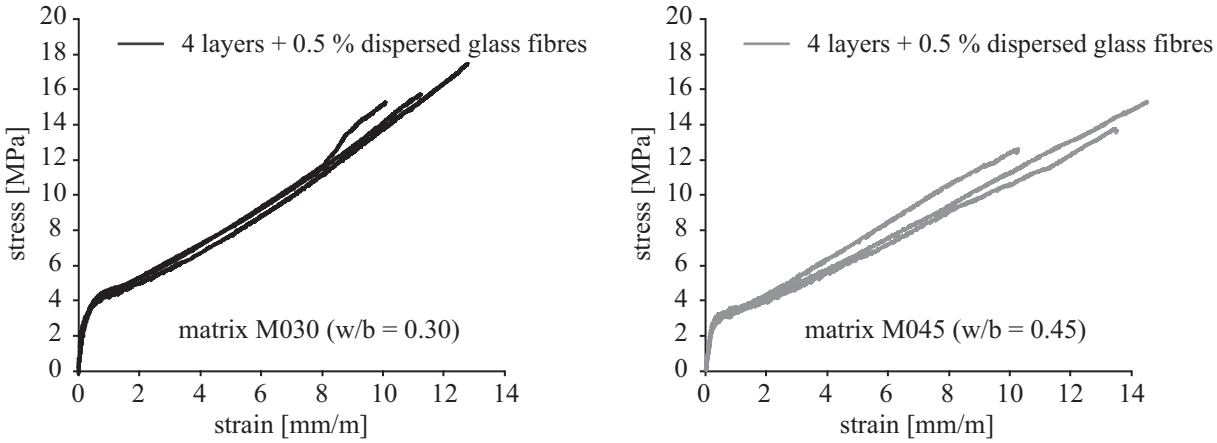

Figure B.2: Stress-strain curves determined in uniaxial tensile tests on specimens reinforced with 4 layers of textile and 0.5 % short dispersed glass fibres made with the matrix M030 (left) and M045 (right)

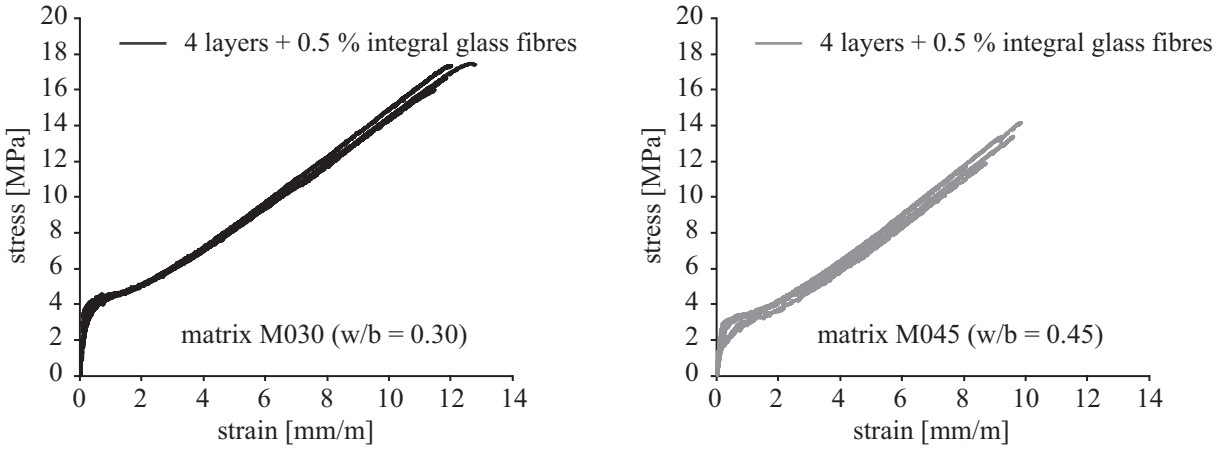

Figure B.3: Stress-strain curves determined in uniaxial tensile tests on specimens reinforced with 4 layers of textile and 0.5 % short integral glass fibres made with the matrix M030 (left) and M045 (right)

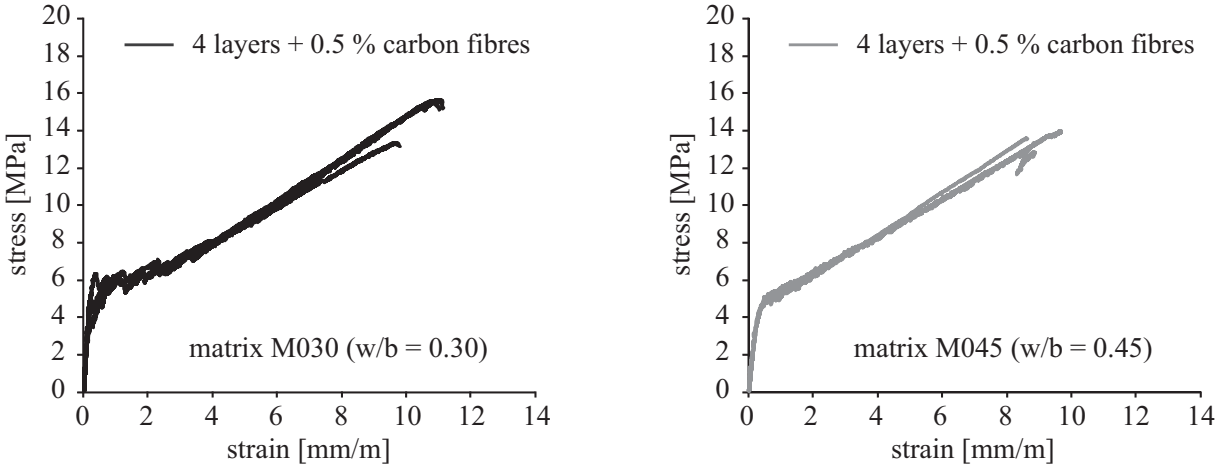

Figure B.4: Stress-strain curves determined in uniaxial tensile tests on specimens reinforced with 4 layers of textile and 0.5 % short carbon fibres made with the matrix M030 (left) and M045 (right)

C Appendix – Effect of short fibres on crack pattern

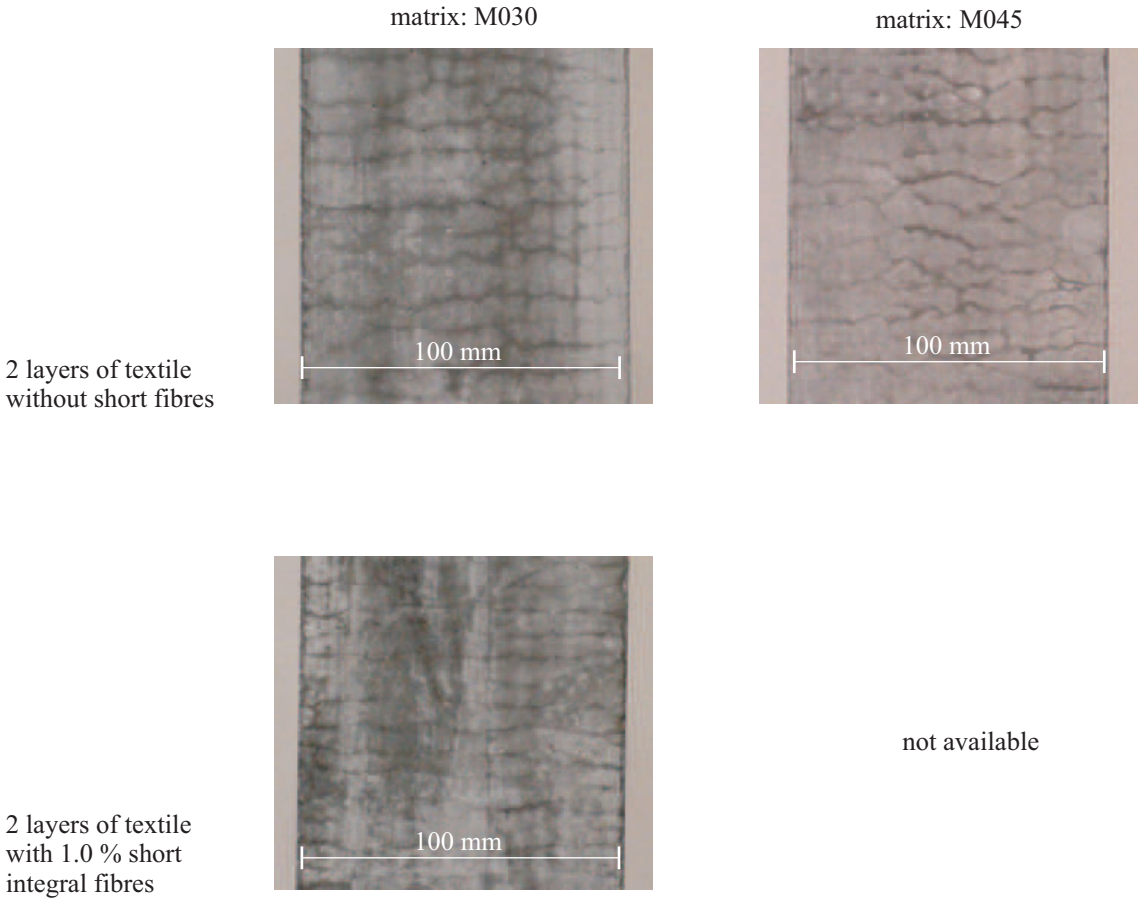

Figure C.1: Effect of short integral glass fibres on crack patterns on specimen' surface; TRC plates with matrix M030 (left) and M045 (right) at strain level of approximately 10 mm/m

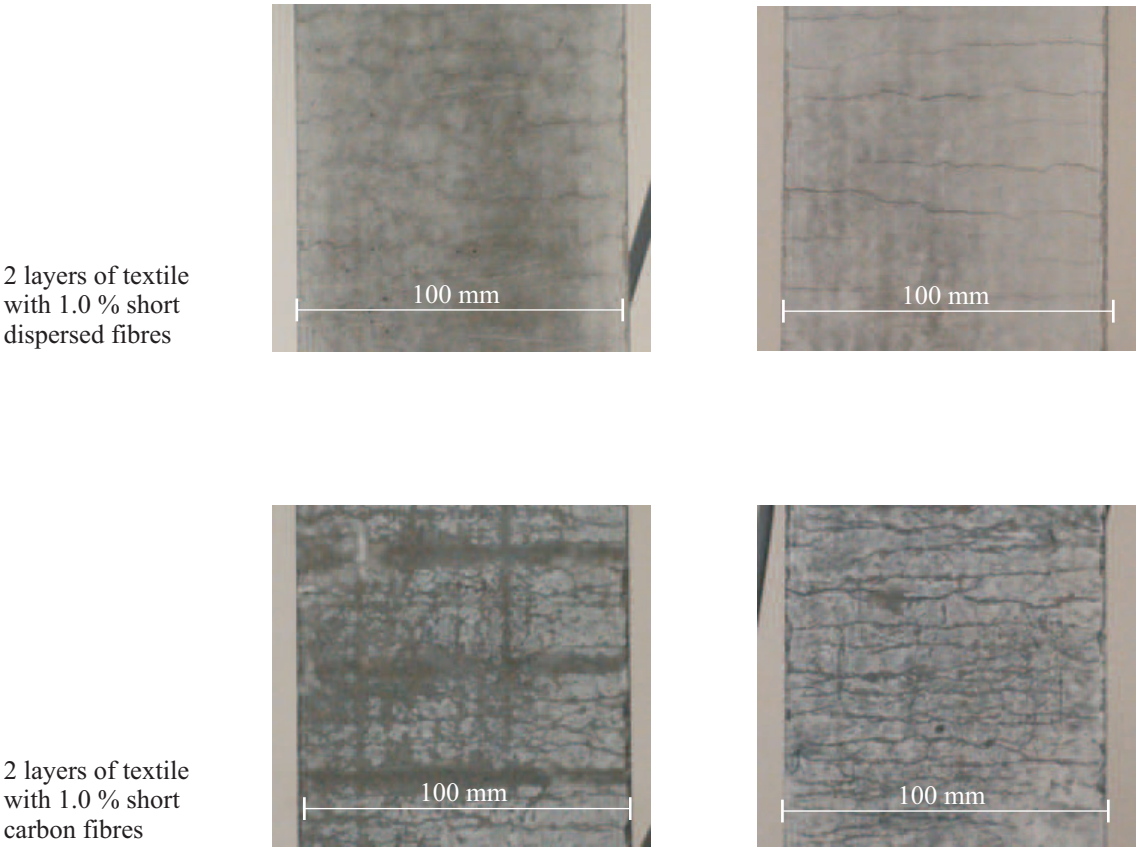

Figure C.2: Effect of short dispersed glass and carbon fibres on crack patterns on specimen' surface; TRC plates with matrix M030 (left) and M045 (right) at strain level of approximately 10 mm/m

D Appendix – List of Symbols

Abbreviations

CSH	Calcium Silicate Hydrate
ESEM	Environmental Scanning Electron Microscope
FRC	Fibre Reinforced Concrete
LVDT	Linear Variable Differential Transformer
PVA	Polyvinyl Alcohol
SHCC	Strain-hardening Cement-based Composites
TRC	Textile-Reinforced Concrete
w/b	Water-to-binder ratio

Latin letters capital

A	cross-sectional area of the fibres / cross-sectional area of the specimen
A_c	unit cross-section area
E	Young's modulus
P	force
F	pullout force
F_{fra}	maximum bearing load of the fibres
$F_{cb,i}$	bond strength of cross-link i
$F_{cf,i}$	frictional force of cross-link i
F_{Si}	maximum bearing load of spring i
$F_{S1,drop1}$	drop is stress after the breakage of the first cross-link
S	stiffness of a spring element
C	stiffness of the system
N	index of the last cross-link
V_f	Volume fraction of fibre

Latin letters small

b	proportion between the actual and unit cross-sectional area
l	length of a segment of fibre between two cross-links
l_e	embedded length of the fibre
n	index of the newly activated cross-link
$w_{c,i}$	distance between cross-link i and crack surface
n_f	number of fibres

Greek letters small

β	shape parameter of Weibull function
η	scale parameter of Weibull function
γ	location parameter of Weibull function
Δl_e	deformation capacity at which the fibre fractures after linear elastic response
α_f	fibre orientation factor
δ	deformation, displacement

Indices

fra	fracture
e	elastic
p	plastic
i	number
j	number